eman ta zabal zazu

Universidad del País Vasco
Euskal Herriko Unibertsitatea

Ingeniaritza Goi Eskola Teknikoa
Escuela Técnica Superior de Ingeniería
Bilbao

Departamento de Ingeniería Química y del Medio Ambiente
ESCUELA TÉCNICA SUPERIOR DE INGENIERÍA
BILBAO

DEVELOPMENT OF THE HETEROGENEOUS CATALYSTS FOR THE PRODUCTION OF LEVULINIC ACID FROM FURFURYL ALCOHOL

A dissertation submitted to the University of the Basque Country to apply for the degree of Ph.D in Chemical Engineering

By

Ilian Guzmán Vélez

Advisors:
Prof. María Belén Güemez Bilbao
Prof. José Cambra Ibáñez

Bilbao 2015

Una especial dedicatoria a mi Familia y a Flavia.....

…….Por su incondicional apoyo y cariño.

Acknowledgements

I would like thanks go to institutions who financed this study. Particularly, this work was supported by funds Spanish Ministry of Economy and Competitiveness (MINECO) and European Union through the European Regional Development Fund (FEDER) (Project: CTQ2012-38204-C03-01 and CTQ2012-38204-C03-03), the Basque Regional Government and University of the Basque Country (UPV/EHU).

I also thank the cooperation of other institutions as the Institute of Catalysis and Petrochemistry (ICP-CSIC), special thanks to the Dr Rafael Mariscal, for their great contribution in this project, as well as to their research group the Sustainable Energy and Chemistry (EQS). I would like thank Dr Benjamin Katryniok, Department of Solid-State Chemistry Unit (UCCS), Lille 1 University, as well as to their research group for his great willingness and collaboration in this study. I also want thank to the research group of Department of Inorganic Chemistry, Crystallography and Mineralogy of Malaga University (UMA), for their unconditional collaboration.

Special thanks go to Thesis Advisors, Dr. María Belén Güemez Bilbao and Dr. José Francisco Cambra Ibañez, for their knowledge, guidance, patience, understanding, and encouragement that have given me during this research. Besides my directors, I would like especially thanks to the members of the Sustainable Process Engineering research group (SUPREN) for all the assistance and fellowship received.

Summary

The object of this thesis belongs to the research on chemical compounds derived from biomass, which in recent years has generated high interest due to multiple applications in the field of chemical industry and energy. Among the compounds of great interest is levulinic acid. Levulinic acid has important characteristics that define it as a precursor of multiple products with applications in various fields of chemical industry. The most known and developed process to obtain levulinic acid is the "Biofine" process. The process is performed in two reaction steps to convert the sugars (with six carbon atoms) by acid hydrolysis using H_2SO_4. The yield to levulinic acid obtained in the “Biofine” process is around of 70-80 % respect to maximum theoretical, and corresponds to 50 % of carbohydrate (C6). In the production of levulinic acid, great efforts are being made to replace homogeneous acid catalysis as H_2SO_4, HCl, HBr by solids heterogeneous catalysis that are more sustainable, easy to recover and recycle and that affect positively the economic balance of the process. For this purpose in general are used lignocellulosic materials, sugars or its derivatives such as furfural or 5-hydroxymethylfurfural. However, the yields to levulinic acid remain low.

Another alternative to obtain levulinic acid, which is primary object of this thesis, is from compounds closest to the productive chain from biomass, in this case from furfuryl alcohol. Levulinic acid formation proceeds by the hydration reaction of furfuryl alcohol using acid catalysts, typically mineral acids. The development of this thesis is focused on the study of novel heterogeneous acid catalysts that can be used in the reaction, also in the incorporation of alternative reaction systems to improve the yield to levulinic acid.

In the first phase of research (chapter 4) a selection of solid acid catalysts with organic support such as ion exchange resins Amberlyst 35 (A35), 47 (A47) and 70 (A70), and inorganic support as SBA-15 and MCM-41 zeolites was performed. The catalytic activity tests initially were conducted on a fixed bed system in continuous flow, obtaining a maximum yield to levulinic acid of 62 mol % with A35 catalyst. However,

despite the positive results, the reaction system was not feasible due to operational problems that generated the furan resins formed in reaction, these generated clogging in the internal connections of the reaction system. Subsequently, the activity tests were focused on the use of a discontinuous stirred reaction system, based on the catalyst with best results in previous system (A35), however, the yield to levulinic acid decreased significantly.

As result of a research stay in the Institute of Catalysis and Petrochemistry (ICP-CSIC) in Madrid (Spain), the synthesis and characterization of catalysts of niobium (Nb) supported on TiO_2 and zeolite USY which are materials with considerable acidity was developed. The catalytic activity was developed using niobium catalysts prepared by two methods and the A35 used as reference material. An alternative reaction system which involves the incorporation of cyclopentyl methyl ether (CPME) as solvent, generating a system reaction in two phases (organic and aqueous) was used. Furfuryl alcohol is located mainly in organic phase and maintains a low concentration in the aqueous phase, while the levulinic acid is concentrated in aqueous phase. The study showed that the yield to levulinic acid increases up to 45 mol %, for the catalyst A35, but, niobium catalysts not showed selectivity to levulinic acid. However, the results concluded that properties such as Brönsted acidity and mesoporosity have high influence in selectivity to levulinic acid. This phase of research is presented in Chapter 6, in which the study of niobium catalysts is extends to obtain two alternative products, the 4-hydroxy-2-cyclopentenone and cyclopentanone.

In a next phase of research (chapter 5) and according to above results was raised modify the reaction system to semi-batch. In this system the use of 2-butanone (MEK) as solvent of furfuryl alcohol was studied. The mixture of furfuryl alcohol and MEK was slowly fed into the reactor, which contains a mixture of water and MEK, allowing maintain low concentrations of furfuryl alcohol in the reactor, thus reducing the formation of furan resins. With this system, a "screening" of catalysts with Bronsted acidity and having mesoporosity was performed, the results showed a yield to levulinic acid of 62 mol % for the catalyst A35 (reference material). However, a very close result in yield to levulinic acid (58 mol %) using HZSM-5 (SiO_2: Al_2O_3 =50) zeolite was obtained, so that with this catalyst the optimization of operating conditions and variables as temperature, amount of catalyst fed, furfuryl alcohol concentration, type of atmosphere (hydrogen or nitrogen), and reaction time was developed. Under optimal

conditions a yield to levulinic acid of 73 mol% was reached. As the acidity of zeolite HZSM-5 is related with silica-alumina ratio (Si/Al), a detailed study of this material was developed. For this, the commercial zeolite HZSM-5 with lower Si/Al ratio (SiO_2/Al_2O_3= 23) was also selected. Both zeolites (HZSM-5 (23) and HZSM-5 (50) were subjected to desilication process for further decrease of Si/Al ratios and increase its acidity and mesoporosity. Should be noted that a part of the characterization was carried out during a stay in the University of Lille 1 (France). The characterization results showed that desilication process decrease the Si/Al ratio and increases the mesoporosity of modified zeolites. The catalytic activity developed over optimal reaction conditions, has allowed achieve a yield to levulinic acid of 81 mol% using the desilicated zeolite HZSM-5 (23).

A series of solid considered as "superacids" which are based on sulfated zirconium oxide (ZrO_2/ SO_4^{2-}) were also prepared and characterized. To improve the acidity properties, it was proposed the lanthanum incorporation using different contents of lanthanum and zirconium precursors (La_xZrO_2/SO_4^{2-}). These catalysts were prepared by a co-precipitation technique using ultrasound at low temperatures; this phase research is discussed in Chapter 7. The yields to levulinic acid obtained in this phase were low.

Resumen

El tema objeto de estudio en esta tesis pertenece a la línea de investigación sobre compuestos químicos derivados de la biomasa, que en recientes años ha generado un alto interés, debido a las múltiples aplicaciones en el sector de la industria química y de la energía. Entre los compuestos de gran interés en este ámbito está el ácido levulínico. El ácido levulínico posee características importantes que lo definen como un compuesto precursor de múltiples subproductos con aplicaciones en varios campos de la industria química. El proceso más conocido y desarrollado para la obtención de ácido levulínico es el proceso "Biofine". Este proceso, se realiza en dos etapas de reacción y trata azúcares de seis átomos de carbono mediante hidrólisis ácida usando ácido sulfúrico (H_2SO_4). El rendimiento obtenido de ácido levulínico en el proceso "Biofine" es de alrededor de 70-80 % del máximo teórico, y corresponde al 50 % de carbohidratos de seis carbonos. En la producción de ácido levulínico y en el ámbito científico, son muchos los esfuerzos que se están realizando para sustituir la catálisis ácida homogénea (H_2SO_4, HCl, HBr) por materiales sólidos (catálisis heterogénea) que sean más sostenibles, fáciles de recuperar y reciclar, y que influyan positivamente en el balance económico del proceso. Para ello, como materia prima se emplean en general material lignocelulósico, azúcares o compuestos derivados de estos últimos, como el furfural o el 5-hidroximetilfurfural. Sin embargo, los rendimientos de ácido levulínico siguen siendo bajos.

Otra alternativa para la obtención de ácido levulínico, objetivo principal de estudio en esta tesis, es a partir de compuestos más próximos en la cadena productiva de los derivados de la biomasa, en este caso, el alcohol furfurílico. La formación de ácido levulínico transcurre mediante la reacción de hidratación de alcohol furfurílico, usando catalizadores ácidos, habitualmente ácidos minerales. El desarrollo de esta tesis se centra en el estudio de catalizadores ácidos heterogéneos novedosos que puedan ser usados en la reacción, y en la incorporación de sistemas de reacción alternativos que permitan mejorar el rendimiento de ácido levulínico.

En la primera fase de investigación (capitulo 4) se realizó una selección de catalizadores sólidos ácidos que incluyeron catalizadores con soporte orgánico como las resinas de intercambio iónico Amberlyst 35 (A35), 47 (A47) y 70 (A70), y de soporte inorgánico como zeolitas tipo SBA-15 y MCM-41. Los ensayos de actividad catalítica, realizados inicialmente en un sistema de lecho fijo y flujo continuo, permitieron obtener con el catalizador A35 un rendimiento máximo de 62 % molar de ácido levulínico. Sin embargo, a pesar de los buenos resultados, el sistema de reacción no fue viable, debido a los problemas de tipo operativo que generaron las resinas furánicas formadas en la reacción y que causan taponamiento en las conexiones internas del sistema de reacción. Posteriormente, los ensayos de actividad se centraron en el uso de un sistema de reacción agitado discontinuo, tomando como base el catalizador con los mejores resultados obtenidos en el sistema anterior (A35), sin embargo los rendimientos disminuyeron considerablemente.

Mediante una estancia de investigación en el Instituto de Catálisis y Petroleoquímica (ICP-CSIC) de Madrid, se desarrolló la síntesis y caracterización de catalizadores de niobio (Nb) soportados sobre dióxido de titanio (TiO_2) y zeolita ultra estable USY los cuales son materiales con una considerable acidez. La actividad catalítica se desarrolló usando los catalizadores preparados de niobio, así como el A35 utilizado como material de referencia. Se utilizó un sistema alternativo de reacción que involucró la incorporación de ciclopentil-metileter (CPME) como disolvente, generándose en el sistema de reacción 2 fases (orgánica y acuosa), el alcohol furfurílico permanece mayoritariamente en la fase orgánica y mantiene una baja concentración en la fase acuosa, mientras que el ácido levulínico se concentra en la fase acuosa. El estudio mostró que el rendimiento de ácido levulínico aumenta hasta un 45 % molar para el catalizador A35, pero los catalizadores de niobio no presentaron selectividad a ácido levulínico. No obstante, los resultados permitieron concluir que propiedades como la acidez tipo Brönsted y la mesoporosidad de los catalizadores, favorecen la selectividad a ácido levulínico en la reacción objeto de estudio. Esta fase de investigación se presenta en el capítulo 6, en el que se extiende el estudio sobre los catalizadores de niobio a la obtención de dos productos alternativos, 4-hidroxi-2-ciclopentenona y ciclopentanona.

En una siguiente fase de investigación (capitulo 5), teniendo en cuenta los resultados anteriores, se optó por modificar el sistema de reacción pasando a ser semicontinuo. En

este sistema se planteó el uso de 2-butanona (MEK) como disolvente del alcohol furfurílico. La disolución de alcohol furfurílico en MEK se alimenta poco a poco al reactor, que a su vez contiene una mezcla de H_2O-MEK, lo que permite mantener en el reactor bajas concentraciones de alcohol furfurílico, disminuyendo así la formación de resinas furánicas. Con este sistema se realizó un "screening" de catalizadores con acidez tipo Brönsted y que poseen mesoporosidad, dos variables importantes de acuerdo a resultados obtenidos hasta ese momento. Los resultados mostraron un rendimiento máximo de 62 % molar de ácido levulínico para el catalizador A35 (material de referencia). Sin embargo, un resultado muy próximo con un rendimiento de ácido levulínico del 58 % molar se obtuvo con la zeolita HZSM-5 (SiO_2:Al_2O_3=50), por lo que con este catalizador se procedió a optimizar las condiciones de operación de las siguientes variables: temperatura, cantidad de catalizador, concentración de alcohol furfurílico alimentado, atmósfera de reacción (hidrógeno o nitrógeno), y tiempo de reacción. En las condiciones óptimas se alcanzó un rendimiento de ácido levulínico del 73 % molar. Debido a que la acidez de la zeolita HZSM-5 está relacionada con el ratio de sílice–alúmina (Si/Al), se optó por desarrollar un estudio más detallado de este material. Para ello también se seleccionó la zeolita comercial HZSM-5 con menor relación Si/Al, (SiO_2:Al_2O_3=23). A ambas zeolitas (HZSM-5 (23) y HZSM-5 (50) se les sometió a un proceso desilicación para disminuir aún más la relación Si/Al y aumentar así la acidez y la mesoporosidad. Indicar que una parte de la caracterización de estos materiales se realizó durante una estancia en la Unidad de Catálisis y Química del Sólido de la Universidad de Lille 1 (Francia). Los resultados de la caracterización mostraron que efectivamente el proceso de desilicación disminuye la relación Si/Al e incrementa la mesoporosidad de las zeolitas tratadas. La actividad catalítica en las condiciones óptimas de reacción permitió alcanzar un rendimiento de ácido levulínico del 81 % molar para la zeolita HZSM-5 (23) desilicada.

También se prepararon y caracterizaron una serie de sólidos considerados como "superácidos" a base de óxido de zirconio sulfatado (ZrO_2/SO_4^{2-}). Para mejorar las propiedades de acidez de este material, de acuerdo a los reportes encontrados en la bibliografía se planteo la incorporación de lantano, usando diferentes contenidos (La_xZrO_2/SO_4^{2-}), y mediante una técnica de co-precipitacion usando ultrasonido a bajas temperaturas. Esta fase de investigación se trata en el capítulo 6, los resultados de rendimiento de acido levulinico en esta fase de investigación fueron bajos.

Table of contents

Capítulo 1. Introducción

1.1. La biomasa como una alternativa a los recursos de origen fósil 11

1.2. Ácido levulínico (LA) 22

1.3. Catálisis heterogénea aplicada a la obtención de ácido levulínico a partir de alcohol furfurílico. 34

1.4.Referencias..... 45

Capítulo 2. Objetivos 56

Capítulo 3. Materiales y técnicas experimentales

3.1. Resumen 61

3.2. Materiales 62

3.3. Procedimientos de preparación de los catalizadores 63

3.4. Técnicas de caracterización de catalizadores 69

3.5. Sistemas de reacción utilizados 78

3.6. Técnicas de análisis de reactivos y productos 83

3.7. Referencias 87

Chapter 4. Acidic ion exchange resins in the production of levulinic acid

4.1. Summary 90

4.2. Introduction 91

4.3. Selection and properties of ion exchange resins 93

4.4. Reaction in continuous flow (packed bed reactor) 96

4.5. Reaction in batch system 101

4.6. Conclusions 113

4.7. References 114

Chapter 5. Inorganic solid catalysts in the production of levulinic acid

5.1. Summary 117

5.2. Introduction 118

5.3. Preliminary screening of acid solid catalysts 119

5.4. Optimization of operating parameters using HZSM-5 zeolite (H-Z(50)) 127
5.5. ZSM-5 zeolite modified 135
5.6. Conclusions 149
5.7. References 150

Chapter 6. Study of "superacid" catalysts sulfated lanthanum-zirconium oxide in the synthesis of levulinic acid from furfuryl alcohol

6.1. Summary 157
6.2. Introduction 158
6.3. Experimental 159
6.4. Results and discussion 161
6.5. Conclusions 167
6.6. References 168

Chapter 7. Valorization of furfuryl alcohol as an alternative to produce precursor of 4-hydroxy-2-cyclopentenone and cyclopentanone.

7.1. Summary 170
7.2. Introduction 171
7.3. Experimental 173
7.4. Results and discussion 174
7.5. Conclusions 200
7.6. References 201

Chapter 8. Conclusions and proposals for futures research on this topic

8.1. Conclusions 203
8.2. Proposals for futures research on this topic 206

Holdings derived from Doctoral Thesis 207

Index of Figures

Capítulo 3

Figura 3.1. Montaje para las reacciones en sistema discontinuo (“batch”) 79

Figura 3.2. Reactor autoclave de acero inoxidable con controlador de temperatura y agitación 80

Figura 3.3. Planta PID Microactivity usada para los ensayos en reacción de flujo continuo.. 82

Figura 3.4. Elementos para toma y tratamiento de las muestras liquidas de reacción..... ….85

Figura 3.5. Tratamiento de toma de muestras de gases del reactor y análisis en GC..... ….86

Chapter 4

Figure 4.1. DRIFT Spectra of pyridine adsorbed on A35 (fresh)..... 96

Figure 4.2. Effect of WHSV on yield to LA 98

Figure 4.3. Variation of LA yield using A35 and A47 99

Figure 4.4. Effect of the temperature in yield to LA. 100

Figure 4.5. Ternary diagram for the H_2O-FA-CPME system 102

Figure 4.6. GC characteristic chromatogram of compounds obtained at 2 hours reaction . 105

Figure 4.7. Behavior of FA conversion and yield to LA with reaction time..... 105

Figure 4.8. Evolution of relative chromatographic peak areas of compounds on reaction time 107

Figure 4.9. variation of selectivity on time at different temperatures 107

Figure 4.10. Influence of the concentration of FA in conversion and yield to LA..... 108

Figure 4.11. Influence the amount of water in yield to LA and conversion of FA. 109

Figure 4.12. Influence of catalyst loading over yield to LA and conversion of FA. 110

Chapter 5

Figure 5.1. Variation of FA conversion and yield to LA by modification of gas media used.. 128

Figure 5.2. Comparative study of organic co-solvents in the reaction of FA to LA..... 129

Figure 5.3. Variation of yield to LA, by the modification of FA concentration in the mixture fed 130

Figure 5.4. Variation of yield to LA for different values of mol FA/ gcat. 131

Figure 5.5. Variation of yield to LA by the increases of the temperature 132

Figure 5.6. Evolution of catalytic activity the main products and reagents during the initials two hours, reported in peak areas. 133

Figure 5.7. Evolution of yield to LA on time of reaction 134

Figure 5.8. Signal of energy dispersion X-ray analysis (EDX) for H-Z(50) zeolite 137

Figure 5.9.1. Nitrogen adsorption and desorption isotherms of a) H-Z(50), b) H-ZD(50). ... 139

Figure 5.9.2. Nitrogen adsorption and desorption isotherms of c) H-ZR(50), d) H-ZDR(50). 140

Figure 5.10. Nitrogen adsorption and desorption isotherms of a) H-Z(23), b) H-ZD(23), c) H-ZDR(23). 141

Figure 5.11. TPD-NH_3 profiles of the parent and desilicated zeolites: a) H-Z(23), H-ZD(23) and H-ZDR(23). b) H-Z(50), H-ZD(50) and H-ZDR(50). 143

Figure 5.12. FT-IR spectra of pyridine chemisorbed on HZSM-5 catalysts at 313 K 144

Figure 5.13. Deconvolution spectra of pyridine chemisorbed on H-Z(50) at 313 K. 145

Figure 5.14. Yield to LA by the use of parent and desilicated zeolites 147

Figure 5.15. Yield to LA on the reaction time for H-Z(23) and H-ZD (23) zeolites. 147

Figure 5.16. Comparison of yields to LA between desilicated H-ZD(23) and recovery H-ZDR(23). 148

Chapter 6

Figure 6.1. Signal of energy dispersion X-ray analysis for $La_{0.53}ZrO_2/SO_4^{2-}$ and $La_{1.06}ZrO_2/SO_4^{2-}$**.** 162

Figure 6.2. XPS data analysis for A) $La_{0.53}ZrO_2/SO_4^{2-}$, B) $La_{1.06}ZrO_2/SO_4^{2-}$.. 163

Figure 6.3. Evolution of furfuryl alcohol conversion with reaction time for La_xZrO_2/SO^{2-}.... 164

Figure 6.4. Distribution of by-products obtained with La_xZrO_2/SO_4^{2-}catalysts**.** 166

Chapter 7

Figure 7.1. Evolution of temperature programmed oxidation (TPO) of Nb_1TiO_2 catalyst 175

Figure 7.2. Thermogravimetric analysis (TGA) of H-USY and Nb_xUSY catalysts..... 176

Figure 7.3. X-ray diffraction of H-USY zeolite and Nb_xUSY 178

Figure 7.4. X-ray diffraction analysis of Nb_xTiO_2 catalysts 178

Figure 7.5. XPS analysis of Nb_xTiO_2 and Nb_xUSYM2 179

Figure 7.6. XPS analysis of Nb_1USYM2, Nb_4USYM2, Nb_8USYM2. 180

Figure 7.7. Acidity determined by FTIR pyridine adsorption method. 393 K: (a) TiO_2 (b) Nb_8TiO_2 (c) $Nb_{24}TiO_2$. 182

Figure 7.8. Acidity determined by pyridine adsorption FTIR at 473 K: (a) H-USY, (b) Nb_4USYM1, (c) Nb_8USYM1, (d) Nb_4USYM2, (e) Nb_8USYM2. 183

Figure 7.9. Isothermal cycles of ammonia chemisorption for Nb_xTiO_2 at 373 K..... 184

Figure 7.10. Temperature programmed reduction (TPR) of γ-Al_2O_3, WO_x/Al_2O_3 and Pt*WO_x/Al_2O_3 catalysts. 186

Figure 7.11. Nitrogen adsorption desorption isotherm of Pt*WO_x/Al_2O_3 catalyst..... 187

Figure 7.12. X-ray diffraction (XRD) of Pt/Al_2O_3, Pt*WO_x/Al_2O_3 and WO_x/Al_2O_3 catalysts.... 188

Figure 7.13. Conversion of furfuryl alcohol using a) Nb_xUSY, b) Nb_xTiO_2. 189

Figure 7.14. Relative peak area of 4-HCP formation for Nb_xUSY and Nb_xTiO_2. 190

Figure 7.15. Representation of reactants and products in second stage. Yield to (CPN+CPOL) and relative peak area of 4-HCP..... 191

Figure 7.16. Variation of CPN+CPOL yield with the operating pressure..... 192

Figure 7.17. Effect of temperature in FA conversion and yields to main products..... 193

Figure 7.18. Variation of yields to CPN with amount of FA fed (moles FA/ mass of catalyst). 194

Figure 7.19. Conversion of FA by the use of WO_x/Al_2O_3, Pt/Al_2O_3 and Pt*WO_x/Al_2O_3catalysts 195

Figure 7.20. Main products obtained by the use of different catalysts. a) WO_x/Al_2O_3, b) Pt/Al_2O_3 and c) Pt*WO_x/Al_2O_3 196

Figure 7.21. Selectivity to CPN using Pt/Al_2O_3, WO_x/Al_2O_3 and Pt*WO_x/Al_2O_3 catalysts..... 197

Figure 7.22. Selectivity of products obtained for different catalysts. 198

Index of Schemes

Capítulo 1.

Esquema 1.1. Producción mundial por tipo de energía para los años comprendidos entre 1973 y 2011. 12

Esquema 1.2. Demanda mundial de energía primaria entre el año 1980 y 2009 y su proyección hasta 2035..... 12

Esquema 1.3. Derivados potenciales de la plataforma de azúcares. 15

Esquema 1.4. Fuente, origen y aprovechamiento de la biomasa. 17

Esquema 1.5. Representación de los grupos funcionales del LA. 23

Esquema 1.6. Principales productos obtenidos a partir del LA. 24

Esquema 1.7. Diagrama representativo de obtención de LA a partir de hemicelulosa y celulosa 27

Esquema 1.8. Proceso "Biofine" de producción de LA..... 28

Esquema 1.9. Mecanismo de reacción de FA a LA 30

Esquema 1.10. Mecanismo de resinificación del FA en medio ácido 32

Esquema 1.11. Obtencion de LA a partir de: (1) 5-metilfurfural, (2) butirolactona, (3) nitroetano y acroleína 33

Esquema 1.12. Estructura característica de las zeolitas ácidas, acidez Brönsted y Lewis 40

Esquema 1.13. Estructura de la resina de intercambio iónico con grupos sulfónicos. 42

Capítulo 3.

Esquema 3.1. Diagrama representativo del sistema semi-continuo utilizado..... 81

Esquema 3.2. Reactor tubular de lecho fijo. 83

Chapter 4.

Scheme 4.1. Main products of hydration reaction of furfuryl alcohol with acid catalysts 91

Scheme 4.2. Representation of two liquid phases in batch reactor 101

Chapter 5.

Scheme 5.1. Construction of three-dimensional structure of ZSM-5 zeolite 120

Scheme 5.2. Construction of three-dimensional structure of Y zeolite 121

Scheme 5.3. Construction of three-dimensional structure of Beta zeolite, (structure BEA). 122

Scheme 5.4. Structure type Keggin of heteropoliacids 122

Scheme 5.5. Surface structure of sulfated zirconium oxide 123

Chapter 6.

Scheme 6.1. Surface structure proposed for sulfated zirconia 158

Scheme 6.2. Main products obtained from FA, with ZrO_2/SO_4^{2-} and La_xZrO_2/SO_4^{2-} catalysts. 165

Chapter 7.

Scheme 7.1. Mechanism of reaction in two stages for the conversion of furfuryl alcohol to cyclopentanone 172

Scheme 7.2. Proposed routes of obtaining CPN from furfuryl alcohol. a) reaction route for catalysts with platinum content, b) reaction route for catalysts with metallic oxide content. 199

Index of Tables

Capítulo 1

Tabla 1.1. Contenido (% en peso) de celulosa, hemicelulosa y lignina en algunos residuos agrícolas y forestales 16

Tabla 1.2. Lista de los 12 compuestos principales "building blocks" 20

Tabla 1.3. Derivados de los 12 compuestos base 21

Tabla 1.4. Propiedades fisicoquímicas del ácido levulínico 23

Tabla 1.5. Rendimientos de ácido levulínico obtenido a partir de diferentes materias primas y con diferentes catalizadores 29

Tabla 1.6. Lista general de catalizadores sólidos ácidos 36

Capítulo 3

Tabla 3.1. Compuestos químicos utilizados en las reacciones 62

Tabla 3.2. Compuestos químicos utilizados en la preparación de los catalizadores 62

Tabla 3.3. Compuestos químicos utilizados en las técnicas de caracterización y en la medición de la actividad catalítica 63

Tabla 3.4. Cantidades usadas en la preparación de los catalizadores de Nb_x/TiO_2 64

Tabla 3.5. Cantidades usadas en la preparación de los catalizadores Nb_x/USY por el método de impregnación húmeda (WI) 65

Tabla 3.6. Cantidades usadas en la preparación de los catalizadores Nb_x/USY por el método de precipitación 66

Tabla 3.7. Cantidades usadas en la preparación de los catalizadores $Pt*WO_x/Al_2O_3$ por el método de impregnación húmeda 68

Tabla 3.8. Especificaciones y condiciones de operación del reactor autoclave de acero inoxidable 80

Chapter 4

Table 4.1. List of several commercial Amberlyst with its main properties 94

Table 4.2. Physical and chemical specifications of Amberlyst 35 Wet and Amberlyst 47 95

Table 4.3. Product distribution predicted for H_2O-FA-CPME system. 103

Table 4.4. Catalytic activity results with different systems of reaction at 393 K , 3h of reaction 111

Table 4.5. Analysis of sulfur percentage in fresh and used catalyst, using an Amberlyst 35 Wet 112

Chapter 5

Table 5.1. Properties of different solid acid catalysts studied and activity results obtained. 126

Table 5.2. Summary the optimal conditions obtained using H-Z(50) catalysts 134

Table 5.3. Summary of textural properties and elemental composition of the zeolites studied 138

Table 5.4. Results of acidity by TPD-NH_3 142

Table 5.5. Result of acidity by FTIR spectra of adsorbed pyridine 146

Chapter 6

Table 6.1. Elemental quantification of catalysts by EDX and XPS analysis 162

Table 6.2. Total acidity determined by TPD-NH_3 163

Table 6.3. Summary of FA conversions and yields to LA on reaction time 165

Chapter 7

Table 7.1. Textural properties and chemical composition of Nb_xUSY and Nb_xTiO_2 catalysts ..... .177

Table 7.2. Binding energy (eV) and surface content of niobium (Nb) by XPS analysis 181

Table 7.3. Brönsted and Lewis peak areas ratio 182

Table 7.4. Total acidity determined by ammonia chemisorption at 373 K..... 185

Table 7.5. Textural properties and chemical composition of platinum and wolframium catalysts..... 186

Table 7.6. Metal particle sizes from XRD measurements 188

Capítulo 1. Introducción

Tabla de Contenido

1.1. La biomasa como una alternativa a los recursos de origen fósil 11

1.1.1. Recursos de origen renovable: la biomasa. 11

1.1.2. El aprovechamiento de la biomasa: justificación 17

1.1.3. El concepto de biorrefineria 18

1.1.4. Compuestos base o "building blocks" 20

1.2. Ácido levulinico 22

1.2.1. Importancia, propiedades físicas y aplicaciones 22

1.2.1.1. Reacciones del grupo carboxilo 24

1.2.1.2. Reacciones del grupo carbonilo 25

1.2.1.3. Reacciones del grupo metilo 25

1.2.1.4. Reacciones de oxidación y reducción 26

1.2.2. Obtención de ácido levulínico a partir de biomasa (lignocelulosa) 26

1.2.3. Obtención de ácido levulínico a partir de alcohol furfurílico 30

1.2.4. Otros procesos de obtención de ácido levulínico 33

1.3. Catálisis heterogénea aplicada a la obtención de ácido levulínico a partir de alcohol furfurílico. 34

1.3.1. Catalizadores sólidos ácidos. 35

1.3.1.1. Óxidos metálicos 37

1.3.1.2. Catalizadores sólidos ácidos tipo aluminosilicatos. 39

1.3.1.3. Resinas de intercambio iónico ácidas. 41

1.3.1.4. Sólidos superácidos 44

1.4. Referencias 45

1.1. La biomasa como una alternativa a los recursos de origen fósil

1.1.1. Recursos de origen renovable: la biomasa.

El consumo de petróleo a nivel mundial ha ido en aumento desde 1960, año en que se constituye la Organización de Países Exportadores de Petróleo (OPEP), organización que ha permitido coordinar y unificar las políticas petroleras en todo el mundo. Este recurso natural no renovable ha generado una verdadera transformación en todos los ámbitos de la humanidad: los sectores transporte, energético e industrial, proporcionando a la sociedad un estado de bienestar social y económico. Con el aumento de la población mundial, el incremento en el consumo de los productos derivados del petróleo ha generado una gran dependencia de este mercado. La mayor parte de dichas reservas están situadas en regiones geopolíticamente inestables, lo que ocasiona una alta volatilidad en los precios produciendo desestabilización e incertidumbre en la economía mundial. Además, gran parte de las reservas probadas de petróleo garantizan un abastecimiento hasta mediados del presente siglo según el informe de la "BP Statistical Review of World Energy" del 2014 [1]; en este informe se estima que el planeta contaba con reservas probadas de petróleo de casi 1,687 billones de barriles a finales de 2012, garantizando durante 53 años más el suministro si se mantiene el consumo a los ritmos actuales.

Por otra parte, el uso de combustibles fósiles (petróleo, carbón, gas natural y sus derivados), especialmente en el sector transporte y energético, es la principal fuente de emisiones de gases de efecto invernadero (CO_2, NO_x, SO_x, HC's,..), responsables del cambio climático. Estos hechos han conducido a que en los últimos veinticinco años, países altamente dependientes de los recursos petrolíferos se hayan volcado en desarrollar políticas energéticas basadas en recursos naturales renovables (hidráulica, eólica, solar-fotovoltaica, biomasa), que minimicen la dependencia energética de países exportadores de petróleo y las emisiones de gases contaminantes. La producción mundial por tipo de energía en los años 1973 y 2011 se muestra en el Esquema 1.1 [1]. En el se observa que se ha reducido de manera significativa la contribución de la producción de petróleo, pasando de 46 % en 1973 al 31,3 % en 2011, no así la de gas

natural y combustibles sólidos que han experimentado un aumento. Asimismo, la demanda mundial de energía primaria se ha incrementado considerablemente, y según datos reportados en la *BP Statical Review of World Energy* [1], se prevé que para el año 2035 será de 16961 millones de toneladas equivalentes de petróleo (ver Esquema 1.2).

En resumen, todo lo comentado anteriormente indica claramente la necesidad mundial de promover la incorporación de nuevas tecnologías limpias para cubrir en las próximas décadas no solo las necesidades energéticas sino también las industriales dependientes de los recursos fósiles.

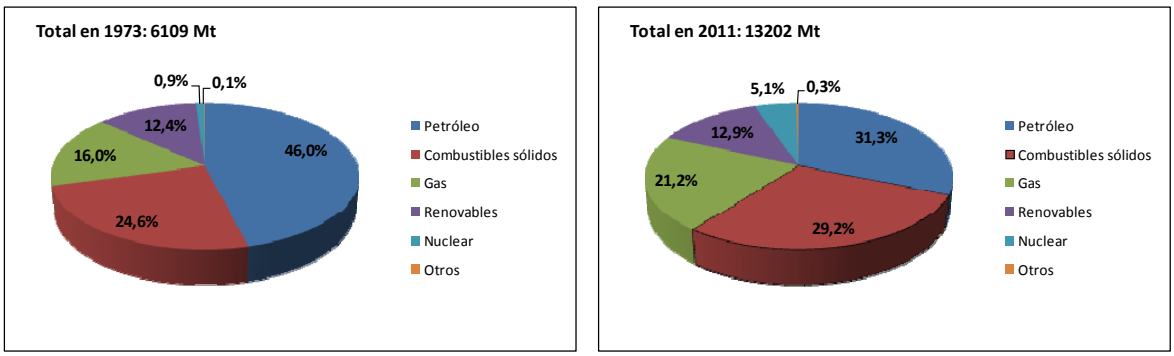

Esquema 1.1. Producción mundial por tipo de energía para los años comprendidos entre 1973 y 2011.[2]. Mt: millones de toneladas.

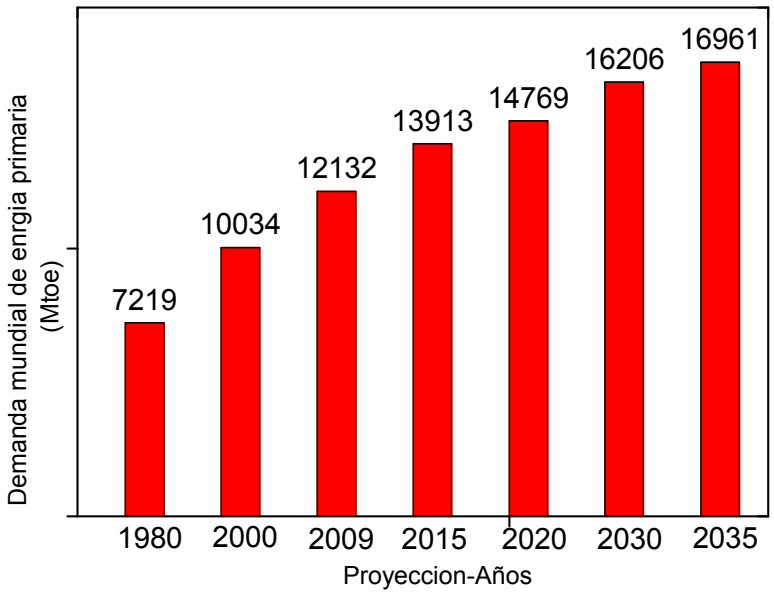

Esquema 1.2. Demanda mundial de energía primaria entre el año 1980 y 2009 y su proyección hasta 2035.; Mtoe: Millones de toneladas de petróleo equivalentes [1].

Muchos de los principales productos derivados del petróleo (crudo) como son las gasolinas, gas licuado, aceites lubricantes, parafinas o ceras, plásticos, pinturas, barnices, disolventes, fertilizantes e insecticidas, cauchos artificiales, negro de humo, poliéster y muchos más, pueden ser obtenidos y/o sustituidos, al menos parcialmente, por otros compuestos químicos que cumplen la misma función y que provienen de la ***biomasa*** [3, 4]**.**

La **biomasa** es la materia orgánica originada en un proceso biológico, excluyendo aquella que ha sufrido cambios profundos en su composición, tales como los que han tenido lugar durante los procesos de mineralización ocurridos en la formación del carbón, petróleo o gas. La biomasa es utilizable como fuente de energía renovable y se produce a partir de la energía contenida en la radiación solar, fijada por los vegetales en el proceso de fotosíntesis. De acuerdo a su origen la biomasa se puede clasificar en:

- *Biomasa natural*: Materia orgánica producida en la naturaleza sin intervención humana.
- Biomasa residual: Subproducto generado en actividades agrícolas, ganaderas agroalimentarias, en la industria de la transformación de la madera, etc.
- *Cultivos energéticos*: Biomasa cultivada para la producción de biocombustibles.

Por tanto, la biomasa engloba la materia orgánica procedente de residuos forestales (árboles, ramas, cortezas, astillas, podas, etc.)[3], residuos agrícolas (residuos procedentes de los cultivos alimentarios, como podas de olivos, paja de cereales, bagazo del maíz, etc.), cultivos energéticos como soja y girasol, residuos urbanos (aceites de fritura, restos de comida, fangos de depuradora de aguas residuales), residuos de las industrias de pasta de papel y papeleras, etc.

Al contrario de lo que sucede con los productos derivados de las materias primas fósiles, la transformación de la biomasa posee un balance neutro de dióxido de carbono, ya que la cantidad que se libera a la atmósfera al final del ciclo de vida de los bioproductos es idéntica a la cantidad de CO_2 atmosférico que es capturado y fijado por los organismos unicelulares durante la formación de dicha biomasa.

Entre los productos derivados de biomasa que se utilizan como alternativa de los combustibles de origen fósil están los *bio-alcoholes* [5]. En principio, el bio-alcohol más extraido usado como sustituto de la gasolina, fue el etanol, pero su uso directo decayó progresivamente, y en la actualidad se propone como aditivo de la gasolina y no como sustitutivo directo de ésta. Por ejemplo, el carburante de los coches que circulan por Estados Unidos, la Unión Europea y Brasil, entre otros lugares, contiene etanol pero la cantidad de éste no supera generalmente el 10 % de la mezcla total [6].

Otro caso es el de los bioaceites o aceites vegetales, que mediante un proceso de esterificación usando un alcohol (habitualmente metanol) son transformados en *biodiesel*, que a su vez es empleado con eficiencia en motores de combustión de inyección indirecta, ya que son más viscosos que el gasóleo tradicional. En el mencionado proceso, las moléculas de los enlaces éster de los triglicéridos se hidrolizan y se transforman en glicerina y cadenas de los ácidos grasos que posteriormente reaccionan con metanol, formando ésteres lineales denominados *biodiesel* [7]. La glicerina obtenida, una vez refinada se puede utilizar en las industrias química, cosmética y farmacéutica [3-5].

Dado que la biomasa se compone mayoritariamente de carbohidratos (celulosa, hemicelulosa, almidón, sacarosa,) y lignina (polímero formado por cadenas de compuestos aromáticos), la extracción de azúcares (glucosa, xilosa, maltosa, etc) de los carbohidratos abre un amplio abanico de posibilidades en la síntesis de compuestos químicos de alto valor añadido para el sector industrial químico, como por ejemplo 5-hidroximetil-furfural, furfural, anhídrido máleico, alcohol furfurílico, 2-metil-tetrahidrofurano, metilfurano, ácido levulínico, angelicalactona, γ-valerolactona, ácido acrílico, 1,4 pentanodiol, y múltiples derivados de ellos, cuyos procesos en muchos casos aún son objeto de estudio.

Las tecnologías aplicadas a la transformación de azúcares en productos químicos se agrupan en una plataforma denominada "*Plataforma de Azúcares*". En el Esquema 1.3 se puede apreciar la gran variedad de compuestos químicos derivados de la plataforma de azúcares, algunos de ellos con aplicaciones en el campo de los biocombustibles, otros con aplicaciones en la industria química, farmacéutica y de alimentos [4, 8-13].

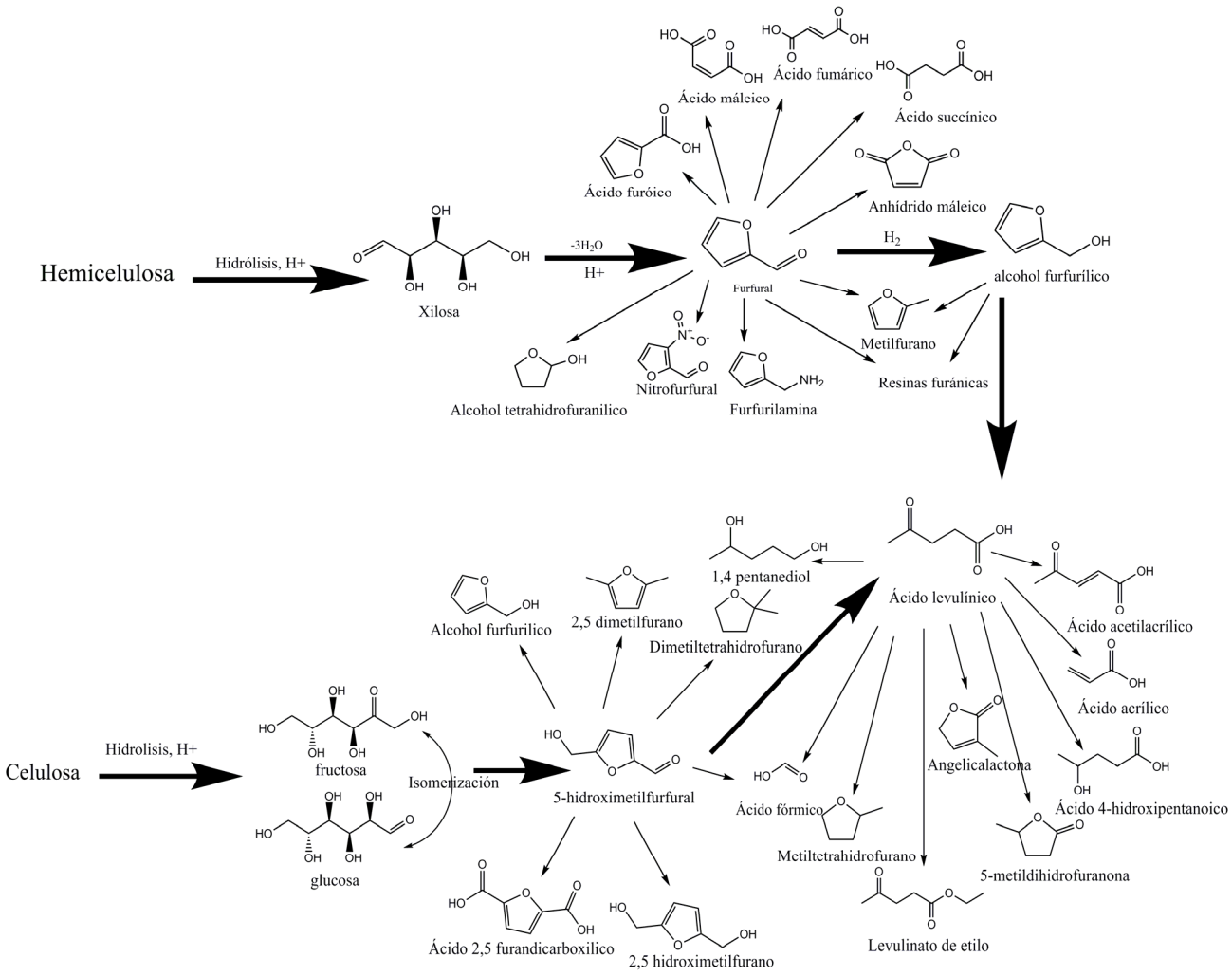

Esquema 1.3. Derivados potenciales de la plataforma de azúcares.

La hemicelulosa es un polisacárido que está compuesto generalmente de cinco diferentes monómeros de azúcar, de 5 y 6 átomos de carbono: D-xilosa, L-arabinosa, D-galactosa, D-glucosa y D-manosa, siendo la xilosa la más abundante. La extracción de hemicelulosa de la biomasa puede realizarse por medios físicos o por combinación de métodos físicos y químicos. En general, los métodos físicos, tales como tratamiento con vapor o tratamiento con agua caliente, producen polímeros de xilanos que pueden ser subsecuentemente hidrolizados, bajo leves condiciones de acidez (a través de hidrólisis con ácido sulfúrico diluido), para producir monómeros de xilosa con buenos rendimientos [14]. La D-xilosa obtenida puede ser utilizada para la obtención de furfural mediante un proceso de reacción de deshidratación usando catalizadores ácidos en medio acuoso [15-20]. El furfural obtenido es un importante compuesto químico a

nivel industrial, precursor de múltiples compuestos químicos, algunos de los cuales se representan en el Esquema 1.3.

La celulosa es un polímero formado por unidades de glucosa, con una estructura de cristalinidad rígida típicamente aislada dentro de la matriz lignina-hemicelulosa. El pre-tratamiento usado para separar la celulosa de la biomasa suele ser mediante combinación de procesos mecánicos de molienda y procesos fisicoquímicos, mediante la extracción de la lignina presente usando NaOH diluido en agua (5 % en peso), seguido de un tratamiento de lavado con agua a temperatura de 373 K. Este proceso sirve para separar la lignina y extraer la hemicelulosa, obteniendo así la "pulpa celulósica" pura. Como se muestra en el Esquema 1.3, la celulosa en medio acuoso puede ser hidrolizada a glucosa y fructosa mediante el uso de catalizadores ácidos, habitualmente a una temperatura de 423 K [21-25]. De acuerdo a las condiciones de operación de la hidrólisis de la celulosa, los productos obtenidos pueden ser mayoritariamente: glucosa, 5- hidroximetilfurfural (5-HMF), ácido fórmico y ácido levulínico (LA).

En la Tabla 1.1, se puede observar la composición de celulosa, hemicelulosa y lignina de algunos residuos agrícolas [26]. Los porcentajes de hemicelulosa y celulosa varían de acuerdo al tipo de biomasa. Los mayores contenidos de celulosa se encuentran en la madera, alcanzando hasta el 50 % en peso; en el caso de la hemicelulosa, los máximos valores están alrededor del 30 % en peso para determinados materiales.

Tabla 1.1. Contenido (% en peso) de celulosa, hemicelulosa y lignina en algunos residuos agrícolas y forestales [26].

Material	Celulosa (%)	Hemicelulosa (%)	Lignina (%)
Madera de Álamo	48,9	17,3	27,7
Paja de trigo	35,8	26,8	16,7
Sorgo	44,6	25,3	18,0
Hojas de maíz	36,4	22,6	16,6
Mazorcas de maíz	38,5	32,8	18,7
Paja de arroz	35,6	11,9	15,3
Paja de frijol	30,6	23,1	9,3

En todos los casos el porcentaje de celulosa es superior al 30 %, lo que hace viable económicamente el proceso de separación y su posible uso como precursor de productos de alto valor añadido.

1.1.2. El aprovechamiento de la biomasa: justificación

Desde el punto de vista energético y ambiental, así como para el desarrollo socioeconómico de las zonas rurales, la biomasa puede constituir un recurso básico para la sociedad a mediano plazo. Actualmente, como se muestra en el Esquema 1.1 aproximadamente más del 80 % del abastecimiento energético en el mundo proviene de las energías fósiles, un 2 % de la energía nuclear, y alrededor del 10 % de las *energías renovables* (hidráulica, eólica, solar-fotovoltáica, biomasa). Ese alto valor porcentual de fuente de energía no renovable conlleva a importantes implicaciones medioambientales y causa preocupación en todos los ámbitos de la economía global. Las instalaciones de producción energética y de obtención de compuestos químicos derivados de la biomasa pueden abastecerse de una amplia gama de tipos de biomasa, preferentemente de biomasa residual como la forestal y agrícola (como podas de árboles, astillas, cardos, paja, huesos de frutos, así como cáscaras de almendras, de arroz, trigo), o la proveniente de residuos industriales y urbanos (Esquema 1.4).

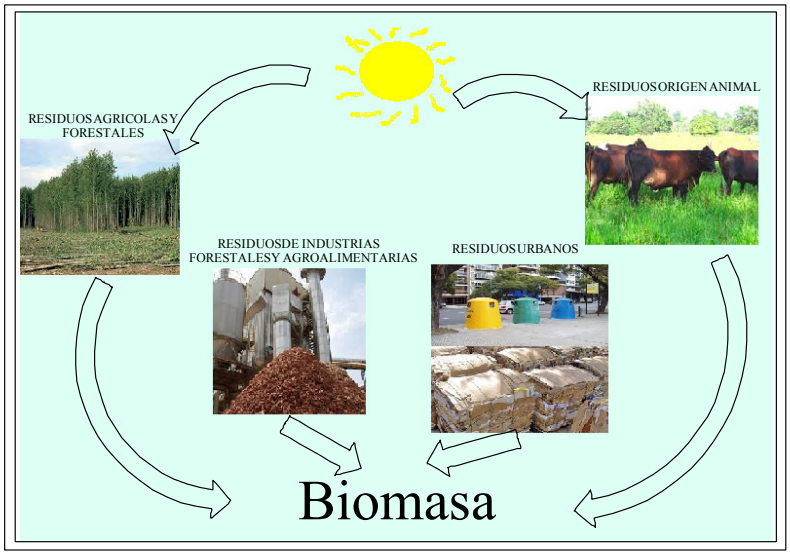

Esquema 1.4. Fuente, origen y aprovechamiento de la biomasa.

El uso de la biomasa como recurso energético tiene distintas ventajas de tipo medioambiental, social y económico, entre las que figuran:

- Disminución de las emisiones de azufre y de partículas sólidas.
- Reducción en la emisión de gases contaminantes como CO y NO_X.
- Ciclo neutro de CO_2, sin contribución al efecto invernadero.
- Reducción de riesgos de incendios forestales y de plagas de insectos al potenciar la limpieza y poda de bosques.
- Aprovechamiento de residuos agrícolas, evitando su quema en el terreno.
- Disminución de la dependencia de la importación de combustibles fósiles y de las repercusiones económicas de fluctuaciones de sus precios (no son combustibles importados).
- Mejora socioeconómica de las áreas rurales.

La industria basada en la biomasa puede ser sostenible si se implementa de manera integrada, es decir relacionando la abundancia del recurso renovable disponible con la preservación del medio ambiente. Sin embargo, estos productos son en su mayoría poli-funcionales y transformarlos requiere un control estricto de la química y de la selectividad de los procesos. La mayor parte de los procesos de transformación son procesos catalíticos. La catálisis puede jugar un rol crítico para incrementar la selectividad a un determinado producto, y por tanto, hacer viable económicamente el proceso de transformación de la biomasa.

1.1.3. El concepto de biorrefineria

La producción de bio-productos es un mercado en crecimiento con implicaciones en el sector industrial, sea químico, alimentario o de transporte, pero aún es preciso un mayor desarrollo experimental y tecnológico que permita obtener los productos con mayor selectividad y de manera más eficiente y continua.

El ***concepto de biorrefinería*** engloba la integración de procesos y tecnologías para un uso eficaz de las materias primas, con instalaciones que operen de una manera sostenible y en equilibrio con el medio ambiente. Es decir, una biorrefinería es la combinación óptima de procesos biológicos, termoquímicos y químicos para la obtención de una variada gama de productos, que posibilita el empleo de numerosas

materias primas gracias a las sinergías establecidas entre las diferentes tecnologías [6, 8-14, 27-34].

El término de biorrefinería es análogo al de las refinerías de petróleo, sin embargo, la heterogeneidad de la biomasa y sus numerosas posibilidades de conversión, multiplican los posibles esquemas de operación que pueden desarrollarse en una biorrefinería. Por lo tanto, no existe un único esquema de proceso de biorrefinería, sino que cada una de ellas se debe diseñar acorde a las necesidades de orden tecnológico, marcadas por el tipo de biomasa usada como materia prima [5, 6, 8-14, 27-35]. Además para ser competitivas, las biorrefinerías deben operar de la misma forma que las refinerías de petróleo, tanto en lo que se refiere a la escala de producción como en relación a la cartera de productos; y para ser económicamente viables, es necesario que sean versátiles con la producción direccionada a suplir las tendencias mundiales de mercado [6].

Actualmente, dentro de la plataforma de azúcar, la del procesamiento de la caña de azúcar es la que más se adapta al proceso de una biorrefinería. Sin embargo, existe la tendencia en otros segmentos, tales como las industrias de aceites vegetales, y las empresas de papel y celulosa, entre otras, que también se adecuan a este concepto [27].

Con base en los diferentes procesos bioquímicos y químicos disponibles para la conversión de la biomasa, y dependiendo de la materia prima y/o de los productos que se pretende obtener en esas instalaciones, diversas configuraciones de biorrefinerías pueden ser adoptadas. Los procesos bioquímicos involucran los procesos enzimáticos, los procesos fermentativos y la producción de algas [5], mientras que los procesos químicos engloban los procesos termoquímicos, la transesterificación química, el hidroprocesamiento, el craqueo catalítico y la síntesis de Fischer-Tropsch (FT) [3, 9, 12, 13, 28]. Los procesos químicos desarrollados principalmente por la industria de petróleo, están siendo adaptados para uso de la biomasa y sus derivados como materia prima.

1.1.4. Compuestos base o "building blocks".

Como se ha mostrado en el Esquema 1.3, una considerable cantidad de compuestos químicos se obtienen a partir de la celulosa y hemicelulosa extraída de la biomasa. Así, se entiende por compuestos ***base o "building blocks"*** aquellos compuestos químicos que son punto de partida para la obtención de una gran variedad de productos, y que por lo tanto, son indispensables para el desarrollo de la industria química sostenible. La Tabla 1.2, muestra una lista de estos compuestos derivados de la plataforma de azúcares de acuerdo a un informe elaborado por el Departamento de Energía de los Estados Unidos, sub-división de Energía Eficiente y Energías Renovables [13]. El informe identifica y selecciona 12 compuestos que pueden ser obtenidos a partir de azúcares por vía biológica o química. Estos compuestos poseen moléculas con múltiples grupos funcionales que tienen el potencial de transformarse en nuevas familias de moléculas útiles de alto valor para el sector industrial (químico, alimentario, cosméticos, farmacéutico, industrias de lubricantes, etc).

Tabla 1.2. Lista de los 12 compuestos principales "building blocks" [13].

Compuestos base	
✓ Ácido 1,4 succínico, fumárico y maléico	✓ Ácido itacónico
✓ Ácido 2,5 furandicarboxílico	✓ Ácido levulínico
✓ Ácido 3-hidroxipropanóico	✓ 3-hidroxibutirolactona
✓ Ácido aspártico	✓ Glicerol
✓ Ácido glucárico	✓ Xilitol / arabinitol
✓ Ácido glutámico	✓ Sorbitol

La selección final de los 12 compuestos base mostrados en la Tabla 1.2 comenzó con una lista de más de 300 moléculas. Una lista más corta de 30 posibles compuestos se seleccionó mediante un proceso de revisión iterativa basada en el modelo de compuestos base petroquímico, los datos químicos, los datos conocidos del mercado, las propiedades y el potencial de aplicaciones de las moléculas. Esta lista de 30

compuestos, se redujo finalmente a 12 mediante el examen de los mercados potenciales de los "building blocks" y sus derivados y la complejidad técnica de las vías de síntesis. Un grupo de moléculas de segundo nivel también fue identificado. Estas incluyen ácido glucónico, ácido láctico, ácido malónico, ácido propiónico, ácido cítrico, ácido aconítico y ácido xilónico, también la acetoína, furfural, levoglucosano, lisina, serina y treonina. En la Tabla 1.3, se representan los principales compuestos con gran potencial derivados de los 12 primeros compuestos base.

Tabla 1.3. Derivados de los 12 compuestos base [13].

Compuesto base	Compuesto derivado
➢ Ácido 2,5 furandicarboxílico	✓ Ácido succínico ✓ Furan-2,5-dicarbaldehído ✓ Dihidroxi-2,5-metilfurano ✓ Dihidroxi-2,5-metiltetrahidrofurano ✓ Aminometil-2,5 bis-tetrahidrofurano
➢ Ácido succínico	✓ γ-butirolactona ✓ 1,4-butanediol ✓ Tetrahidrofurano ✓ 2-pirrolidona ✓ Succinonitrilo ✓ 1,4 diaminobutano ✓ Succindiamida
➢ Ácido-3-hidroxipropiónico	✓ Ácido acrílico ✓ Metilacrilato ✓ Acrilamida ✓ Acrilonitrilo ✓ Propiolactona ✓ Ácido malónico ✓ 1,3-Propanediol
➢ Ácido aspártico	✓ 2-Amino-1,4-butanediol ✓ Amino-2-pirrolidona ✓ Anhídrido aspartico ✓ Amino-γ-butirolactona ✓ 3-Aminotetrahidrofurano
➢ Ácido glucárico	✓ α-Cetoglucarato ✓ Polihidroxipoliamidas ✓ Glucarodilactona ✓ Glucaro-δ-lactona ✓ Glucaro-γ-lactona
➢ Ácido glutámico	✓ Ácido glutárico ✓ 1,5-Pentanodiol ✓ 5-Amino-1-butanol ✓ Ácido piroglutamico ✓ Prolinol ✓ Prolina ✓ Piroglutaminol ✓ Norvolina ✓ Glutaminol

Tabla 1.3. Continuacion

➢ Ácido itaconico	✓ 2-Metill-1,4-butanodiamina ✓ Diamidaitaconico ✓ 3-Metilpirrolidina ✓ 3-Metil-tetrahidrofurano ✓ 4-Metil- γ- valerolactona
➢ Ácido levulínico	✓ 2-Metil-tetrahidrofurano ✓ Ácido acrílico ✓ d-Aminolevulínato ✓ Ácido difenolico ✓ Ácido β-Acetilacrilico ✓ Esteres de levulinato ✓ 1,4-Pentanediol ✓ Angelicalactona ✓ γ-valerolactona
➢ 3-Hidróxibutirolactona	✓ 3-Hidroxibutirolactona ✓ γ-Butenilactona ✓ Epoxilactona ✓ Acrilatolactona ✓ 2-Amino-3-hidroxitetrahidrofurano ✓ 3-Aminotetrahidrofurano ✓ 3-Hidroxitetrahidrofurano
➢ Glicerol	✓ Glicidol ✓ 1,3-Propanediol ✓ Propilenglicol ✓ Poliésteres y nylons ✓ Mono-, di-, o triglicerato ✓ Digliceraldehído ✓ Glicerol carbonato ✓ Ácido glicérico
➢ Sorbitol	✓ Propilenglicol ✓ Etilenglicol ✓ Glicerol ✓ Ácido láctico

1.2. Ácido levulinico

1.2.1. Importancia, propiedades físicas y aplicaciones

Como se ha descrito en el apartado anterior, el ácido levulinico (LA), es un importante compuesto derivado de subproductos de la biomasa, por lo que está incluido dentro de los primeros 12 productos compuestos base o "building blocks" [13]. Posee características importantes que lo definen como un compuesto precursor de múltiples productos con aplicaciones en varios campos de la industria. El LA es un ácido orgánico débil que contiene tres grupos funcionales en su estructura molecular (ver Esquema

1.5), dos de ellos altamente reactivos: el grupo carboxilo (–COOH) y el grupo carbonilo (=C=O), lo que permite la posibilidad de una variedad de transformaciones sintéticas mediante reacciones de esterificación, condensación, hidrogenación, oxidación y halogenación [36-39].

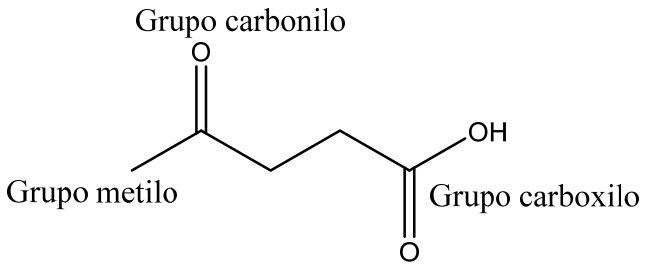

Esquema 1.5. Representación de los grupos funcionales del LA.

Las propiedades fisicoquímicas del LA se presentan en la Tabla 1.4, la baja temperatura de fusión en condiciones estándar indican que el ácido levulinico se encuentra en fase sólida, bajo la forma de cristales. Otra característica a resaltar es el alto valor de la temperatura de ebullición (518 K), lo que facilita la separación de los disolventes más volátiles mediante destilación. Además, el LA se disuelve con facilidad en agua, etanol y éter.

Tabla 1.4. Propiedades fisicoquímicas del ácido levulínico [40].

Propiedad	Valor
Fórmula Molecular	$C_5H_8O_3$
Peso molecular	116,1152
Densidad (g/mL)	1,134
Índice de refracción	1,4396
Temperatura de fusión (K)	306
Temperatura de ebullición (K)	518,7
Presión de vapor a 375 K (mm Hg)	1
$\Delta_{fus}H$ a 306 K (kJ/mol)	9,22
Δ_rH^0 (kJ/mol)	1425
Δ_rG^0 (kJ/mol)	1396

El LA ha sido producido desde 1870, pero nunca ha alcanzado un uso comercial en grandes volúmenes. Una razón para la baja comercialización puede ser debida a que la mayoría de las investigaciones sobre este compuesto se hicieron en los primeros cuarenta años del siglo pasado, cuando las materias primas eran costosas, los rendimientos de producción bajos y una tecnología poca desarrollada para la separación y purificación, sumado a un desconocimiento de su potencial en cuanto aplicaciones industriales. En la actualidad, la sobreproducción de materias primas y el desarrollo en ciencia y tecnología ha abierto la puerta a reevaluar el potencial industrial del LA, que es precursor de una considerable serie de productos (Esquema 1.6) que poseen múltiples aplicaciones industriales (resinas, plastificantes, anticongelantes, recubrimientos, alimentos, farmacéutica…etc).

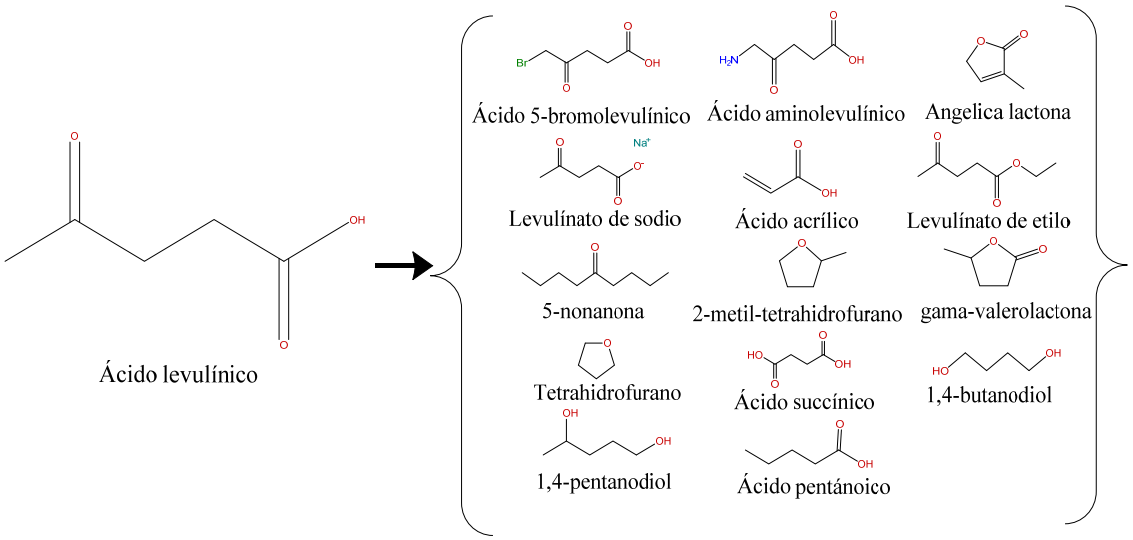

Esquema 1.6. Principales productos obtenidos a partir del LA.

1.2.1.1. Reacciones del grupo carboxilo

El grupo carboxilo del LA participa en una serie de reacciones de esterificación en los que varios ésteres de levulinato son producidos en presencia de catalizadores ácidos, especialmente el ácido sulfúrico. Recientemente se han publicado métodos novedosos para la obtención de ésteres de levulinato que implican la reacción del LA con alcoholes

orgánicos mediante extracción-reactiva, en la que la fase del alcohol orgánico actúa como agente esterificante y fase extrayente [38]. Un ejemplo es el *levulinato de etilo* producido por esterificación del LA con etanol [37]. Este levulinato es usado como aditivo oxigenado de combustibles diesel o como aromatizante en fragancias industriales. También otros ésteres de levulinato obtenidos a partir de alcoholes de más elevado punto de ebullición son usados como plastificantes especiales para los plásticos de celulosa.

1.2.1.2. Reacciones del grupo carbonilo

Las reacciones que involucran el grupo carbonilo del LA proporcionan una amplia gama de compuestos interesantes. Esto ocurre por adición nucleofílica al grupo funcional. Entre las más importantes están las del LA con varias aminas para formar amidas. Las amidas formadas son de interés debido a su actividad biológica y a que pueden ser usadas en la industria farmacéutica como antibióticos [38]. El LA reacciona con amoníaco o hidróxido de amonio en presencia de un catalizador metálico y de gas hidrógeno para formar *5-metil-2-pirrolidona* que es un compuesto intermedio útil en la industria farmacéutica [38]. También mediante la reacción del LA con fenol en medio ácido se obtiene el *ácido difenólico*, que tiene varios usos en la producción de polímeros, lubricantes, materiales retardantes de fuego y en pinturas [39]. Estudios recientes han estimado que el ácido difenólico podría abarcar un mercado de unas $4{,}5x10^4$ toneladas/año en sustitución del bisfenol A, y también unas $2{,}3x10^3$ toneladas/año como material de recubrimiento [39].

1.2.1.3. Reacciones del grupo metilo

Finalmente están las reacciones que involucran el grupo metilo del LA. Éste es fácilmente halogenado usando bromuro o cloruro para producir halogenuros orgánicos. Por ejemplo, el *ácido 5-bromolevulínico* obtenido por la bromación del LA en metanol y que es un precursor del *ácido δ-aminolevulínico*, ingrediente de un herbicida biodegradable utilizado también en la industria farmacéutica como componente activo en el tratamiento de cáncer [38].

1.2.1.4. Reacciones de oxidación y reducción

El LA puede ser oxidado a varios derivados interesantes. La selectividad es alta dependiendo del tipo de oxidante. Así, a altas temperaturas de oxidación (602-663 K) en presencia de oxígeno y de un catalizador como V_2O_5 se produce el *ácido succínico* [38]. El ácido succínico (ácido 1,4-butanedioico) es otro compuesto de gran valor con una demanda de $2{,}7x10^5$ toneladas/año y con diferentes aplicaciones para la síntesis de una gama amplia de productos de mucho interés, entre los que están la *butirolactona (GBL)*, el *1,4-butanediol (BDO)* y el *tetrahidrofurano (THF)***,** importante disolvente con innumerables aplicaciones. Por otra parte, el LA puede ser reducido a *γ-valerolactona (GVL)* mediante hidrogenación catalítica con catalizadores de platino [41, 42]. La GVL se usa como un disolvente para lacas, insecticidas, aditivos y como precursor de un importante compuesto, el *metil-tetrahidrofurano (MTHF)*, que tiene un alto potencial como aditivo oxigenado en gasolinas con un mercado de $2{,}6x10^5$ m^3 por año [38].

1.2.2. Obtención de ácido levulínico a partir de biomasa (lignocelulosa)

El proceso de obtención de LA a partir de biomasa [30-33, 35, 43-64], involucra la hidrólisis de celulosa y/o de hemicelulosa previamente separada de la biomasa usando catalizadores ácidos (Esquema 1.7). La hidrólisis de celulosa para formar hexosas se realiza en medio ácido acuoso generando isómeros de glucosa y fructosa, estos son deshidratados en medio ácido para formar el 5-hidroximetilfurfural (HMF) como compuesto central [43, 65]. A continuación, la conversión de HMF en LA es el resultado de la adición de dos moléculas de agua al enlace C_2-C_3 del anillo furánico. En la reacción también se produce ácido fórmico [14, 30, 46].

Por otro lado, la hidrólisis ácida de la hemicelulosa produce mayoritariamente xilosa [64], la cual mediante una reacción de deshidratación produce furfural [33, 44, 46, 50], este reacciona a alcohol furfurílico y finalmente, el alcohol es hidratado para producir el LA.

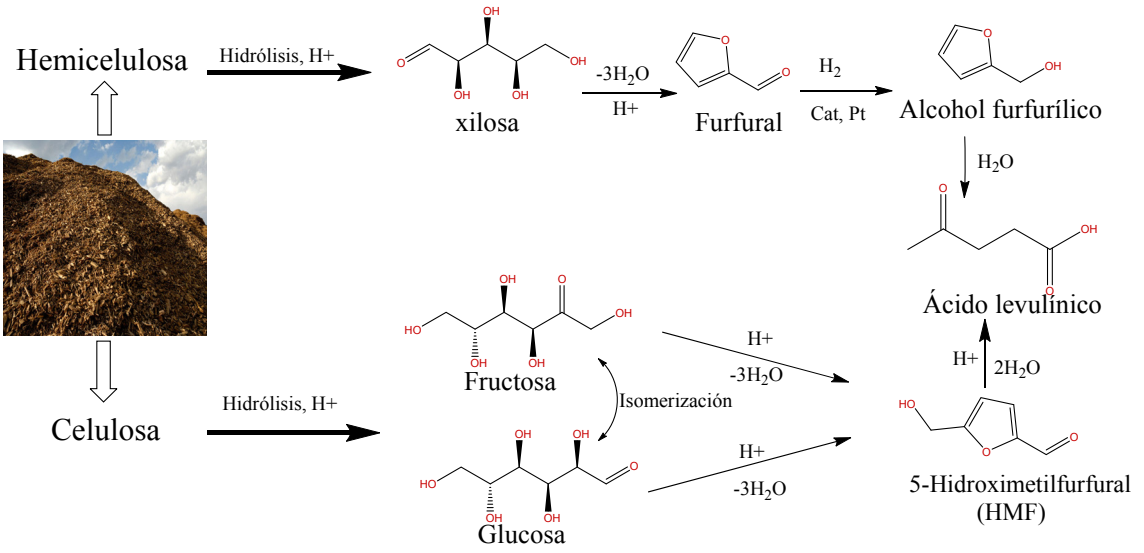

Esquema 1.7. Diagrama representativo de obtención de LA a partir de hemicelulosa y celulosa [8, 30, 60, 66].

El proceso más conocido y desarrollado para la obtención de LA es el proceso "Biofine" [60]. Este proceso proporciona una interesante vía para convertir biomasa lignocelulósica en plataformas químicas de alto valor, específicamente LA a partir de fracciones de C_6 y furfural de C_5. El proceso "Biofine", que se describe en el Esquema 1.8, consiste en hacer reaccionar la biomasa con ácido sulfúrico diluido (entre el 1,5 y 3 % en peso), en un reactor de flujo pistón, donde ocurre la hidrólisis de los carbohidratos a 5-HMF, operando a 483-493 K, 25 bar y a cortos tiempos de residencia (12 segundos), para minimizar la formación de productos de degradación. A continuación, en un segundo reactor, los compuestos intermedios son convertidos a LA y ácido fórmico a 463-473 K y 14 bar, con un tiempo de residencia de 20 min. El rendimiento a LA del proceso "Biofine" es de alrededor de 70-80 % del máximo teórico, y corresponde al 50 % de carbohidratos (C6) [60, 67]. La restante materia carbonosa es recogida como ácido fórmico (20 %) y residuos sólidos insolubles llamados "húminas" (30 %), los cuales se producen por reacciones de degradación de los compuestos intermedios.

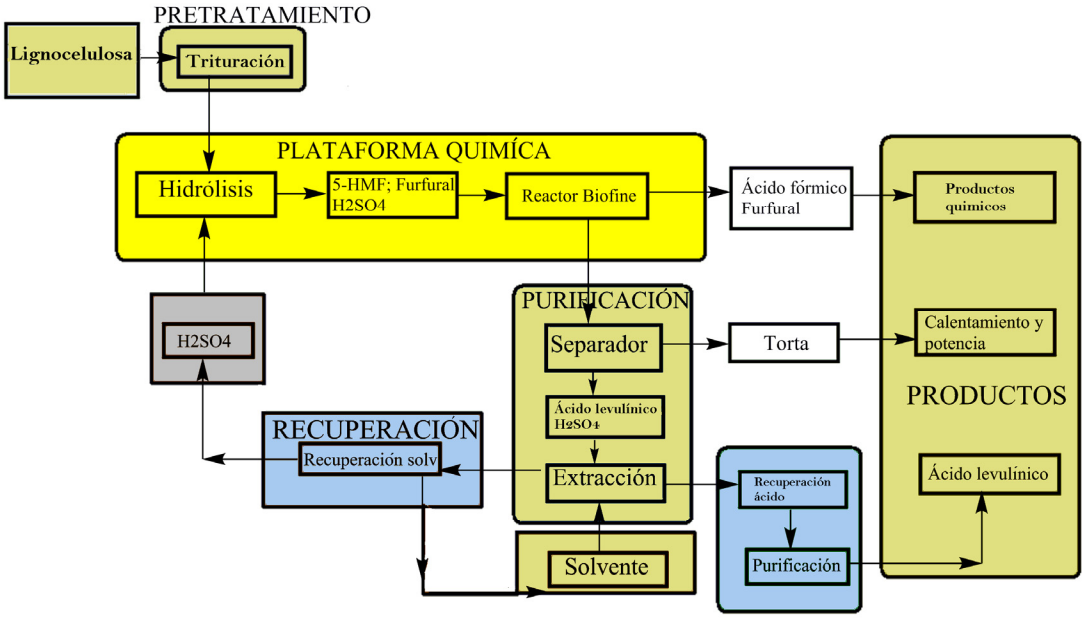

Esquema 1.8. Proceso "Biofine" de producción de LA [67].

Hasta hace relativamente poco tiempo los estudios sobre la producción de ácido levulinico a partir de biomasa se han desarrollado usando ácido sulfúrico como catalizador, debido a la alta disociación de iones H^+ en medio acuoso, lo que ha hecho insustituible el ácido mineral como catalizador en muchos procesos actuales. Sin embargo, la catálisis ácida homogénea presenta algunos aspectos negativos que instan a buscar su sustitución, principalmente debido a que los ácidos minerales no son reutilizables y causan problemas de corrosión en las instalaciones del proceso, por lo que requieren materiales especiales.

En la Tabla 1.5 se muestran algunos rendimientos a LA obtenido a partir de distintas materias primas y diferentes catalizadores. Zeng Shanshan et al (2012) [68], han estudiado la obtención de LA mediante hidrólisis de glucosa, usando catalizadores sólidos ácidos (heteropoliácidos modificados) tipo $M_XH_{3-2X}PW_{12}O_{40}$ donde M es Zn, Cu, Cs o Ag, de los cuales el $Ag_3W_{12}O_{40}$, ha mostrado el mejor rendimiento a LA (81,6 %). Por otra parte Chang et al (2006) [57], han obtenido rendimientos a LA de hasta un 80,7 % molar usando H_2SO_4 diluido al 5 % en peso a 443 K en un reactor discontinuo. Weingarten et al (2012) [69], han señalado que en la conversión de glucosa con H_2SO_4

diluido como catalizador, moderas temperaturas (413-433 K) de reacción y largos tiempos de residencia (100 min) fueron claves para obtener un buen rendimiento a LA (68% molar); en contraste, altas temperaturas (453-473 K) y cortos tiempos de reacción (≤ 1 min) favorecen la formación de 5-HMF. Sun Zhong et al. (2012) [70] han publicado rendimientos a LA de 63,1 % usando heteropoliácidos iónicos líquidos del tipo $[C_4H_6N_2(CH_2)_3\ SO_3H]_3$-nHn$PW_{12}O_{40}$, partiendo de celulosa, en un sistema bifásico agua-metil-isobutil cetona. Mientras que Girisuta et al. (2007) [71] estudiaron la conversión de celulosa a 423 K en presencia de H_2SO_4 1M a bajas concentraciones iniciales de celulosa, obteniendo un rendimiento a LA del 60 % e indicando que en las condiciones estudiadas la formación de residuos carbonosos insolubles ("huminas") disminuye.

Tabla 1.5. Rendimientos de ácido levulínico obtenido a partir de diferentes materias primas y con diferentes catalizadores.

Biomasa	Catalizador	Rendimiento a LA	Referencias
Glucosa	Heteropoliácido $Ag_3PW_{12}O_{40}$	81,6%	[68]
	H_2SO_4, 3% (V/V)	80,7% (molar, teórico)	[57]
	H_2SO_4,5% en peso	68% (molar, teórico)	[69]
	$CrCl_3$ y zeolita HY	55,2%	[51]
Celulosa	Líquido iónico HPA	63,1%	[70]
	H_2SO_4-(0,05-1M)	60%	[1]
	Ru/C +ácido fórmico	53%	[71]
	Zeolita LZY	43,2%	[62]
Sacarosa	$S_2O_8^{2-}/ZrO_2$-TiO_2-Al_2O_3	72,3%	[68]
	H_2SO_4, 3,5 mol/L	43,3%	[72]
	SO_4^{2-}/Fe_2O_3-Al_2O_3-Al_2O_3-SiO_2	33,1%	[73]

1.2.3. Obtención de ácido levulínico a partir de alcohol furfurílico

Los procesos de hidrólisis ácida de derivados primarios de biomasa expuestos en el apartado anterior se desarrollan en la mayoría de los casos en una sola etapa de reacción generando una serie amplia de subproductos con diferentes aplicaciones. Sin embargo, algunos de estos productos exigen mayor demanda que otros de acuerdo a las necesidades del mercado. Por lo tanto, es necesario implementar procesos de biorrefineria integrada que involucren múltiples etapas de reacción y separación, y así permitir la producción constante y efectiva de un determinado producto. De esta forma cada etapa de reacción se estudia bajo las condiciones óptimas que buscan incrementar al máximo el rendimiento del producto. Por ello, se considera necesario estudiar la viabilidad en la obtención de LA a partir de los compuestos más próximos en la cadena productiva de los derivados de la biomasa, en este caso el alcohol furfurílico (FA).

En presencia de agua y de un catalizador ácido, el FA reacciona para formar LA mediante la reacción de hidratación y apertura de su anillo furánico. El mecanismo de reacción produce una serie de productos intermedios, algunos de ellos inestables (ver Esquema 1.9).

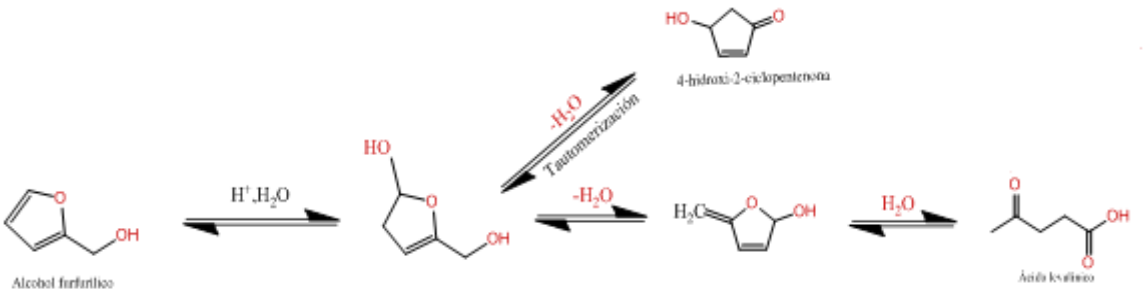

Esquema 1.9. Mecanismo de reacción de FA a LA adaptado de la referencia [72]

Los compuestos intermedios más estables son los hidroxifuranos que se forman en un paso previo a la apertura del anillo furánico durante la formación del LA. La apertura del anillo furánico requiere de catalizadores de una considerable fuerza ácida. Los

estudios desarrollados usando catalizadores minerales ácidos como ácido sulfúrico (H_2SO_4), ácido clorhídrico (HCl), ácido bromhídrico (HBr) y ácido yodhídrico (HI), hasta el día de hoy han mostrado los mejores resultados en rendimiento a LA. Masatomi et al.(1971) [63], estudiaron el proceso de obtención de LA a partir de FA disuelto en un disolvente orgánico, como metiletilcetona (MEK), dietílcetona, etilcetona y ciclohexanona, y haciéndolo reaccionar con una disolución acuosa de mismo disolvente orgánico. El proceso fue desarrollado en semicontinuo a 413 K y con ácido clorhídrico (HCl) como catalizador. El rendimiento máximo de LA obtenido fue de un 93 % molar, usando MEK como disolvente. Estos rendimientos de LA constituyen los mejores resultados reportados en la bibliografía consultada. Capai et al (1992) [61], incorporaron hasta un 40 % en peso de LA al medio de reacción y emplearon HCl como catalizador, obteniendo un rendimiento a LA del 83 % en peso. Bajo las mismas condiciones de reacción, pero usando ácido bromhídrico (HBr), el rendimiento de LA disminuyó a 73,1 % en peso y cuando se sustituyó el LA del medio de reacción por un disolvente orgánico como MEK o metil-isobutílcetona y HCl como catalizador, los rendimientos se redujeron a 76,1 % y 72,1 % respectivamente.

La sustitución de los ácidos minerales por catalizadores ácidos sólidos en la síntesis de reacción de LA a partir de FA ha sido estudiada también por otros autores, aunque la cantidad de publicaciones es mucho menor, y los resultados de rendimiento a LA son más bajos. Redmon et al (1956) [73], patentaron los resultados de la reacción de FA en medio acuoso usando una resina de intercambio iónico (Amberlite IR-120) como catalizador. Ellos alcanzaron un rendimiento máximo de 65 % en peso de LA, equivalente a un 55 % molar. Este es el máximo valor de rendimiento en catálisis heterogénea reflejado en la literatura científica consultada hasta el momento para la reacción señalada.

Van de Graaf et al (2007) [74], emplearon Amberlyst ^{TM} 35 y Dowex 50WX4, también en un medio de reacción acuoso, sin embargo no mostraron resultados de rendimiento a LA, centrando su estudio en la obtención de ésteres de levulinato, en los que habían incorporado previamente alcohol etílico a la reacción. En este caso obtuvieron un rendimiento del 91 % molar de levulinato de etilo. González-Maldonado et al (2012) [75], se centraron en el estudio de la reacción de FA en medio acuoso usando la resina de intercambio iónico Amberlyst ^{TM}15 como catalizador. En este estudio presentan un

análisis de los posibles productos intermedios de la reacción, sin embargo no muestran resultados de rendimiento de LA. Finalmente, están los estudios realizados por Milan Hronec et al. [76, 77], en los que el medio ácido de reacción se crea mediante la auto-disociación del agua (H^+, OH^-) a alta temperatura. Los resultados indican que se obtiene un rendimiento aceptable (50% mol) al compuesto 4-hidroxi-2-ciclopentenona (4-HCP), pero el rendimiento a LA es prácticamente nulo. En el Esquema 1.9, se incluye la formación del subproducto 4-HCP, el cual contribuye a la disminución del rendimiento a LA.

La hidrólisis ácida de FA produce también otro tipo de compuestos como las resinas furánicas. Esto obliga a realizar un estudio profundo sobre las condiciones óptimas de reacción y las propiedades que deben tener los catalizadores sólidos para incrementar el rendimiento a LA.

La reactividad del FA es muy alta en medio ácido. Su estructura molecular es susceptible de reacción en los enlaces C-O del anillo furánico al igual que del enlace C-O de su grupo hidroximetilo, cuyo enlace es más débil y es el principal punto de reacción del protón H^+ (ver Esquema 1.10). Tras la deshidratación del alcohol, el carbono que ha perdido el grupo OH queda con carga positiva ($^+CH_2$), y es precursor de las reacciones de resinificación, tras la unión con la 2ª posición del anillo furánico.

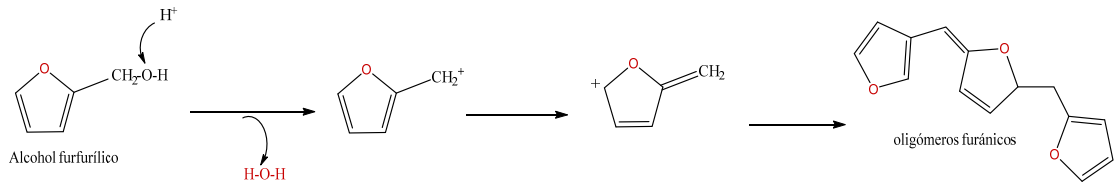

Esquema 1.10. Mecanismo de resinificación del FA en medio ácido, adaptado de la referencia [78].

Para evitar las reacciones no deseadas de resinificación y aumentar el rendimiento a LA, los estudios muestran que trabajar con bajas concentraciones de FA disminuye la formación de resinas. Este hecho es aplicable en mayor o menor medida dependiendo si el disolvente de la reacción es agua o si se trata de un disolvente orgánico. Por ejemplo, en la reacción del FA para formar levulinato de etilo, Taejin Kim et al (2013) [78]

estudiaron el efecto de etanol y butanol como disolventes orgánicos en la polimerización del FA. Esta reacción también es catalizada por un ácido mineral (H_2SO_4) y los resultados indican un incremento en la formación de resinas con el aumento de la concentración del FA. Otro aspecto a tener en cuenta para incrementar la selectividad a ácido levulinico es evitar la formación del subproducto 4-HCP [79].

1.2.4. Otros procesos de obtención de ácido levulínico

El LA también puede obtenerse tras la oxidación del 5-metilfurfural con peróxido de hidrógeno (H_2O_2, 28 %) a 333 K en presencia de ácido fórmico (HCOOH) (ver Esquema 1.11, reacción (1)). Esta reacción da una mezcla de productos de LA y 4-oxopentenoico [38] con un rendimiento masico a LA de hasta el 98,5 % para un tiempo de reacción de 540 minutos.

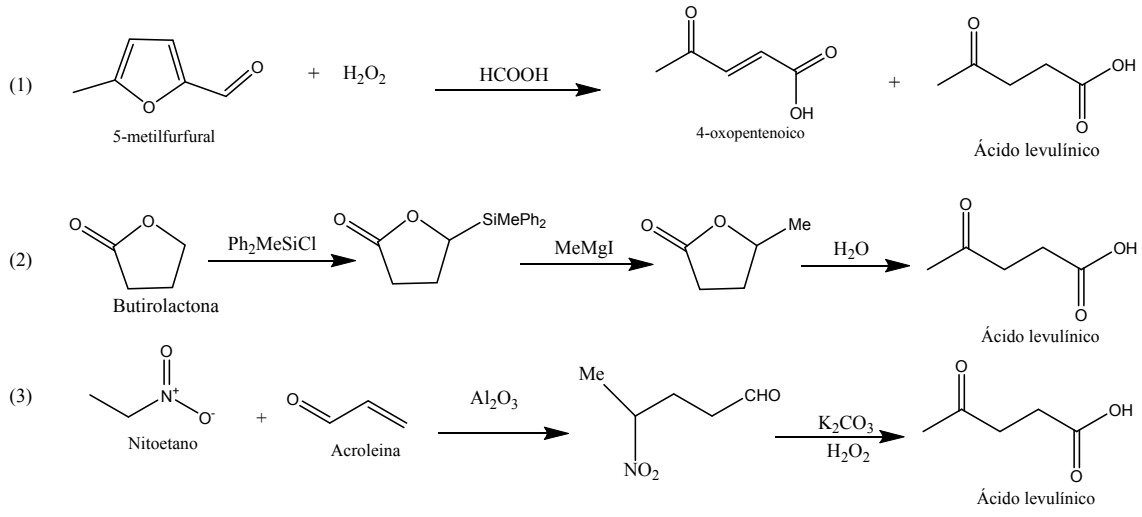

Esquema 1.11. Obtencion de LA a partir de: (1) 5-metilfurfural, (2) butirolactona, (3) nitroetano y acroleína [38].

Otra alternativa para producir LA es a partir de 4-(difenil-metil-silil)-butirolactona en presencia de un catalizador de yodo–magnesio (CH_3MgI) (Esquema 1.11, reacción 2);

en este caso el rendimiento masico de LA es del 71,2 % [80]. También el LA puede ser obtenido a partir de la reacción de nitroetano y acroleína en presencia de Al_2O_3 como catalizador, con la subsecuente oxidación de 4-nitropentanal formado en un sistema oxidante de H_2O_2-K_2CO_3 (Esquema 1.11, reacción (3)) [38]. A pesar de los buenos rendimientos que presentan las reacciones citadas, todavía no es posible llevarlas a cabo a escala industrial, debido a las dificultades de obtención de los reactivos en las cantidades requeridas.

1.3. Catálisis heterogénea aplicada a la obtención de ácido levulínico a partir de alcohol furfurílico.

Como se ha descrito en el apartado 1.2.3, los estudios mostrados en la bibliografía consultada sobre catálisis heterogénea aplicada a la síntesis de LA a partir de FA, hasta el momento se limitan a algunos catalizadores tipo resinas de intercambio catiónico como Amberlyst 15, Dowex y Amberlyte IR-120 [73-75], obteniendo rendimientos relativamente bajos de LA. De acuerdo a la información recopilada, Redmond [81] ha reportado un rendimiento de 55 % molar de LA, usando Amberlite IR-120, que es el mas alto valor reportado a la fecha, debido a que los demás estudios se extienden hacia la obtencion de esteres de levulinato (levulinato de etilo, levulinato de butilo.etc.), en cuyo caso los rendimientos superan el 90 % [74, 82, 83].

Los catalizadores sólidos ácidos han sido usados a lo largo de la historia, en principio adquirieron gran importancia en procesos de craqueo catalítico, sin embargo su uso se ha extendido a infinidad de procesos diferentes en la industria química, y más recientemente, en los procesos de biorrefineria. Los primeros catalizadores de este tipo fueron las arcillas ácidas naturales tipo bentonita, más tarde sobre los años de 1940, se empezaron a sintetizar algunos catalizadores ácidos. En esta segunda generación se desarrollaron catalizadores para uso en craqueo catalítico basados en aluminosilicatos amorfos, que posteriormente, en el año 1962, fueron remplazados por aluminosilicatos cristalinos (*zeolitas*). Estos aluminosilicatos cristalinos tienen disponibles un mayor número de centros ácidos que los materiales amorfos, y su fuerza ácida puede incrementarse durante su preparación. Una descripción de los principales sólidos ácidos

que han sido objeto de estudio en diferentes procesos de reacción y que pueden ser una alternativa para su uso en la reacción de FA a LA se presenta a continuación.

1.3.1. Catalizadores sólidos ácidos.

Los catalizadores sólidos ácidos difieren entre sí en la acidez, en su superficie específica, resistencia mecánica, estabilidad térmica e hidrotérmica y/o el coste de producción. Por lo tanto, un catalizador puede ser elegido y/o diseñado dependiendo de los requerimientos del sistema. Un catalizador sólido ácido además puede poseer diferente variedad de sitios ácidos y de fuerza ácida. De acuerdo a la definición, un ácido de Lewis es una sustancia capaz de aceptar o compartir un par de electrones de una base de Lewis para conformar un ácido-base. Un ácido Brönsted es una especie capaz de donar un protón [84]. Ambos conceptos Brönsted y Lewis son aplicables también a los catalizadores sólidos. Muchos metales, fundamentalmente metales de transición, se consideran ácidos de Lewis y se utilizan como tales en diferentes reacciones [85]. Entre ellos cabe destacar: aluminio, antimonio, azufre, boro, cerio, cobalto, cobre, estaño, europio, fósforo, hierro, lantano, molibdeno, níquel, paladio, plata, silicio, talio, titanio, vanadio, iterbio, zinc y zirconio. Distintos compuestos de los mencionados metales se utilizan como catalizadores ácidos de Lewis en reacciones de síntesis orgánica, destacando entre ellos BF_3, $AlCl_3$, $SnCl_4$ o $TiCl_4$ [85,86]. Estos compuestos activan los grupos funcionales de los sustratos con relativamente baja estéreo-selectividad, regio-selectividad y quimio-selectividad. Sin embargo, la acidez Lewis de estos metales puede ser modulada cuando se coordinan con diferentes ligandos orgánicos.

En general, todos los ácidos de Lewis se caracterizan por poseer una fuerte afinidad por varios heteroátomos presentes en moléculas orgánicas, particularmente nitrógeno y oxígeno por lo que son capaces de generar complejos de coordinación 1:1, donde el sustrato orgánico se comporta como una base de Lewis. La coordinación del ácido de Lewis induce la polarización de la molécula reactante como consecuencia de la pérdida de densidad electrónica del reactivo en beneficio del catalizador, activando la primera y produciendo la reacción química y el producto deseado. Finalmente, en una última etapa, el complejo (ácido de Lewis-producto) se disocia, regenerando el centro ácido para otro ciclo catalítico [85]

Un buen ejemplo de los materiales catalíticos que poseen acidez tipo Brönsted y Lewis son las zeolitas. En el Esquema 1.12, la acidez Brönsted está representada mediante el enlace O-H^+. Si se calienta la zeolita, se puede eliminar el agua de los sitios de Brönsted dejando átomos de aluminio coordinados solamente con tres átomos de oxígeno. Estos actúan como ácidos de Lewis. La Tabla 1.6 muestra un resumen de algunos de los catalizadores sólidos ácidos principalmente estudiados en reacciones orgánicas.

Tabla 1.6. Lista general de catalizadores sólidos ácidos [84, 86]

Clasificación	Compuestos
Arcillas minerales naturales	Bentonita, Mordenita, Kaolina, Montmorilonita, Zeolitas (X,Y,A, ZSM-5…….)
Resinas de intercambio catiónico	Amberlyst, Amberlite, Nafion, Smopex 101, Dowex.
Óxidos de metales y sulfuros	ZnO, CdO, Al_2O_3, ThO_2, TiO_2, ZrO_2, SnO_2, PbO, CuO, Cu_2O, Bi_2O_3, Sb_2O_5, V_2O_5, Cr_2O_3, MoO_3, WO_3, CdS, ZnS, Nb_2O_5.
Sales metálicas	$SrSO_4$, $CuSO_4$, $ZnSO_4$, $CdSO_4$, $Al_2(SO_4)_3$, $FeSO_4$, $Fe_2(SO_4)_3$, $CoSO_4$, $NiSO_4$, $Cr_2(SO4)_3$, $KHSO_4$, K_2SO_4, $Co_3(PO_4)_2$, BPO_4, $AlPO_4$, $Cu_3(PO_4)_2$, $Ti_3(PO_4)_4$, $AlCl_3$, $TiCl_3$
Mezcla de óxidos	SiO_2-Al_2O_3, SiO_2-TiO_2, SiO_2-ZrO_2, SiO_2-ZnO, SiO_2-La_2O_3, SiO_2-MoO_3, SiO_2-WO_3, SiO_2-V_2O_5, Al_2O_3-ZnO, Al_2O_3-TiO_2, Al_2O_3-CdO, Al_2O_3-B_2O_3, Al_2O_3-ZrO_2, Al_2O_3-V_2O_5, Al_2O_3-MoO_3, Al_2O_3-WO_3, Al_2O_3-Mn_2O_3, Al_2O_3-Co_3O_4, Al_2O_3-CuO, TiO_2-Sb_2O_5, TiO_2-WO_3, TiO_2-MoO_3, TiO_2-Mn_2O_3, TiO_2-V_2O_5, ZrO_2-CdO, ZrO_2-ZnO, ZrO_2-WO_3, ZnO-Fe_2O_3, MoO_3-CoO, Heteropoliácidos ($H_3PW_{12}O_{40}$).

Tabla 1.6. continuacion

Sólidos súper ácidos	*Soporte*
- SbF_5, TaF_5……	- SiO_2-Al_2O_3, SiO_2-TiO_2, SiO_2-ZrO_2, TiO_2-ZrO_2, Al_2O_3-B_2O_3, SiO_2, SiO_2-WO_3, HF-Al_2O_3.
- SbF_5, BF_3…….....	- Al_2O_3, MoO_3, ThO_2, Al_2O_3-WO_3
- BF_3, $AlCl_3$, $AlBr_3$…….	- Grafito, Pt-grafito
- SbF_5-HF, SbF_5-FSO_3H….	- Resinas de intercambio iónico
- SbF_5-CF_3SO_3H……. - Nafion	- Metales (Pt,Al), aleación (Pt-Au, Ni-Mo, Al-Mg), poliestireno, SiO_2-Al_2O_3, kaolin, carbón activado, grafito.
- ZrO_2-SO_4^{2-}, Fe_2O_3-SO_4^{2-}, TiO_2-SO_4^{2-},ZrO_2,Fe-ZrO_3/SO_4^{2-} ,TiO_2-$La_2O_3/SO4^{2-}$, ZrO_2-La_2O_3/SO_4^{2-}.	- Al_2O_3, $AlPO_4$

Los sólidos ácidos mostrados en la Tabla 1.6 presentan diferentes propiedades y características, algunas de las cuales se abordan a continuación.

1.3.1.1. Óxidos metálicos

Una buena parte de los óxidos metálicos y de sus mezclas pueden ser también materiales con características ácidas. Los óxidos de metales de transición tienen una amplia variedad de estructuras de superficie que afectan a la energía superficial de estos

compuestos e influyen en sus propiedades químicas. La acidez y basicidad relativa de los átomos presentes en la superficie de óxidos metálicos se ve afectada por la coordinación del catión metálico y el anión oxígeno, lo que altera las propiedades catalíticas de estos compuestos. La superficie de un óxido metálico consta de matrices ordenadas de centros ácido-base. Los centros de metal catiónico actúan como sitios ácidos de Lewis, mientras que los centros de oxígeno aniónicos actúan como bases de Lewis. Los grupos hidroxilo superficiales son capaces de actuar como ácido o base Brönsted, ya que son capaces de rechazar o aceptar un protón. La superficie de la mayoría de los óxidos metálicos será, en cierta medida hidroxilada en condiciones normales, cuando el vapor de agua está presente. La fuerza y la cantidad de sitios ácidos Lewis y Brönsted determinan la actividad catalítica de muchos óxidos metálicos [87].
La principal ventaja de los óxidos metálicos es su bajo coste, y si se seleccionan las composiciones adecuadas se puede lograr una buena estabilidad térmica. Sin embargo, en lo referente a la acidez, hay que resaltar que los óxidos metálicos, generalmente por si solos, no presentan valores altos de acidez [87]; sólo mediante combinaciones adecuadas entre ellos se puede incrementar esta característica. Por ejemplo, en la síntesis de dicloro-pentafluoropropano, catalizadores de óxido de zirconio activado con flúor o diclorodifluorometano se comportaron como un ácido Lewis, incrementado la actividad catalítica en dicha reacción [87].

En la deshidratación de glicerol a acroleína se combinan óxidos de niobio y zirconio, observándose que el rendimiento aumenta con el incremento de niobio [88]. También para incrementar la actividad en reacciones de deshidratación de glicerol se han utilizado una serie de catalizadores de zirconio dopado con sílice mesoporosa a diferentes relaciones Zr/Si, observándose una buena dispersión de sitios ácidos, principalmente de tipo Lewis [89]. Un catalizador de óxido de niobio mesoporoso (Nb_2O_5) ha sido utilizado en la reacción de deshidratación de xilosa a furfural, mostrando una conversión superior respecto al óxido de niobio comercial [90]. Otros autores han utilizado óxido de niobio soportado sobre óxido de titanio en la reacción de deshidratación de metanol a dimetil-eter [91] o un catalizador mesoporoso de óxido de fosfato-niobio en la reacción de deshidratación de fructosa a 5-HMF en medio acuoso [92]. Las propiedades ácidas del óxido de zirconio soportado sobre óxido de wolframio han sido investigadas en la reacción de deshidratación de metanol [93].

Por otra parte, los óxidos de silicio y aluminio (SiO_2, γ-Al_2O_3) generalmente se usan como soportes debido a que tienen una alta superficie específica. Un soporte muy utilizado es la γ-Al_2O_3 obtenido a partir de las sales de aluminio, como el nitrato de aluminio ($Al(NO_3)_3.9H_2O$), empleando procesos hidrotérmicos con posterior calcinación. Este proceso también se puede utilizar para preparar mezclas de óxidos de titanio y aluminio. Por ejemplo, los catalizadores de TiO_2-Al_2O_3 preparados por el método de co-precipitación han sido usados para la esterificación de ácido láctico con n-butanol, exhibiendo una alta acidez [94]. Catalizadores híbridos de CuO-ZnO, CuO-ZnO-Al_2O_3, según estudios realizados por Flores et al (2008) [95], poseen mayoritariamente acidez tipo Lewis.

La mezcla de catalizadores de óxido de aluminio y óxido de silicio (aluminosilicatos) posee gran potencial como catalizadores ácidos en el campo de la catálisis heterogénea por su mesoporosidad, permitiendo ser funcionalizados por síntesis directa o mediante procedimientos post-síntesis. La funcionalización de los materiales mesoporosos permite el empleo de estos como catalizadores en una gran variedad de reacciones catalizadas por centros ácidos. La descripción de este tipo de materiales se realiza en el siguiente apartado.

1.3.1.2. Catalizadores sólidos ácidos tipo aluminosilicatos.

Los aluminosilicatos son minerales compuestos de aluminio, silicio y oxígeno que se encuentran de manera natural o sintética. Un amplio grupo de zeolitas se pueden encontrar de manera natural (aluminosilicatos naturales) en rocas sedimentarias, volcánicas y metamórficas. Estos materiales fueron los primeros catalizadores comerciales usados a gran escala en procesos de craqueo; sin embargo, los impactos negativos de las impurezas presentes como el hierro, en la selectividad del proceso promovieron el desarrollo de aluminosilicatos cristalinos sintetizados (zeolitas). Los aluminosilicatos se han utilizado como catalizadores en un gran número de transformaciones químicas, especialmente en el ámbito de los hidrocarburos [96-101]. Entre ellos, han sido particularmente útiles en reacciones de isomerización de olefinas [98-100], parafinas, alquilación de aromáticos con alcoholes [105-121], oligomerización de olefinas y craqueo catalítico [119, 120]. Durante los años 1950-1969, estos materiales de aluminosilicatos tuvieron gran importancia, evolucionando

posteriormente, a materiales sintetizados de aluminosilicatos cristalinos (zeolitas), aluminofosfatos (ALPOS) o fosfatos de aluminosilicatos (SAPOS), los cuales son materiales con mejores características texturales y ácidas que las de origen natural.

Las zeolitas son aluminosilicatos cristalinos hidratados que constan de un armazón de tetraedros de $[SiO_4]^{4-}$ y $[AlO_4]^{5-}$ conectados el uno al otro por medio de átomos de oxígeno (Esquema 1.12). La estructura presenta canales y cavidades de dimensiones moleculares en las cuales se encuentran los cationes de compensación, moléculas de agua u otros adsorbatos y sales. Este tipo de estructura microscópica hace que las zeolitas presenten una superficie interna extremadamente grande con relación a su superficie externa (entre 500 y 1000 m^2/g). Sin embargo, esta superficie es poco accesible para algunos compuestos de tipo macromolecular. La microporosidad de estos sólidos es abierta y la estructura permite la transferencia de materia entre el espacio intracristalino y el medio que lo rodea. Esta transferencia está limitada por el diámetro de los poros de la zeolita, ya que sólo podrán acceder o salir del espacio intracristalino aquellas moléculas cuyas dimensiones sean inferiores a un cierto valor, el cual varía de una zeolita a otra, dependiendo especialmente de la relación de sílice-alúmina.

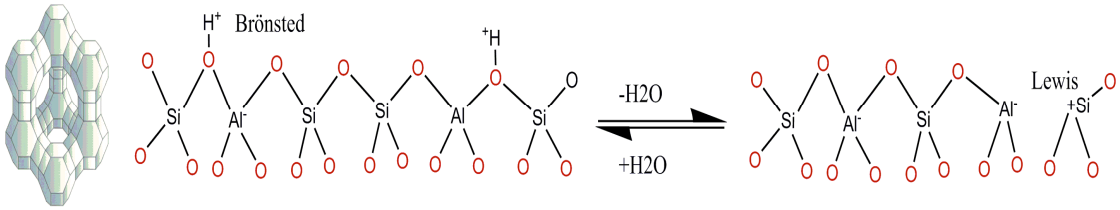

Esquema 1.12. Estructura característica de las zeolitas ácidas, acidez Brönsted y Lewis [84].

Dependiendo de su composición química, las zeolitas pueden actuar como catalizadores ácidos, básicos o de reducción-oxidación (redox), siendo sus aplicaciones en catálisis ácida las de mayor importancia industrial [121]. La funcionalidad ácida de las zeolitas procede de la presencia de la carga negativa neta asociada a cada átomo de aluminio incorporado a la estructura. Si ésta se compensa mediante un protón enlazado al oxígeno, puente entre un átomo de silicio y otro de aluminio, el grupo hidroxilo formado (=O-H) presenta un enlace mucho más fuerte que el existente cuando se

compensa la carga de un oxígeno unido a un átomo de silicio (grupo silanol), lo que le convierte en un centro ácido tipo Brönsted por su posibilidad de ceder un protón (Esquema 1.12).

La acidez de las zeolitas no se limita a la presencia de centros de tipo Brönsted, ya que también presentan centros de tipo Lewis, capaces de aceptar pares de electrones. Estos se forman tras la deshidroxilación y la desaluminización de las zeolitas. Así, pueden aparecer en forma de aluminio o silicio tri-coordinados (≡Al, $\equiv Si^{+}$), y/o como aluminio extra-red conteniendo especies como AlO^{+} [122]. Los centros ácidos de Lewis son inestables en tratamientos con vapor de agua o a altas temperaturas. Este tipo de tratamientos puede provocar la extracción del aluminio de la estructura, dando lugar a la aparición de especies de Al extra-red.

El número de centros ácidos está directamente relacionado con la cantidad de átomos trivalentes. Sin embargo, la fuerza ácida asociada a cada centro activo depende de diversos factores, como la relación Si/Al, la geometría, el grado de intercambio iónico, etc. De este modo, se ha comprobado que la fuerza ácida de un determinado centro es mayor cuanto menor sea el número de átomos de aluminio situados en la segunda esfera de coordinación, por lo que un centro aislado presentará mayor fuerza como centro ácido Brönsted [123].

1.3.1.3. Resinas de intercambio iónico ácidas.

Las resinas de intercambio iónico ácidas son materiales orgánicos sintéticos cuya estructura se presenta como una matriz polimérica tridimensional que posee polaridad, la cual se encuentra neutralizada por iones de carga opuesta. En su estructura, estos materiales llevan un exceso de carga ya sea positiva o negativa, por lo que la naturaleza de los grupos polares unidos a la matriz polimérica determina el comportamiento de la resina.

Las resinas ácidas presentan grupos de intercambio catiónico distribuidos entre la estructura polimérica, siendo los más frecuentes los grupos sulfónicos, fosfóricos, carboxílicos y fenólicos, los cuales presentan diferencias de acidez para ser usadas en diferentes aplicaciones [124]. Concretamente, las resinas sulfónicas (ver Esquema 1.13)

son resinas fuertemente ácidas, debido a que la acidez que le confiere el grupo sulfónico hace que se comporte de manera similar a la de un ácido fuerte.

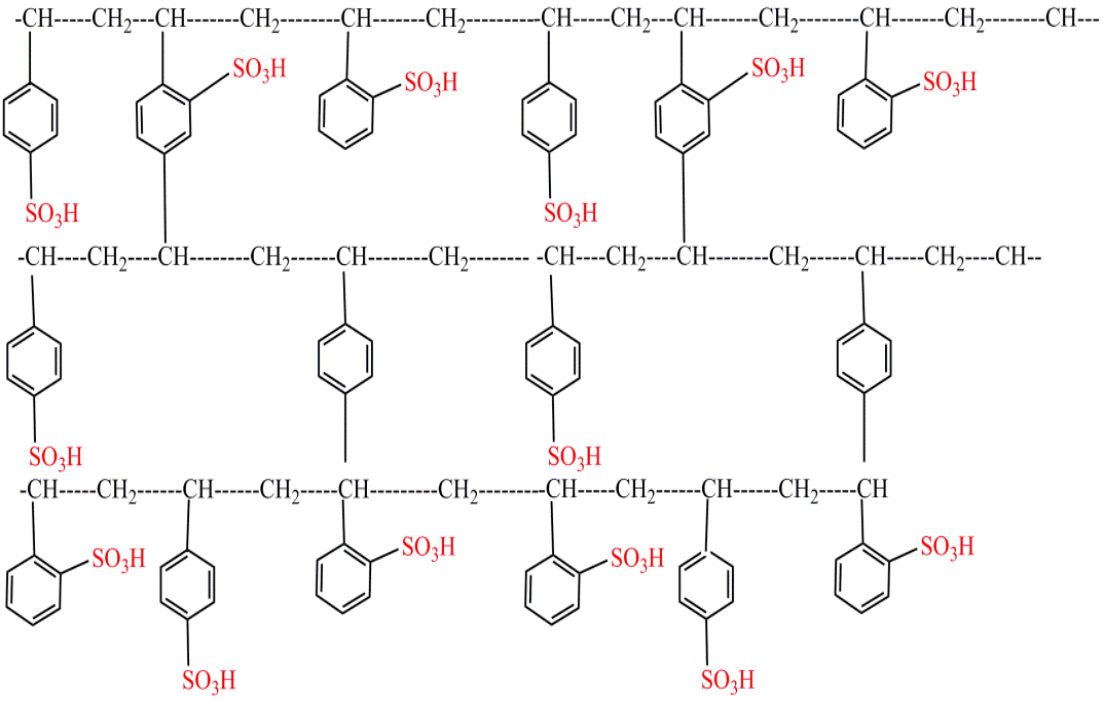

Esquema 1.13. Estructura de la resina de intercambio iónico con grupos sulfónicos.

Las propiedades de las resinas de intercambio iónico se encuentran determinadas específicamente por la naturaleza de la matriz polimérica de la que está compuesta, y de los grupos polares unidos a ella. De esta manera, las propiedades más importantes son: el grado de entrecruzamiento, capacidad de intercambio, porosidad, estabilidad térmica y adsorción selectiva. El grado de entrecruzamiento se define como el porcentaje del agente entrecruzante respecto del monómero de la matriz polimérica, tal como se puede observar en el Esquema 1.13. La función principal del agente entrecruzante es unir las cadenas del polímero, de tal manera que se formen redes tridimensionales fuertemente unidas entre sí, confiriéndole insolubilidad y resistencia térmica. La capacidad de intercambio se define como el número de grupos intercambiables, capaces de incorporarse en reacciones de intercambio, y por tanto, representa el número de sitios activos disponibles. Así por ejemplo, para resinas catiónicas se usan habitualmente como medida los miliequivalentes de cationes intercambiados por gramo de resina seca

o por mililitro de resina húmeda. Este valor fluctúa comúnmente entre 2 y 5 meq/g, como es el caso de resinas de marca registrada Amberlyst [125].

La porosidad y la estabilidad térmica de estos materiales dependen en gran medida del grado de entrecruzamiento. Así las resinas con un bajo grado de entrecruzamiento tienen tamaños de poro alto y poseen menor estabilidad térmica que las resinas sintetizadas con alto grado de entrecruzamiento. Sin embargo, su carácter polimérico orgánico sólo permite tener una resistencia térmica adecuada hasta 463 K para el caso de las resinas sulfónicas, como las Amberlyst, y de 493 K para las resinas fluoradas. Por tanto, esta es una propiedad que limita su uso a procesos que sean efectivos a temperaturas superiores.

Las resinas de intercambio iónico Amberlyst se han utilizado en reacciones de alquilación [126], en procesos de purificación [127], y recuperación de metales [128], además de reacciones de hidrogenación, cuando es dopada con paladio. Entre estas últimas reacciones están incluidas las de producción de compuestos oxigenados (MTBE, TAME e isooctano) para ser utilizados como aditivos de las gasolinas [130-132]. Las resinas Amberlyst se comercializan en forma de perlas esféricas de resina o una estructura macro-reticular. Este tipo de resina presenta la desventaja de su baja superficie específica (50 m^2/g) [125].

En las resinas Amberlyst, la reacción catalítica se lleva a cabo cuando los reactivos son transportados desde la fase fluida hasta la superficie de la resina, donde se ponen en contacto con los grupos catalíticamente activos (grupos sulfónicos) que poseen el contra-ion H^+:

$$Matriz - SO_3.H^+ \rightarrow Matriz - SO_3.^- + H^+$$

El transporte de las moléculas reactivas desde el seno del fluido hasta el interior de matriz polimérica se efectúa a través de una delgada capa de fluido que rodea la superficie de la resina conocida como capa de Nerst, de tal forma que el transporte a través de esta película ocurre únicamente por difusión.

1.3.1.4. Sólidos superácidos

Otros materiales recientemente utilizados son los denominados "sólidos superácidos". Este concepto se aplica a aquellos materiales catalíticos que poseen una acidez igual o mayor que el 100 % de la acidez del ácido sulfúrico puro, es decir, con valores iguales o superiores a la función Hammett (Ho) de -11,93 (valor del ácido sulfúrico). La función de acidez Hammett (Ho) es una medida de la acidez usada en soluciones altamente ácidas, propuesta por el químico orgánico y físico Louis Planck Hammett y que se usa para extender la acidez Brönsted-Lowry mas allá de las disoluciones acuosas diluidas para la cual la escala de pH es útil [133].

La elevada fuerza ácida de los materiales superácidos permite catalizar reacciones como las de isomerización [134-136] a más bajas temperaturas (habitualmente entre 373- 573 K). Aunque se han ensayado diferentes tipos de sólidos superácidos como el SbF_5 [137-139], el más ampliamente investigado y el que mejor resultado ha mostrado es el óxido de zirconio sulfatado (ZrO_2/SO_4^{2-}) [134, 140-143], pese a que presenta algunos inconvenientes como la inestabilidad y su rápida desactivación por perdida de sulfatos.

Materiales ácidos de estructura SO_4^{2-}/M_xO_y, donde M puede ser un metal como Fe, Ti, Zr, Mo, W, Sn, Si o Al, han despertado también gran interés en los últimos años dentro del campo de la catálisis [101-103], debido no sólo a sus propiedades ácidas, sino también a la alta resistencia a la corrosión y a la elevada estabilidad térmica. Las publicaciones científicas hacen referencia a su efectividad como catalizador en reacciones de deshidratación, isomerización, alquilación, acetilación, y reducción selectiva de NO_x, entre otras [102, 104-108].

Los catalizadores ácidos WO_x/ZrO_2 son mucho más estables a altas temperaturas, frente a los catalizadores SO_x/ZrO_2. La acidez observada en ellos es de tipo Brönsted y Lewis. La acidez Brönsted se asocia a su estructura superficial de heteropolioxoaniones, en los que se requieren protones para garantizar la neutralidad o compensación de cargas. Por otro lado la acidez tipo Lewis está referida a la presencia de cationes Zr^{+4} en la superficie. La densidad de estos sitios ácidos disminuye significativamente cuando el contenido de wolframio se aproxima a la saturación superficial y simultáneamente los grupos Zr-OH desaparecen [103].

1.4. Referencias

[1] U.S International Energy Agency, (I. E. A). 1 (2011) 1-659. http:// www.iea.org/publications/freepublications/publication/weo2011_web.pdf

[2] European Commission, EU Energy in Figures. Statistical Pocketbook, European Union, Bélgica (2014). http://ec.europa.eu/energy/sites/ener/files/documents/2014 _pocketbook.pdf

[3] L. Mei Wu, C. Hui Zhou, D. Shen Tong, W. Hua Yu, Chapter 15 - Catalytic thermochemical processes for biomass conversion to biofuels and chemicals, in: V.K. Gupta, M.G. Tuohy, C.P. Kubicek, J. Saddler, F. Xu (Eds.), Bioenergy Res.: Advances and Applications, Elsevier, Amsterdam, 2014, pp. 243-254.

[4] J.C. Serrano-Ruiz, A. Pineda, A.M. Balu, R. Luque, J.M. Campelo, A.A. Romero, J.M. Ramos-Fernández, Catalytic transformations of biomass-derived acids into advanced biofuels, Catal. Today. 195 (2012) 162-168.

[5] W. K.W (Ed.), Bioalcohol Production; Biochemical Conversion of Lignocellulosic Biomass, 1 ed., Woodhead, 2010.

[6] S.J.T. Pollar, C.A. Velis, P.J. Longhurst, G.H. Drew, R. Smith, Biodrying for mechanical-biological treatment of wastes: a review of process science and engineering, Bioresource. Technol. 100 (2009) 2747-2761.

[7] X. Castells, Aprovechamiento de residuos agricolas y forestales, (Ed.) Díaz de Santos. 1 (2012) 723.

[8] S. Dutta, S. De, B. Saha, Advances in biomass transformation to 5-hydroxy methylfurfural and mechanistic aspects, Biomass Bioenergy. 55 (2013) 355-369.

[9] S. Murat Sen, C.A. Henao, D.J. Braden, J.A. Dumesic, C.T. Maravelias, Catalytic conversion of lignocellulosic biomass to fuels: Process development and technoeconomic evaluation, Chem. Eng. Sci. 67 (2012) 57-67.

[10] S.G. Wettstein, D.M. Alonso, E.I. Gürbüz, J.A. Dumesic, A roadmap for conversion of lignocellulosic biomass to chemicals and fuels, Current Opinion in Chemical Engineering. 1 (2012) 218-224.

[11] J.C. Serrano Ruiz, R.M. West, J.A. Dumesic, Catalytic Conversion of Renewable Biomass Resources to Fuels and Chemicals , Annu. Rev. Chem. Biomol. Eng. 1 (2010) 79-100.

[12] A. Corma, S. Iborra, A. Velty, Chemical routes for the transformation of biomass into chemicals, Chem. Rev. 107 (2007) 2411.

[13] T. Werpy, G. Petersen, Top Value Added Chemicals From Biomass, Pacific Northwest National Laboratory (PNNL) National Renewable Energy Laboratory (NREL). 1 (2004) 45-48. http://www.nrel.gov/docs/fy04osti/35523.pdf

[14] S. Yoon, S. Han, S. Shin, The effect of hemicelluloses and lignin on acid hydrolysis of cellulose, Energy. 77 (2014) 19-24

[15] C. Rong, X. Ding, Y. Zhu, Y. Li, L. Wang, Y. Qu, X. Ma, Z. Wang, Production of furfural from xylose at atmospheric pressure by dilute sulfuric acid and inorganic salts, Carbohydr. Res. 350 (2012) 77-80.

[16] I. Agirrezabal-Telleria, J. Requies, M.B. Güemez, P.L. Arias, Dehydration of d-xylose to furfural using selective and hydrothermally stable arenesulfonic SBA-15 catalysts, Appl. Catal. B: Environmental. 145 (2014) 34-42.

[17] C. García-Sancho, I. Agirrezabal-Telleria, M.B. Güemez, P. Maireles-Torres, Dehydration of d-xylose to furfural using different supported niobia catalysts, Appl. Catal. B: Environmental. 152–153 (2014) 1-10.

[18] I. Agirrezabal-Telleria, C. García-Sancho, P. Maireles-Torres, P.L. Arias, Dehydration of xylose to furfural using a Lewis or Brönsted acid catalyst and N_2 stripping, Chin. J. Catal. 34 (2013) 1402-1406.

[19] B. Pholjaroen, N. Li, Z. Wang, A. Wang, T. Zhang, Dehydration of xylose to furfural over niobium phosphate catalyst in biphasic solvent system, J. Energy. Chem. 22 (2013) 826-832.

[20] S. Lima, M. Pillinger, A.A. Valente, Dehydration of d-xylose into furfural catalysed by solid acids derived from the layered zeolite Nu-6(1), Catal. Commun. 9 (2008) 2144-2148.

[21] H.T. Vo, V.T. Widyaya, J. Jae, H.S. Kim, H. Lee, Hydrolysis of ionic cellulose to glucose, Bioresour. Technol. 167 (2014) 484-489.

[22] S. Shen, C. Wang, B. Cai, H. Li, Y. Han, T. Wang, H. Qin, Heterogeneous hydrolysis of cellulose into glucose over phenolic residue-derived solid acid, Fuel. 113 (2013) 644-649.

[23] B. Yang, Z. Dai, S.Y. Ding, Ch.E. Wyman, Hydrolysis of cellulosic biomass, Biofuels. 2 (2011) 421-450

[24] G. Fan, C. Liao, T. Fang, M. Wang, G. Song, Hydrolysis of cellulose catalyzed by sulfonated poly(styrene-co-divinylbenzene) in the ionic liquid 1-n-butyl-3-methylimidazolium bromide, Fuel Process. Technol. 116 (2013) 142-148.

[25] K. Zhuo, Q. Du, G. Bai, C. Wang, Y. Chen, J. Wang, Hydrolysis of cellulose catalyzed by novel acidic ionic liquids, Carbohydr. Polym. 115 (2015) 49-53

[26] S.Gonzáles, N.O. Soto, O.M. Rutiaga, H. Medrano, J.G. Rutiaga, J. Lopez, O ptimization of the enzimatic hydrolysis process of four straw bean varieties., Revista Mexicana de Ingenieria Quimica. 10 (2011) 17-28.

[27] S. Dutta, S. Pal, Promises in direct conversion of cellulose and lignocellulosic biomass to chemicals and fuels: Combined solvent–nanocatalysis approach for biorefinary, Biomass Bioenergy. 62 (2014) 182-197.

[28] P. Gallezot, Chapter 1 - Metal Catalysts for the Conversion of Biomass to Chemicals, in: S.L. Suib (Ed.), New and Future Developments in Catalysis, Elsevier, Amsterdam, (2013), pp. 1-27.

[29] Z. Lipeng, S. Meiting, Qiyong Cai, Lin Wua, Xiaopeng Hua, Xiaomei Yang, Chen Chen, Jie Xu., Hydrolysis of hemicellulose catalyzed by hierarchical H-USY zeolites The role of acidity and pore structure, Microporous Mesoporous Mater. 169 (2013) 54-59.

[30] W. Deng, Q. Zhang, Y. Wang, Catalytic transformations of cellulose and cellulose-derived carbohydrates into organic acids, Catal. Today. 234 (2014) 31-41

[31] D.B. Bevilaqua, M.K.D. Rambo, T.M. Rizzetti, A.L. Cardoso, A.F. Martins, Cleaner production: levulinic acid from rice husks, J. Clean. Prod. 47 (2013) 96-101.

[32] H. Ren, Y. Zhou, L. Liu, Selective conversion of cellulose to levulinic acid via microwave-assisted synthesis in ionic liquids, Bioresour. Technol. 129 (2013) 616-619.

[33] E.L. Gurbuz, S.G. Wettstein, D.M. Alonso, J.A. Dumesic, Conversion of hemicellulose to furfural and levulinic acid in biphasic reactors with alkylphenol solvents, American Chemical Society, Division of Fuel Chemistry. 57 (2012) 129-130.

[34] B.Kamm, P.R.Gruber, M.Kamm (Eds.), Biorefineries-industrial processes and products, 1 ed, (2006) Wiley-VCH,.

[35] J.C. Serrano-Ruiz, A. Pineda, A.M. Balu, R. Luque, J.M. Campelo, A.A. Romero, J.M. Ramos-Fernández, Catalytic transformations of biomass-derived acids into advanced biofuels, Catal. Today. 195 (2012) 162-168.

[36] D.R. Fernandes, A.S. Rocha, E.F. Mai, C.J.A. Mota, V. Teixeira da Silva, Levulinic acid esterification with ethanol to ethyl levulinate production over solid acid catalysts, Appl. Catal. A: General. 425–426 (2012) 199-204.

[37] Y. Kuwahara, W. Kaburagi, K. Nemoto, T. Fujitani, Esterification of levulinic acid with ethanol over sulfated Si-doped ZrO2 solid acid catalyst: Study of the structure–activity relationships, Appl. Catal. A: General. 476 (2014) 186-196.

[38] B.V. Timokhin, V.A. Baransky, G.D. Eliseeva, Levulinic acid in organic synthesis, Russ. Chem. Rev. 68 (1999) 73-84.

[39] X. Yu, Y. Guo, K. Li, X. Yang, L. Xu, Y. Guo, J. Hu, Catalytic synthesis of diphenolic acid from levulinic acid over cesium partly substituted Wells–Dawson type heteropolyacid, Journal of Mol. Catal. A: Chemical. 290 (2008) 44-53.

[40] National Institute of Standards and Thechnology, Nist.(2014) http://webbook.nist.gov/cgi/cbook.cgi?Name=levulinic+acid&Units=SI

[41] M. Sudhakar, M. Lakshmi Kantam, V. Swarna Jaya, R. Kishore, K.V. Ramanujachary, A. Venugopal, Hydroxyapatite as a novel support for Ru in the hydrogenation of levulinic acid to γ-valerolactone, Catal. Commun. 50 (2014) 101-104

[42] K. Yan, T. Lafleur, C. Jarvis, G. Wu, Clean and selective production of γ-valerolactone from biomass-derived levulinic acid catalyzed by recyclable Pd nanoparticle catalyst, J. Clean. Prod. 72 (2014) 230-232

[43] Y. Shen, Y. Xu, J. Sun, B. Wang, F. Xu, R. Sun, Efficient conversion of monosaccharides into 5-hydroxymethylfurfural and levulinic acid in $InCl_3$–H_2O medium, Catalysis Communications. 50 (2014) 17-20.

[44] K. Dussan, B. Girisuta, D. Haverty, J.J. Leahy, M.H.B. Hayes, Kinetics of levulinic acid and furfural production from Miscanthus × giganteus, Bioresour. Technol. 149 (2013) 216-224.

[45] B. Girisuta, K. Dussan, D. Haverty, J.J. Leahy, M.H.B. Hayes, A kinetic study of acid catalysed hydrolysis of sugar cane bagasse to levulinic acid, Chem. Eng. J. 217 (2013) 61-70.

[46] B. Kamm, M. Gerhardt, G. Dautzenberg, Chapter 5 - Catalytic Processes of Lignocellulosic Feedstock Conversion for Production of Furfural, Levulinic Acid, and Formic Acid-Based Fuel Components, in: S.L. Suib (Ed.), New and Future Developments in Catalysis, Elsevier, Amsterdam, (2013) 91-113.

[47] M. Kang, S.W. Kim, J. Kim, T.H. Kim, J.S. Kim, Optimization of levulinic acid production from Gelidium amansii, Ren. Energy. 54 (2013) 173-179.

[48] R. Weingarten, Y.T. Kim, G.A. Tompsett, A. Fernández, K.S. Han, E.W. Hagaman, W.C. Conner Jr., J.A. Dumesic, G.W. Huber, Conversion of glucose into levulinic acid with solid metal(IV) phosphate catalysts, J. Catal. 304 (2013) 123-134.

[49] N. Ya'aini, N.A.S. Amin, S. Endud, Characterization and performance of hybrid catalysts for levulinic acid production from glucose, Microporous Mesoporous Mat. 171 (2013) 14-23.

[50] K. Yan, A. Chen, Efficient hydrogenation of biomass-derived furfural and levulinic acid on the facilely synthesized noble-metal-free Cu–Cr catalyst, Energy. 58 (2013) 357-363.

[51] N. Ya'aini, N.A.S. Amin, M. Asmadi, Optimization of levulinic acid from lignocellulosic biomass using a new hybrid catalyst, Bioresour. Technol. 116 (2012) 58-65.

[52] H. Chen, B. Yu, S. Jin, Production of levulinic acid from steam exploded rice straw via solid superacid, Bioresour. Technol. 102 (2011) 3568-3570.

[53] D.W. Rackemann, W. Doherty, The conversion of lignocellulosics to levulinic acid, Biofuels Bioproducts Biorefining. 5 (2011) 198-214.

[54] J. Hegner, K.C. Pereira, B. DeBoef, B.L. Lucht, Conversion of cellulose to glucose and levulinic acid via solid-supported acid catalysis, Tetrahedron Lett. 51 (2010) 2356-2358.

[55] C. Chang, X. Ma, P. Cen, Kinetic Studies on Wheat Straw Hydrolysis to Levulinic Acid, Chin. J. Chem. Eng. 17 (2009) 835-839.

[56] C. Chang, P. Cen, X. Ma, Levulinic acid production from wheat straw, Bioresour. Technol. 98 (2007) 1448-1453.

[57] C. Chang, X. Ma, P. Cen, Kinetics of Levulinic Acid Formation from Glucose Decomposition at High Temperature, Chin. J. Chem. Eng. 14 (2006) 708-712.

[58] B. Girisuta, L.P.B.M. Janssen, H.J. Heeres, GREEN CHEMICALS A Kinetic Study on the Conversion of Glucose to Levulinic Acid, Chem. Eng. Res. Des. 84 (2006) 339-349.

[59] Q. Fang, M.A. Hanna, Experimental studies for levulinic acid production from whole kernel grain sorghum, Bioresour. Technol. 81 (2002) 187-192.

[60] J.J. Bozell, L. Moens, D.C. Elliott, Y. Wang, G.G. Neuenscwander, S.W. Fitzpatrick, R.J. Bilski, J.L. Jarnefeld, Production of levulinic acid and use as a platform chemical for derived products, Resour. Conserv. Recycling. 28 (2000) 227-239.

[61] B. Capai, G. Lartigau, Preparation of Levulinic acid, United States Patent. 5,175,358 (1992).

[62] J. Jow, G.L. Rorrer, M.C. Hawley, D.T.A. Lamport, Dehydration of d-fructose to levulinic acid over LZY zeolite catalyst, Biomass. 14 (1987) 185-194.

[63] O.N. Masatomi, H.T. Yoshio, Kinoshita, T.M. Tokushima, J. Naruto, Manufacture of Levulinic Acid, US.Patent: 3.752.849 (1971).

[64] D.W. Rackemann, J.P. Bartley, W.O.S. Doherty, Methanesulfonic acid-catalyzed conversion of glucose and xylose mixtures to levulinic acid and furfural, Ind. Crops Prod. 52 (2014) 46-57.

[65] I. Jiménez-Morales, A. Teckchandani-Ortiz, J. Santamaría-González, P. Maireles-Torres, A. Jiménez-López, Selective dehydration of glucose to 5-hydroxymethylfurfural on acidic mesoporous tantalum phosphate, Appl. Catal. B: Environmental. 144 (2014) 22-28.

[66] P. Dornath, W. Fan, Dehydration of fructose into furans over zeolite catalyst using carbon black as adsorbent, Microporous Mesoporous Mat. 191 (2014) 10-17.

[67] D.M. - Alonso, J.Q. - Bond, J.A. - Dumesic, - Catalytic conversion of biomass to biofuels, Green Chem. 12 (2010) 1493-1513.

[68] Z. Shanshan, L. Lu, L. Di, P. Lincai, Catalytic conversion of glucose to levulinic acid by solid heteropolyacid salts, CIESC Journal. 63 (2012) 3881.

[69] R. Weingarten, J. Cho, R. Xing, W.C. Conner, G.W. Huber, Kinetics and Reaction Engineering of Levulinic Acid Production from Aqueous Glucose Solutions., ChemSusChem. 5 (2012) 1280-1290.

[70] Z. Sun, M. Cheng, H. Li, T. Shi, M. Yuan, X. Wang, Z. Jiang, One-pot depolymerization of cellulose into glucose and levulinic acid by heteropolyacid ionic liquid catalysis, - RSC Adv. 2 (2012) 9058-9065

[71] B. Girisuta, B.M. Janssen, H.J. Heeres, Kinetic Study on the Acid-Catalyzed Hydrolysis of Cellulose to Levulinic Acid, Ind. Eng. Chem. Res. 46 (2007) 1696-1708.

[72] T. Kim, R.S. Assary, R.E. Pauls, C.L. Marshall, L.A. Curtiss, P.C. Stair, Thermodynamics and reaction pathways of furfuryl alcohol oligomer formation, Catal. Commun. 46 (2014) 66-70.

[73] R. B.C, Process for the production of levulinic acid, US Patent: 2,738,367 (1956).

[74] W.D. Van De Graaf, J.P. Lange, Process for the conversion of Furfuryl Alcohol into Levulinic Acid or Alkyl Levulinate, US patent: 7,265,239B2 (2007).

[75] G.Maldonado, R. Assary, J. Dumesic, L. Curtiss, Experimental and theoretical studies of the acid-catalyzed conversion offurfuryl alcohol to levulinic acid in aqueous solution, Energy & Environment Science. 5 (2012) 6981-6989.

[76] M. Hronec, K. Fulajtárová, T. Soták, Kinetics of high temperature conversion of furfuryl alcohol in water, J. Ind. Eng. Chem. 20 (2014) 650-655.

[77] M. Hronec, K. Fulajta, T. Sota, Highly selective rearrangement of furfuryl alcohol to cyclopentanone, Appl. Catal B: Environmental, 154-155 (2014) 294-300

[78] T. Kim, R.S. Assary, H. Kim, C.L. Marshall, D.J. Gosztola, L.A. Curtiss, P.C. Stair, Effects of solvent on the furfuryl alcohol polymerization reaction: UV Raman spectroscopy study, Catal. Today. 205 (2013) 60-66.

[79] M. Hronec, K. Fulajta, T. Liptaj, Effect of catalyst and solvent on the furan ring rearrangement to cyclopentanone, Appl. Catal. A: General, 437-438 (2012) 104-111.

[80] L.M. Fuentes, G.L. Larson, A facile synthesis of 4-oxo carboxylic acids from γ-butyrolactone., Tetrahedron Lett. 23 (1982) 271-274.

[81] B.C. Redmond, Process for the production of levulinic acid, US Patent. 2,738,367 (1952).

[82] P. Neves, S. Lima, M. Pillinger, S.M. Rocha, J. Rocha, A.A. Valente, Conversion of furfuryl alcohol to ethyl levulinate using porous aluminosilicate acid catalysts, Catal. Today. 218–219 (2013) 76-84.

[83] Z. Zhang, K. Dong, Z. Zhao, Efficient Conversion of Furfuryl Alcohol into Alkyl Levulinates Catalyzed by an Organic–Inorganic Hybrid Solid Acid Catalyst, ChemSusChem. 4 (2011) 112-118.

[84] K. Tanabe, M. Misono, H. Hattori, Y. Ono, Solid Ácids and Bases their catalytic properties, 1 ed., Kodansha Ltd., 1989.

[85] H. Yamamoto, K. Maruoka, K. Furuta, Acid-Base Catalysis , Ed. Kodansha, Tokyo,. 1 (1988) 81-92.

[86] G. Busca, Chapter 6 - Metal Oxides as Acid-Base Catalytic Materials, in: G. Busca (Ed.), Heterogeneous Catalytic Materials, Elsevier, Amsterdam,(2014) 103-195.

[87] M. Tamura, K. Shimizu, A. Satsuma, Comprehensive IR study on acid/base properties of metal oxides, Appl. Catal A: General. 433–434 (2012) 135-145.

[88] P. Lauriol-Garbey, G. Postole, S. Loridant, A. Auroux, V. Belliere-Baca, P. Rey, J.M.M. Millet, Acid–base properties of niobium-zirconium mixed oxide catalysts for glycerol dehydration by calorimetric and catalytic investigation, Appl. Catal. B: Environmental. 106 (2011) 94-102.

[89] C. García-Sancho, R. Moreno-Tost, J. Mérida-Robles, J. Santamaría-González, A. Jiménez-López, P. Maireles-Torres, Zirconium doped mesoporous silica catalysts for dehydration of glycerol to high added-value products, Appl. Catal. A: General. 433–434 (2012) 179-187.

[90] C. García-Sancho, J.M. Rubio-Caballero, J.M. Mérida-Robles, R. Moreno-Tost, J. Santamaría-González, P. Maireles-Torres, Mesoporous Nb_2O_5 as solid acid catalyst for dehydration of d-xylose into furfural, Catal. Today. 234 (2014) 119-124.

[91] R. Ladera, E. Finocchio, S. Rojas, J.L.G. Fierro, M. Ojeda, Supported niobium catalysts for methanol dehydration to dimethyl ether: FTIR studies of acid properties, Catal. Today. 192 (2012) 136-143.

[92] Z. Yu, J. Wang, J. Ren, X. Liu, X. Li, Y. Xia, G. Lu, Y. Wang, Mesoporous niobium phosphate: an excellent solid acid for the dehydration of fructose to 5-hydroxymethylfurfural in water., Catal. Sci. Technol. 2 (2012) 2485-2491.

[93] E.I. Ross-Medgaarden, W.V. Knowles, T. Kim, M.S. Wong, W. Zhou, C.J. Kiely, I.E. Wachs, New insights into the nature of the acidic catalytic active sites present in ZrO2-supported tungsten oxide catalysts, J. Catal. 256 (2008) 108-125.

[94] K. Li, C. Wang, Esterification of lactic acid over TiO2–Al2O3 catalysts, Appl. Catal. A: General. 433–434 (2012) 275-279.

[95] J.H. Flores, M.I. Pais da Silva, Acid properties of the hybrid catalyst CuO–ZnO or CuO–ZnO–Al2O3/H-ferrierite: An infrared study, Colloids Surf. Physicochem. Eng. Aspects. 322 (2008) 113-123.

[96] H. Kao, H. Wu, Y. Liao, A.S.T. Chiang, Aluminosilicate MCM-48 mesostructures assembled from dried zeolite precursors and Gemini surfactant, Microporous Mesoporous Mater. 86 (2005) 256-267.

[97] J. Jolivet, C. Chanéac, D. Chiche, S. Cassaignon, O. Durupthy, J. Hernandez, Basic concepts of the crystallization from aqueous solutions: The example of aluminum oxy(hydroxi)des and aluminosilicates, Comptes Rendus Geoscience. 343 (2011) 113-122.

[98] J.A. Boscoboinik, X. Yu, B. Yang, S. Shaikhutdinov, H. Freund, Building blocks of zeolites on an aluminosilicate ultra-thin film, Microporous Mesoporous Mater. 165 (2013) 158-162.

[99] J.M. Thomas, J. Klinowski, The Study of Aluminosilicate and Related Catalysts by High-Resolution Solid-State NMR Spectroscopy, Adv. Catal. 33 (1985) 199-374.

[100] K.J.D. Mackenzie, M. Welter, 18 - Geopolymer (aluminosilicate) composites: synthesis, properties and applications, in: I.M. Low (Ed.), Advances in Ceramic Matrix Composites, Woodhead Publishing, (2014) 445-470.

[101] G. Perego, M. Cesari, G. Allegra, Ordered and disordered structures in borosilicates with a pentasil-type framework , J. Appl. Cryst. 17 (1984) 403.

[102] E. Babůrek, J. Nováková, Isomerization of n-butane over acid zeolites: Role of Broensted and Lewis acid sites, Appl. Catal A: General. 185 (1999) 123-130.

[103] K.M. Minachev, V.V. Kharlamov, A.M. Shkitov, A.S. Fomin, The Effect of Modification of H-Mordenite on its Activity and Selectivity in n-Pentane Isomerization in the Presence of Benzene, Mendeleev Commun. 3 (1993) 166-168.

[104] H. Förster, J. Seebode, Sorption and isomerization of cyclopropane in A-type zeolites studied by infrared spectroscopy, Zeolites. 3 (1983) 63-71.

[105] W. Aslam, M.A.B. Siddiqui, B. Rabindran Jermy, A. Aitani, J. Čejka, S. Al-Khattaf, Selective synthesis of linear alkylbenzene by alkylation of benzene with 1-dodecene over desilicated zeolites, Catal. Today. 227 (2014) 187-197.

[106] G.C. Laredo, R. Quintana-Solórzano, J.J. Castillo, H. Armendáriz-Herrera, J.L. Garcia-Gutierrez, Benzene reduction in gasoline by alkylation with propylene over MCM-22 zeolite with a different Brønsted/Lewis acidity ratios, Appl. Catal. A: General. 454 (2013) 37-45.

[107] T. Odedairo, S. Al-Khattaf, Comparative study of zeolite catalyzed alkylation of benzene with alcohols of different chain length: H-ZSM-5 versus mordenite, Catal. Today. 204 (2013) 73-84.

[108] H. Yamashita, Y. Mitsukura, H. Kobashi, K. Hiroki, J. Sugiyama, K. Onishi, T. Sakamoto, Microwave-assisted regioselective alkylation of naphthalene compounds using alcohols and zeolite catalysts, Appl. Catal. A: Gen. 381 (2010) 145-149.

[109] Z. Zhu, Q. Chen, Z. Xie, W. Yang, C. Li, The roles of acidity and structure of zeolite for catalyzing toluene alkylation with methanol to xylene, Microporous Mesoporous Mater. 88 (2006) 16-21.

[110] R. Anand, S.S. Khaire, R. Maheswari, K.U. Gore, Alkylation of biphenyl with t-butylalcohol over modified Y zeolites, J. Mol. Catal. A: Chem. 218 (2004) 241-246.

[111] S.R. Kirumakki, N. Nagaraju, K.V.R. Chary, S. Narayanan, A facile O-alkylation of 2-naphthol over zeolites Hβ, HY, and HZSM5 using dimethyl carbonate and methanol, J. Catal. 221 (2004) 549-559.

[112] Z. Zhu, Q. Chen, W. Zhu, D. Kong, C. Li, Catalytic performance of MCM-22 zeolite for alkylation of toluene with methanol, Catal. Today. 93–95 (2004) 321-325.

[113] R. Anand, S.S. Khaire, R. Maheswari, K.U. Gore, V.R. Chumbhale, N-Alkylation of aniline with ethanol over HY and dealuminated HY zeolites, Appl. Catal. A: Gen. 242 (2003) 171-177.

[114] R. Anand, R. Maheswari, K.U. Gore, V.R. Chumbhale, Selective alkylation of catechol with t-butyl alcohol over HY and modified HY zeolites, Catal. Commun. 3 (2002) 321-326.

[115] D. Venu Gopal, B. Srinivas, V. Durgakumari, M. Subrahmanyam, Vapor-phase alkylation of indole with methanol over zeolites, Appl. Catal. A: Gen. 224 (2002) 121-128.

[116] K. Zhang, H. Zhang, G. Xu, S. Xiang, D. Xu, S. Liu, H. Li, Alkylation of phenol with tert-butyl alcohol catalyzed by large pore zeolites, Appl. Catal. A: Gen. 207 (2001) 183-190.

[117] J. Aguilar, F.V. Melo, E. Sastre, Alkylation of biphenyl with methanol over Y zeolites, Appl. Catal. A: Gen. 175 (1998) 181-189.

[118] M. Hunger, U. Schenk, J. Weitkamp, Mechanistic studies of the side-chain alkylation of toluene with methanol on basic zeolites Y by multi-nuclear NMR spectroscopy, J. Mol. Catal. A: Chem. 134 (1998) 97-109.

[119] X. By: Meng, B. Ma, X. Zhang, F. Ling, Z. Zhang, F. Fan, Research progress in modification of USY zeolite as catalyst for petrochemical industry, Huagong Keji. 17 (2009) 59-65.

[120] O. Kazu, T. Takuya, O. Shizuyo, Y. Hiroyuki, N. Miki, Origin of the excellent catalytic activity of Pd loaded on ultra-stable Y zeolites in Suzuki–Miyaura reactions, J. Catal.. 273 (2010) 156-166.

[121] A. Corma, From microporous to mesoporous molecular sieve materials and their use in catalysis , Chem. Rev. 97 (1997) 2373.

[122] V.B. Kazansky, Catalytic site from a chemical point of view , Stud. Surf. Sci. Catal. 85 (1994) 251.

[123] L.A. Pine, P.J. Maher, W.A. Wachter, Prediction of cracking catalyst behavior by a zeolite unit cell size model , J. Catal. 85 (1984) 466.

[124] M.B. Pera-Titus, J. Tejero, M. Iborra, C. Fite´, F. Cunill, J.F. Izquierdo, Liquid-phase synthesis of isopropyl tert-butyl ether by addition of 2-propanol to isobutene on the oversulfonated ion-exchange resin Amberlyst-35, Appl. Catal. A. 323 (2007) 38-50.

[125] Rohm & Haas, Product data sheet of Amberlyst resin (2003) 1. http://www.dow.com/assets/attachments/business/process_chemicals/amberlyst/amberlyst_35wet/tds/amberlyst_35wet.pdf

[126] R. Bringué, E. Ramírez, M. Iborra, J. Tejero, F. Cunill, Kinetics of 1-hexanol etherification on Amberlyst 70, Chem. Eng. J. 246 (2014) 71-78.

[127] M. Naushad, Z.A. ALOthman, M.R. Khan, N.J. ALQahtani, I.H. ALSohaimi, Equilibrium, kinetics and thermodynamic studies for the removal of organophosphorus pesticide using Amberlyst-15 resin: Quantitative analysis by liquid chromatography–mass spectrometry, J. Ind. Eng. Chem. 20 (2014) 4393-4400

[128] S. Mustafa, K.H. Shah, A. Naeem, T. Ahmad, M. Waseem, Counter-ion effect on the kinetics of chromium (III) sorption by Amberlyst.15 in H+, Li+, Na+, Ca++, Al+++ forms, Desalination. 264 (2010) 108-114.

[129] R. Bringué, M. Cadenas, C. Fité, M. Iborra, F. Cunill, Study of the oligomerization of 1-octene catalyzed by macroreticular ion-exchange resins, Chem. Eng. J. 207–208 (2012) 226-234.

[130] K.F. Yee, A.R. Mohamed, S.H. Tan, A review on the evolution of ethyl tert-butyl ether (ETBE) and its future prospects, Renewable Sustainable Energy Rev. 22 (2013) 604-620.

[131] F. Collignon, R. Loenders, J.A. Martens, P.A. Jacobs, G. Poncelet, Liquid Phase Synthesis of MTBE from Methanol and Isobutene over Acid Zeolites and Amberlyst-15, J. Catal. 182 (1999) 302-312.

[132] N.S. Caetano, J.M. Loureiro, A.E. Rodrigues, MTBE synthesis catalysed by acid ion exchange resins: Kinetic studies and modeling of multiphase batch reactors, Chem. Eng. Sci. 49 (1994) 4589-4604.

[133] R.J. Gillespie, T.E. Peel, - Hammett acidity function for some superacid systems. II. Systems sulfuric acid-[fsa], potassium fluorosulfate-[fsa], [fsa]-sulfur trioxide, [fsa]-arsenic pentafluoride, [sfa]-antimony pentafluoride and [fsa]-antimony pentafluoride-sulfur trioxide, - J. Am. Chem. Soc. 95 (1973) 5173-5178.

[134] H. Matsuhashi, H. Shibata, H. Nakamura, K. Arata, Skeletal isomerization mechanism of alkanes over solid superacid of sulfated zirconia, Appl. Catal. A: Gen. 187 (1999) 99-106.

[135] V.M. Benítez, C.R. Vera, C.L. Pieck, F.G. Lacamoire, J.C. Yori, J.M. Grau, J.M. Parera, Silica supported superacid isomerization catalysts, Catal. Today. 107–108 (2005) 651-656.

[136] V.V. Brei, O.V. Melezhyk, S.V. Prudius, M.M. Levchuk, K.I. Patrylak, Superacid WOx/ZrO2 catalysts for isomerization of n-hexane and for nitration of benzene, Stud. Surf. Sci. Catal. 143 (2000) 387-395.

[137] M. Marczewski, H. Marczewska, K. Witosławski, Superacid properties of Al_2O_3-SbF5 catalytic system, J. Mol. Catal. A: Chem. 97 (1995) 101-110.

[138] Y. Saito, K. Ado, T. Asai, H. Kageyama, O. Nakamura, Y. Yamamoto, Enhancement of ionic conductivity of Na4Zr2Si3O12 by the dispersion of SbF5-adsorbed solid superacid particles, Solid State Ionics. 53–56, Part 2 (1992) 728-732.

[139] P. Fabre, J. Devynck, B. Tremillon, Electrochemical study of the methylcyclopentane oxidation in anhydrous hydrogen fluoride and HF−SbF5 superacid solutions, J. Electroanalytical. Chem. Interfacial. Electrochem. 113 (1980) 251-264.

[140] J.R. Sohn, D.H. Seo, Preparation of new solid superacid catalyst, zirconium sulfate supported on γ-alumina and activity for acid catalysis, Catal. Today. 87 (2003) 219-226.

[141] A. Corma, V. Fornés, M.I. Juan-Rajadell, J.M.L. Nieto, Influence of preparation conditions on the structure and catalytic properties of SO42−/ZrO2 superacid catalysts, Appl. Catal. A: Gen. 116 (1994) 151-163.

[142] K. Arata, H. Matsuhashi, M. Hino, H. Nakamura, Synthesis of solid superacids and their activities for reactions of alkanes, Catal. Today. 81 (2003) 17-30.

[143] K. Arata, Solid Superacids, Adv. Catal. 37 (1990) 165-211.

Capitulo 2. Objetivos

2.1. Objetivo principal

Tal como se ha mencionado en el capítulo 1, el ácido levulínico es un compuesto químico de alto valor añadido que puede ser obtenido a partir de la biomasa. El ácido levulínico se obtiene tradicionalmente mediante hidrólisis ácida de lignocelulosas (celulosa, hemicelulosa y lignina), mediante procesos de catálisis homogénea usando catalizadores ácidos inorgánicos (minerales), los cuales presentan serias desventajas económicas en aspectos importantes como la integración de procesos, la preservación de los equipos y la incompatibilidad ambiental.

En el marco de los procesos integrados de biorrefineria, una alternativa para la obtención de ácido levulínico es a partir de alcohol furfurílico, un compuesto más próximo en la cadena de producción de productos derivados de la biomasa. El alcohol furfurílico se obtiene a escala industrial a partir de furfural, lo que puede garantizar una producción continua de ácido levulínico. En este contexto el objetivo principal de esta Tesis Doctoral es **la preparación y evaluación de materiales catalíticos novedosos** para la obtención de ácido levulínico a partir de alcohol furfurílico mediante un proceso de catálisis heterogénea.

Para el desarrollo de este objetivo principal, se han planteado los objetivos específicos que se describen en el apartado siguiente.

2.2. Objetivos específicos

Para cumplir con el objetivo principal expuesto anteriormente, se proponen los siguientes objetivos parciales.

- Realizar una amplia revisión bibliográfica sobre los catalizadores sólidos ácidos que puedan ser utilizados en la reacción de obtención de ácido levulínico a partir de alcohol furfurílico. Entre el grupo de catalizadores ácidos están los de estructura orgánica, como las resinas de intercambio iónico tipo Amberlyst y Nafion que poseen grupos sulfónicos que le dan una característica de acidez fuerte. Por otro

lado están los catalizadores de estructura inorgánica como las zeolitas con distintas configuraciones de sílice-alúmina entre los que se destacan, HZSM-5, H-Y, H-USY, H-β, SBA-15, los óxidos metálicos de carácter ácido, los heteropoliácidos como el ácido fosfotungstico en diferentes soportes, así como los sólidos superácidos entre los que se destacan los óxidos de zirconio sulfatado.

- Estudiar la actividad catalítica de los catalizadores seleccionados. Para esto se plantean ensayos de actividad catalítica en diferentes sistemas de reacción que incluyen los sistemas de flujo continuo en un reactor de lecho fijo, semi-continuo y discontinuo (batch), y diferentes condiciones de operación.

- Caracterizar los catalizadores que presenten los mejores resultados de actividad catalítica en la obtención de ácido levulínico usando las técnicas de caracterización que aporten la mayor información fundamental respecto a la composición química, estructura, textura y propiedades termo-mecánicas de los catalizadores. En este sentido, la caracterización de los catalizadores debe centrarse en el estudio de las propiedades de los catalizadores que ejerzan mayor efecto en la reacción estudiada, como la acidez total, el tipo de acidez Brönsted y Lewis, el área superficial y el tamaño de poro.

- De acuerdo a los resultados de caracterización, centrar el estudio en la influencia de estas propiedades en la actividad catalítica. Para ello, aquellas formulaciones que mejores resultados presenten, se plantea mejorar las características físico-químicas (aumento de la acidez y/o tamaño de poro) y analizar su efecto sobre el rendimiento a ácido levulinico. Así mismo, realizar un ajuste de las principales variables de proceso usando el catalizador que presente los mejores resultados de actividad. Los ajustes en las condiciones de reacción incluiran la modificación de variables como la presión, temperatura, atmosfera de reacción, agitación, concentraciones óptimas de alimentación y la inclusión de elementos a la reacción como solventes inertes que permitan mejorar los rendimientos al ácido levulínico y minimizar los subproductos no deseados.

Capítulo 3. Materiales y técnicas experimentales

Tabla de contenido

3.1. Resumen 61

3.2. Materiales 62

3.3. Procedimiento de preparación de los catalizadores 63

3.3.1. Catalizadores de Nb_x/TiO_2 63

3.3.2. Catalizadores de Nb_x/USY 65

3.3.2.1. Preparación de los catalizadores de Nbx/USY por el método de impregnación húmeda 65

3.3.2.2. Preparación de los catalizadores de Nb_x/USY por el método de precipitación . 66

3.3.3. Preparación de los catalizadores de WO_x/Al_2O_3, Pt/Al_2O_3 y $Pt*WO_x/Al_2O_3$ 66

3.3.3.1. Preparación de los catalizadores Pt/Al_2O_3 y WO_x/Al_2O_3 67

3.3.3.2. Preparación de los catalizadores bimetálicos $Pt*WO_x/Al_2O_3$ 67

3.3.4. Preparación de los catalizadores "superácidos" La_xZrO_2/SO_4^{2-} 68

3.4. Técnicas de caracterización de catalizadores. 69

3.4.1. Espectroscopía de emisión óptica con plasma de acoplamiento inductivo (ICP-OES) 70

3.4.2. Energía de dispersión de rayos X (EDX-SEM) 70

3.4.3. Difracción de rayos X (XRD) 71

3.4.4. Isotermas de adsorción-desorción de nitrógeno 72

3.4.5. Temperatura programada de oxidación (TPO) 72

3.4.6. Desorción de amoníaco a temperatura programada (NH_3-TPD) 74

3.4.7. Espectroscopía infrarroja por transformada de Fourier (FT-IR) 75

3.4.8. Análisis de CHNS 76

3.4.9. Espectroscopía fotoelectrónica de rayos X (XPS) 77

3.5. Sistemas de reacción utilizados 78

3.5.1. Sistema de reacción en discontinuo ("batch") 78

3.5.2. Sistema de reacción en semicontinuo ("semi-batch") 81

3.5.3. Sistema de reacción en flujo continuo 82

3.6. Técnicas de análisis de reactivos y productos 83

3.6.1. Cromatografía gaseosa con detectores FID, TCD y espectrometría de masas 84

3.6.2. Toma de muestras para análisis 85

3.7. Referencias 87

3.1. Resumen

En este capítulo se realiza una descripción detallada de los elementos más importantes utilizados para el desarrollo de la parte experimental de la presente Tesis. El capítulo se inicia con una descripción de los materiales utilizados como reactivos, catalizadores y solventes, describiendo su pureza y las especificaciones del proveedor. Posteriormente, se describen los procedimientos empleados en la preparación de los catalizadores utilizados. Asimismo, se describen las técnicas de análisis utilizadas para la determinación cuantitativa y cualitativa de los reactivos y productos de reacción. A continuación se realiza una descripción de las diferentes técnicas de caracterización de los catalizadores usados, acorde a las necesidades del proyecto. En la parte final, se realiza una descripción de los sistemas de reacción utilizados para el estudio de la actividad catalítica.

3.2. Materiales

Los reactivos utilizados para el desarrollo de la actividad catalítica, para la preparación de los catalizadores usados en este proyecto y para el análisis mediante algunas técnicas de caracterización se muestran en las Tablas 3.1, 3.2 y 3.3 respectivamente, indicando en ellas el porcentaje de pureza, la marca del suministrador y el tipo de reacción en la que se utilizaron.

Tabla 3.1. Compuestos químicos utilizados en las reacciones.

Nombre del compuesto	Pureza (%)	Suministrador	Tipo de uso
Alcohol furfurílico	98,0	Merck	Reac- (1) - (2)
Ácido levulínico	98,0	Aldrich	Pat-Reac- (1)
Ciclopentanona	99,0	Aldrich	Reac- (1)
Ciclopentilmetileter	99,9	Aldrich	Sol-Reac (1)
2-Butanona (MEK)	99,5	Aldrich	Sol-Reac (1)
Ácido clorhídrico	37,0	Panreac	Cat-Reac (1)
Ácido sulfúrico	96,0	Panreac	Cat-Reac (1)
Tetrahidrofurano	99,9	Aldrich	Sol-Reac (1)
Acetona	99,5	Panreac	Sol-Reac (1)

Reac (1): Reacción de obtención de ácido levulínico a partir de alcohol furfurílico; Reac (2): Reacción obtención de 4-HCP y ciclopentanona a partir de alcohol furfurílico; Pat: patrón estándar; Sol: solvente; Cat: catalizador.

Tabla 3.2. Compuestos químicos utilizados en la preparación de los catalizadores

Nombre del compuesto	Pureza (%)	Suministrador	Tipo de uso
Zeolita ZSM-5, forma amoniacal Si/Al: 23, (23:1), hidratado	-	Alfa Aesar	Cat
Zeolita ZSM-5, forma amoniacal Si/Al: 52, (50:1), hidratado	-	Zeolyst International	Cat
Zeolita β, forma amoniacal (5:1), hidratado	-	Zeolyst International	Cat
Zeolita Y, forma amoniacal (5,1:1), hidratado	-	Alfa Aesar	Cat
Ácido fosfotungstico	99,995	Alfa Aesar	Cat
Hidróxido de sodio, pellets	97,000	Panreac	S- Cat
Cloruro de amonio	99,500	Panreac	S- Cat
Ácido clorhídrico	37,000	Panreac	S- Cat

Tabla 3.2. Continuación

Ácido sulfúrico	96,000	Panreac	S- Cat
AmberlystTM 47	-	Rohm Haas	Cat
Oxalato de niobio (V) hidratado	Hidratado	Alfa Aesar	S- Cat
Ácido oxálico	99,0	Aldrich	S- Cat
γ-Al_2O_3	99,9	Aldrich	S- Cat
Metatungstato de amonio	99,9	Aldrich	S- Cat
Nitrato-tetraaminoplatino	99,9	Aldrich	S- Cat
Oxido de titanio (Degusa P25)	99,5	Degussa	S- Cat
Nitrato de lantano (III) hidratado	99,9	Alfa Aesar	S- Cat
Zirconio (IV) oxinitrato, hidratado	99,0	Panreac	S-Cat

Cat: catalizador; S-Cat: Síntesis de catalizadores.

Tabla 3.3. Compuestos químicos utilizados en las técnicas de caracterización y en la medición de la actividad catalitica.

Nombre del compuesto	Pureza (%)	Suministrador	Tipo de uso
Tetrahidrofurano (THF)	99,000	Panreac	Solvente y lavado
Dimetisulfóxido (DMSO)	99,900	Aldrich	Lavado
Ácido fluorhídrico	60,000	Aldrich	Solvente
Nitrógeno líquido	98,000	Air liquide	Refrigerante
Nitrógeno (gas)	99,999	Air liquide	TPR, TGA, G,C, reactor
Helio	99,999	Air liquide	G.C
Oxígeno	99,995	Air liquide	TGA
Hidrógeno	99,993	Air liquide	TPR, Reactor.

TPR: Reducción a Temperatura Programada, TGA: Análisis Termogravimétrico, GC: Cromatografía de gases.

3.3. Procedimiento de preparación de los catalizadores

3.3.1. Catalizadores de Nb_x/TiO_2

Los catalizadores de óxido de niobio (Nb_2O_5) soportados sobre dióxido de titanio (TiO_2) se prepararon usando el método de impregnación húmeda (WI). Para ello, el soporte de TiO_2 se desgasifica usando un sistema de vacío en un rotavapor. Posteriormente, se

impregna el soporte con el niobio que se encuentra en su forma de oxalato de niobio diluido en ácido oxálico. La nomenclatura de los catalizadores preparados es Nb_x/TiO_2, donde "x" hace referencia al contenido teórico en peso. A manera de ejemplo, a continuación se detalla el procedimiento seguido para preparar el catalizador con un contenido de 1 % en peso de niobio (Nb_1/TiO_2). Siguiendo la misma metodología se prepararon catalizadores de niobio con contenidos entre 4 % y 24 % en peso. La Tabla 3.4 muestra las cantidades empleadas en la preparación de los distintos contenidos.

- Se pesaron 0,1158 g de oxalato de niobio y se disolvieron hasta 50 ml con una solución de ácido oxálico 0,1 M. A continuación se agitó la disolución a 500 rpm durante 12 horas hasta la completa disolución del sólido (solución de oxalato de niobio).
- Se pesaron 2,0033 gramos de TiO_2 y se llevó a un rotavapor, donde se desgasificó a una presión de vacío de 50 mmHg y 318 K, durante 40 minutos para eliminar algunos posibles contaminantes.
- Se incorporó la solución de oxalato de niobio al rotavapor y a continuación se volvió a ajustar la presión y temperatura a 50 mmHg y 318 K respectivamente. Seguidamente se procedió a la impregnación con la solución de oxalato de niobio previamente preparada.
- Aproximadamente 1 hora después, el material sólido seco se calcinó a 573 K para eliminar los restos de oxalato.

Tabla 3.4. Cantidades usadas en la preparación de los catalizadores de Nb_x/TiO_2

Catalizador	Masa oxalato-Nb (g)	Masa TiO_2 (g)	Volumen de aforo (mL)
Nb_1/TiO_2	0,1158	2,0033	50
Nb_4/TiO_2	0,4628	2,0015	50
Nb_8/TiO_2	0,9266	2,0033	50
Nb_{16}/TiO_2	1,8527	2,0002	50
Nb_{24}/TiO_2	2,7755	2,0009	50

X : contenido metálico teórico en porcentaje en peso respecto al soporte.

3.3.2. Catalizadores de Nb_x/USY

Los catalizadores de niobio soportados sobre la zeolita USY se prepararon por dos métodos: impregnación húmeda (M1) y precipitación-deposición (M2). En cada método se prepararon catalizadores con tres contenidos de niobio metálico: 1 %, 4 % y 8 % (% en peso).

3.3.2.1. Preparación de los catalizadores de Nb_x/USY por el método de impregnación húmeda

Para obtener la zeolita en la forma ultra estable y protonada (H-USY), una muestra de 20 gramos de zeolita Y, en su forma amoniacal, se calcinó hasta 773 K a 10 K/min durante 8 horas, en una atmósfera de aire húmedo. El oxalato de niobio en las cantidades especificadas en la Tabla 3.5 se disolvió hasta 50 ml con una disolución de ácido oxálico 0,1 M. La impregnación se realizó mediante la adición cuantitativa de la disolución de oxalato de niobio a 5 gramos de la zeolita H-USY, previamente desgasificado en un rotavapor a temperatura de 313 K, presión de vacío de 80 mbar y una velocidad de agitación de 100 rpm. Posteriormente, las muestras sólidas secas con el niobio impregnado se retiraron del sistema de rotavapor y se redujeron a menor tamaño "polvo fino" mediante pulverización manual usando un mortero. Finalmente, las muestras son calcinadas en aire a 773 K durante 4 horas.

Tabla 3.5. Cantidades usadas en la preparación de los catalizadores Nb_x/USY por el método de impregnación húmeda (WI).

Catalizador	Oxalato de Nb (g)	H- USY (g)	Volumen total (ml)
Nb_1/USYM1	0,1025	2,0010	50
Nb_4/USYM1	0,4303	2,0015	50
Nb_8/USYM1	0,9050	2,0005	50

x: contenido metálico teórico en porcentaje en peso respecto al soporte.

3.3.2.2. Preparación de los catalizadores de Nb_x/USY por el método de precipitación

A 5 gramos de la zeolita amoniacal tipo Y, se les incorporó la cantidad necesaria de una disolución de oxalato de niobio 0,1 M (ver Tabla 3.6) para obtener el contenido de niobio requerido. La reacción de intercambio iónico entre el ion oxalato y el amonio se llevó a cabo durante 24 horas con agitación a 600 rpm, generándose oxalato de amonio y un precipitado catiónico de niobio, que se deposita en el soporte (zeolita). Transcurrido el tiempo indicado, el sólido se separó del remanente líquido por filtración y se realizaron repetidos lavados del sólido retenido en el filtro con agua bidestilada hasta eliminar los oxalatos presentes. Las muestras se secaron a 378 K y fueron pulverizadas manualmente usando un mortero hasta obtener tamaños de partículas menores. Finalmente, las muestras se calcinaron a 773 K, en atmósfera de aire húmedo para obtener la forma ultra estable y protónica del material Nb_x/USY.

Tabla 3.6. Cantidades usadas en la preparación de los catalizadores Nb_x/USY por el método de precipitación

Catalizador	Oxalato de Nb (g)	NH_4-USY (g)	Volumen total (ml)
Nb_1/USYM2	0,2889	5,0005	100
Nb_4/USYM2	1,1563	5,0010	100
Nb_8/USYM2	2,3101	5,0001	100

x: contenido metálico teórico en porcentaje en peso respecto al soporte.

3.3.3. Preparación de los catalizadores de WO_x/Al_2O_3, Pt/Al_2O_3 y $Pt*WO_x/Al_2O_3$

Estos catalizadores fueron preparados usando el método de impregnación húmeda. El procedimiento para la preparación de los catalizadores bimetálicos, platino-wolframio, se desarrollo incorporando primero el wolframio en el soporte de γ-Al_2O_3 (WO_x/Al_2O_3), y sobre éste material, posteriormente se impregnó el platino. Antes del estudio de actividad, todos los catalizadores fueron calcinados a 723 K usando un flujo de aire de

20 mL/min y posteriormente, fueron reducidos con un flujo de hidrógeno a la misma temperatura. Las cantidades usadas para la preparación de todos los catalizadores (tabla 3.7) se eligieron para obtener aproximadamente un 5 wt% de cada metal en el soporte.

3.3.3.1. Preparación de los catalizadores Pt/Al_2O_3 y WO_x/Al_2O_3

Metatungstato de amonio ($(NH_4)_6(H_2W_{12}O_{40})*nH_2O$) o tetra-amino-platino ($(Pt(NH_3)_4(NO_3)_2$) en la cantidad descrita en Tabla 3.7, se disolvió hasta 100 mL con agua bidestilada. A continuación la disolución metálica se adicionó cuantitativamente a 2 gramos de soporte (γ-Al_2O_3) que previamente fue des-gasificado a temperatura de 313 K y presión de vacío de 50 mmHg en un rotavapor. La mezcla ubicada en el rotavapor fue tratada a las mismas condiciones de temperatura y presión durante aproximadamente 1 hora, para generar la evacuación del agua y permitir la impregnación del metal en el soporte. El sólido obtenido se secó a 383 K durante 2 horas y posteriormente se calcinó a 723 K en aire con una rampa de calentamiento de 2 K/min, durante 4 horas.

3.3.3.2. Preparación de los catalizadores bimetálicos $Pt*WO_x/Al_2O_3$

La preparación del catalizador bimetálico de platino y wolframio soportado en γ-Al_2O_3 se hizo añadiendo la cantidad de tetra-amino-platino ($(Pt(NH_3)_4(NO_3)_2$) (descrita en Tabla 3.7) en 2 gramos de catalizador WO_x/Al_2O_3, que previamente fue preparado siguiendo el procedimiento descrito en la sección 3.3.3.1. La impregnación se realizó usando el mismo procedimiento y bajo las mismas condiciones de temperatura y presión descritas en la sección 3.3.3.1.

Tabla 3.7. Cantidades usadas en la preparación de los catalizadores $Pt*WO_x/Al_2O_3$ por el método de impregnación húmeda.

Catalizador	Metatungstato de amonio (g)	cloruro de tetraminoplatino(II) (ml)
WO_x/Al_2O_3	1,6085	-
Pt/Al_2O_3	-	0,1732
$Pt*WO_x/Al_2O_3$	1,6077	0,1715

3.3.4. Preparación de los catalizadores "superácidos" La_xZrO_2/SO_4^{2-}

Para la preparación de los catalizadores "superácidos", diferentes valores de lantano (La) fueron usados respecto al zirconio (Zr). Los porcentajes de relación molar de La/Zr empleados para la preparación de los catalizadores fueron: 0,00; 0,53; 1,06. El procedimiento de preparación detallado se describe a continuación:

6 gramos de $ZrN_2O_7*xH_2O$ se disolvieron en 20 ml de H_2O bidestilada, a continuación 0,06 gramos de $La(NO_3)_3*6H_2O$ se disolvieron en 10 ml de H_2O, y ambas soluciones se unieron, completando hasta 50 ml con H_2O bidestilada. Se ajusto el pH de la disolución final a valores entre 9 y 10, usando hidróxido de amonio concentrado, en un equipo de ultrasonidos; el ajuste de pH generó la formación de un precipitado, compuesto por una mezcla de hidróxidos de zirconio y lantano. A continuación se traslado el precipitado a un congelador cuya temperatura se estableció a 255 K, durante 4 horas. El sólido se separó de la solución acuosa mediante el uso de un papel de filtro común, con ayuda de un sistema de vacío. El sólido retenido se secó a 383 K durante 6 horas hasta que los cristales estuvieron completamente secos. El contenido total, seco y pulverizado, se sumergió en 25 ml de una disolución de H_2SO_4 0,5 M, durante 12 horas, a continuación se separo nuevamente el sólido presente en la disolución y se secó a 383 K. La muestra seca fue calcinada durante 4 horas a 923 K, con incrementos de temperatura de 5 K/min y un flujo de aire de 1 L/min. Se repitió el mismo procedimiento usando 0,12 g de lantano. Las muestras fueron nombradas como ZrO_2/SO_4^{2-}, $La_{0.53}ZrO_2/SO_4^{2-}$, $La_{1.06}ZrO_2/SO_4^{2-}$.

3.4. Técnicas de caracterización de catalizadores.

Las técnicas de caracterización utilizadas para la determinación de las propiedades de los catalizadores desarrollados en esta investigación se describen en este apartado. La elección de cada una de estas técnicas responde a las necesidades y requerimientos de cada etapa de la investigación y la información obtenida se ha empleado para estimar la importancia de una propiedad u otra del catalizador en el desarrollo de la reacción objeto de estudio en cada capítulo. La caracterización de los catalizadores se realizó en diferentes centros de investigación los cuales se nombran a continuación; en alguno de los cuales el Doctorando pudo realizar estancias de al menos tres meses.

- Instituto de Catálisis y Petroleoquímica (ICP), que está adscrito al Consejo Superior de Investigaciones Científicas (CSIC) en Madrid (España). Estancia predoctoral de 3 meses.
  -Técnicas empleadas: acidez total (Quimisorción), acidez Bronsted y Lewis (FT-IR), TPO, XPS.

- Unidad de Catálisis y de Química del Sólido (UCCS), de la Universidad de Lille 1, Lille (Francia). Estancia predoctoral de 4 meses.
  -Técnicas empleadas: acidez total (NH_3-TPD), EDX, BET.

- Servicios Generales de Investigación de la UPV/EHU, (SGIker).
  -Técnicas empleadas: XPS, XRD.

- Laboratorios de Análisis e Investigación del Departamento de Ingeniería Química y del Medio Ambiente, Escuela Técnica Superior de Ingeniería de Bilbao (ETSI), grupo de Investigación SUPREN.
  -Técnicas empleadas: ICP(OES), TGA, CHNS, acidez Bronsted y Lewis (FT-IR), BET.

- Departamento de Química Inorgánica, Cristalografía y Mineralogía, Facultad de Ciencias, Universidad de Málaga (UMA).
  -Técnicas empleadas: acidez total NH_3-TPD, acidez Bronsted y Lewis FT-IR, BET.

3.4.1. Espectroscopía de emisión óptica con plasma de acoplamiento inductivo (ICP-OES)

La determinación de la composición química de algunos catalizadores se efectuó mediante la técnica de espectroscopía de emisión óptica con plasma de acoplamiento inductivo (ICP-OES), usando un equipo Perkin Elmer Optima 2000 DV con cámara de spray SCOTT. La técnica se basa en la radiación emitida cuando un átomo o ión excitado por absorción de energía de una fuente caliente, se relaja a su estado fundamental [1, 2]. La cantidad de energía emitida dependerá de la cantidad de átomos presentes del metal correspondiente. Por tanto, el primer paso es la atomización de la muestra. Para excitar los átomos se utiliza plasma de argón a $1x10^4$ K, constituido por una mezcla gaseosa conductora de electrones y cationes de la muestra a analizar. Para determinar la concentración, esencialmente, se necesita un nebulizador para conseguir un aerosol de partículas y un atomizador que mediante calentamiento (plasma) produce átomos o iones independientes. Así, solo se necesita un sistema de excitación térmico, la propia fuente de atomización, y un detector.

Para determinar la concentración de los metales, se realizan en primer lugar las curvas de calibración correspondientes a cada metal en el intervalo de concentración comprendido entre 0 y 10 mg/L. Para cada metal se emplean tres puntos de calibración, los límites de detección están alrededor de 0,1 ppb. Las disoluciones se prepararon a partir de disoluciones patrón certificadas para análisis de emisión atómica de 1000 mg/L en medio ácido. Antes de realizar el análisis, las muestras se sometieron a un tratamiento de digestión hasta conseguir la disolución de todos los componentes metálicos presentes en las muestras sólidas.

3.4.2. Energía de dispersión de rayos X (EDX-SEM)

El equipo de energía de dispersión de rayos X provisto de un detector SEM (EDX-SEM) se utilizó para cuantificar el contenido metálico de algunos catalizadores. Esta técnica analítica es utilizada para el análisis elemental o caracterización química de una amplia gama de elementos de la tabla periódica [3-5]. La técnica se basa en la

interacción de una fuente de excitación de rayos X sobre un sólido. Su capacidad de caracterización se debe en gran parte al principio fundamental de que cada elemento tiene una estructura atómica única, que permite un único conjunto de picos en su espectro de rayos X.

El microscopio utilizado fue un Hitachi S3600N SEM, equipado con un detector (Thermo Ultra Dry) a un voltaje de aceleración de 15 kV. El detector de rayos X es capaz de detectar elementos químicos de número atómico comprendido entre los del carbono y el uranio. Se tomaron imágenes de las distintas partes analizadas a diferentes aumentos para establecer el punto exacto de análisis de la muestra. La microscopía electrónica de barrido presenta la ventaja frente a las demás técnicas, de poder observar la zona microscópica que se está analizando, así como la posibilidad de obtener imágenes de dicha zona.

3.4.3. Difracción de rayos X (XRD)

La difracción es un fenómeno de dispersión, mediante el cual los átomos dispersan la radiación incidente en todas las direcciones; en algunas direcciones los rayos dispersados están en fase completamente, por lo que se obtienen rayos difractados según la constitución de la red cristalina y la separación entre planos de átomos [6]. Los rayos dispersados estarán en fase completamente cuando la diferencia de fase sea igual a un número entero de n-longitudes de onda, esta relación se conoce como ley de Bragg [7].

Esta técnica de rayos X se utilizó con el fin de determinar la cristalinidad y el ordenamiento estructural de los metales en los catalizadores objeto de investigación. La técnica consiste en analizar los picos obtenidos en un difractograma para obtener la estructura química que tiene un compuesto determinado. Esta técnica analiza las intensidades de los picos y les asigna un ángulo de rotación a cada uno de ellos, de esta forma se puede determinar las características estructurales del sólido, la disposición de los átomos metálicos en la red cristalina y las distancias entre los planos de red.

Los espectros XRD de los catalizadores se obtuvieron en un equipo Philips X'Pert Pro, trabajando a 40 kV y 40 mA. Se utilizó un monocromador secundario con radiación Cu-Ka (λ = 1,5418 Å) y un detector de estado sólido Pixcel (longitud activa en 2θ 3,347 º).

Los datos fueron analizados en ángulos de Bragg 2θ entre 5 º a 80 ° (tamaño de paso = 0,02606 y tiempo por paso = 51s).

3.4.4. Isotermas de adsorción-desorción de nitrógeno

Las isotermas de adsorción de nitrógeno a 77 K se realizaron con objeto de determinar las propiedades texturales (superficie específica, tamaño y volumen de poro) de los diversos catalizadores preparados. Estos análisis se llevaron a cabo en los equipos Autosorb 1C-Quantachrome (instalaciones del grupo SUPREN), Micromeritics ASAP 2010 V3 (instalaciones del grupo UCCS) y ASAP 2020 V4 (instalaciones de UMA). Como procedimiento básico previo a la adsorción, las muestras se sometieron a un tratamiento de desgasificación a vacío, con el fin de eliminar todo tipo de compuestos inicialmente adsorbidos sobre su superficie. Posteriormente, se dosificó la cantidad adecuada de nitrógeno para cubrir todo el intervalo de presiones relativas hasta aproximarse al valor de saturación (P/P_0= 0,976), registrándose en todos los casos los valores de adsorción y desorción de la isoterma. La determinación de la superficie específica de los catalizadores se llevó a cabo mediante la aplicación de los procedimientos BET (Brunauer, Emmett y Teller, 1938) y Langmuir, este ultimo apropiado para materiales microporosos [8].

3.4.5. Temperatura programada de oxidación (TPO)

El análisis de temperatura programada de oxidación (TPO) es una técnica de análisis térmico que se realiza en atmósfera de aire o de oxígeno en mezcla con nitrógeno o argón. Esta técnica consiste en incrementar la temperatura de un sólido (catalizador) en atmósfera oxidante y fijar los valores de temperatura de oxidación de las especies metálicas presentes en el catalizador. También se puede utilizar para estudiar la eliminación de coque incrustado en los catalizadores.

En el desarrollo de este trabajo se emplearon dos métodos para determinar las temperaturas de oxidación. El primer método fue usado en los catalizadores de niobio

soportados sobre la zeolita USY y consistió en una modificación del método termogravimétrico TGA. Usualmente la técnica de análisis termogravimétrico permite determinar la pérdida de peso de una muestra en función de la temperatura y la estabilidad térmica de un material. Sin embargo, cuando el incremento de temperatura se hace en una atmosfera oxidante, los elementos metálicos presentes en la muestra solida se oxidan generando un incremento de peso que es registrado por una micro balanza. Las muestras fueron analizadas en un equipo Mettler Toledo, TGA/SDTA 851^e, que está provisto de entrada de gases y de un sistema de refrigeración. El procedimiento usado para los análisis fue el siguiente: debido a que las muestras analizadas poseen un alto contenido de humedad, se realizaron dos etapas de calentamiento. En la primera etapa, la muestra sólida se depositó en un crisol que fue previamente pesado por la micro balanza (volumen del crisol: 900 µl), y que posteriormente se colocó en la cámara de temperatura de manera automática por un robot. La temperatura se incrementó a 10 K/min hasta 673 K usando una atmósfera de nitrógeno, de manera que se produzca la eliminación de la humedad presente en la muestra. Una vez que la muestra se enfrió hasta los 373 K, se inició la segunda etapa de calentamiento a una rampa de 10 K/min, hasta alcanzar la temperatura de 823 K en atmósfera de aire sintético. Este proceso permite la oxidación de los elementos metálicos presentes. La micro balanza registró el peso exacto de la muestra mediante diferencia con el peso del crisol vacío, los valores de las temperaturas a la que se produce la oxidación del metal se observan mediante un leve incremento del peso de la muestra.

El segundo método usado para realizar la TPO fue empleado en los catalizadores de niobio soportados sobre óxido de titanio. En este caso, 50 mg de catalizador fueron cargados en un reactor de cuarzo en forma de U conectado a un espectrómetro de masas Balzer Prisma TM cuadrupolo QMS 200. El análisis se desarrolló calentando la muestra desde la temperatura ambiente (303 K) hasta 600 K a una velocidad de calentamiento de 10 K/min y con un flujo de 50 mL/min de una mezcla de O_2/Ar 20 vol%. Los fragmentos de m/z = 18 (H_2O+), m/z = 28 (CO+) y m/z = 44 (CO_2+) se monitorizaron de forma continua con el espectrómetro de masas.

3.4.6. Desorción de amoníaco a temperatura programada (NH_3-TPD)

Las medidas de desorción de amoníaco a temperatura programada (NH_3-TPD) se realizaron con el objeto de determinar la acidez total y distribución de fuerza ácida de los diferentes catalizadores sintetizados. El fundamento de la técnica es el de saturar la superficie del catalizador con amoníaco, que se adsorbe en sus centros ácidos accesibles, y someterlo a continuación a un rampa de calentamiento controlada. Al calentar, la desorción del amoníaco se efectúa a mayor o menor temperatura en función de la fuerza de los centros ácidos presentes en el sólido. La selección de amoníaco como molécula sonda se realiza por sus características fuertemente básicas, que permite su adsorción en prácticamente la totalidad de centros ácidos presentes, aún siendo débiles, y por su reducido tamaño, que posibilita su acceso a los centros ácidos que se encuentran en el interior de los micro poros de las zeolitas.

El procedimiento de análisis se llevó a cabo en las instalaciones del grupo de investigación de la UCCS y es resumido a continuación. Los catalizadores se sometieron a un tratamiento de desgasificación a fin de eliminar las sustancias adsorbidas física y químicamente en sus centros ácidos. La desgasificación se hizo bajo una corriente de helio y una rampa de calentamiento de 10 K/min hasta la temperatura programada (823 K para el caso de las zeolitas y 923 K para los materiales "superácidos"), manteniendo la temperatura final durante 30 minutos. Tras la desgasificación, se enfrió la muestra hasta 373 K y se hizo pasar una corriente de NH_3 mediante 15 pulsaciones de 175 μL. Finalmente, se llevó a cabo la desorción térmica de amoníaco, sometiendo la muestra a una rampa de calentamiento controlada (10 K/min) bajo flujo de helio (30 mL/min) hasta que se alcanzó la temperatura establecida, valor al que se mantuvo durante 30 minutos. El amoníaco desorbido a diferentes temperaturas fue arrastrado por la corriente de helio y se registró con un detector de conductividad térmica.

La cantidad total de centros ácidos existentes en el catalizador se calculó a partir del área bajo la curva de desorción mediante la aplicación de un factor de respuesta obtenido en una calibración previa (15 pulsaciones). Asimismo, la temperatura correspondiente al máximo de la curva de desorción se encuentra estrechamente relacionada con la fuerza ácida de los centros, y se considera habitualmente como una

medida directa de la misma con fines comparativos. No obstante, la técnica presenta la limitación de no permitir distinguir entre centros ácidos de tipo Brönsted o Lewis, ya que el amoníaco se adsorbe en ambos.

3.4.7. Espectroscopía infrarroja por transformada de Fourier (FT-IR)

Los espectros de reflectancia difusa en el infrarrojo por transformada de Fourier (FT-IR) de piridina se realizaron para determinar la naturaleza, distribución y fuerza de los centros ácidos Brönsted y Lewis presentes en los catalizadores utilizados en los ensayos catalíticos. La técnica consiste en tratar el catalizador con piridina que es una base que se adsorbe en los centros ácidos accesibles, para después calentar el material de forma controlada y producir la desorción de la molécula (piridina) en función de la fuerza de los centros ácidos presentes en el sólido. Muchos autores han usado piridina como molécula sonda por sus características básicas, que permiten su adsorción en prácticamente la totalidad de centros ácidos presentes y distinguir entre centros ácidos tipo Lewis o tipo Brönsted [9-15].

Una parte de la caracterización de esta propiedad se realizó en el Instituto de Catálisis y Petroleoquímica de Madrid, ICP- CSIC. Este centro de investigación cuenta con un espectrofotómetro Nicolet 5700 equipado con una fuente global y un tipo de crio-detector de Hg-Te-Cd que trabaja en el rango de 4000 a 650 cm^{-1} de longitud de onda. También se utilizó un accesorio óptico Praying Mantis y una cámara in-situ Harrick Scientific Products NY, donde se colocaron las muestras en cantidad aproximadamente de 50 mg finamente pulverizadas. Previamente, las muestras se secaron a 398 K durante 1 hora bajo flujo de argón. Posteriormente, las muestras se impregnaron con piridina y la fracción de piridina fisisorbida se eliminó haciendo pasar un flujo de argón durante 1 h antes de la recogida de los espectros a diferentes temperaturas.

En los Servicios Generales de la UPV/EHU se cuenta con un espectrómetro VERTEX 70 BRUKER XSA con dos módulos: Vertex 70 con detector DTGS y XSA con detector MCT. El equipo posee una cámara de alta temperatura de reacción diseñada para operar hasta 1183 K en alto vacío, el controlador de temperatura es ATC-024-3. En este equipo se realizó la determinación de los sitios ácidos Brönsted y Lewis para los catalizadores

tipo zeolita H-ZSM5 que son estudiados en el capítulo 5. Las condiciones de análisis se resumen a continuación:

Pre-tratamiento de la muestra:

Desgasificación a 723 K, a vacío durante 2 horas.

Adsorción de piridina:

A 313 K durante 1 hora.

Desorción de piridina y toma de espectros:
313 K y 413 K

La naturaleza de los centros ácidos presentes en las muestras analizadas se determinaron a partir de las correspondientes bandas asociadas con la adsorción de moléculas de piridina en centros Lewis o Brönsted.

3.4.8. Análisis de CHNS

Esta técnica de análisis químico elemental permite determinar el contenido total de carbono, hidrógeno, nitrógeno y azufre (C, H, N, S) presente en muestras sólidas o líquidas. Específicamente esta técnica se empleó para determinar la proporción de azufre presente en los catalizadores sólidos frescos y usados, con el objeto de analizar el grado de desactivación de los mismos, determinando la pérdida de dichos grupos por lixiviado, durante el proceso de reacción.

Los análisis se realizaron en un analizador elemental LECO TruSpec Micro delivers y el método analítico se basa en la oxidación completa e instantánea de la muestra que transforma todos los compuestos presentes en productos de combustión. Los gases resultantes de la combustión son transportados mediante un caudal de 100 mL/min de gas portador (He) a través de un tubo de reducción y después selectivamente separados en columnas específicas para luego ser resorbidos térmicamente. Finalmente, los gases pasan de forma separada por un detector de conductividad térmica que proporciona una señal proporcional a la concentración de cada uno de los componentes individuales de la muestra.

3.4.9. Espectroscopía fotoelectrónica de rayos X (XPS)

La espectroscopía fotoelectrónica de rayos X es uno de los métodos de caracterización de superficie más ampliamente utilizado en la actualidad. La popularidad de esta técnica deriva del alto contenido de información que suministra y la flexibilidad para ser utilizada en una gran variedad de muestras. La técnica XPS se cataloga dentro de las técnicas analíticas de espectroscopía electrónica, denominadas de este modo porque se miden electrones [16]. El análisis XPS más básico de una superficie puede proporcionar información cualitativa y cuantitativa de todos los elementos presentes, excepto hidrógeno y helio. Con aplicaciones más sofisticadas de la técnica se obtiene información detallada de la organización y morfología de la superficie. La técnica XPS es muy específica de la superficie, debido al corto alcance de los fotoelectrones que son excitados del sólido. La energía de los fotoelectrones que salen de la muestra se determina usando un analizador (entre los más usados son el hemisférico concéntrico (CHA)), el cual da un espectro con una serie de picos de fotoelectrones. La energía de enlace de los picos es característica de cada elemento. Las áreas de los picos se pueden utilizar para determinar la composición de la superficie de los materiales. La forma de cada pico y la energía de enlace pueden ser alterados ligeramente por el estado químico del átomo emisor de luz. Por lo tanto, el análisis de XPS puede proporcionar también información sobre los enlaces químicos.

En este trabajo, los espectros XPS fueron obtenidos por dos equipos. Los resultados correspondientes al estudio de catalizadores de niobio se realizaron en el ICP-CSIC. Este centro de investigación cuenta con un equipo provisto de un analizador Phoibos 150 1D-DLD con radiación monocromática Al Ka (1486,6 eV) y fuentes de rayos X. En este caso, las energías de enlace fueron calibradas con respecto al pico C1s.

Los espectros XPS correspondientes al estudio sobre los catalizadores "superácidos" (Zr y La) se obtuvieron en los Servicios Generales de la UPV/EHU (SGIker). El equipo es un sistema SPECS (Berlin, Alemania) equipado con analizador Phoibos 150 1D-DLD y fuente radiación monocromática Al Kα (1486,6 eV). Se llevó a cabo un análisis inicial de los elementos presentes (wide scan: step energy 1 eV, dwell time 0,1 s, pass energy 80 eV) y se realizaron análisis detallados de los elementos presentes (detail scan: step energy 0,1 eV, dwell time 0,1 s, pass energy 30 eV) con un ángulo de salida de

electrones de 90º. Los espectros fueron ajustados mediante el software CasaXPS 2.3.16, que modeliza las contribuciones Gauss-Lorentzian, después de una substracción del fondo (Shirley).

3.5. Sistemas de reacción utilizados

Los ensayos de actividad catalítica se realizaron en las instalaciones de los laboratorios de investigación del Departamento de Ingeniería Química y del Medio Ambiente de la Escuela Técnica Superior de Ingeniería de la Universidad del País Vasco/Euskal Herriko Unibertsitatea (UPV/EHU) y en las instalaciones del Grupo de Investigación de Energía y Química Sostenible del Instituto de Catálisis y Petroleoquímica (ICP-CSIC). Las infraestructuras empleadas tanto para los procesos de reacción como para los análisis de reactivos y productos se describen a continuación.

3.5.1. Sistema de reacción en discontinuo ("batch")

El estudio de la actividad catalítica en sistema de reacción discontinuo se realizó en una serie de reactores de vidrio marca "Vineland N.J, Ace glass incorporated USA", de 15 cm de longitud y 17 mm de diámetro interno con capacidad de 15 mL. Una vez que los reactivos y el catalizador son cargados en el reactor, se introduce un agitador magnético, se purga durante 3 minutos con nitrógeno para desplazar el aire presente, a continuación se cierra herméticamente y se coloca en un baño de aceite, el cual está a la temperatura de reacción. El baño de aceite es calentado por una placa calefactora tipo IKA RTC Basic, con límites de regulación de temperatura de 0 a 583 K y de agitación entre 0-1200 rpm (Figura 3.1). La placa posee un termopar para el control de temperatura. Este tipo de dispositivo de reacción es usado en reacciones que se llevan a cabo en condiciones de temperatura y presión bajas.

En este trabajo, la presión de operación corresponde a la presión autógena generada cuando el sistema de reacción alcanza la temperatura de operación mediante el incremento de la temperatura en el sistema de reacción cerrado.

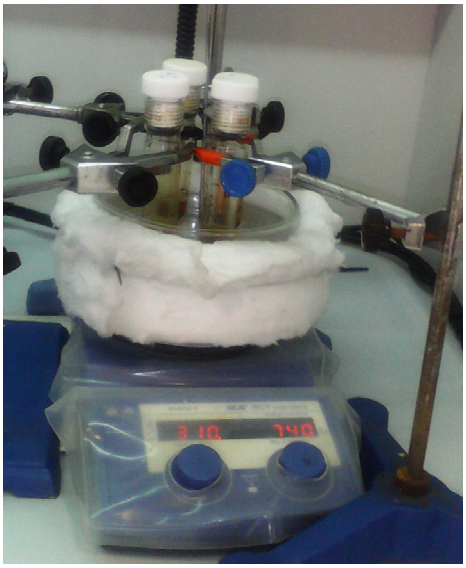

Figura 3.1. Montaje para las reacciones en sistema discontinuo ("batch").

Por otro lado, cuando se desarrollaron estudios de actividad a presiones superiores a la autógena y cuando fue necesario incluir gas hidrógeno en el medio de reacción, se utilizó un mini-reactor agitado de acero inoxidable (Parker Autoclave Engineers, Iberfluid Instruments S.A) con capacidad de 50 mL, equipado con una camisa calefactora que recubre el reactor para su calentamiento (Figura 3.2).

El sistema de la Figura 3.2 está equipado con un control automático para la regulación de la de temperatura y velocidad de agitación, y un indicador de presión (manómetro Bourdon). Además, dispone de conexiones para la recogida de muestras líquidas y para la entrada y salida de gases.

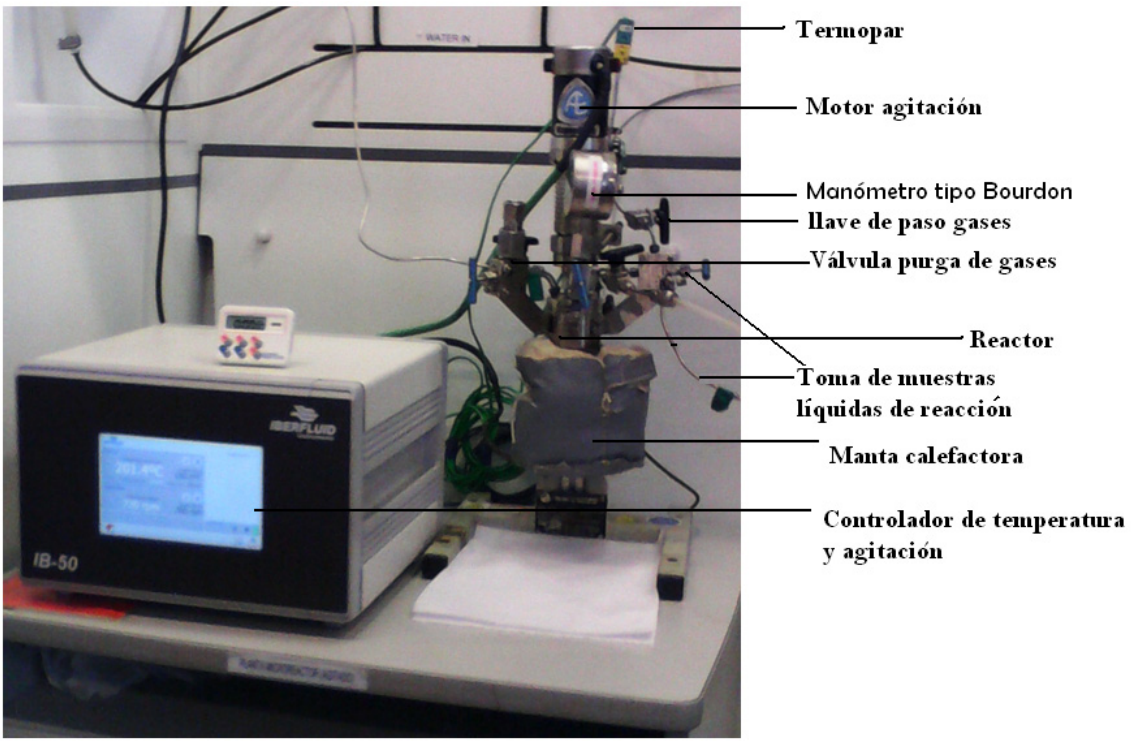

Figura 3.2. Reactor autoclave de acero inoxidable con controlador de temperatura y agitación

Las especificaciones del reactor están resumidas en la Tabla 3.8. El procedimiento de operación en general consiste en introducir en el reactor la mezcla de reacción y el catalizador, a continuación se cierra el sistema y se introduce el gas (nitrógeno o hidrógeno) para eliminar el aire del reactor mediante repetidas purgas del sistema. Con el gas correspondiente se fija la presión de operación, se cierra todo el sistema de carga de gases, se inicia la agitación a 700 rpm y el calentamiento hasta la temperatura de operación deseada.

Tabla 3.8. Especificaciones y condiciones de operación del reactor autoclave de acero inoxidable.

Parámetro	*Valor*
Diámetro interno	35 mm
Volumen	50 mL
Longitud	85 mm
Temperatura máxima de operación	588 K
Presión máxima de operación	200 bar
Agitación	0-3000 rpm

3.5.2. Sistema de reacción en semicontinuo ("semi-batch")

Como una alternativa al proceso de reacción en "batch", el proceso semi-batch incluye una o más corrientes líquidas de alimentación controladas por una bomba peristáltica dosificadora. El reactor utilizado para los ensayos de actividad corresponde al descrito previamente en el apartado 3.5.1, al que se le incorporó una bomba de pistón marca Gilson 305 para la alimentación de reactivos líquidos. El esquema 3.1 muestra el diagrama del proceso.

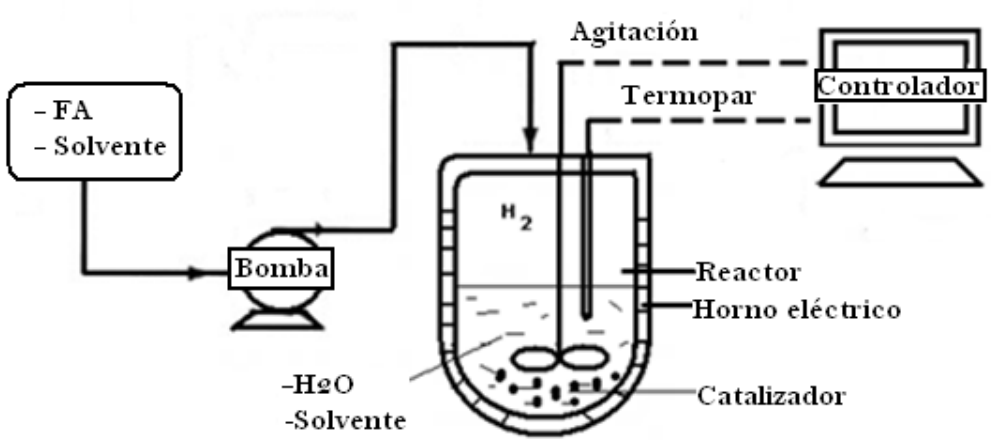

Esquema 3.1. Diagrama representativo del sistema semi-continuo utilizado

Cuando en el sistema de reacción se emplea agua y un co-solvente orgánico, se carga en el reactor una cantidad específica de catalizador, H_2O y de disolvente orgánico. El sistema se cierra y el aire del sistema es purgado con el gas hidrógeno o nitrógeno, según sea la atmósfera de reacción empleada (reductora o inerte). A continuación se presuriza el sistema con el gas correspondiente a la presión de operación, se pone en marcha la agitación y se comienza el calentamiento hasta alcanzar la temperatura de operación. Cuando la temperatura del sistema se estabiliza, se inicia la alimentación de flujo de una disolución que contiene una mezcla del reactivo principal y del disolvente orgánico, durante un tiempo tal que la concentración total del reactivo sea la establecida, tiempo a partir del cual el sistema comienza a operar como discontinuo.

3.5.3. Sistema de reacción en flujo continuo

Los ensayos de actividad en flujo continuo se desarrollaron en un reactor de lecho fijo incorporado en una planta piloto tipo PID Microactivity (Figura 3.3). La planta dispone de sistemas de medida y control de flujo másico de gases de alimentación y de temperatura y presión del reactor. Además, dispone de un horno eléctrico de potencia regulable, sistema separador gas- líquido mediante enfriamiento tipo peltier. El líquido es alimentado a la planta mediante una bomba Gilson modelo 307-30x v2.11.

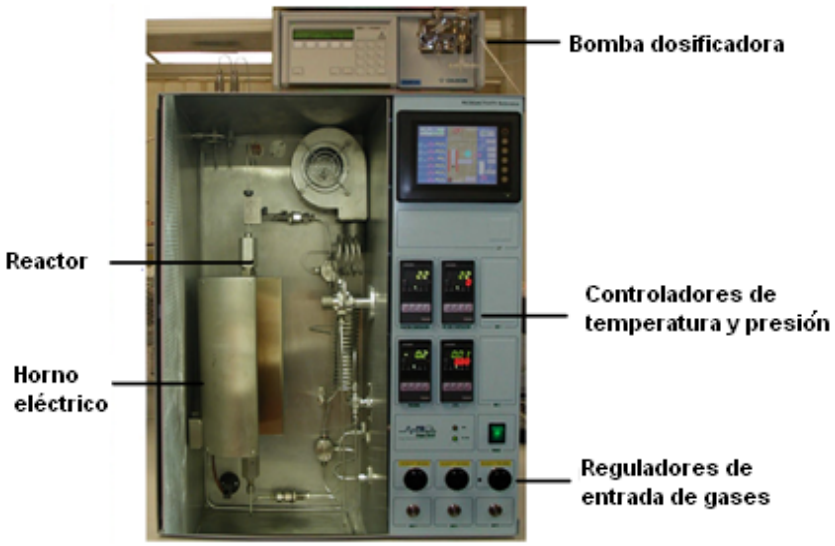

Figura 3.3. Planta PID Microactivity usada para los ensayos en reacción de flujo continuo

El reactor es de lecho fijo de 11,5 mm de diámetro interior y 300 mm de longitud. El lecho catalítico se sitúa en el centro del reactor y la parte superior e inferior del mismo se rellena con carburo de silicio que tiene un diámetro de partícula de 3,5 mm (ver Esquema 3.2). En el centro del lecho catalítico se mide la temperatura con un termopar tipo K. En los extremos internos del reactor empacado se colocan unas mallas metálicas y lana de cuarzo que sirven como soporte y filtro de posibles partículas sólidas finas.

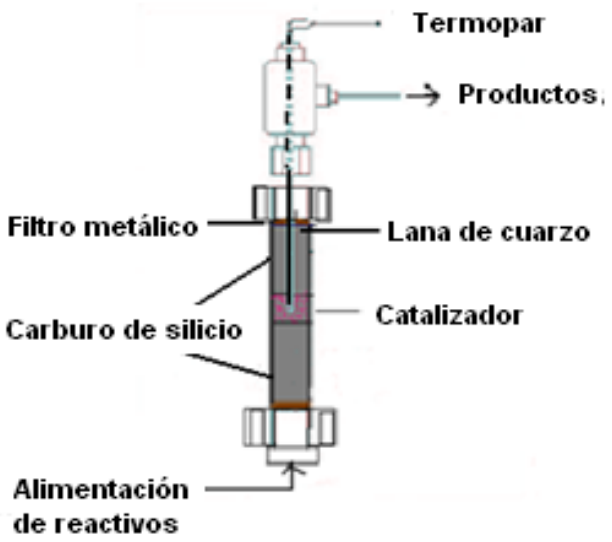

Esquema 3.2 Reactor tubular de lecho fijo.

El montaje del reactor consta de tres zonas. La primera zona está constituida por carburo de silicio (diámetro superior a 1 mm) hasta un nivel cercano al centro del reactor. A continuación una segunda zona formada por una mezcla de carburo de silicio (diámetro promedio $\leq$ 0,1 mm) y el catalizador con tamaño granular aproximado de 0,42 mm (esquema 3.2). Finalmente, la última zona constituida también por un lecho de carburo de silicio. Cuando el reactor ya está cargado, se colocó en el centro del horno y se conectaron las entradas y salidas de la planta. Se fijó la presión de operación con gas nitrógeno y a continuación se calentó hasta la temperatura de operación deseada. Una vez alcanzada la temperatura de operación, se comenzó a alimentar el flujo de la mezcla reaccionante. Durante la reacción, a intervalos de tiempo establecidos, se procedió a tomar muestras del producto líquido obtenido, para posteriormente ser analizados.

3.6. Técnicas de análisis de reactivos y productos

Los reactivos (líquidos) y productos de reacción (líquidos y gases) se identificaron y cuantificaron empleando diversas técnicas de análisis, las cuales se detallan a continuación.

3.6.1. Cromatografía gaseosa con detectores FID, TCD y espectrometría de masas

Esta técnica permitió la identificación y cuantificación de los reactivos y los productos de reacción. Para ello se emplearon dos equipos diferentes de cromatografía de gases. El primero es un cromatógrafo de gases Agilent Technologies modelo 6890N. Este cromatógrafo fue usado para la cuantificación de los principales compuestos de reacción. El cromatógrafo está equipado con dos detectores, uno de conductividad térmica (TCD) y otro de ionización de llama (FID). La columna capilar empleada para la separación de los compuestos es de tipo apolar, con un material 100 % de dimetil-polisiloxano, marca J&W Scientific, de 60 m x 0,53 mm. Las condiciones de operación del equipo para cada análisis fueron:

- Volumen de inyección: 0,5 µL
- Split: 50:1
- Flujo total He: 359 mL/min
- Flujo de aire: 325 mL/min
- Flujo H_2: 50 mL/min
- Flujo N_2: 5 mL/min

El segundo cromatógrafo de gases cuenta con un detector de espectrometría de masas (MS) usado para la identificación de los compuestos principales, mediante la obtención de los correspondientes espectros de masas y su comparación con la base de datos disponible en el software del equipo. Este cromatógrafo de gases Agilent Technologies modelo 6890 está equipado con una columna de alta polaridad de ácido nitro-teraptálico, modificada con poli etilenglicol y de dimensiones 60 m x 0,32 mm. El cromatógrafo esta acoplado a un detector de espectrometría de masas (MS) Agilent 5973 Network.

- Volumen de inyección: 0,1 µL
- Split: 50:1
- Flujo Split : 114 mL/min
- Flujo total He: 25,3 mL/min

3.6.2. Toma de muestras para análisis

El tratamiento de las muestras líquidas y/o de gases se desarrolló de la misma forma en todos los casos. Los elementos usados para la toma de muestra se pueden observar en la Figura 3.4. El procedimiento utilizado se explica a continuación.

Las muestras de reacción ***líquidas*** se recogen en frascos de vidrio topacio para protección de los rayos UV que pueden lentamente favorecer reacciones de oxidación y alterar los resultados. La muestra a analizar se extrae del frasco mediante una jeringuilla y se filtra a un vial de cromatografía a través de un filtro de 0,23 μm (Figura 3.4).

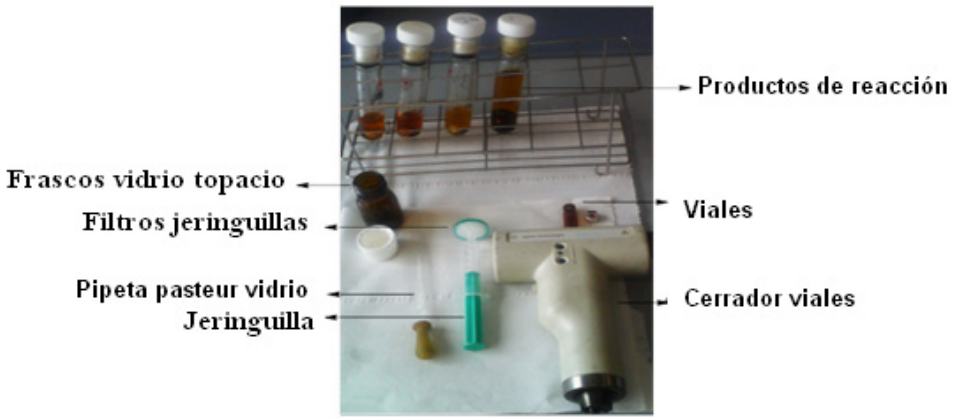

Figura 3.4. Elementos para toma y tratamiento de las muestras liquidas de reacción.

En el caso del sistema de reacción con autoclave, se recogieron muestras de gas en bolsas de polipropileno de 1 litro. Estas bolsas están provistas de una válvula manual que permite la entrada y salida del gas. Las muestras se tomaron en la línea de salida de gases del reactor al finalizar el ensayo correspondiente y a la temperatura de 303 K.

El gas es inyectado al cromatógrafo mediante succión con una bomba de membrana (Figura 3.5).

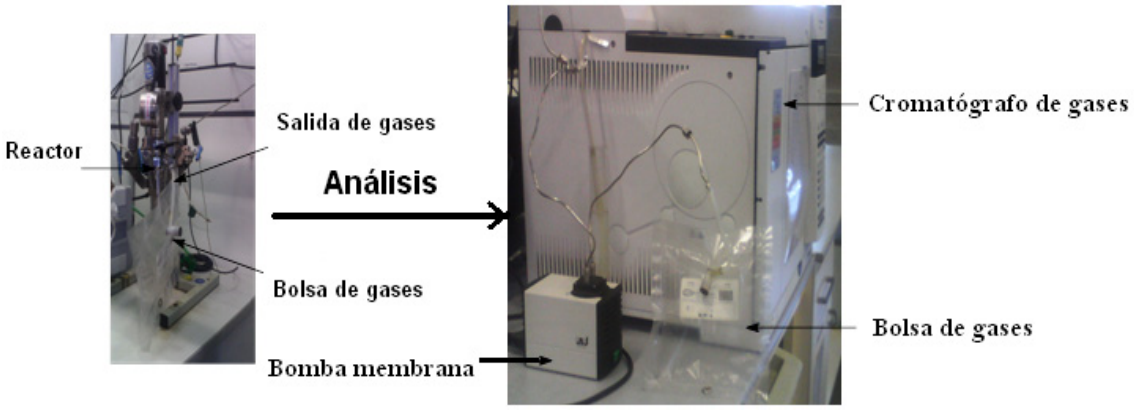

Figura 3.5. Tratamiento de toma de muestras de gases del reactor y análisis en GC

3.7 Referencias

[1] T.R Crompton (Ed.), Analysis of Seawater: A Guide for the Analytical and Environmental Chemist, 2 ed., Springer Science & Business Media, Berlin, Germany, (2006).

[2] V. F, D. P (Eds.), Isotopic Analysis: Fundamentals and Applications Using ICP-MS, 2 ed., Wiley-VCH, Weinheim, Germany, (2012).

[3] S. Erat, H. Metin, M. Ari, Influence of the annealing in nitrogen atmosphere on the XRD, EDX, SEM and electrical properties of chemical bath deposited CdSe thin films, Mater. Chem. Phys. 111 (2008) 114-120.

[4] B. Buehn, A.H. Rankin, M. Radtke, M. Haller, A. Knoechel, Burbankite, a (Sr, REE, Na, Ca)-carbonate in fluid inclusions from carbonatite-derived fluids: Identification and characterization using Laser Raman spectroscopy, SEM-EDX, and synchrotron micro-XRF analysis, Am. Min. 84 (1999) 1117-1125.

[5] A. De los Rios, F. Fernández, F. Alonso, J. Palacios, D. Gómez, M. Rubio, G. Víllora, A SEM–EDX study of highly stable supported liquid membranes based on ionic liquids, J. Membr. Sci. 300 (2007) 88-94.

[6] S. M, N. G (Eds.), X-Ray Diffraction: A Practical Approach, 1 ed., Plenum Publishing Corporation, New York, (1998).

[7] Bragg's Law and Diffraction: How waves reveal the atomic structure of crystals, University of Washington. 3 (2014). http://skuld.bmsc.washington.edu/~merritt/bc530/bragg/

[8] R. J.C, M. S (Eds.), Handbook of Surface and Interface Analysis: Methods for Problem-Solving, 2 ed., CRC Press; Taylor and Francis Group, Florida, US, (2009).

[9] D. Meloni, S. Laforge, D. Martin, M. Guisnet, E. Rombi, V. Solinas, Acidic and catalytic properties of H-MCM-22 zeolites: 1. Characterization of the acidity by pyridine adsorption, Appl. Catal., A: 215 (2001) 55-66.

[10] B. Chakraborty, B. Viswanathan, Surface acidity of MCM-41 by in situ IR studies of pyridine adsorption, Catal. Today. 49 (1999) 253-260.

[11] E. Selli, L. Forni, Comparison between the surface acidity of solid catalysts determined by TPD and FTIR analysis of pre-adsorbed pyridine, Microporous Mesoporous Mater. 31 (1999) 129-140.

[12] X. Zhao, G. Lu, A. Whittaker, G. Millar, H. Zhu, Comprehensive study of surface chemistry of MCM-41 using 29Si CP/MAS NMR, FTIR, Pyridine-TPD, and TGA, The J. Phys. Chem. B. 101 (1997) 6525-6531.

[13] A. Ahmet, M. Holger, H. Dieter, Investigation of acid sites on V2O5/TiO2 catalysts by FTIR with Adsorption of Pyridine, Tr. J. Chem. 20 (1996) 38-42.

[14] T. Barzetti, E. Selli, D. Moscotti, L. Forni, Pyridine and ammonia as probes for FTIR analysis of solid acid catalysts, J.Chem.Soc., Faraday Trans. 92 (1996) 1401-1407.

[15] N. Topsøe, K. Pedersen, E.G. Derouane, Infrared and temperature-programmed desorption study of the acidic properties of ZSM-5-type zeolites, J. Catal. 70 (1981) 41-52.

[16] D. Briggs, Surface Analysis of Polymers by XPS and Static SIMS, Cambridge University Press, (1998).

Chapter 4. Acidic ion exchange resins in the production of levulinic acid

Table of contents

4.1. Summary 90

4.2. Introduction 91

4.3. Selection and properties of ion exchange resins 93

4.3.1. Physicochemical properties 93

4.3.2. Acidity of Amberlyst catalysts 95

4.4. Reaction in continuous flow (packed bed reactor) 96

4.4.1. Materials and methods 96

4.4.2. Experimental procedure 96

4.4.3. Catalytic activity 97

4.4.3.1. Effect of liquid hourly space velocity (WHSV) on yield to LA 97

4.4.3.2. Comparative study between A35 and A47 99

4.4.3.3. Effect of the temperature 100

4.5. Reaction in batch system 101

4.5.1. Materials and methods 101

4.5.2. Experimental procedure 103

4.5.3. Catalytic activity 104

4.5.3.1. Effect of temperature, feed composition and catalyst loading 104

4.5.3.2. Effect of type of solvent and catalytic system used 110

4.5.3.3. Thermal- mechanical stability of catalyst 112

4.6. Conclusions 113

4.7 References 114

4.1. Summary

In this chapter a study of activity using Amberlyst catalysts in the synthesis of levulinic acid from furfuryl alcohol is presented. The materials selected were Amberlyst 47 and Amberlyst 35Wet, which are ion exchange resins with high porosity and acidity. Continuous and batch reaction systems were selected. The preliminary tests were developed in continuous flow using a packed bed reactor, and optimal conditions as concentration of furfuryl alcohol and temperature were evaluated. In this system, the best results were obtained using Amberlyst 35Wet, which showed a yield to levulinic acid up to 60 mol%. However, the formation and accumulation of furan resins on the catalyst generated operational problems in the system.

Due to the above mentioned operational problems in the continuous system, tests in batch reactor were developed. In this case oligomeric furan resins were also formed through undesired side reactions having a great influence on the final yield. Therefore, the addition of organic solvents to the reaction system was considered in order to reduce this problem. The cyclopentyl methyl ether (CPME) was added as a co-solvent and after optimization of several parameters, the yield to levulinic acid increased up to 44 mol%, with a complete conversion of furfuryl alcohol, after 3 hours of reaction time. This result is significantly higher when compared with the equivalent reaction systems without CPME or with other solvents.

4.2. Introduction

Such as described in Chapter 1.2.3, one route to synthesize levulinic acid (LA) from furfuryl alcohol (FA) is the hydration and ring opening of FA (see in Scheme 4.1) [1-7]. This reaction has been studied since the mid-twentieth century and the majority of studies have been patented by various authors [1,3-5], but the scientific literature published is not abundant.

Usually, The FA hydration to LA takes place using homogeneous strong acid catalysts such as sulfuric or hydrochloric acids [1,5,7]. The disadvantages of using homogeneous acid catalysts are well known: risks in handling, high toxicity, the need of special infrastructures for their use with the corresponding associated cost, high amounts of catalysts, and the difficulty of their separation and recovery. Therefore, promising studies about this reaction have been included using heterogeneous catalysts [2-4,6], with adequate acidity and textural properties. Catalysts such as ion exchange resins, zeolites and acidic clays are gaining importance to obtain high purity products. These new processes, with an easier separation step of the catalyst from the reaction mixture and lower corrosion issues, minimize the need for additional work-up procedures (which can often be expensive) and avoid the generation of large volumes of toxic waste.

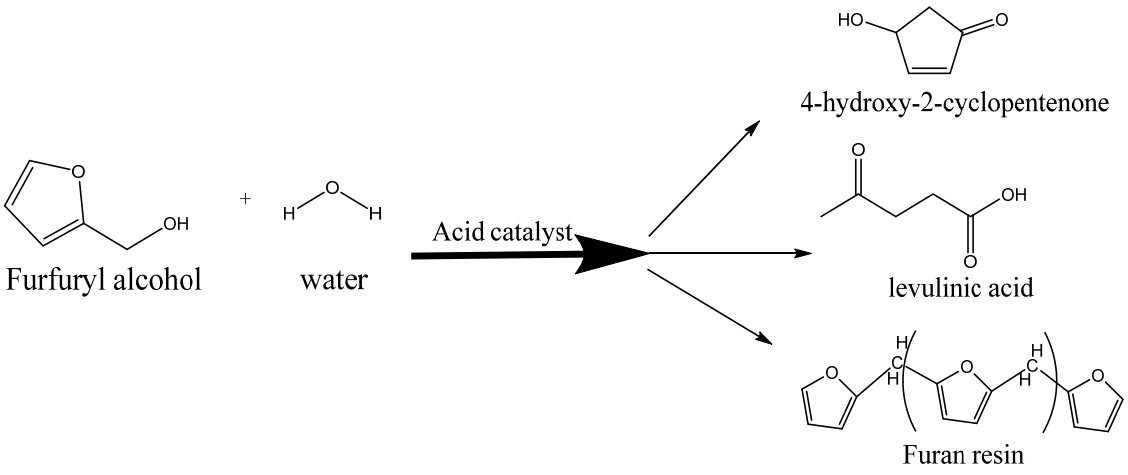

Scheme 4.1. Main products of hydration reaction of furfuryl alcohol with acid catalyst

With homogeneous catalysis, the best result found in the bibliography was reported by Masatomi et al. (1971) [1]. They showed a 93 % yield to LA using also a semi-batch

process with hydrochloric acid as catalyst and 2-butanone as solvent to dilute the FA fed. Whilst with heterogeneous catalysis, Redmond et al. (1956) [3], obtained a 55 mol% yield to LA, using Amberlite IR-120 as catalyst in a semi-batch process by the addition of concentrated FA to water.

In this way, the main objective of this research is to study the production of LA by hydration and ring opening of furfuryl alcohol using the commercial ion exchange acid resins: Amberlyst 35Wet (A35) and Amberlyst 47 (A47). These resins were chosen for its high concentration of acid sites (> 4.7 meq/g) and because they can operate at moderately high temperatures [8]. For the activity test, batch and packed bed reactors were used. This last type of systems is usually the preferred one due to its high economic viability, because it operates continuously; although its use is more suitable for gas phase reactions, many reactions in liquid phase perform well. The advantage of using packed bed reactor is the higher conversion per weight of catalyst and particularly in this reaction which requires strong acid sites.

On the other hand, when the furfuryl alcohol is in acidic aqueous medium it polymerizes to oligomeric products such as described in chapter 1.2.3 (Scheme 1.10.) [9-12]. The formation of oligomeric resins in the hydration reaction of FA causes not only low yields, but also generates some operational problems in the process. The oligomerization occurs via a condensation reaction between the ***OH*** of the methyl group of one furan ring and the hydrogen atom in the fifth position of another furan ring, leading to water elimination and formation of a methylene linkage [11]. Due to these reactions, very low concentrations of FA are used in the liquid reaction medium: concentrations below 2 wt% are recommended [12]. To achieve low concentrations of FA and limit the formation of undesirable byproducts, organic inert co-solvents may be added to the reaction medium [12].

Some authors have studied the effect of using organic solvents to extract organic molecules from the aqueous acidic reaction medium and minimize the formation of undesired condensation products [12-16]. Thus, solvents such as alkyl alcohols [13], alkyl phenols [14], cyclopentyl methyl ether [15] or traditional solvents as toluene or tetrahydrofuran [16] were analyzed in transformation reactions of carbohydrates and subsequent purification steps. Furthermore, if an alcohol is incorporated in the FA acid reaction medium, then high yields to levulinate esters are obtained [4,17]. Masatomi et

al. (1973) [1] reported that when a water soluble aliphatic ketone is present in the reaction medium, the levulinic acid can be obtained with high efficiency. Moreover, Capai et al. (1992) [5] also reported that when a ketone is used as the solvent, condensation reactions occur during acid hydrolysis of furfuryl acohol.

In this chapter, the cyclopentyl methyl ether (CPME) was chosen as inert co-solvent for the reaction in batch system. According to GlaxoSmithKline´s solvent selection guide [18], CPME solvent presents some advantages in terms of environmental, health, and safety aspects, over other solvents that are commonly used in this type of processes. In addition, due to its low vaporization energy (69.2 kcal/kg), this solvent can be recovered and easily reused. This solvent also presents high hydrophobicity but FA is soluble in it. Hence, two liquid phases coexist in the reactor. FA is dissolved in both phases, but mostly in the organic one, so in the aqueous phase FA concentration remains quiet low. As the reaction occurs in the aqueous phase where it is also placed most of the catalyst, the FA gradually crosses to the aqueous phase through the interface to maintain the equilibrium. The LA formed is mostly situated in the aqueous phase, but a small fraction of LA is soluble in the CPME and subsequently must be recovered.

4.3. Selection and properties of ion exchange resins

4.3.1. Physicochemical properties

The ion exchange resins Amberlyst are manufactured by the incorporation of functional sulfonic groups into a crosslinked polymeric matrix, such as described in chapter 1.3.1.3., the polymeric matrix is a co-polymer made from two monomers divinylbenzene and styrene. The styrene and divinylbenzene copolymer do not absorb water, and it gains such strong water adsorption capacity after modification with ion-exchangeable functional groups (sulfonic group SO_3H^+). Mostly, the ion exchange resins are insoluble by the introduction of crosslinks which interconnect various hydrocarbon chains. Thus, the resins are insoluble in all solvents without suffering any severe modification in their properties. However, the matrix is elastic and can be expanded.

A list of commercial Amberlyst resins with properties as acidity and maximum operating temperatures is reported in Table 4.1, where is also included Amberlyst 70 (A70) which exhibits the highest thermal stability, as well as Amberlyst 35 (A35) and 36 (A36), which show the highest ion exchange capacity.

Table 4.1. List of several commercial Amberlyst with its main properties [8].

Name	Matrix	Functional group	Ion exchange capacity (meq/g)	Max-Temp (K)
Amberlyst 131 Wet	Gel	SO_3H	4.8	403
Amberlyst 15 Dry	MR*	SO_3H	4.7	393
Amberlyst 15 Wet	MR*	SO_3H	4.7	393
Amberlyst 16 Wet	MR*	SO_3H	4.8	403
Amberlyst 31 Wet	Gel	SO_3H	4.8	403
Amberlyst 33	Gel	SO_3H	4.8	403
Amberlyst 35 Dry	MR*	SO_3H	5.2	423
Amberlyst 35 Wet	MR*	SO_3H	5.2	423
Amberlyst 36 Wet	MR*	SO_3H	5.4	423
Amberlyst 39 Wet	MR*	SO_3H	5.0	403
Amberlyst 47	MR*	SO_3H	4.7	403
Amberlyst 70	MR*	SO_3H	2.6	463
Amberlyst CH10	MR*	SO_3H	4.8	403
Amberlyst CH28	MR*	SO_3H	4.8	403

The Amberlyst 47 (A47) and Amberlyst 35 wet (A35) were selected for the development of activity tests. The physical and chemical properties of both materials are shown in Table 4.2. The main properties differences between these catalysts are related to concentration of acid sites, average pore diameter and thermal stability.

Table 4.2. Physical and chemical specifications of Amberlyst 35 Wet and Amberlyst 47 [8].

Property	Amberlyst ™ 47	Amberlyst ™35 Wet
Physical form	Opaque spherical mixture	Opaque spherical mixture
Functional group	SO_3H	SO_3H
Concentration of acid sites	≥ 4.7 meq/g	≥ 5.2 meq/g
Moisture retention capacity	50 a 57 %	51 a 57 %
Surface area	50 m^2/g	50 m^2/g
Average pore diameter	240 Å	300Å
Max- Operating Temperature	393 K	423K
Flow velocity	1 a 5 BV* /h (WHSV)	1 a 5 BV* /h (WHSV)
Pressure drop limit	1 bar (15 psig) through the bed	1 bar (15 psig) through the bed

* 1BV= 1 m^3 of solution / m^3 of resin.

4.3.2. Acidity of Amberlyst catalysts

The active acid sites of Amberlyst catalysts are sulfonic groups as showed in Table 4.2. Measurements using Diffuse Reflectance Infrared Fourier Transform Spectroscopy (DRIFTS) were carried out, to identify adsorbed pyridine in Brönsted and Lewis acid sites (described in chapter 3.4.8). Sulfonic acid groups are strong acids with high concentration of Brönsted acid sites as shown in Figure 4.1. The spectrum of pyridine adsorbed on A35 shows major bands at 1545 and 1627 cm^{-1} which correspond to Brönsted acid sites. A lower peak is observed at 1445 cm^{-1}, corresponding to Lewis acid site. The high concentration of Brönsted acid sites was confirmed by the Brönsted and Lewis peak area ratio at 1545 cm^{-1} and 1445 cm^{-1} respectively (Bpy/Lpy = 5.15).

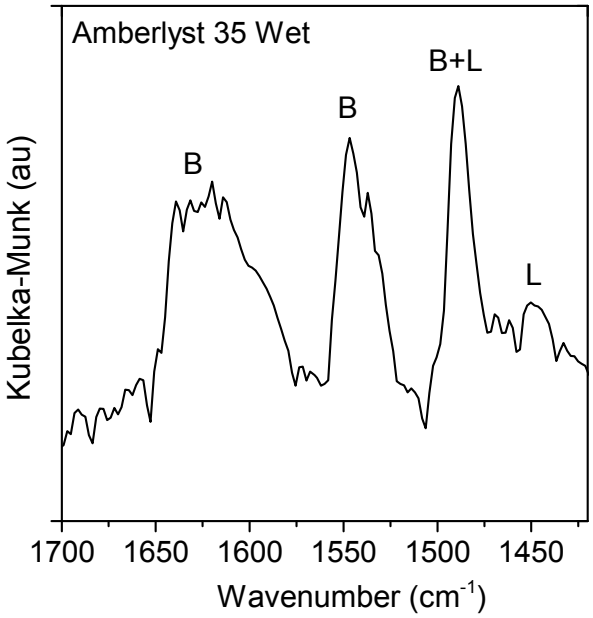

Figure 4.1. DRIFT Spectra of pyridine adsorbed on A35 (fresh). Spectrum conditions: Pyridine desorption at 398 K, after 120 min.

4.4. Reaction in continuous flow (packed bed reactor)

4.4.1. Materials and methods

The tests in continuous flow were developed using the reagents described previously in chapter 3.2: FA and bi-distilled water as reagents, A35 and A47 resins as catalysts, levulinic acid (LA) as standard reagent for its quantification and silicon carbide as bed filler. The tests were carried out in a PID Microactivity reactor system described in chapter 3.5.3. The liquid sample composition and sulfur content of catalyst were analyzed by gas chromatography and CHNS analyzer respectively (see chapters 3.6.1 and 3.4.9).

4.4.2. Experimental procedure

A typical activity test is described below. The catalyst A35 or A47 (0.3 g) previously dried, was located in the bed reactor center as described in Scheme 3.2, chapter 3. The

reactor was assembled in the PID microactivity system (Figure 3.3, chapter 3). The system was purged and pressurized at 5 bar using nitrogen, and then the temperature was increased up to 393 K. When the operating conditions were achieved, 0.1 mL/min of a solution FA at 10 wt% in bi-distilled water was fed to reactor. The products of reaction were taken at several time intervals for analysis. The collected samples were filtered through a filter 0.23 μm for gas chromatographic analysis.

For the tests in continuous flow, FA conversion and yield to LA were determined as:

$$FA\_Conversión(\%) = \frac{[C\_FA]_0 - [C\_FA]_t}{[C\_FA]_0} \cdot 100 \qquad \textbf{(eq.4.1)}$$

$$LA\_Yield(\%) = \frac{[C\_LA]_t}{[C\_FA]_0} \cdot 100 \qquad \textbf{(eq. 4.2)}$$

Where ***C*** is the molar concentration of furfuryl alcohol (FA) or levulinic acid (LA); subscript "0" is the FA fed to reactor, and "t" is the reaction time.

4.4.3. Catalytic activity

4.4.3.1. Effect of liquid hourly space velocity (WHSV) on yield to LA

The weight hourly space velocity (WHSV) is a parameter used for relating the reactant liquid flow rate entering the reactor with the amount of catalyst loaded. WSHV is expressed as:

$$\text{WHSV} = \frac{\text{FA mass flow fed}}{\text{Total catalyst weight}} [=] \, h^{-1} \qquad \textbf{(eq 4.3.)}$$

The influence of this parameter in yield to LA was tested by the variation in the quantity of catalyst loaded and the concentration of FA in the solution fed to reactor. The catalyst selected was A47 and the reaction tests were performed under the conditions specified

in Figure 4.2. The WHSV selected were: 1.7, 2.3 and 3.4 h^{-1} corresponding to 0.4, 0.3 and 0.2 g of catalyst, respectively. In the conditions studied, 100 % FA conversion was obtained. The main product of reaction was levulinic acid (LA). Other two compounds with high GC peak areas were identified by MS-GC as 4-hydroxy-2-cyclopentenone (4-HCP) and α-angelicalactone. Traces of other compounds were also observed, but not identified. The results depicted in Figure 4.2 shows a maximum yield to LA (60 %) at WHSV of 2.3 h^{-1}. And, when the value of WHSV was increased to 3.4 h^{-1}, the yield decreased by half. This behavior is directly related with the optimal amount of acid sites required per mol of FA, which allows the furan ring opening (Scheme 4.1). If the amount of catalyst is low, the furan ring of FA does not open, reacting to other undesirable compounds. On the other hand, when the value of WHSV was decreased to 1.7 h^{-1} (the amount of catalyst was increased), also a decrease in yield to LA was observed, probably due to the formation of furan resins at high concentrations of acid sites per mol of FA, according to results reported by various authors [10-12]. The above indicates that an optimal ratio between FA mol and concentration of acid sites is necessary for obtain high yield to LA.

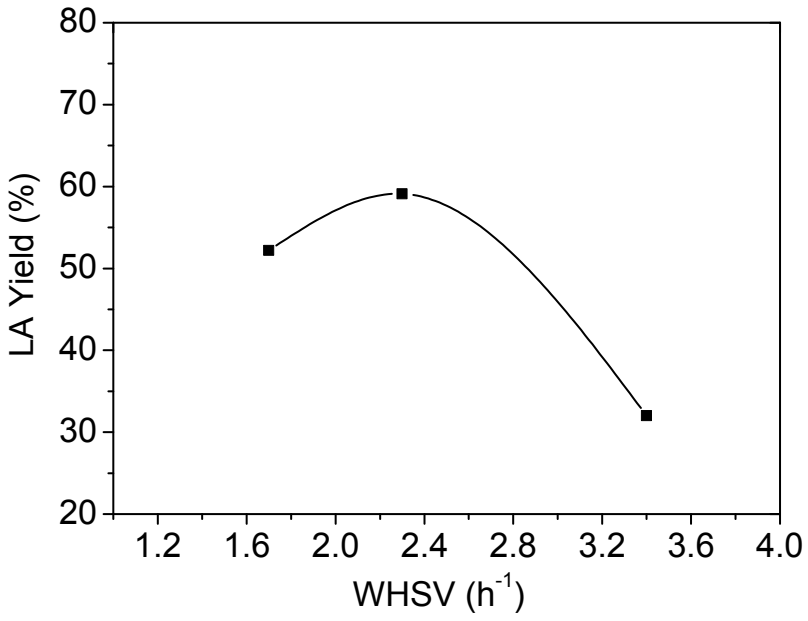

Figure 4.2. Effect of WHSV on yield to LA; general conditions: Flow 0.1 mL/min, temperature: 393 K, pressure: 5 bar N_2; the depicted results correspond to maximum yield obtained for each value of WHSV tested (maximum yield to LA reached at 3 hours of operation), the conversion of FA in all cases was 100 %.

- WHSV (1.7 h^{-1}): 0.4 g cat A47, solution feed of FA at 10 wt%.
- WHSV (2.3 h^{-1}): 0.3 g cat A47, solution feed of FA at 10 wt%.
- WHSV (3.4 h^{-1}): 0.2 g cat A47, solution feed of FA at 10 wt%.

4.4.3.2. Comparative study between A35 and A47

The activity of both catalysts was studied under the conditions described in Figure 4.3. Once again total conversion was achieved, while the difference in maximum yield to LA obtained with both catalysts was insignificant. However, the results with A47 showed a higher yield drop with time on stream when compared to A35. This decrease in yield to LA can be related with its thermal stability; the maximum operation temperature suggested for A47 is 393 K (Table 4.2), which is the operation temperature used in tests, whereas for A35 the temperature limit is 423 K; therefore, A47 catalyst, could have suffered a slight loss of structural stability and a loss of acid sites or difficulty for access to them of FA molecules.

In both cases, the yield to LA decreases by sulfonic group losses, attributed to leaching process (see section 4.5.3.3). Figure 4.3 shows that yield decreased up to 40 % respect to maximum values, but the conversion of FA remained close to 100 %, indicating that other by-products (unidentified) were formed.

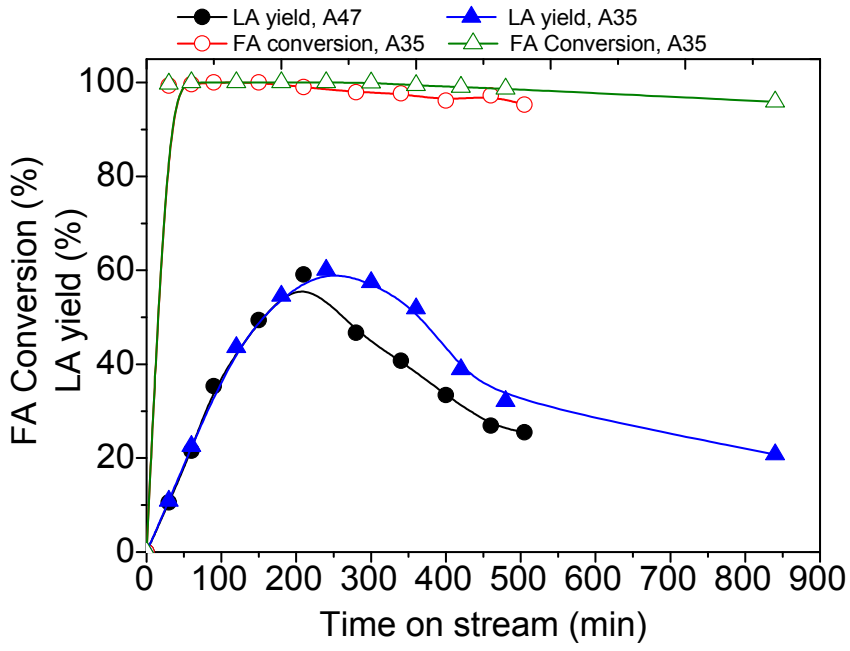

Figure 4.3. Variation of LA yield using A35 and A47. Operation conditions: WHSV: 2.3 h^{-1}, 393K, 5 bar N_2.

4.4.3.3. Effect of the temperature

The effect of the temperature of reaction in FA conversion and yield to LA was studied at 333 K, 393 K and 423 K using A35 as catalyst. Figure 4.4 shows the results obtained including the conversion of FA. This conversion in all cases was complete when the operation time reached 2 hours, and the reactivity of FA and the formation of LA increased with temperature. The results show a difference up to 40 percentage points in yield to LA, between the lowest and the highest temperatures, which correspond to 333 K and 423 K, respectively. The yields to LA showed in Figure 4.4 indicate that rate of reaction increased with the temperature. Subsequently a decrease of yield to LA can be seen, that is most evident a high temperatures. This decrease at high temperatures can be associated to sulfonic group losses of the catalyst, attributed to leaching process. The temperature increases the kinetic energy of sulfonic group bond and thus leads to their weakening (C-SO_3H). The above favors the hydrolysis process, the water can capture sulphonic groups from surface and hydrolyse them to give homogeneous H_2SO_4 [19]. The leaching of sulfonic groups is of great importance in continuous flow systems, because the sulfuric acid formed from sulfonic groups losses goes out of the reaction system, while in batch system these remain within the reaction system (see section 4.5).

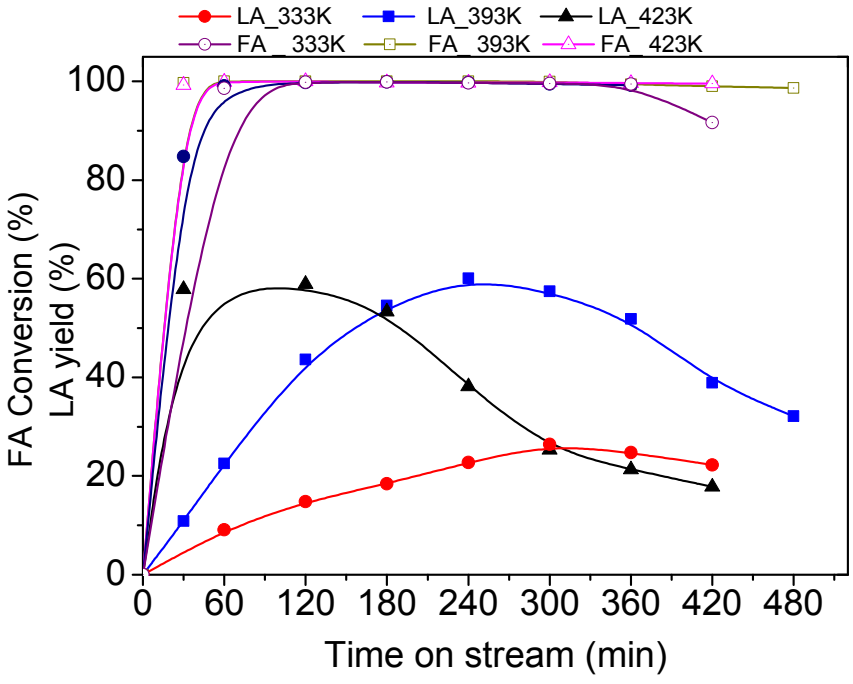

Figure 4.4. Effect of the temperature in yield to LA. Operation conditions: WHSV: 2.3 h^{-1}, Pressure: 5 bar N_2.

The above mentioned acid site losses also could generate an increase in intermediate by-products as the 4,5,5-trihydroxypentan-2-one, proposed by Maldonado et al. (2012) [6], or 4-hydroxy-2-cyclopentanone (4-HCP) [2,20], which could be favored when the acidity in the medium is low, as analyzed in section 4.5.

4.5. Reaction in batch system

4.5.1. Materials and methods

The catalytic tests were carried out in glass pressure stirred reactors (Ace Glass Incorporated, Vineland N.J, USA) described in chapter 3.5.1, Figure 3.1. The system used for the activity tests in micro glass reactors was a two-liquid phase system, composed of an aqueous phase and an organic one, in which cyclopentyl methyl ether (CPME) was used as solvent of FA (Scheme 4.2). Such as is shown in Scheme 4.2, two liquid phases coexist during the reaction: the FA molecules migrate to the aqueous phase through the interface at low rates, and, as a result the FA concentration in this phase remains low through the reaction time. The LA formed is mostly present in the aqueous phase, but a small fraction of LA is soluble in the CPME and subsequently must be recovered from this organic phase.

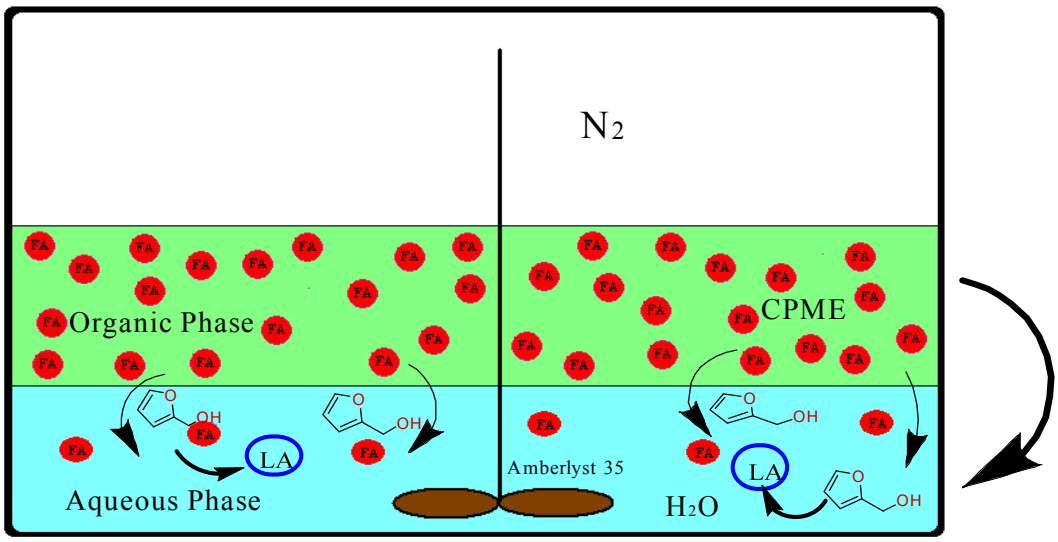

Scheme 4.2. Representation of two liquid phases in batch reactor

Figure 4.5 shows the ternary diagram H_2O-FA-CPME for the initial mixture fed to reactors. The conditions used for the simulation were 393 K and 10 bar, which are the temperature of reaction and autogenous pressure (approximate value) respectively. The mixture fed to the reactor (red point) corresponds to values included in Table 4.3. The distribution of compounds in CPME rich phase (black point) and water rich phase is determined by the interpolation of tie line on red point. The values summarized in Table 4.3 confirm that FA is mostly placed in organic phase (CPME) and that its concentration is low in aqueous phase.

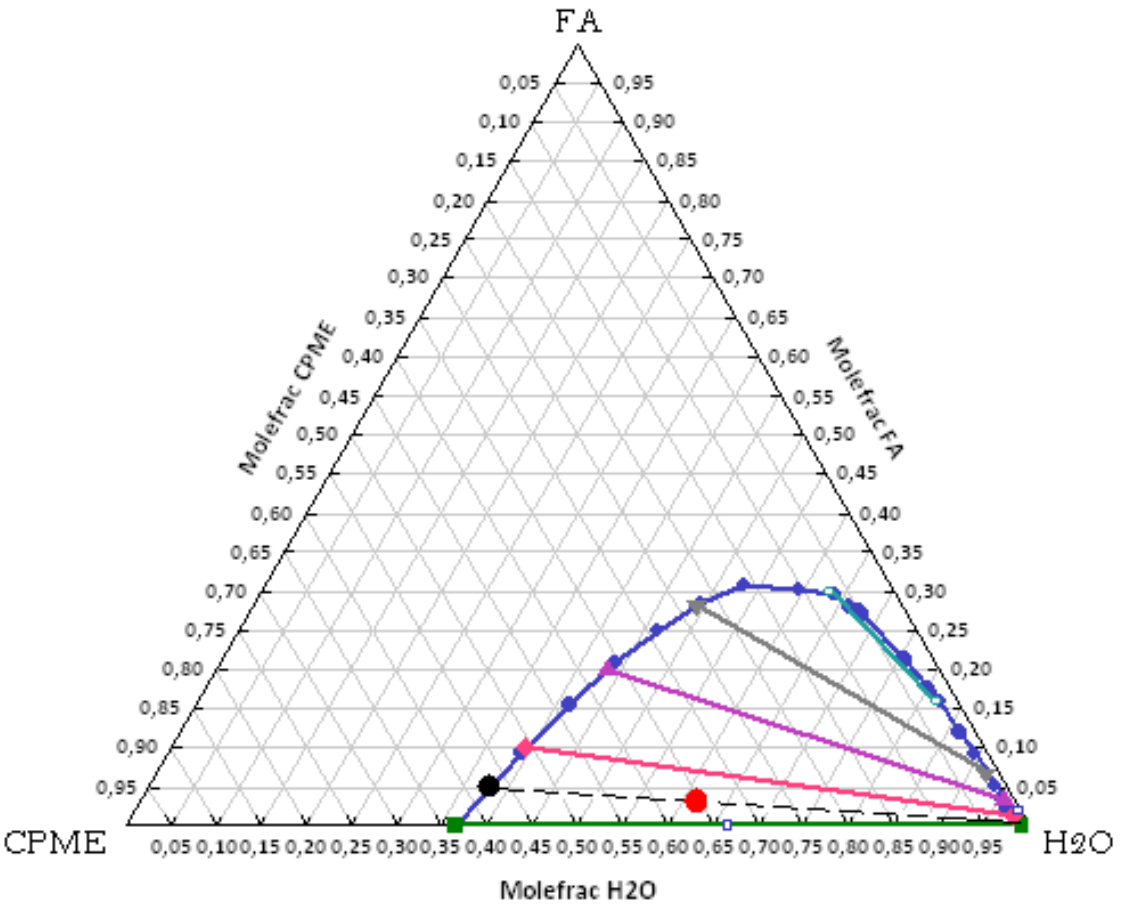

Figure 4.5. Ternary diagram for the H_2O-FA-CPME system at 393 K and 10 bar determined by simulation in Aspen Plus v8.2. Thermodynamic method: NRTL-RK. Red point: Fraction mol of ternary system fed to system. Black point: fraction mol of ternary system in CPME rich phase. Line segment: Tie line distribution.

Table 4.3. Product distribution predicted for H_2O-FA-CPME system.

Compound	mmol added	molar fraction (Red point)	molar fraction in water-rich phase	molar fraction in CPME-rich phase
Water	111	0.61	0.98	0.38
FA	6	0.03	0.01	0.05
CPME	65	0.36	0.01	0.57

4.5.2. Experimental procedure

The catalyst was loaded in the reactor, followed by the addition of FA, deionized water and CPME at different ratios in volume among these compounds. The usual ratio of FA:H_2O:CPME was 1:4:15 (v/v) and the total fluid volume used was 10 mL. Air was previously removed from the reactor by purging with a N_2 flow during 1 min. Then, the glass-pressure reactor was located in an oil bath heated by a hot-plate magnetic-stirrer device. Previously, the oil bath was fixed at the reaction temperature. Reactant mixture was stirred at 800 rpm during the catalytic reaction. Different glass-pressure reactors were used for each run. The reaction in all of them started at the same time. After different reaction times, each reactor was taken out from the oil bath, and the reaction was stopped immediately immersing the reactor in cold water (277 K).

The reaction mixture was quantitatively transferred and subsequently filtered with a millipore filter of 0.22 μm for their immediate analysis by GC. In the case of the tests conducted with CPME, the aqueous and organic phases were separated and then analyzed.

In order to compare activity and yield results obtained with heterogeneous catalytic system, additional experiments were also carried out using H_2SO_4 as homogeneous catalyst in equal amounts of equivalent per gram of acidity than A35 catalyst.

For all the activity tests, FA conversion (X_{FA}), LA selectivity (S_{LA}) and LA yield (Y_{LA}) were determined as:

$$X_{FA} = \frac{\left[N^{0}_{FA} - (N^{aq}_{FA} + N^{org}_{FA})_t \right]}{N^{0}_{FA}} \cdot 100 \qquad \textit{(eq. 4.4)}$$

$$S_{LA} = \frac{(N^{aq}_{LA} + N^{org}_{LA})_t}{N^{0}_{FA} - (N^{aq}_{FA} + N^{org}_{FA})_t} \cdot 100 \qquad \textit{(eq. 4.5)}$$

$$Y_{LA} = \frac{(N^{aq}_{LA} + N^{org}_{LA})_t}{N^{0}_{FA}} \cdot 100 \qquad \textit{(eq. 4.6)}$$

Where N is mole of FA or LA; sub-script "0" is the FA fed to reactor, and "t" is the reaction time, and, in the aqueous and organic phases are represented by "aq" and "org", respectively.

4.5.3. Catalytic activity

4.5.3.1. Effect of temperature, feed composition and catalyst loading

Sample analysis via gas chromatography showed that the highest peaks corresponded to FA, CPME, LA and a main by-product identified by GC-MS as 4-hydroxy-2-cyclopentenone (4-HCP) (Figure 4.6). In Figure 4.6 is shown typical chromatograms obtained at 2 hours of reaction (maximum yield to LA). LA was mostly located in aqueous phase as well as the 4-HCP (top figure), in organic phase (bottom figure), the peak intensity was much lower, but in this phase was observed a significant change in its coloration, shifting from light yellow at red wine color, which evidenced the presence of furan resins. Besides, peaks of very low intensity were also observed.

The evolution of FA conversion and yield to LA with reaction time are shown in Figure 4.7. In this figure, again the high reactivity of FA molecule can be observed, reaching complete conversion after 2 hour of reaction time. Interestingly, once FA was spent, LA yield continued increasing up to 40 %. This yield was practically constant (approximately 39 %, value not represented) after 24 h of reaction time.

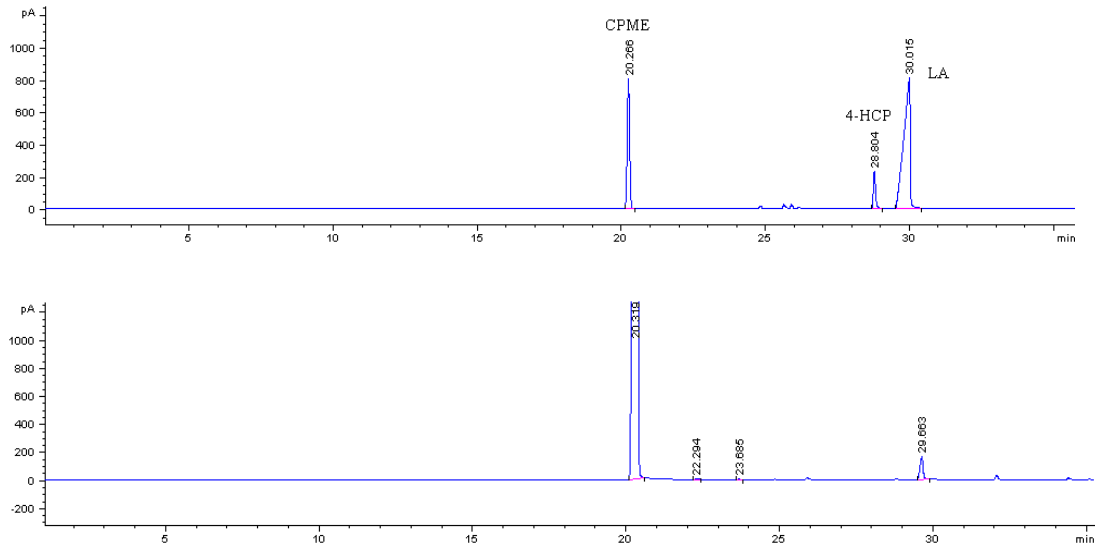

Figure 4.6. GC characteristic chromatogram of main compounds obtained at 2 hours reaction. Operation conditions: 0.2 mL of FA, 2 mL of H_2O, and 7.8 mL of CPME, 5.0 mg/mL of catalyst, 393 K and autogenous pressure. Top: aqueous phase. Bottom: organic phase (rich in CPME).

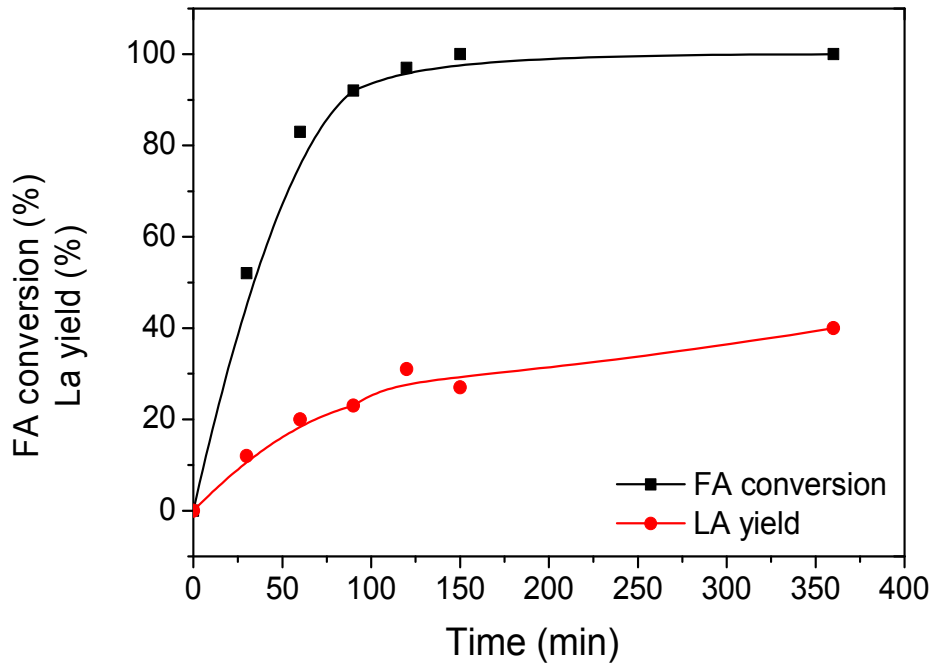

Figure 4.7. Behavior of FA conversion and yield to LA with reaction time. Operation conditions: 0.2 mL of FA, 2 mL of H_2O, and 7.8 mL of CPME, 5.0 mg/mL of A35 catalyst, 393 K and autogenous pressure.

In order to follow the evolution of the main intermediate compound with the reaction time, in Figure 4.8 are shown the chromatographic peak areas of the major products in the aqueous phase: LA and 4-HCP. For reaction time lower than 1.5 h, the LA and 4-HCP signals increased considerably. At this reaction time, the signal of 4-HCP showed a maximum, while the LA signal increased continuously until 6 h. Between 1.5 h and 6 h, the LA signal increased up to 35%, whereas the 4-HCP signal was approximately constant. This behavior can be explained because LA is being formed from different unstable intermediates while that 4-HCP is formed only when FA is present in the reaction media.

Literature indicates that in acid aqueous media, FA reacts to form different intermediate products [2,6]. Maldonado et al. (2012) [6], showed that the FA can be converted to LA by different pathways, mainly through the formation of 4,5,5-trihydroxypentan-2-one. But, according to Hronec et al (2013) [2,20], FA conversion proceeds to form unstable furanic compounds and continues with the formation of levulinic acid and polymerization products. These authors observed that in a highly acid reaction media, the yield to 4-HCP decreased remarkably, and when the reaction was carried out in aqueous media without catalyst, the polymeric compounds and the 4-HCP were the main products.

The results of this study seem to be consistent with the suggested mechanism of Hronec et al.(2012) [2,20]. Under the conditions studied, the formation of LA seems to be favorable, and practically no products derived from it were observed, as confirmed by the yield achieved, nearly constant after 6 h of reaction.

The effect of temperature was tested at three different temperatures: 363 K, 393 K and 423 K. Selectivity to LA variation with the temperature is shown in Figure 4.9. In this figure, it can be observed that after three hours of reaction the selectivity reached its maximum when the temperature was the highest. However, to these conditions, LA selectivity started to decrease, due to the activity loss of A35, attributed to the above mentioned thermo-mechanical limitations.

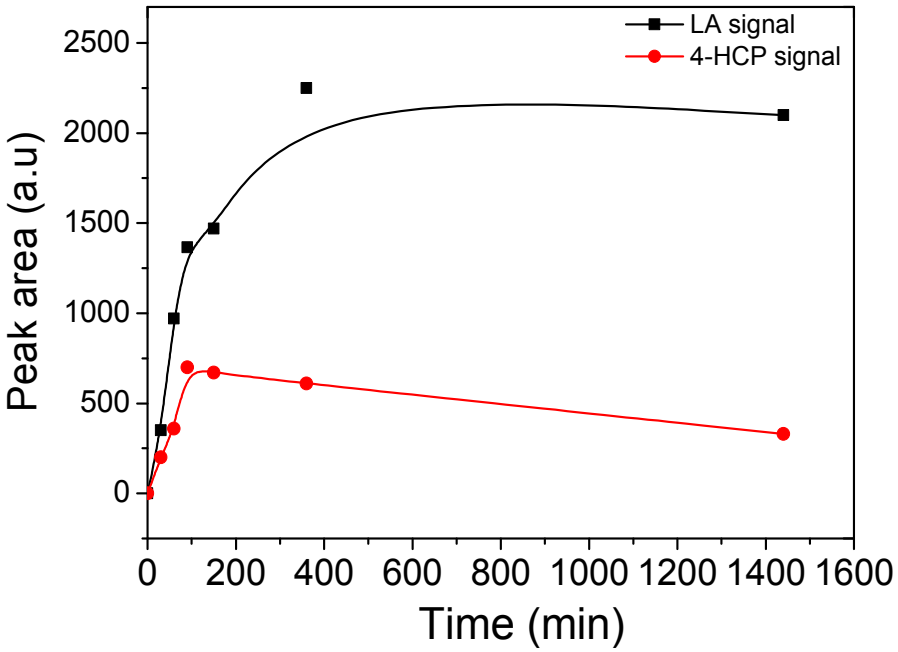

Figure 4.8. Evolution of relative chromatographic peak areas of compounds on reaction time. Operation conditions: 0.2 mL of FA, 2 mL of H_2O, and 7.8 mL of CPME, 5.0 mg/mL of A35 catalyst, 393 K and autogenous pressure, 100 % FA conversion to 150 min.

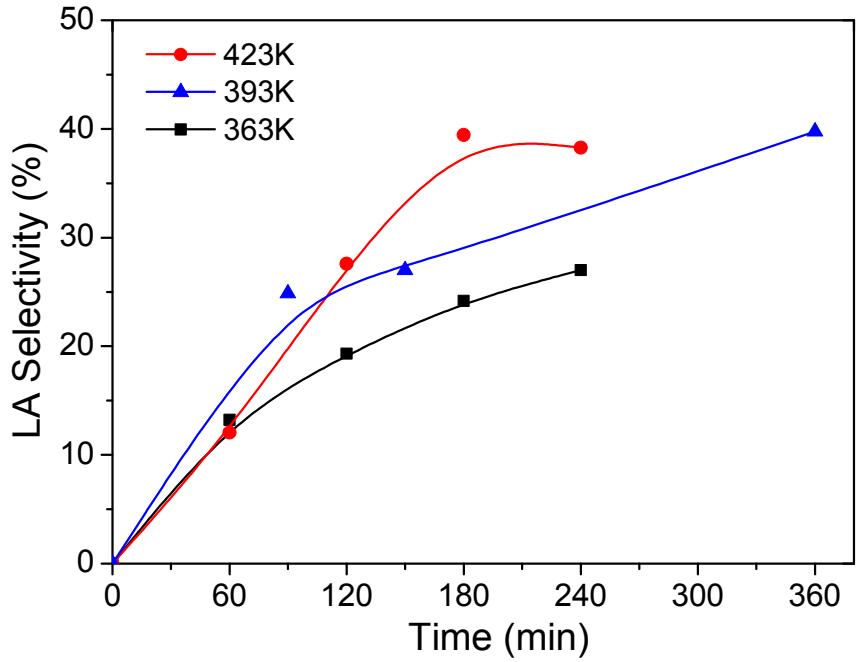

Figure 4.9. Variation of selectivity on time at different temperatures. Operation conditions: 0.2 mL of FA, 2 mL of H_2O, and 7.8 mL of CPME, 5.0 mg/mL of A35 catalyst and autogenous pressure.

The effects of feed composition and catalyst loading were also analyzed. In all activity tests, the operating temperature was set at 393K. The variation of yield to LA as a function of FA and water concentration is shown in Figures 4.10 and 4.11 respectively. The amount of CPME was adjusted to obtain a total reaction volume of 10 mL. The Figure 4.10 shows that initial concentrations above 1.15 mol/L of FA favored the resin formation, causing significant decreases in LA yields. On the other hand, concentrations below this value produced approximately constant LA yields.

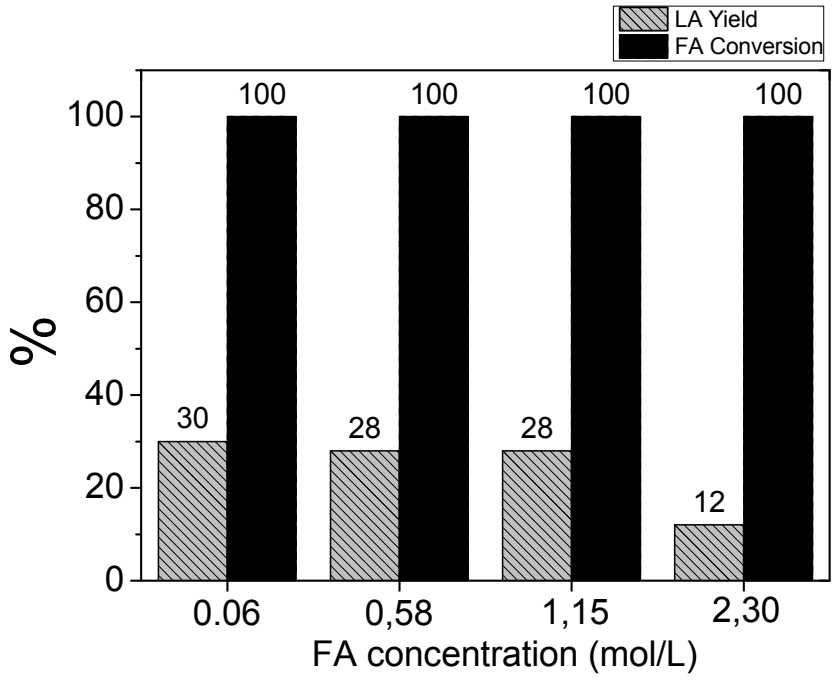

Figure 4.10. Influence of the concentration of FA in conversion and yield to LA. Operation conditions: 20 %(v/v) water, 5.0 mg/mL of catalyst, 2 hours reaction time and different volumes of FA and CPME, 393K, autogenous pressure.

Regarding the amount of water in the reaction media (Figure 4.11), it can be observed that the presence of high amounts of water also decreased the yield to LA. In this case, increases in chromatographic signal of by-products and intermediates compounds (not included in figure) were observed. At higher water concentration the formation of LA decreased because hydrogen ions formed by autodissociation of water have propitiated mostly reaction mechanisms of 4-hydroxy-2-cyclopentanone (4-HCP) formation [2]. Therefore to obtain high LA yield, low amount of water should be added.

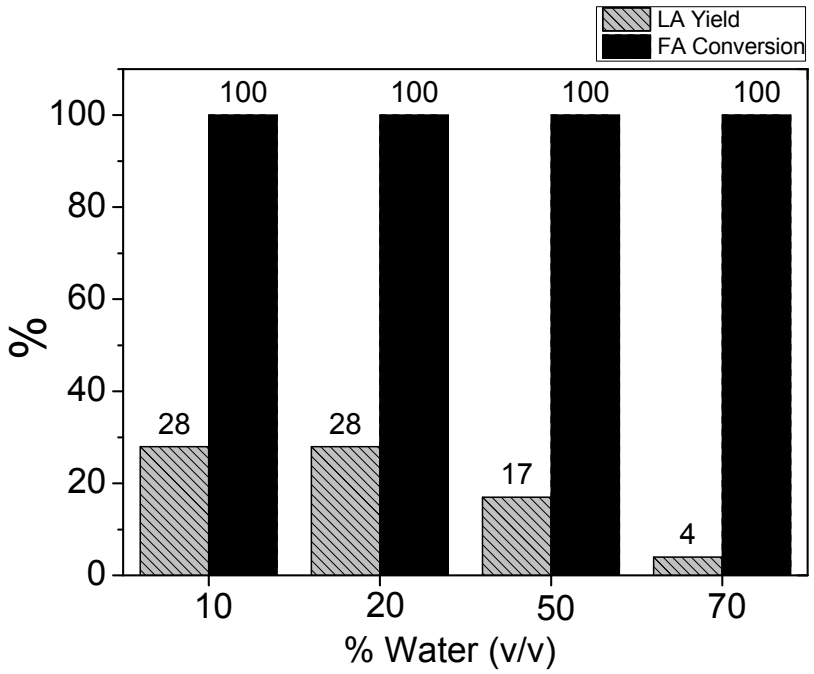

Figure 4.11 Influence the amount of water in yield to LA and conversion of FA. Operation conditions: 0.58 mol/L of FA, 5 mg/mL of catalyst, 2 hours reaction time different volumes of CPME and water, 393 K, autogenous pressure.

In Figure 4.12, the variation of yield to LA with the catalyst loading is represented. As it can be observed, this yield increased with the amount of acid sites, reaching a maximum yield when 5.0 mg/mL of catalyst was used. Low concentration of acid sites in reaction media is not enough to allow the furan ring opening, thus forming intermediate products. However, an excess of acid sites promotes polymerization reactions, causing furan resins formation and the corresponding decreases in yield to LA, in agreement with the results obtained in the packed bed reactor (section 4.4).

In summary, the best operating conditions deduced from the results were: 0.58 mol/L of FA, 20 % (v/v) of water, 75 % (v/v) of CPME and 5.0 mg/mL of catalyst.

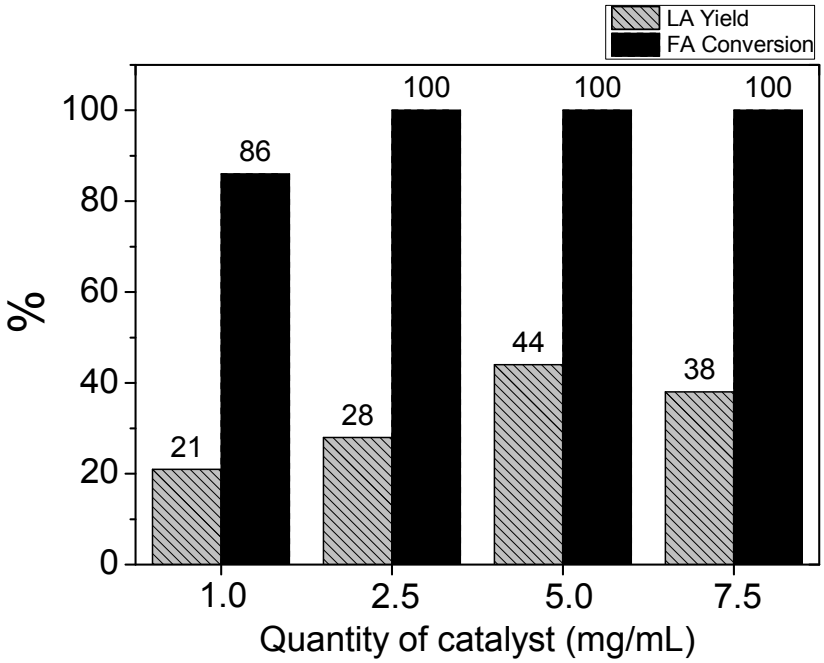

Figure 4.12. Influence of catalyst loading over yield to LA and conversion of FA. Operation conditions: 0.58 mol/L of FA, 20 % (v/v) of water, 75% (v/v) of CPME, 3 hours reaction time and different amounts of catalyst, 393 K, autogenous pressure.

4.5.3.2. Effect of type of solvent and catalytic system used

Table 4.4 shows the results obtained when the organic co-solvent was changed. It can be observed that the experiment developed without catalyst did not present any type of reaction, and the values of yield to LA and FA conversion were zero. Sulfuric acid was used as reference, the milliequivalents (H^+ form) added of this homogeneous catalyst were the same as those added with Amberlyst 35Wet. Using the same operating conditions, but with the presence of an acid catalyst, either H_2SO_4 or A35 catalyst, total conversion was achieved and the LA yield was around 7% after 3 hours of reaction time.

On the other hand, when there was no water in the catalytic reaction system and an inert solvent was used, LA was not formed, but a 44 % FA conversion was observed, possibly due to intermediates and polymeric compounds.

The use of CPME as inert solvent in this aqueous reaction system improved significantly the yield to LA. In this case, the FA conversion was also 100 % and yield to LA reached 44 % for the same reaction time. The feed of CPME in the reaction media allowed only an increase from 7 to 10 % of LA yield when sulfuric acid was the catalyst. This poor result is due to the distribution of homogeneous sulfuric acid catalysts in both phases, catalyzing polymerization reactions in the organic phase (red wine coloration observed).

The result obtained using two industrial solvents as toluene and cyclohexane did not improved the yield when compared to CPME. Toluene and cyclohexane are two solvents obtained from crude oil, while the CPME is a new totally green solvent, independent of the petrochemical industry. These results indicate that the best combination is the use of heterogeneous catalyst and a hydrophobic co-solvent such as the one used in the present study: CPME.

Table 4.4 Catalytic activity results with different systems of reaction at 393 K , 3h of reaction.

Solvent	Catalyst	LA Yield (%)	FA Conversion (%)
Water [a]	-	0	0
Water [b]	H_2SO_4	7	100
Water [c]	A35	7	100
CPME [d]	A35	0	44
water + CPME [e]	H_2SO_4	10	100
water + CPME [f]	A35	44	100
water + Toluene [f]	A35	36	100
water + Cyclohexane [f]	A35	12	100

(a) 0.5 mL of FA and 9.5 mL of water; (b) 0.5 mL of FA, 9.5 mL of water and 0.7µL of H_2SO_4 (96 %); (c) 0.5 mL of FA, 9.5 mL of water and 5.0 mg/mL of A35; (d) 0.5 mL of FA, 2 mL of water, 7.5 mL of CPME and 0.7µL of H_2SO_4 (96 %); (e) 0.5 mL of FA, 2 mL of water, 7.5 mL of CPME and 5.0 mg/mL of A35.

4.5.3.3. Thermal- mechanical stability of catalyst

As discussed above, the structure of resin ionic Amberlyst consists of a copolymer polystyrene-divinylbenzene with sulfonic groups supported on it. The polymeric structure has limited thermostability (Table 4.1), although with the increase in the crosslinking this material can be stable up to 463 K (Amberlyst 70). However, some reactants and products can affect its stability by the interaction with its organic co-polymeric support. This is only a hypothesis according to the test results. Contrary to the above, the significant loss in activity of used catalyst attributed to leaching of sulfonic groups was verified by the sulfur analysis in the fresh and used catalyst. Siril et al. (2008) [21], studied that the thermal stability of Amberlyst 35wet is limited by the tendency of the material to lose sulfonic groups. They observed the evolution of SO_2 at the degradation temperatures, and suggested a rupture of the aromatic carbon to sulfur bond. Therefore the presence of additional electron withdrawing groups on the benzene ring would strengthen this bond and so contribute to improve thermal stability.

The Table 4.5 shows the values of sulfur content reported in weight percentage, respect to total mass. The total loss of sulfur is 65 %wt. This percentage is equivalent to the acidity lost, since the acidity is attributed to the sulfonic groups.

Table 4.5 Analysis of sulfur percentage in fresh and used catalyst, using an Amberlyst 35 Wet.

Catalyst	Sulfur (wt%)
Amberlyst (35W) Fresh	16.6
Amberlyst (35W) Used *	5.8

*Amberlyst used in the following conditions: 393 K, 3 hours of reaction, autogenous pressure (N_2), 0.5 mL of FA, 2 mL of water, 7.5 mL of CPME and 5.0 mg/mL of A35.

The activity of the used catalyst was not evaluated due to its thermo-mechanical deformation evidenced at the end of the reaction and because furan resins were adhered on its surface, thus restraining its reusability.

4.6. Conclusions

In this chapter, the obtaining of levulinic acid from aqueous solutions of furfuryl alcohol via heterogeneous catalysis has been studied. The catalysts used were two Amberlyst resins, and the reaction systems selected were continuous flow and batch reactors. The study of the Amberlyst catalysts in continuous flow system (packed bed reactor), was carried out by the variation of two important parameters, the reaction temperature and concentration of FA fed. The use of the two types of catalysts also enabled to obtain information about the properties of the catalyst and the effect on LA yield. The most significant results were obtained with Amberlyst 35Wet at 393 K and 1 %wt FA, reaching 60 % LA yield. The thermal stability of the Amberlysts materials had a high influence on these results. The Amberlyst 47 has a maximum operating temperature at 393 K, which is the same value of temperature used in the reaction tests. It is possible that operating at the maximum recommended limit caused some instability problems in its structure.

On the other hand, in batch system the effect of an organic solvent, cyclopentyl methyl ether, in the synthesis of levulinic acid from aqueous solutions of furfuryl alcohol via heterogeneous catalysis has been studied. The addition of CPME resulted in lower FA concentrations in the aqueous phase, and this is why the formation of furan resins was partially prevented. Nevertheless, the water amount in the reactor should be kept as low as possible in order to limit the formation of undesirable by-products as 4-hydroxy-2-cyclopentenone (4-HCP). Moreover, this work has demonstrated that the amount of catalytic acid sites must also be limited in order to avoid undesirable side reactions. Under the conditions studied, the results for monophasic reaction mixtures have shown a similar yield to LA in both, homogeneous (H_2SO_4) and heterogeneous (Amberlyst 35Wet) catalysis when in the reaction medium there were the same acid equivalents per gram. However, when A35 and an organic solvent were used in the reaction medium, a considerable increase in the yield to LA was observed. Thus, the maximum LA yield was 44 % for total conversion of FA at 393K.

The recovery and reusability of the catalyst in both systems (continuous and batch) was not possible due to the mechanical stability loss of catalysts generated by sulfonic group loss and temperature limitations of the catalyst.

4.7 References

[1] O.N. Masatomi, H.T. Yoshio, Kinoshita, T.M. Tokushima, J. Naruto, Manufacture of Levulinic Acid, US Patent 3.752.849 (1973).

[2] M. Hronec, K. Fulajtárová, T. Soták, Kinetics of high temperature conversion of furfuryl alcohol in water, J. Ind. Eng. Chem. 20 (2014) 650-655.

[3] B.C. Redmond, Process for the production of levulinic acid, US Patent. 2.738.367 (1956).

[4] W.D. Van De Graaf, J.P. Lange, Process for the conversion of Furfuryl Alcohol into Levulinic Acid or Alkyl Levulinate, US Patent 7.265.239B2 (2007).

[5] B. Capai, G. Lartigau, Preparation of Levulinic acid, US Patent. 5.175.358 (1992).

[6] G. González Maldonado, R. Assary, J. Dumesic, L. Curtiss, Experimental and theoretical studies of the acid-catalyzed conversion offurfuryl alcohol to levulinic acid in aqueous solution, Energy. Environ. Sci. 5 (2012) 6981-6989.

[7] J.J. Bozell, L. Moens, D.C. Elliott, Y. Wang, G.G. Neuenscwander, S.W. Fitzpatrick, R.J. Bilski, J.L. Jarnefeld, Production of levulinic acid and use as a platform chemical for derived products, Resour. Conserv. Recycling. 28 (2000) 227-239.

[8] Rohm & Haas, Product data sheet of Amberlyst resin (2003) 1.

[9] T. Kim, R.S. Assary, H. Kim, C.L. Marshall, D.J. Gosztola, L.A. Curtiss, P.C. Stair, Effects of solvent on the furfuryl alcohol polymerization reaction: UV Raman spectroscopy study, Cat. Today. 205 (2013) 60-66.

[10] M.G. Alimukhamedov, F.A. Magrupov, Kinetics of homopolycondensation of furfuryl alcohol., Polym. Sci. Ser. B. 49 (2007) 1287-1292.

[11] T.A. Krishnan, M. Chanda, Kinetics of Polymerisation of Furfuryl Alcohol in Aqueous Solution, Anyewandte Makromolekulare Chemie. 43 (1975) 145-156.

[12] T. Kim, R.S. Assary, H. Kim, C.L. Marshall, D.J. Gosztola, L.A. Curtiss, P.C. Stair, Effects of solvent on the furfuryl alcohol polymerization reaction: UV Raman spectroscopy study, Catal. Today. 205 (2013) 60-66.

[13] Y. Román-Leshkov, J.A. Dumesic, Solvent effects on fructose dehydration to 5-hydroxymethylfurfural in biphasic systems saturated with inorganic salts, Top. Cat. 52 (2009) 297-303.

[14] D.M. Alonso, S.G. Wettstein, J.Q. Bond, T.W. Root, J.A. Dumesic, Production of Biofuels from Cellulose and Corn Stover Using Alkylphenol Solvents, Chem SusChem. 4 (2011) 1078-1081.

[15] M.J. Campos Molina, R. Mariscal, M. Ojeda, M. López Granados, Cyclopentyl methyl ether: A green co-solvent for the selective dehydration of lignocellulosic pentoses to furfural, Bioresour. Technol. 126 (2012) 321-327.

[16] J.J. Bozell, L. Moens, D.C. Elliott, Y. Wang, G.G. Neuenscwander, S.W. Fitzpatrick, R.J. Bilski, J.L. Jarnefeld, Production of levulinic acid and use as a platform chemical for derived products, Resour. Conserv. Recycling. 28 (2000) 227-239.

[17] R.I. Khusnutdinov, A.R. Baiguzina, A.A. Smirnov, R.R. Mukminov, U.M. Dzhemilev, Furfuryl Alcohol in Synthesis of Levulinic Acid Esters and Difurylmethane with Fe and Rh Complexes, Russ. J. Appl. Chem. 80 (2007) 1687-1690.

[18] The Royal Society of Chemistry, Glaxo Smith Kline (GSK), suplementary material for Green Chemistry, (2010).

[19] A. Kiss, A. Dimian, G. Rothenberg, Solid Acid Catalysts for Biodiesel Production Towards Sustainable Energy, Adv. Synth. Catal. 348 (2006) 75-81.

[20] M. Hronec, K. Fulajtarová, T. Liptaj, Effect of catalyst and solvent on the furan ring rearrangement to cyclopentanone, Appl. Cat. A: 437–438 (2012) 104-111.

[21] P.F. Siril, H.E. Cross, D.R. Brown, New polystyrene sulfonic acid resin catalysts with enhanced acidic and catalytic properties, J. Mol. Catal. A: Chem. 279 (2008) 63-68.

Chapter 5. Inorganic solid catalysts in the production of levulinic acid

Table of contents

5.1. Summary 117

5.2. Introduction 118

5.3 Preliminary screening of acid solid catalysts 119

5.3.1. Description of catalysts tested 120

5.3.1.1. HZSM-5 zeolite 120

5.3.1.2. Y Zeolite 121

5.3.1.3. H-β Zeolite 121

5.3.1.4. Phosphotungstic acid (PTA), supported on Zeolites 122

5.3.1.5. Superacid catalysts-type sulfated zirconium (SO_4^{2-}/ZrO_2) 123

5.3.2. Experimental 123

5.3.2.1. Preparation of catalysts 123

5.3.2.2. Activity tests 125

5.3.3. Results of the preliminary screening of catalysts 126

5.4. Optimization of operating parameters using HZSM-5 zeolite (H-Z(50)) 127

5.4.1. Effect of the atmosphere of reaction 127

5.4.2. Effect of solvent 128

5.4.3. Effect of the variation in the concentration of FA and the amount of catalyst loaded in the feed stream 130

5.4.4. Effect of temperature 132

5.4.5. Effect of reaction time 133

5.4.6. Summary of optimal conditions obtained 134

5.5. ZSM-5 zeolite modified 135

5.5.1. Use and applications of desilicated zeolites 135

5.5.2. Experimental procedure 135

5.5.2.1. Desilication of HZSM-5 zeolite 135

5.5.2.2. Characterization of catalysts 136

5.5.2.3. Catalytic activity 136

5.5.3. Results 137

5.5.3.1. Results of characterization 137

5.5.3.2. Results of catalytic activity 146

5.6 Conclusions 149

5.7 References 150

5.1. Summary

In this chapter, a series of catalysts with inorganic structure were studied in the hydration reaction of furfuryl alcohol to levulinic acid. The study was focused in some materials with considerable high acidity. Initially catalysts based on zeolites, heteropolyacids and "superacid" solids were studied. The activity of these catalysts was tested using a semi-batch process and 2-butanone as co-solvent of furfuryl alcohol, process whereby decreases the formation of furan resin and therefore increases the yield to levulinic acid.

This initial screening resulted in the selection of HZSM-5 zeolite as the most active catalyst in the formation of levulinic acid. Then, HZSM-5 was used for the optimization of main conditions, as the initial concentration of reactants, amount of catalyst, temperature and pressure of operation. Through optimization process, the yield to levulinic acid was increased up to about 78 mol%. To increase these results, a modification of zeolite HZSM-5 was studied, which involved a desilication process using various silice-alumina ratios. The desilication of HZSM-5 zeolite increases the mesoporosity allowing access to acid sites. The catalytic activity increased when the ratio SiO_2:Al_2O_3 was set to 23, reaching a yield to LA up to 81 mol%. Even more, this catalyst showed a successful reusability.

5.2. Introduction

As discussed in previous chapters, the obtention of levulinic acid (LA) from furfuryl alcohol (FA) in aqueous media was developed over catalysts with strong acidity allowing the furan ring opening [1-5]. In chapter 4, the study over the polymeric ion exchange resin Amberlyst, which possess a considerable presence of Brönsted acid sites, was included. This property has shown an influence in the selectivity to levulinic acid, and therefore was considered in this chapter for the selection of catalysts with similar characteristics. Some materials provide major thermal and mechanical stability and acceptable acidity respect to Amberlyst, as the zeolites, which have been widely used in last decades, due to the variety and structural conformation which provide various alternatives of synthesis.

Due to the above mentioned properties, zeolites are mostly used in reactions such as catalytic cracking, alkylation, isomerization and phenol hydroxylation [6-20]. The amount of acid sites in the zeolites is related with the SiO_2:Al_2O_3 ratios: higher acid sites are present in the zeolite at lower SiO_2:Al_2O_3 ratio. A large group of zeolites with Brönsted acid sites include the HZSM-5, H-USY, H-β and H-Y [21-27].

The porosity is also affected by the SiO_2:Al_2O_3 ratio and determined by the number and spatial arrangement of the bond Si-O-Al in the formation of its tetrahedral structure. Through desilication treatment the SiO_2:Al_2O_3 ratio is modified causing an increase in this important property of the catalyst [28-31].

Many researches show that alkaline desilication of zeolite is an economical and effective procedure to create mesoporous intraparticles in zeolites, the controlled desilication generates a significant decrease in SiO_2:Al_2O_3 atomic ratio favoring the increase in cation exchange capacity [6, 22, 28, 31-35]. An effective control of alkalinization is needed to perform the optimal desilication and prevent the destruction of its structure.

Other materials recently studied with inorganic structure and strong acidity are the denominated “superacids”, specifically the sulfated zirconia described in chapter 1.3.1.4. The strong acidity of sulfated zirconia oxide has attracted much attention due to its ability to catalyze many reactions, such as cracking, alkylation and isomerization

[36-39]. A "superacid" is defined to be an acid stronger than 100 % of sulfuric acid, (Hammett acidity function $H_0 < -11.9$). Therefore, they are materials which can replace the traditional catalytic processes which involve sulfuric acid, but, they are deactivated rapidly at high temperatures. That is why in recent years, rare earth elements as cerium and lanthanum have been supported on sulfated zirconia to increase their acidity and thermal stability [40, 41].

The catalytic activity of these catalysts was studied in a semi-continuous system. This reaction system allows different alternatives of feeding reagents to the reactor, such as the gradual feeding of one the reactants in order to reduce undesired side reactions. Some authors have used the semi-continuous system to diminish the formation of furan resins in this reaction. Masatomi et al. (1971) [42] showed a 93 % yield to LA using a semi-continuous process with hydrochloric acid as catalyst and 2-butanone as co-solvent to dilute the FA fed. The results obtained by Masatomi et al. shows that 2-butanone is a suitable co-solvent of FA in this reaction. This study has been focused on the substitution of the hydrochloric acid catalyst used by Masatomi et al. by the above named heterogeneous catalysts.

5.3 Preliminary screening of acid solid catalysts

As a first step in this research, the results obtained by Masatomi et al. (1971) [42] were initially reproduced using hydrochloric acid (35 %) as catalyst, obtaining equivalent yield to LA (93 %). Then the screening of catalysts was carried out under the same conditions. These catalysts included inorganic catalysts: HZSM-5 zeolite (H-Z(50)), beta zeolite (H-β), ultra stable zeolite (H-USY), heteropolyacid type phosphotungstic acid (PTA), zirconia sulfated superacid (ZrO_2/ SO_4^{2-}) and the organic commercial ion exchange resins Amberlyst 35wet (A35) and Amberlyst 47 (A47) as reference materials according to results obtained in chapter 4. These materials have a substantial amount of Brönsted acid sites [21,23-26], and several alternatives of surface area, pore size, as well as thermal stability.

The screening of the above mentioned catalysts was developed using the semi-continuous system described in chapter 3.5.2.

5.3.1. Description of catalysts tested

5.3.1.1. HZSM-5 zeolite

The HZSM-5 zeolite is a synthetic alumino-silicate with formula $Na_nAl_nSi_{96-n}O_{192}\cdot 16H_2O$ ($0<n<27$) patented by Mobil Oil Company in 1975. This zeolite presents a three dimensional channel, with two systems limited by rings with ten members. Its structure belongs to the ***pentasil*** family: pentasil is the secondary unit formed by the union through oxygen atoms as shown in Scheme 5.1. By the binding of units, chains are formed, which are assembled to form layers, then are grouped in three dimensional structures corresponding to the ZSM-5. The union of structural drawings generates sinusoidal channels and straight channels, parallel between them and perpendicular to the first ones. The pores in the sinusoidal system present dimensions of 5.1x5.5 Å, while the straight ones show a size of 5.3x5.6 Å [43]. In the synthesis of ZSM-5 zeolite, usually done in presence of Na^+ and organic additives, up to twenty five organic agents can be used as directors of the structure, being the tetrapropylammonium bromide and tetrapropylammonium hydroxide (TPABr, TPAOH) the most commonly used. Furthermore, different silicon and aluminum precursors (tetraethyl orthosilicate, sodium silicate, aluminum nitrate, aluminum isopropóxide, etc.) have been used [44, 45].

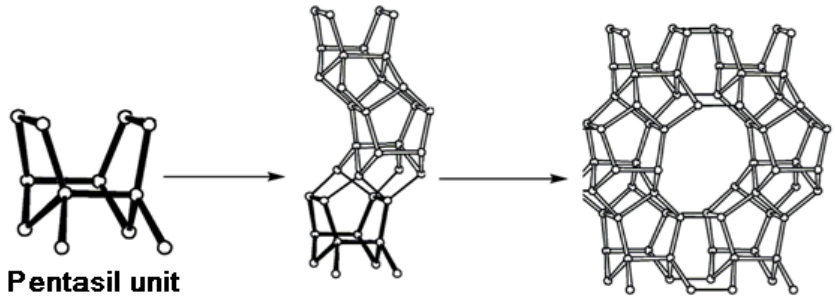

Scheme 5.1. Construction of three-dimensional structure of zeolite ZSM-5[43].

5.3.1.2. Y Zeolite

The zeolite type Y is an isomorphic synthetic zeolite type faujasite, whose structural unit is the ***sodalite*** which consists of truncated octahedron, composed by twenty four tetrahedrons of silice and aluminum [43]. The connection between different units of sodalite is performed by oxygen bridges through the sides with windows of six members, resulting in the structure presented in Scheme 5.2.

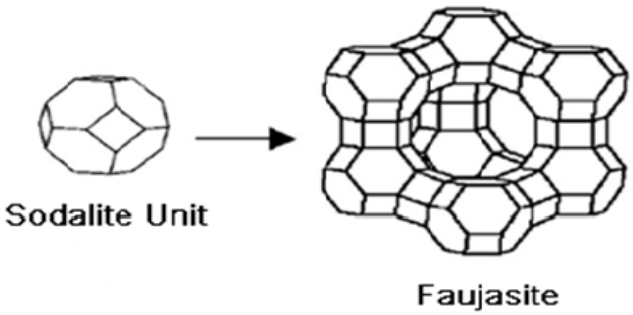

Scheme 5.2. Construction of three-dimensional structure of Y zeolite [43].

The structure of Y zeolite has a large central cavity, which is linked tridimensionally to the following units through the channels limited by links of two oxygen atoms [46]. All pores are dimensionally identical, so that they have a diameter of 7.4 Å. Y Zeolite is synthesized in a gelation process, in which sources of alumina (sodium aluminate) and silica (sodium silicate) are mixed in an aqueous alkaline solution (NaOH) to give a gel, then gel is heated to crystallize the zeolite. The zeolite is present in Na^+ form and must be converted into its acid form. However, to avoid the disintegration of its structure by acid attack it is first converted to ammonium form (NH_4^+), before being converted to acid form. The most important application of zeolite Y includes, principally, its use as catalyst in the units of catalytic cracking in oil refineries [20].

5.3.1.3. H-β Zeolite

The H-β zeolite was cataloged in 1967 [47] as an active catalyst which could possess a three-dimensional pore system with twelve rings as shown in Scheme 5.3. The reflections found experimentally on X-ray diffraction technique can be attributed to the presence of tetragonal structure. The structure of H-β is named as “beta polymorph A”

(BEA), which is characterized by the three channels interconnected by twelve units with dimensions of 6.6x6.7 Å and 5.6x5.6 Å. The chemical formula of H-β is $[Na^{+}_{7}][Al_7Si_{57}O_{128}]$, and its most important application is once again in the petrochemical industry[48].

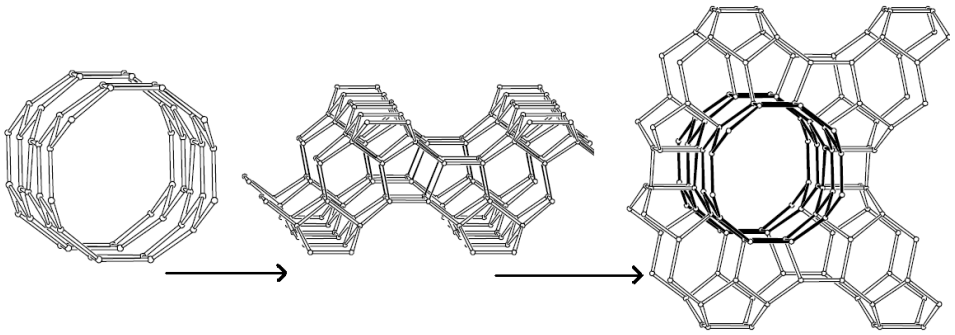

Scheme 5.3. Construction of three-dimensional structure of Beta zeolite, (structure BEA) [43].

5.3.1.4. Phosphotungstic acid (PTA), supported on Zeolites

Heteropolyacids (HPA), typically represented by the chemical formula $H_{8-x}[XM_{12}O_{40}]$, where X is the heteroatom, *x* the oxidation state and M the metal atom added, are a type of material with a particular combination of hydrogen and oxygen with certain metals and non-metals (Scheme 5.4). When the heteroatom is phosphorus (P^{5+}) and tungsten is the metal atom, the phosphotungstic acid is formed (PTA). Usually PTA is supported on zeolites such as MCM-41, to increase its dispersion [49, 50].

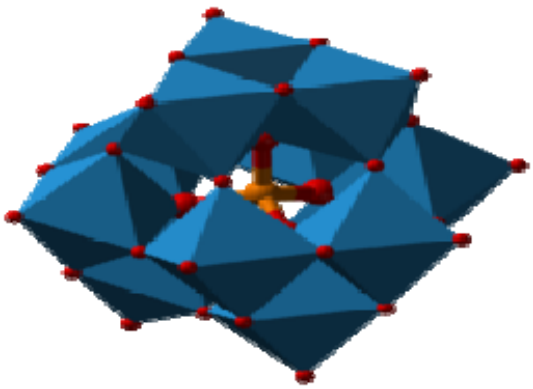

Scheme 5.4. Structure type Keggin of heteropoliacids (depicted from Benjah-bmm27).

Additionally to the increase in dispersion, the supported HPA (HPAs) can diminish the coke formation during the reactions [51, 52], and it have been used in dehydration and oxidation reactions, that exhibit this problem [53]. The structure of HPA, possess qualities such as good thermal stability and high acidity, which can be used to obtain the levulinic acid.

5.3.1.5. Superacid catalysts-type sulfated zirconium (SO_4^{2-}/ZrO_2)

Sulfated zirconium belongs to superacid group of catalysts which were described in chapter 1.3.1.4. When zirconium oxide is modified with sulfate ions, catalysts with high acidity are formed, whose surface structure can be composed of bisulfate species (Scheme 5.5.a), monosulfate species (Scheme 5.5.b) and monosulfate species with geminal S=O groups (Scheme 5.5c) [54].

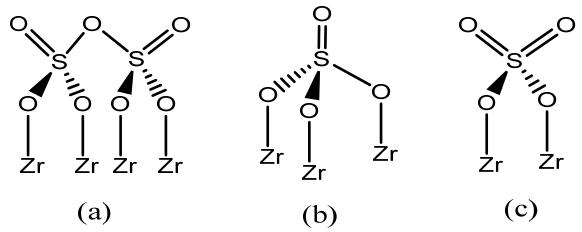

Scheme 5.5. Surface structure of sulfated zirconium oxide

The incorporation of sulfate anions on the ZrO_2 surface has been found to probably increase the number and strength of the Lewis acid sites [55].

5.3.2. Experimental

5.3.2.1. Preparation of catalysts

The ***H-β*** zeolite used (SiO_2/Al_2O_3:25) was the one described in Table 3.2 (chapter 3) prepared in protonated form (H^+) and calcined at 823 K, at heating rate of 10 K/min. The ***H-Z(50)*** is the HZSM-5 zeolite (SiO_2/Al_2O_3:50) described in Table 3.2 (chapter 3). The ***H-ZD(50)*** is the H-Z(50) zeolite which was subjected to desilication process using extraction of silica in a solution NaOH (0.2M) according to the following procedure:

3 grams of H-Z(50) were added to 100 mL of NaOH (0.2M) to 353 K and stirred at 200 rpm, for two hours. Then, the solids were separated by centrifugation and washed with bi-distilled water until neutral pH, afterwards these were dried overnight at 383 K. The zeolites obtained were treated with 50 mL of NH_4Cl (0.5M) to 333 K; the samples were newly centrifuged and washed until all chlorides were eliminated; then the solid was dried to 383 K and subsequently calcined to 823 K during 4 h, to exchange NH_4 to H^+ form.

The ***superacid SO_4^{2-}/ZrO_2*** catalyst was synthesized by the precipitation method using an ultrasound system at low temperature according to the following procedure: 6 grams of $ZrN_2O_7.xH_2O$ (Panreac) were dissolved in bi-distilled water (50mL), then the pH was adjusted at 9.0 by the addition dropwise of aqueous ammonium (NH_4OH, 30 %). The solution was immersed into ultrasound equipment during 5 min. Then, a precipitate of zirconium hydroxide was formed. The precipitate was located in a freezer at 255 K during 4 hours. The solid precipitate was filtered and washed with bi-distilled water until neutral pH, and then was dried at 383 K by 6 hours to obtain dry crystals. The dry solid was immersed in 50 mL of H_2SO_4 (0.5M) by 12 hours, then was separated by filtration and was dried at 383 K. Finally, the solid was calcined at 923 K with heating rate at 5 K/min under air flow (1 L/min).

The ***PTA-USY*** and ***PTA-Z(50)*** were prepared containing 10 wt% of PTA ($12WO_3.H_3PO_4.xH_2O$), equivalent to 7.6 wt% tungsten. The choice of this percentage was consistent with the range used by Nandhini et al. (2006) [50] in the ring opening of succinic anhydride, where an Al-MCM-41 supported phosphotungstic acid was used. The PTA was supported on ultra stable Y zeolite (SiO_2/Al_2O_3:5) and H-Z(50), in both cases 0.3 grams of PTA were dissolved in bi-distilled water (50mL), and the content was transferred to rotary evaporator with 3 grams of zeolite previously degasified. The impregnation was developed at 313 K and 5 mbar. The solids obtained were calcined in air at 523 K. The ***A47 and A35*** are the commercial ion exchange resins Amberlyst 47 and Amberlyst 35 Wet respectively, dried at 333 K (studied in chapter 4).

All the reactants and catalysts aforementioned were described in chapter 3.2.

5.3.2.2. Activity tests

The activity tests were performed in the semi-continuous type reactor described in chapter 3.5.2. In a typical procedure, the reactor was loaded with 20 mL of a mixture which consisted of 4.2 ml of bi-destilled water and 15.8 ml of organic solvent. The organic solvents used were 2-butanone (MEK), cyclophentyl-methyl ether (CPME), tetrahydrofuran (THF) and acetone which were described in chapter 3.2, Table 3.1. The amount of catalyst selected was also introduced in the reactor, and once the reactor was closed, it was purged with N_2 gas; then the pressure was increased up to 10 bar using gas, N_2 or H_2. Finally, the mixture of reaction was preheated up to the selected temperature. To start the reaction, a solution consisting of a mixture of FA and organic solvent (26 vol% FA) was pumped for 3.5 hours at a liquid flow of 0.03 mL/min. After this time, the pump was switched off and the time set in t=0. The test continued with heating and stirring on. Once finished the test, the products inside the reactor were filtered with 0.45 μm filters and weighted for later calculations. A sample was taken to be analyzed via gas chromatography (described in chapter 3.3.1).

The yield (Y) was calculated as the ratio between the number of LA mol formed and the number of FA mol fed (eq.5.1). The conversion (X) was calculated as the ratio between the numbers of FA mol reacted and the number of FA mol fed (eq.5.2). As in some cases two phases were found at the end of the test, each phase was analyzed separately and both the number of moles of the aqueous phase and the number of moles of the organic phase were determined.

$$Y = \frac{(n_{LA,f}^{AP} + n_{LA,f}^{OP})}{n_{FA,i}} \cdot 100 \qquad \textit{(eq.5.1)}$$

$$X = \frac{[n_{FA,i} - (n_{FA,f}^{AP} + n_{FA,f}^{OP})]}{n_{FA,i}} \cdot 100 \qquad \textit{(eq.5.2)}$$

Where:

$n_{LA,f}^{AP}$, $n_{LA,f}^{OP}$ = Final number of LA mol in the aqueous and organic phase, respectively.
$n_{FA,f}^{AP}$, $n_{FA,f}^{OP}$ = Final number of FA mol in the aqueous and organic phase, respectively.

5.3.3. Results of the preliminary screening of catalysts

The results obtained in this preliminary screening are shown in Table 5.1. The results indicate that under the conditions studied, the ion exchange resin A35 was the one showing the best performance (yield to LA, 62 mol%), followed by H-Z(50) zeolite (yield to LA, 58 mol%) and PTA-Z(50) (yield to LA, 58 mol%). The high acidity and pore diameter of A35 were important factors to increase yield to LA. This material was used as reference according to results obtained in chapter 4. The incorporation of PTA on H-Z(50) zeolite did not present improvements in yield to LA respect to support. The characterization results presented in Table 5.1 show a small decrease in both surface area and acidity. The modified H-ZD(50) zeolite did not shown big differences in yield to LA respect to original support, although the desilication process caused a slight increase in pore diameter and surface area, the decrease in yield to LA can be related to acidity loss. The activity results using H-β zeolite (Table 5.1) shows a low yield to LA. The surface characterization indicates that H-β has a high acidity, but a low value of pore diameter, this property can affect the reaction mechanism related to the access of molecules to acid sites, causing the low yield to LA.

Table 5.1 Properties of different solid acid catalysts studied and activity results obtained.

Catalyst	Yield to LA %	Conversion %	S_{BET} (m^2/g)	d_p (Å)	Mesoporosity (%)	Acidity (mmol NH_3/g)
A 47	26.01	99.55	50	240	100	>4.7*
A35	62.39	99.12	50	300	100	≥5.2*
H-β	20.70	91.56	441	6	-	1.282
PTA-USY	19.79	90.18	494	20	10	0.720
H-Z(50)	58.22	99.45	395	24	50	0.826
H-ZD(50)	56.38	99.80	407	37	75	0.661
PTA-Z(50)	58.10	100.00	342	25	34	0.703
ZrO_2/SO_4^{2-}	0.18	58.93	108	34	95	0.338

Reaction conditions: 0.4 g of catalyst, 413 K, 10 bar of H_2, MEK as solvent, 26.2 vol % FA in MEK, 1 h of reaction after 3.5 h of FA feeding. H-ZD(50): zeolite with a desilication process. SBET: surface area determined by BET method, *dp*: Average pore diameter. * Date reported by Rohm and Haas [67] and replicated by Brown et al. (2008) [68].

Very low activity was also observed for the sulfated zirconium catalyst which showed the lowest FA conversion (59 mol %), without a relevant selectivity to LA. The low acidity values reported in Table 5.1 could explain the low activity of the catalyst in this reaction.

The Amberlyst catalysts were included as reference material because they presented good activity in the reaction studied, according to results showed in chapter 4. However, due to their mechanical and thermal limitations which generates active site loss caused by leaching process, the H-Z(50) zeolite, in its protonated form, was selected to be used for optimization of operating parameters in the reaction system.

5.4. Optimization of operating parameters using HZSM-5 zeolite (H-Z(50))

As described in the previous section 5.3.3, the H-Z(50) zeolite was selected as catalyst for optimization of reaction conditions. The optimization consisted in the evaluation of main operation variables and its effect in yield to LA. The variables that were considered for optimization were: the atmosphere of reaction (N_2 and H_2), effect of solvent, effect of the amount of catalyst loaded, variation in the concentration of FA in the feed stream and effect of temperature.

5.4.1. Effect of the atmosphere of reaction

The reaction was studied at different atmospheres, excluding, of course, the oxidant atmosphere that is not suitable for this reaction due to negative effect that produce the formation of undesirable byproducts. In Figure 5.1 it can be seen the difference between the use of an inert (N_2) and hydrogenating (H_2) atmosphere. In the latter case, the yield increases respect to inert atmosphere in almost 20 mol%. The increase in yield to LA can be again attributed to the decrease in formation of resins observed in the remaining mixture in the reactor. The steric effects of hydrogen ("steric bulk") related with space occupied by atoms within a molecule can interpose on the polymerization mechanism.

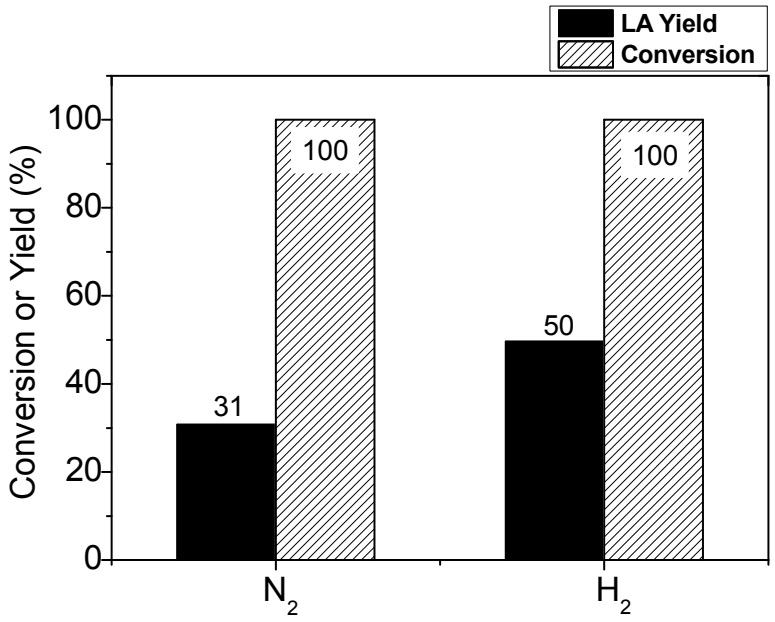

Figure 5.1. Variation of FA conversion and yield to LA by modification of gas media used. Operation conditions: 0.7 g H-Z(50), 20 bar, 463 K, mixture loaded to reactor: 4.2 mL H_2O, 15.8 mL of MEK; flow fed: 0.03 mL/min, 26.2 vol % of FA in MEK.

5.4.2. Effect of solvent

The use of solvent has a high importance in this reaction because its presence in the reaction media also limits the formation of resins. The effect of solvent is related to the mechanism of formation of furan resins by interactions as the solvation process discussed by some authors [56]. The marked tendency of furan derivatives to form resins have motivated studies related to the incorporation of organic co-solvents. Principally, alcohols as ethanol, methanol, butanol and 2-propanol have been used, preventing completely the formation of furan resins. However, these alcohols react with furfuryl alcohol to form the corresponding levulinate esters (ethyl-levulinate, methyl-levulinate, butyl-levulinate) instead of levulinic acid. In various reaction processes related to biomass, solvents have been used to dilute reagents or included into the reaction media as hydrogen donor or extractant agent by the formation of biphasic media. For example, in the obtaining of 5-hydroxymethylfurfural from biomass as cellulose or sugars, the acetonitrile, ethyl acetate, tetrahydrofuran and 2-butylphenol were used as solvents [57]. In the obtaining of furfural from xylose solvents as dioxane,

γ-valerolactone and tetrahydrofuran were also used [58]. The solvents used as hydrogen-donor are tetralin, formic acid, acetic acid and 2-propanol [59]. The compounds with ketone group are also usually used as solvents. These include the acetone, 2-butanone and pentanone [42].

For the study of organic solvents in this chapter, MEK, THF, CPME and acetone were selected. The results obtained are shown in Figure 5.2. The FA conversion in most cases was closer to 100 %. However, the effect of solvent in yield to LA was very significant, specifically in the cases of MEK and acetone. The high value of yield obtained with MEK and acetone, indicates that the ketone group can act as an inhibitor of resin formation. The characteristic cyclic structure of CPME and THF solvents against linear ketone form generated a low association with FA molecules, allowing the activation of the mechanism of polymerization.

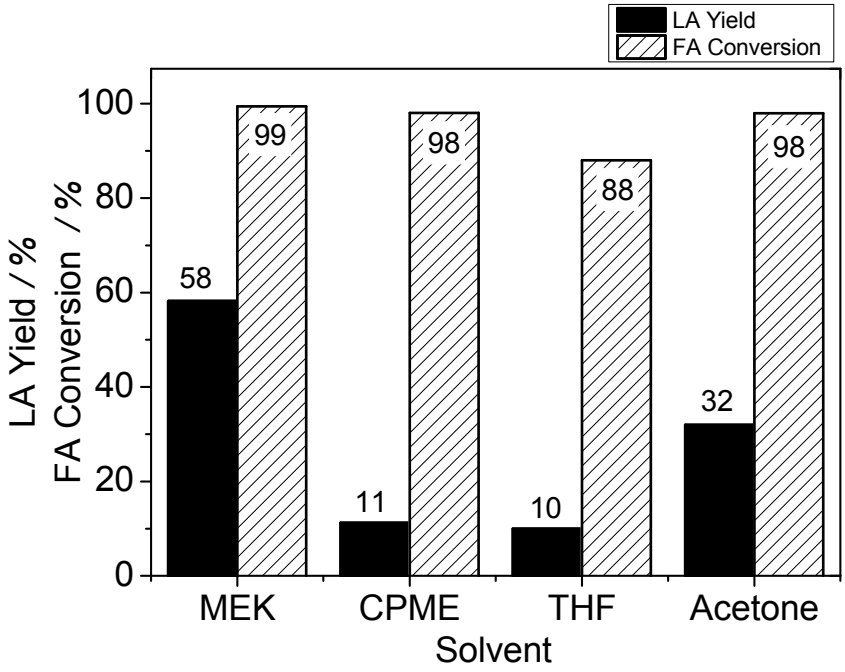

Figure 5.2. Comparative study of organic co-solvents in the reaction of FA to LA. Operation conditions: 413 K, 20 bar of H_2, 0.4 g cat. H-Z(50), 26.2 vol % of FA in organic solvent and 1 h of reaction time.

5.4.3. Effect of the variation in the concentration of FA and the amount of catalyst loaded in the feed stream

The concentration of furfuryl alcohol in the reaction media had influence in the results obtained in previous chapter (4.5.3.1), probably due to the formation of furan resins as reported some authors [2,5,56]; due to this fact, the following parameter of optimization selected was the effect of concentration of FA in the yield to LA.

Figure 5.3 shows LA yield in function of FA concentration, in all cases the conversion of FA was 100%. It can be appreciated an increase in yield to LA with a maximum value of yield to 33.8 vol% of FA in MEK. After this value, a substantial decrease in yield is also observed. Thus, low yield to LA at high concentration of FA could be attributed to the tendency of FA to form furan resin, according to the above referenced. The low values in the concentration of FA fed, also exhibited low yields to LA, in this case attributed to formation of 4-HCP which is a byproduct of reaction analyzed in chapter 4. The formation of 4-HCP is favored at low ratios of FA/H_2O, as was evaluated in chapter 4.5.3.1. The high range of variation of yield to LA shown in Figure 5.3, which represents up to forty percentage points, indicates that it is an important variable to be controlled in this process.

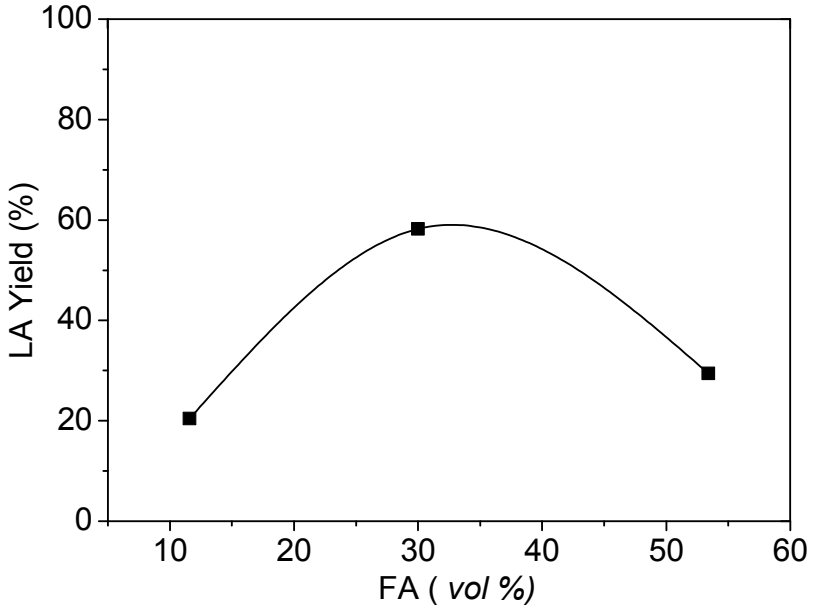

Figure 5.3. Variation of yield to LA, by the modification of FA concentration in the mixture fed. Operation conditions: 413 K, 20 bar H_2, 0.4 g cat H-Z(50), mixture loaded to reactor: 4.2 mL H_2O, 15.8 mL of MEK; flow fed: 0.03 mL/min.

The FA mol fed per gram of catalyst (mol FA/g_{cat}) was also one parameter selected for the optimization in semi-batch system using H-Z(50) as catalyst. The effect of this variable was also evaluated in previous chapter 4.5.3.1, over other reaction system. Those results were conclusive establishing a relationship between the ratios of concentration of FA to mass of catalyst with the yield to LA.

The evolution of yields to LA with this parameter is shown in Figure 5.4. The representation of results indicates that the yield increases with increasing the ratio mol FA/g_{cat}, however, the yield is stable between values of 0.04 and 0.06. So that, the optimal FA concentration was defined as 33 vol% (Figure 5.3) and the quantity of catalysts was chosen as the average value between the two maximum points obtained in Figure 5.4, this value corresponds to 0.5 g of catalyst. Finally, the decrease in LA yield observed at low FA/cat ratios was probably due to an excess of acid sites favoring polymerization reactions.

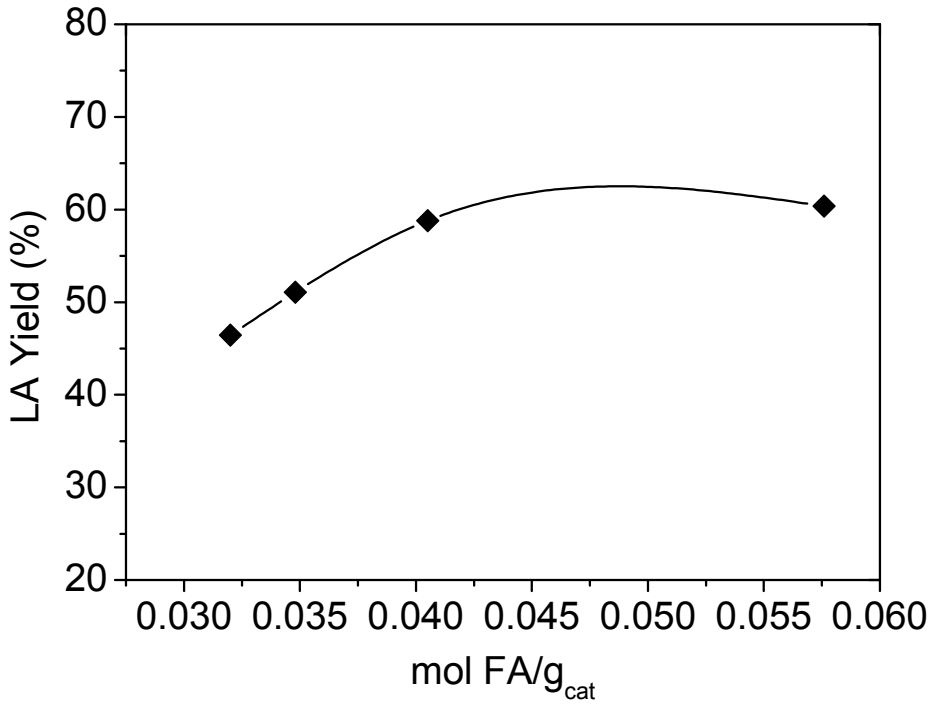

Figure 5.4. Variation of yield to LA for different values of mol FA/ g_{cat}. Operation conditions: 413 K, 20 bar H_2, mixture loaded to reactor: 4.2 mL H_2O, 15.8 mL of MEK, flow fed: 0.03 mL/min, H-Z(50) catalyst.

5.4.4. Effect of temperature

Figure 5.5 shows the effect of temperature in the yield to LA. A slight decrease in the LA yield was observed when the temperature was increased in the range between 413 and 463 K, being more remarkable at 463 K. But, the differences only reached a variation of five percentage points in the yield to LA, which is consistent with the results obtained in previous chapter in continuous flow (chapter 4.4.3.3, Figure 4.7), as well as in chapter 4.5.3.1 (Figure 4.7) in discontinuous system.

Although the effect of temperature in yield to LA was insignificant in the range studied, the formation of some by-products was affected by such changes. This is the case of by-product 4-HCP, which is formed mainly at low temperatures. On the other hand, the increase in temperature can favor the reactions of formation of furan resins as reported by some authors [5, 56].

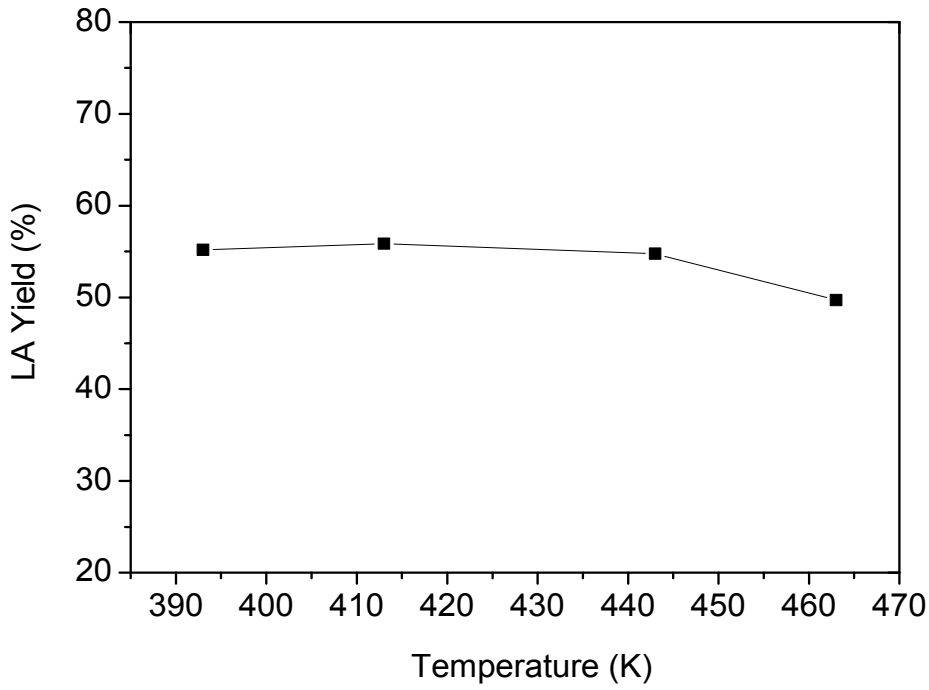

Figure 5.5. Variation of yield to LA by the increases of the temperature. Operation conditions: 20 bar H_2, mixture loaded to reactor: 4.2 mL H_2O, 15.8 mL of MEK, flow fed: 0.03 mL/min at 29 vol% FA, 0.7 g catalyst H-Z(50).

5.4.5. Effect of reaction time

The Figure 5.6 shows the signal intensity corresponding to the three main compounds identified in the reaction: FA, LA and 4-HCP. As it can be seen, the LA signal increased, even when the FA not was already present. This confirms the existence of other intermediate compounds in the reaction which were detected in chromatographic analysis but not identified by the mass spectrometry coupled with gas chromatography (described in chapter 3). The behavior presented by 4-HCP confirms that is a by-product of reaction and it's not an intermediate precursor of LA, because its concentration does not decrease to form LA or other compounds.

A maximum yield to LA was found at 23 h after stopping the feeding pump (Figure 5.7). This value corresponds to 77.7 mol% of yield to LA and 100 mol% of FA conversion. In Figure 5.7 are plotted only the last ten hours of reaction, to show the interval of maximum yield to LA. The differences in yield obtained between 1 hour and 23 hours of reaction reached up to eighteen percentage points. This little difference in yield compared to the long reaction time may not be economically feasible. Therefore, in order to avoid high energy consumption, a low reaction time must be selected considering a slight loss in yield.

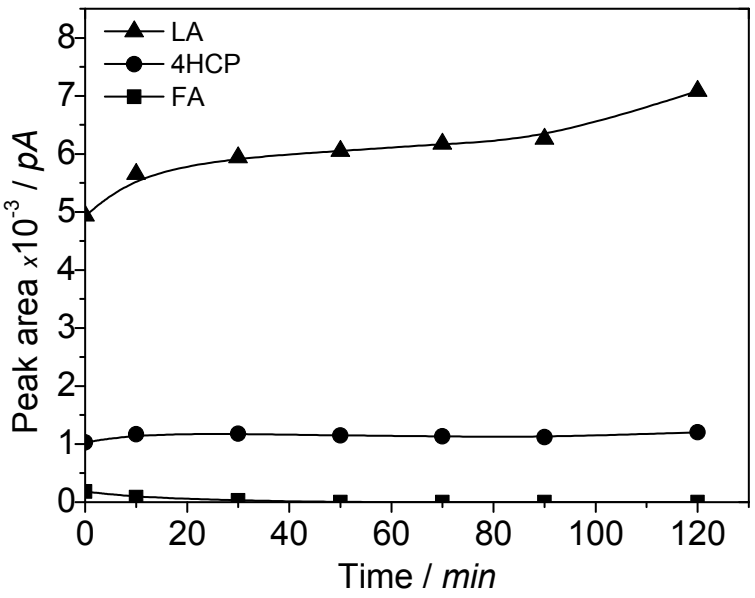

Figure 5.6. Evolution of catalytic activity the main products and reagents during the initials two hours, reported in peak areas. Operation conditions: 0.5 g catalyst H-Z(50), 413 K, 20 bar (H_2), MEK as co-solvent, 36.8 vol % FA.

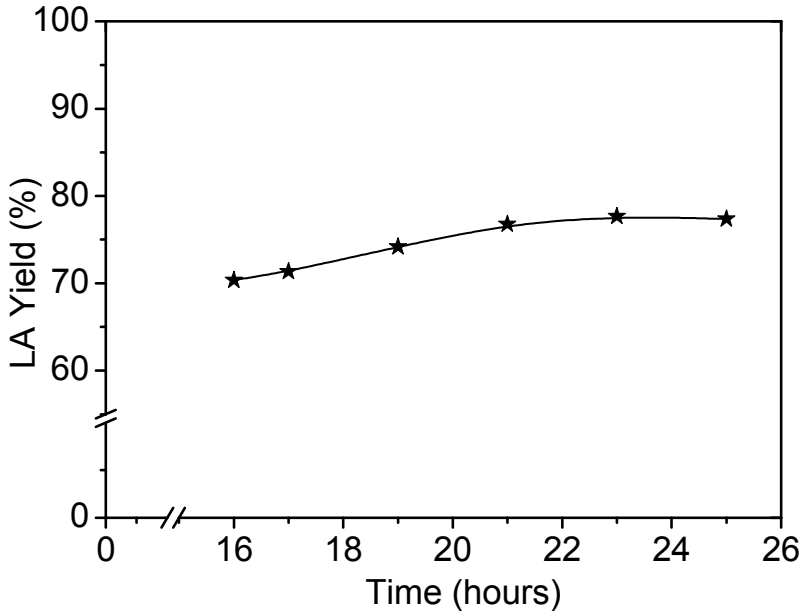

Figure 5.7. Evolution of yield to LA on time of reaction. Operation conditions: 0.5 g cat H-Z(50), 413 K, 20 bar of H_2, MEK as co-solvent, 36.8 vol % FA.

5.4.6. Summary of optimal conditions obtained

After optimization of the main variables, a summary of optimal conditions is shown in Table 5.2. According to results obtained, the most influential variables were: the variation of FA concentration in the mixture fed (increase of yield to LA: 40 %), the effect of solvent (increase in yield to LA: 30 %), the effect of gas medium used (increase in yield to LA: 15%) the variation of quantity of catalyst (increase in yield to LA: 15%) and the variation of temperature (increase in yield to LA: 30 %).

Table 5.2. Summary the optimal conditions obtained using H-Z(50) catalysts

Optimization	Value
Catalyst	HZSM-5
Mass of catalyst (g)	0.5
Temperature (K)	413
Pressure (bar)	20
Gas	H_2
Solvent	MEK
Residence time (h)	23
Concentration of FA fed (vol %)	36.77
Ratio mol FA/g_{cat}	0.057

5.5. ZSM-5 zeolite modified

5.5.1. Use and applications of desilicated zeolites

The modification of zeolite ZSM-5 by desilication is an alternative treatment to obtain materials with high porosity respect to the original. Such as described previously in section 5.2.1, the high thermal stability of HZSM-5 and its significant resistance to deactivation by coke formation, as well as its strong acidity, makes it a catalyst useful for many processes. However, the porosity of the zeolites has an important role in catalytic reactions. By their large size, some molecules need mesoporous materials to access the active sites of catalyst. The desilication has been proven to be an effective method to generate mesoporosity in different types of structures [29-32, 34, 35]. The decrease in silica content (Si/Al ratio), causes an increase in aluminum density, which acts as pore regulator increasing also its acidity [60].

5.5.2. Experimental procedure

5.5.2.1. Desilication of HZSM-5 zeolite

Two ZSM-5 zeolites with different ratios of silica and aluminum were selected for the desilication. The ZSM-5 zeolites (SiO_2/AlO_3:50 and Si/Al: 23) were purchased from the commercial company described in Table 3.2. Previously to the desilication process, the zeolites were calcined to protoned H^+ form at 823 K for 4 hours with a heating rate of 10 K/min. These zeolites were referred as H-Z(50) and H-Z(23). The desilication of H-ZSM-5 zeolites was developed by the following procedure: three grams of parent H-ZSM-5 were mixed with 100 mL of NaOH (0.2M) at 353 K for 2 h. After treatment, the solids were separated by centrifugation and washed with bi-distilled water until neutral pH, then the solid was dried at 383 K overnight. Afterwards, the treated zeolites were exchanged with 50 mL of NH_4Cl (0.5M) at 333 K; the samples again were centrifuged and washed until they were free of chlorides followed by overnight drying at 383 K. Finally, the solid samples were calcined at 823 K for 4 h to exchange NH_4 to H^+ form.

In the following sections the desilicated zeolites are referred as H-ZD(50) and H-ZD(23). The zeolites after reaction were recovered and calcined again for its activation, these were named as H-ZR(50), H-ZDR(50), H-ZDR(23).

5.5.2.2. Characterization of catalysts

The elemental composition of catalysts was determined by energy dispersion X-ray analysis (EDX), described in chapter 3.4.2.

Textural parameters were determined by N_2 adsorption-desorption techniques at 77.35 K, specific surface area was obtained by applying BET method and the total pore volume was calculated at P/P_0= 0.976.

Temperature-programmed desorption of ammonia (NH_3-TPD) was used in order to measure the amount and strength of acid sites on the catalysts. The TPD profiles were monitored by a thermal conductivity detector and recorded from 373 to 823 K with a heating rate of 10 K/min. 15 mg of catalyst was pretreated in a helium flow (30 mL/min) at 773 K for 1 h to remove the physisorbed water and the intracrystalline water. The sample was cooled to 373 K and then, NH_3 was absorbed using pulsed injections at 373 K until saturation. The TCD signal was collected for processing of results.

5.5.2.3. Catalytic activity

The catalytic activity was tested in the semi-continuous system described in chapter 3.5.2, the conditions were established according to the results of optimization, which are summarized in Table 5.2. For all test, the procedure was as follows: the reactor was loaded with a mixture of 4.2 mL of bi-distilled water and 15.8 mL of solvent MEK. Exactly 500 mg of catalyst were introduced in the reactor. Once the reactor was closed, it was purged three times with H_2 gas, and then the pressure was established to 10 bar. Finally, the system was preheated to 413 K, and the stirring was started at 700 rpm. A solution consisting of a mixture of FA (37 vol%) and MEK was pumped up to 3.5 hours with a flow of 0.03 mL/min. After this time, the pump was switched off and the time set to t=0. The test continued with heating and stirring on, up to 23 hours. Once finished the

test, the products inside of reactor were filtered with 0.45 µm filters and then weighted for later calculations. A sample was taken to be analyzed by the gas chromatograph described in paragraph 3.3.1.

5.5.3. Results

5.5.3.1. Results of characterization

The content of silicon and aluminum in the zeolites was measured by EDX technique, the signal of the scanning electron microscope is shown in Figure 5.8. Three points were selected at 100 µm to determine the elemental composition of the materials corresponding to an average of the three points.

The atomic silica-alumina ratio is represented for all samples in Table 5.3. The results indicates that desilication process was effective for both zeolites H-Z(50) and H-Z(23). The silica-alumina ratios decreased in greater proportion in the case of the H-Z(50) zeolite, respect to H-Z(23). The effectivity of desilication is associated to the concentration of NaOH and content of silicon. In this study a concentration 0.2 M of NaOH was previously selected, supported by the best results obtained by Sadowska et al [61].

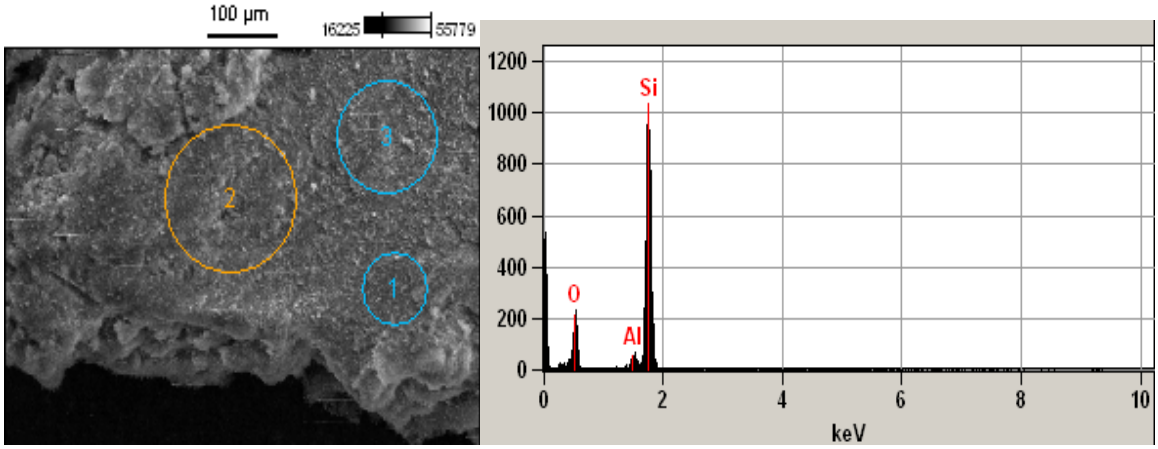

Figure 5.8. Signal of energy dispersion X-ray analysis (EDX) for zeolite H-Z(50)

Table 5.3. Summary of textural properties and elemental composition of the zeolites studied

Catalyst	Si/Al Atom ratio*	S_{BET} (m^2/g)	Mesopore area (m^2/g)	Dp (Å)	Volume (cm^3/g)	
					Mesopore	Micropore
H-Z(50)	25.7	395	138	24	0.24	0.12
H-ZD(50)	21.6	407	203	37	0.29	0.09
H-ZR(50)	26.2	386	168	25	0.14	0.10
H-ZDR(50)	21.8	300	106	42	0.23	0.09
H-Z(23)	11.6	314	80	23	0.07	0.11
H-ZD(23)	10.7	296	104	30	0.13	0.09
H-ZDR(23)	11.5	332	95	27	0.12	0.11

*Determined by EDX analysis, S_{BET}: surface area determined by BET method, Dp: average pore diameter.

The nitrogen physisorbed isotherms are shown in Figures 5.9 and 5.10. The larger slopes of hysteresis loops indicate a higher adsorption capacity of samples desilicated in comparison to parent zeolite. The adsorption desorption-isotherms obtained for each sample are typical of materials with micro and mesoporosity in its structure and can be classified as type IV isotherms with H3 type hysteresis loops closing at P/P_0=0.4.

The results of textural properties are also included in Table 5.3, corresponding to surface area (BET), micro and mesoporosity volumes, and pore size. The effect of desilication on surface properties of zeolites is evident: the mesoporosity increased in both catalysts (H-ZD(50) and H-ZD(23)) respect to parent zeolites. Mesopore volumes increased up to 85% in the case of H-Z(23) and 21% in H-Z(50). These results are consistent with the mesopore surface area obtained, where its increase reaches up to 47% in the case of H-Z(50) zeolite. The pore diameter also increased up to 54% for H-Z(50) and 30% for H-Z(23).

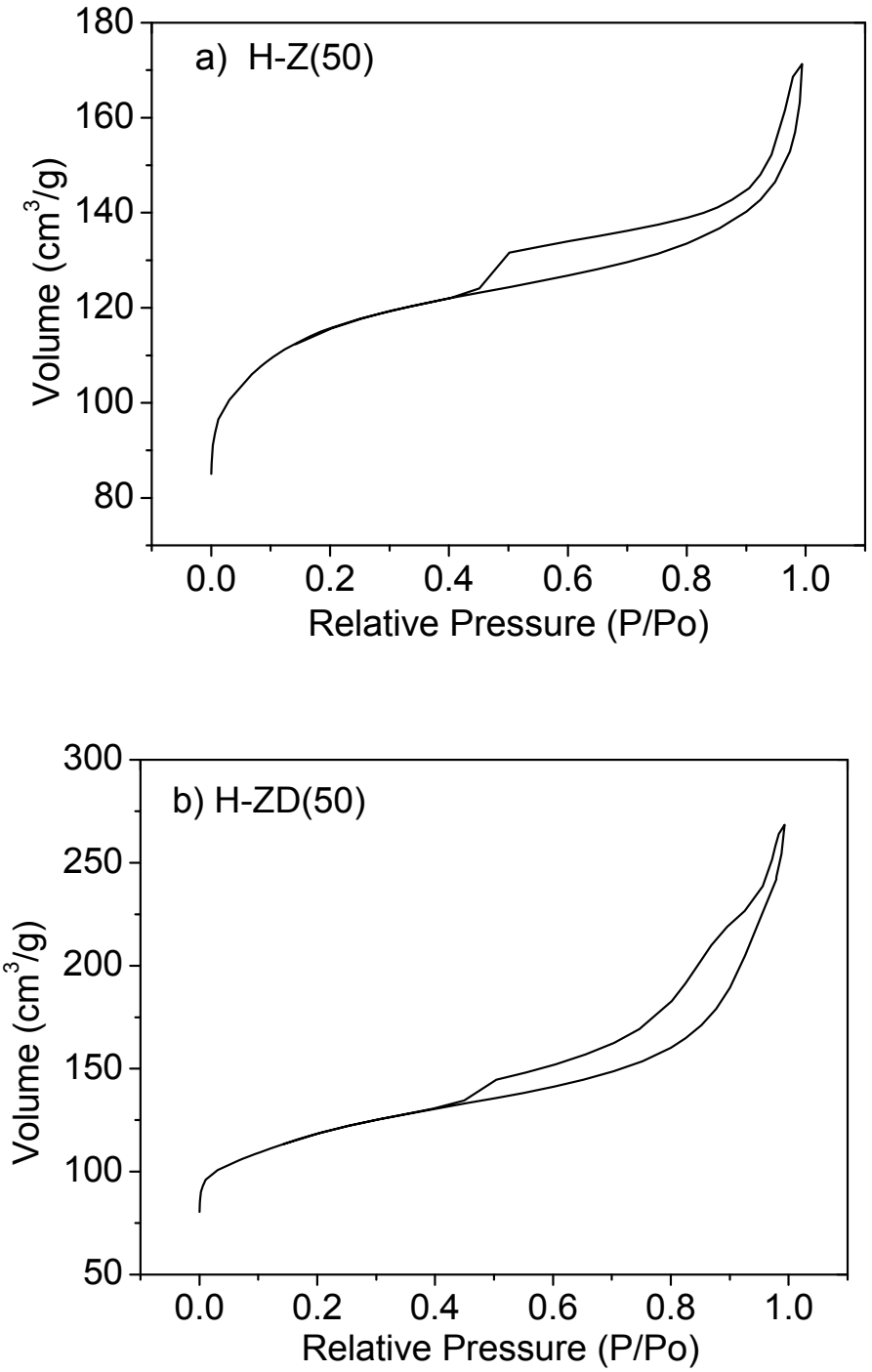

Figure 5.9.1 Nitrogen adsorption and desorption isotherms of a) H-Z(50), b) H-ZD(50).

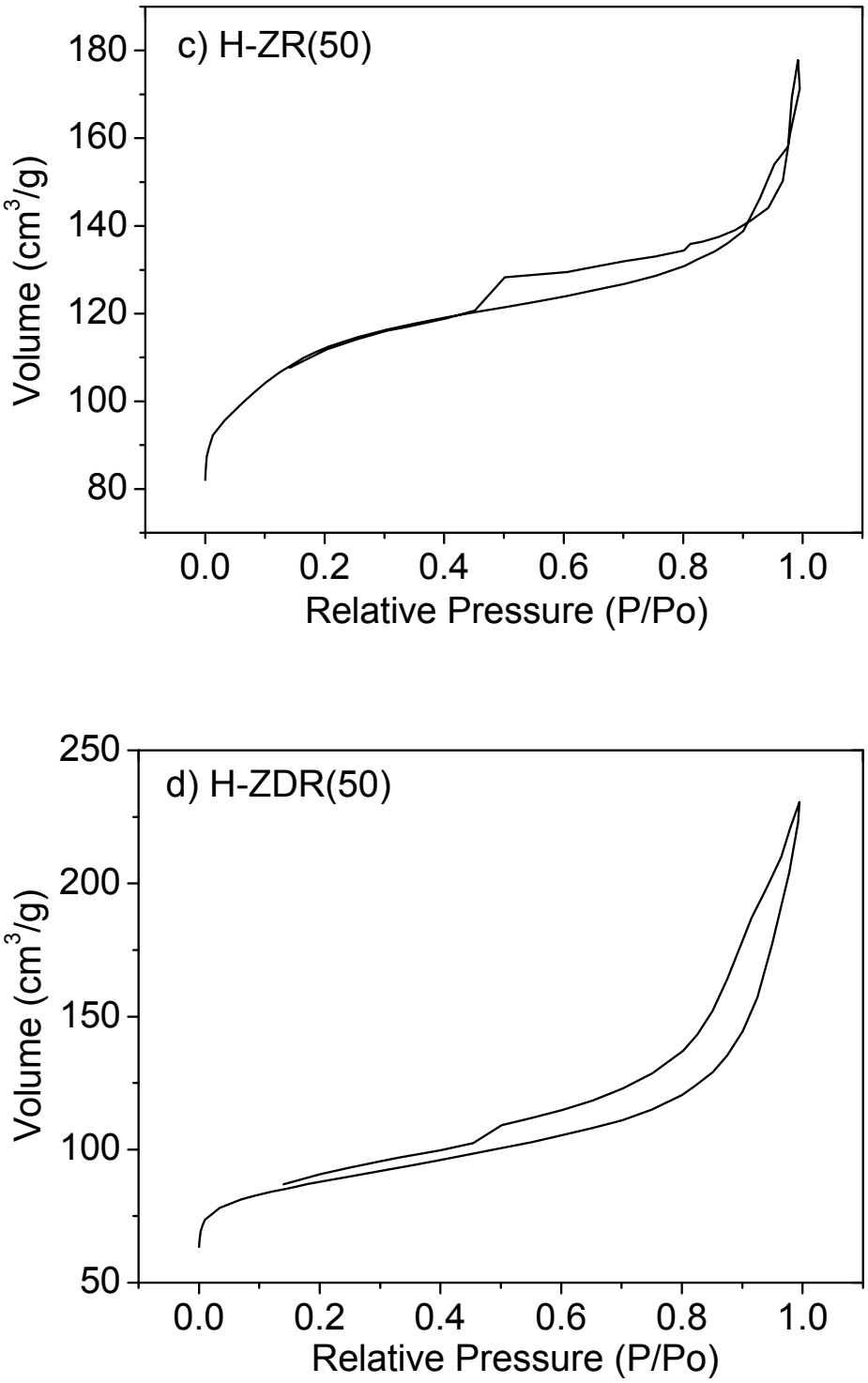

Figure 5.9.2 Nitrogen adsorption and desorption isotherms of c) H-ZR(50), d) H-ZDR(50).

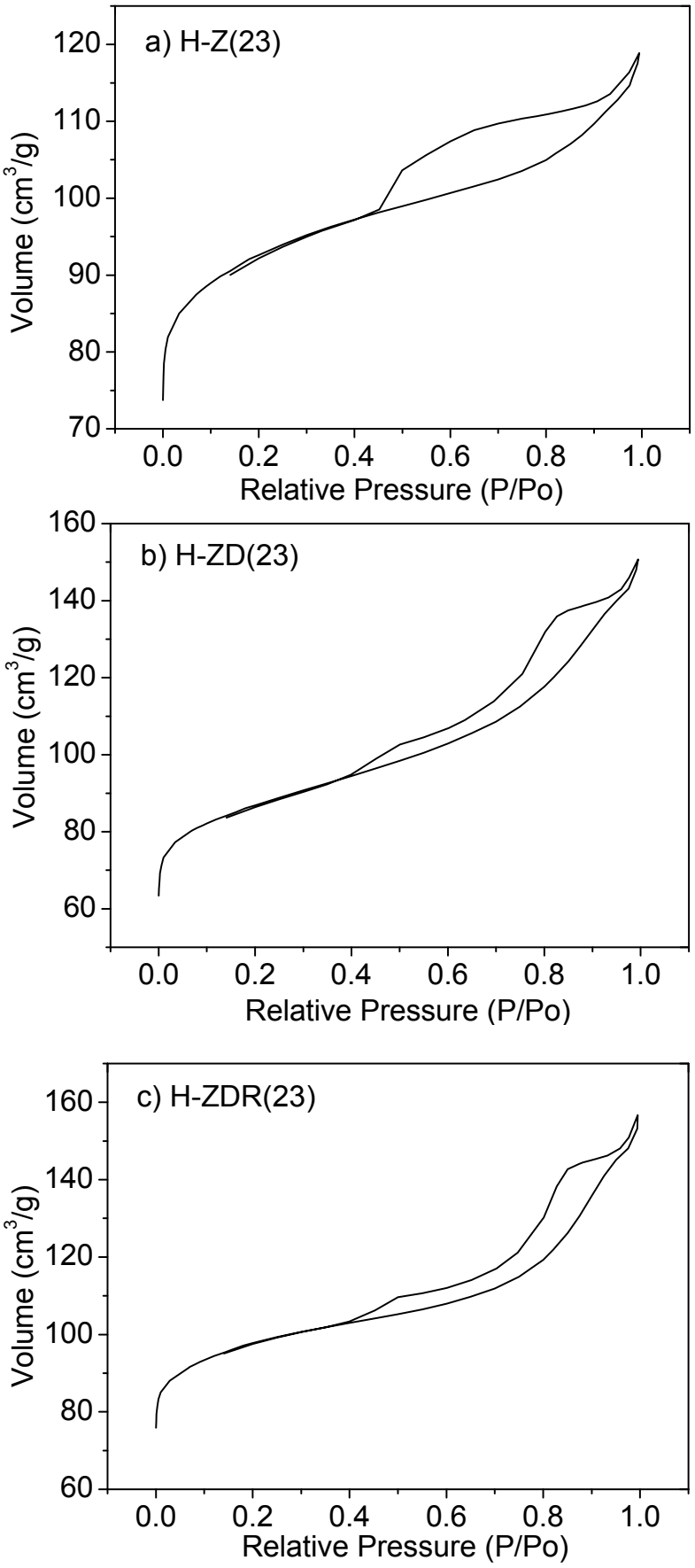

Figure 5.10. Nitrogen adsorption and desorption isotherms of a) H-Z(23), b) H-ZD(23), c) H-ZDR(23).

The acidity was also modified by the desilication process of the zeolites studied. The results of total acidity analyzed by ammonium TPD are shown in Table 5.4. The results show that weak acid sites increased by the desilication of H-Z(50) and H-Z(23), whereas the strong acid sites only increased slightly for H-Z(23).

Table 5.4. Results of acidity by TPD-NH_3

Catalyst	*Acid strength (mmol NH_3/g)		Total acidity (mmol NH_3/g)
	Weak	Strong	
H-Z(50)	0.356	0.470	0.826
H-ZD(50)	0.545	0.116	0.661
H-ZR(50)	0.484	0.243	0.727
H-ZDR(50)	0.412	0.221	0.633
H-Z(23)	0.818	0.126	0.944
H-ZD(23)	1.048	0.158	1.206
H-ZDR(23)	0.801	0.137	0.938

*Average acid strenght weak: 503 K; strong: 678 K.

Figure 5.11 shows the TPD-NH_3 profile for H-Z(50) and H-Z(23). This is compared with TPD-NH_3 of modified and recovered zeolites H-ZD(50), H-ZR(50), H-ZDR(50), H-ZD(23) and H-ZDR(23). Two regions are observed in the profiles of ammonia desorption. The region I is referred as low temperature region at 400-550 K corresponding to the weak acidity. The region II is referred as high temperature region which is comprised in a range of 550-750 K, which represents the strong acid sites.

The zeolite H-Z(50) has a considerable strong acid strength, compared with other zeolites (Figure 5.11 and Table 5.4). The peak at high temperature can be attributed to desorption of NH_3 from strong Brönsted and Lewis sites, whereas the peak at low temperature range is ascribed to desorption from weakly acidic silanol groups, according to various authors [62-65]. Meshram et al. (1986) [65] suggested the possibility that the weak strength acid sites are terminal silanol groups $[Al(OH)_2]^+$ and $[Al(OH)]^{2+}$, which could be sorption sites of weak Lewis acid type [65].

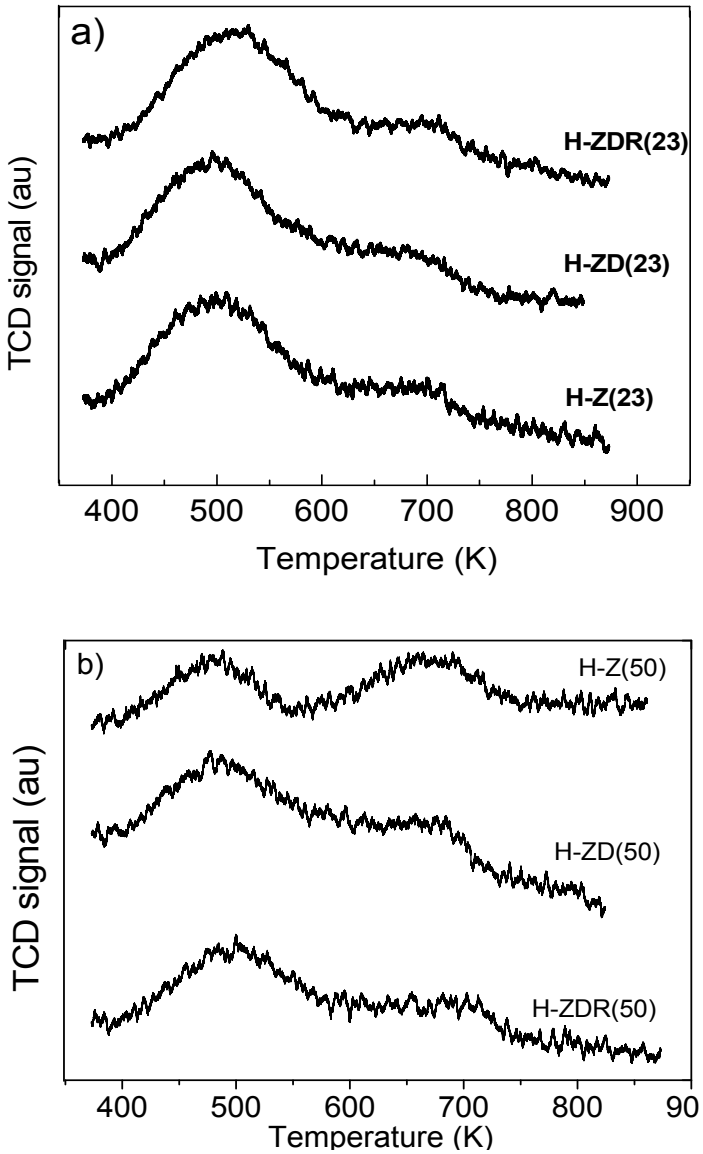

Figure 5.11. TPD-NH_3 profiles of the parent and desilicated zeolites: a) H-Z(23), H-ZD(23) and H-ZDR(23). b) H-Z(50), H-ZD(50) and H-ZDR(50).

FT-IR analyses were developed in a VERTEX 70 Bruker XSA apparatus described in chapter 3.4.8. IR spectra were collected at 423 K which was the temperature selected for activity tests. Pyridine was adsorbed at 313 K after two hours of dehumidification treatment at 723 K under vacuum; the presence of water could affect the quantification of pyridine coordinatively bonded on Lewis acid sites (Lpy), because hydrogen bonded pyridine (Hpy) can be detected at 1440 cm^{-1} [66]. IR spectra after pyridine evacuation were collected for all zeolites studied in this section.

Focusing the study on chemisorbed pyridine species in Lewis and Brönsted acid sites, in Figure 5.12 is summarized the IR spectra. Two bands at 1445 and 1540 cm^{-1} corresponding to chemisorbed pyridine on Lewis acid site (Lpy) and Brönsted acid site (Bpy) respectively are marked by a dotted line in Figure 5.12. Its corresponding peak areas were obtained by integration of IR spectra peak such as shown in Figure 5.13.

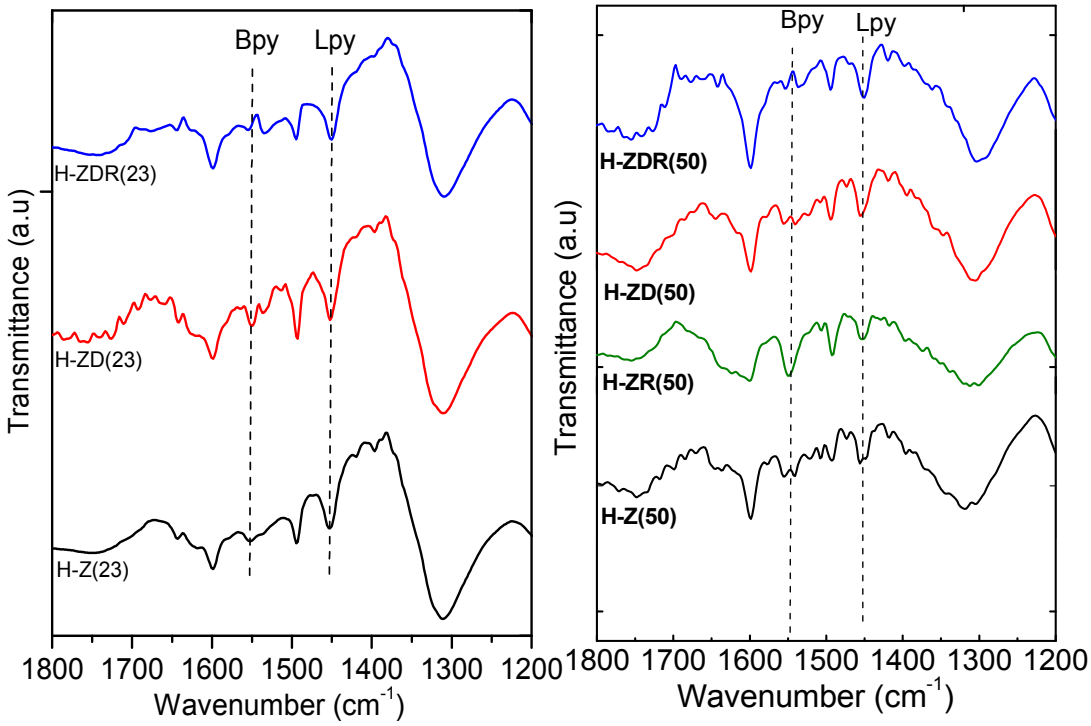

Figure 5.12. FT-IR spectra of pyridine chemisorbed on HZSM-5 catalysts at 313 K. Spectra collected at 413 K in the region of 1200–1800 cm^{-1}. Samples dehumidified at 723 K, 2 hours.

The results of Brönsted and Lewis acidity, summarized in Table 5.5, showed a decrease of Brönsted acidity on H-ZD(50) respect to the parent H-Z(50). This result is offset by a slight increase in Lewis acidity, indicating an increase in alumina density of the catalyst (Table 5.3) caused by desilication process, favors the formation of coordinated Lewis bond, such as is also evidenced in the case of H-ZD(23) respect to its precursor H-Z(23).

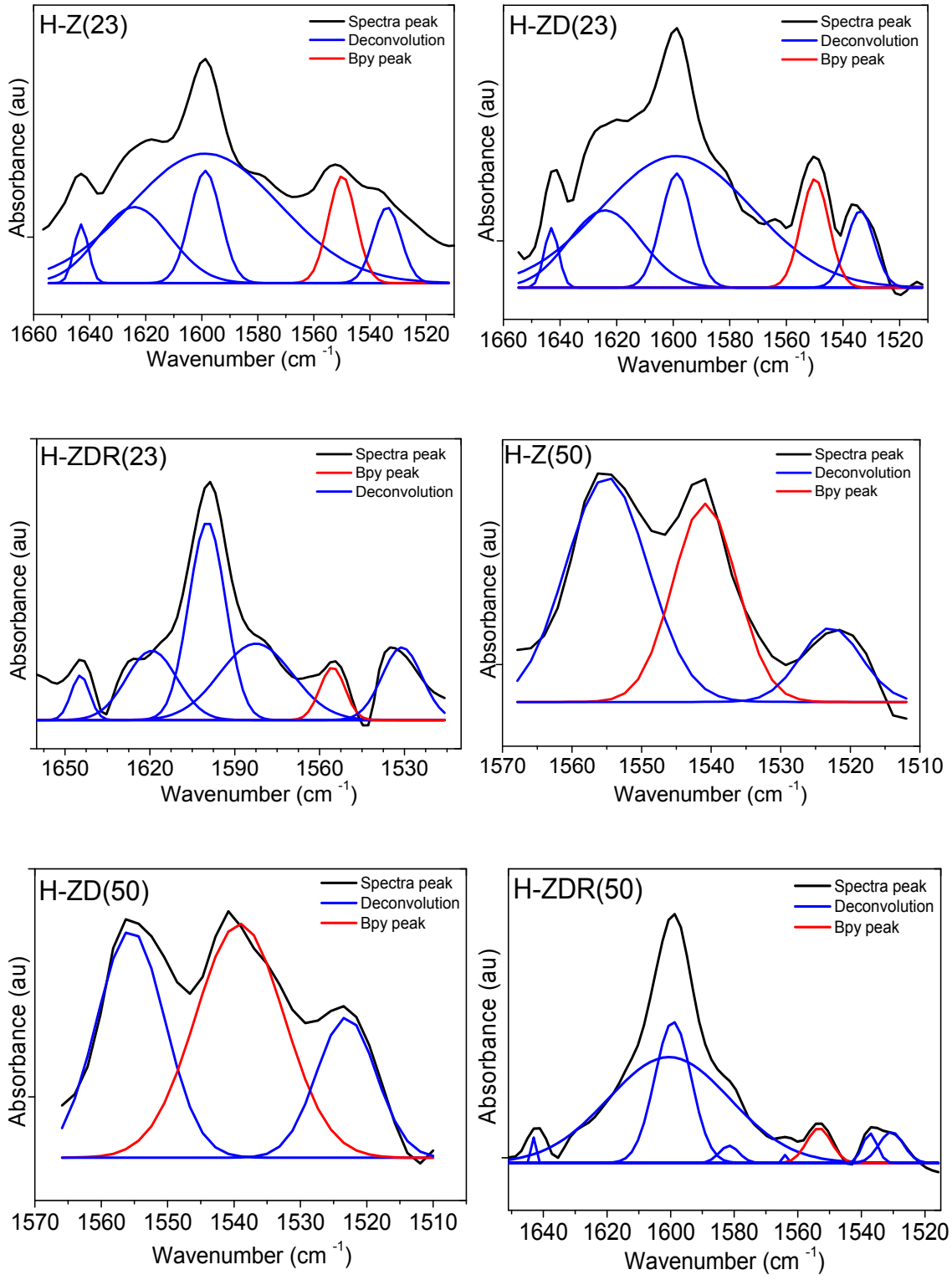

Figure 5.13. Deconvolution spectra of pyridine chemisorbed on H-Z(50) at 313 K. Spectra collected at 413 K in the region of 1570–1530 cm^{-1}. Samples dehumidified at 723 K, 2 hours.

Table 5.5. Result of acidity by FTIR spectra of adsorbed pyridine

Catalyst	Bpy and Lpy peak area fraction		Type of acidity (mmol NH_3/g)	
	Bpy	Lpy	Bpy	Lpy
H-Z(50)	0.561	0.439	0.463	0.363
H-ZD(50)	0.313	0.687	0.207	0.454
H-ZR(50)	0.711	0.289	0.517	0.210
H-ZDR(50)	0.216	0.784	0.137	0.496
H-Z(23)	0.153	0.847	0.144	0.800
H-ZD(23)	0.161	0.839	0.194	1.012
H-ZDR(23)	0.067	0.933	0.063	0.875

Lpy: pyridine coordinatively bonded on Lewis acid sites, Bpy: Protonated bonded pyridine (Brönsted).

5.5.3.2. Results of catalytic activity

The catalytic activity of H-Z(23), H-Z(50) and desilicated H-ZD(50), H-ZD(23) zeolites was evaluated in the reaction of obtaining LA from FA, using the semi-batch system specified in section 5.4.2.3. In Figure 5.14 are shown the yields to LA and conversions of FA obtained with the above referenced catalysts. The results show that zeolite H-ZD(23) has highest yield to LA, respect to the other zeolites tested. This zeolite showed an increase up to 18 percentage points in yield with respect to the parent H-Z(23), indicating the effectiveness the desilication process, which is highly related with increases in its mesoporosity and acidity. However, the results are not positive for H-ZD(50) that decreased up to 16 percentage points in yield respect to the parent H-Z(50), this decrease can be related to Brönsted acidity loss evidenced in Table 5.5.

Due to the high yield shown by H-ZD(23), a comparative study of its catalytic activity with reaction time respect to H-Z(23) is shown in Figure 5.15. The results shows that H-Z(23) presented lower yield to LA that the desilicated H-ZD(23), which reaches a maximum yield at 14 hours of reaction (81 %), while H-Z(23) only reaches 65 % in 23

hours. After the maximum yield obtained at 14 hours, the yield to LA decreased up to 71 mol% at 23 hours. This decrease in yield to LA can be related to dehydration reaction of LA to form α-angelica lactone, which was identified in the gas chromatograph-coupled to mass spectrometry detector (described in chapter 3.4.1) with a 72 % probability.

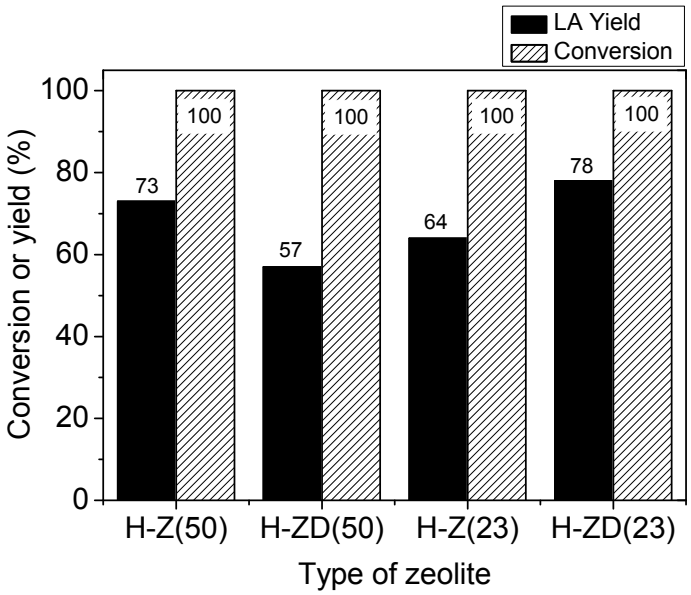

Figure 5.14. Yield to LA by the use of parent and desilicated zeolites. Operation conditions: 413K, 10 bar of H_2, 0.5 g catalyst, 36 vol% of FA in MEK and 23 h of reaction time.

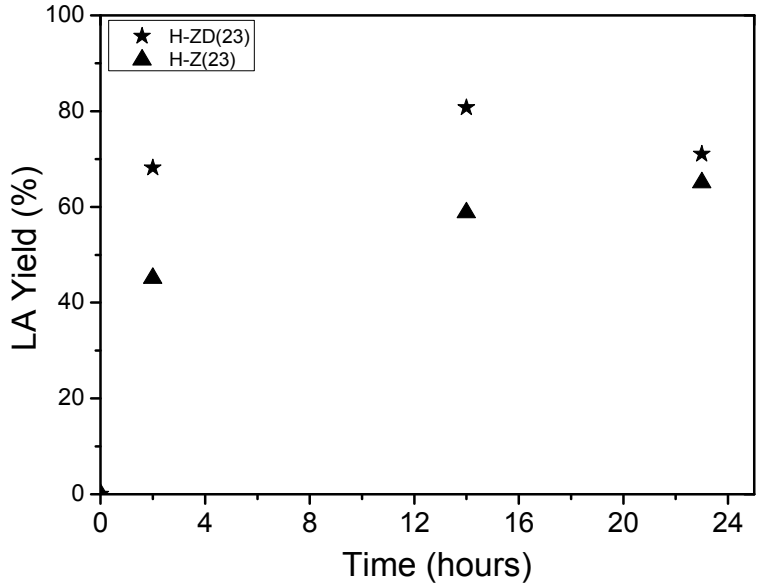

Figure 5.15. Yield to LA on the reaction time for H-Z(23) and H-ZD (23) zeolites. Operation conditions: 413K, 10 bar of H_2, 0.5 g catalyst, 36 vol% of FA in MEK.

The comparative of the activity tests between H-ZD(23) and the recycled H-ZDR(23) are shown in Figure 5.16. The recovered zeolite correspond to H-ZD(23) which was collected after 23 hours of reaction and then calcined to 823 K.

A little difference in the results is observed between both zeolites. The yield to LA obtained with H-ZDR(23) reaches a 74 %, showing a similar behavior than H-ZD(23). The slight difference in yield to LA can be related with variations in some surface properties summarized in Table 5.3. The H-ZDR(23) has a slight decrease of mesoporosity, which includes a little decrease of mesopore area and pore diameter, and greater loss of acidity. Nonetheless, the viability of recovery and recycling of the H-ZD(23) zeolite is highly positive, because the yield only decreased up to 7 mol%, which is a factor very important related with the economical feasibility.

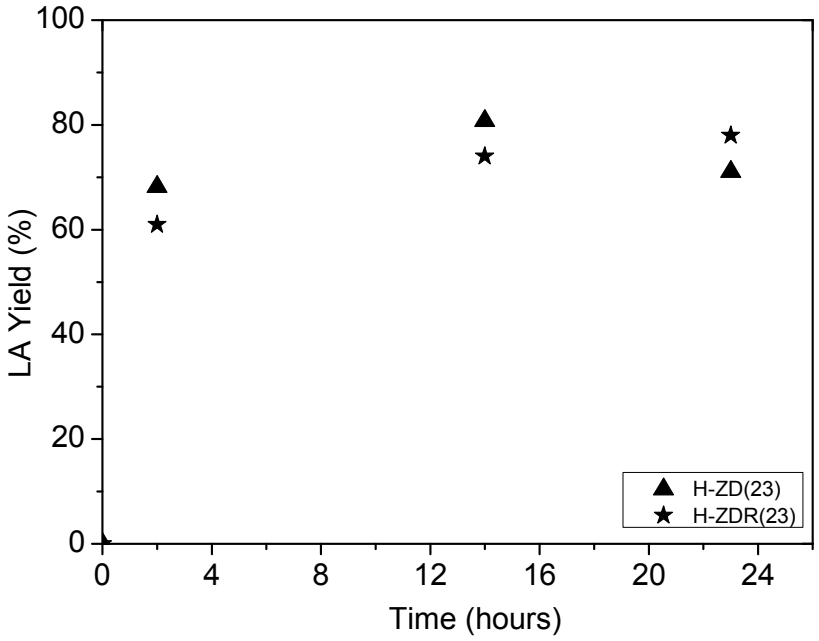

Figure 5.16. Comparison of yields to LA between desilicated H-ZD(23) and recovery H-ZDR(23). Operation conditions: 413K, 10 bar of H_2, 0.5 g catalyst, 36 vol% of FA in MEK.

According to results reported above, the maximum yield to LA obtained by the use of H-ZD(23) reached a 81 mol%, the remaining 19 % that does not react to LA, comprises a series of compound which were observed in the chromatogram at low intensity peaks, most of them not identified by mass spectroscopy. Between the

components with most probability obtained by GC-MS are α-angelicalactone and 4-HCP which was completely identified. It should be noted that during all activity tests, formation of furan resins was not observed (because furan resins were not adhered to wall of reactor and yellow coloration was not observed).

5.6 Conclusions

The ketone group was evaluated against other solvents which showed lower yield to LA. After the screening of catalysts with inorganic structure, the HZSM-5 zeolite showed higher yields to LA compared to other materials evaluated as heteropolyacids (PTA), superacids (zirconium sulfated) and other zeolites. The structure of HZSM-5 allows many configuration options which are related with the silica-alumina ratios. The surface properties can be modified by varying the alumina content. The increase of alumina content on HZSM-5 zeolite by the desilication process was effective, increasing the pore diameter and mesopore volumes, as well as its total acidity. The desilicated H-ZSM-5 with a lower Si/Al ratio (H-ZD(23)) showed the best yield to LA, up to 81 mol%, which represents eleven percentage points higher than parent H-Z(23), a positive recycling also is noteworthy, because the yield only decreased about 7 mol%.

The desilication process on H-Z(5O) also was effective respect to the increase of mesoporosity and pore diameter, but the yield to LA decreased notoriously due to acidity loss, as determined in the characterization. The reaction system used was a semicontinuous system which allowed the increase of yield to LA, minimizing the formation of undesired furan resins, by the incorporation of MEK as solvent of FA in feeding.

5.7 References

[1] J.J. Bozell, L. Moens, D.C. Elliott, Y. Wang, G.G. Neuenscwander, S.W. Fitzpatrick, R.J. Bilski, J.L. Jarnefeld, Production of levulinic acid and use as a platform chemical for derived products, Resour. Conserv. Recycling. 28 (2000) 227-239.

[2] B. Capai, G. Lartigau, Preparation of Levulinic acid, US Patent. 5,175,358 (1992).

[3] G. González Maldonado, R. Assary, J. Dumesic, L. Curtiss, Experimental and theoretical studies of the acid-catalyzed conversion of furfuryl alcohol to levulinic acid in aqueous solution, Energy. Environ. Sci. 5 (2012) 6981-6989.

[4] R.I. Khusnutdinov, A.R. Baiguzina, A.A. Smirnov, R.R. Mukminov, U.M. Dzhemilev, Furfuryl Alcohol in Synthesis of Levulinic Acid Esters and Difurylmethane with Fe and Rh Complexes, Russ. J. Appl. Chem. 80 (2007) 1687-1690.

[5] M.Hronec,K.Fulajta,T.Sota, Kinetics of high temperature conversion of furfuryl alcohol in water, J. Ind. Eng. Chem. (2014) 650-655.

[6] W. Aslam, M.A.B. Siddiqui, B. Rabindran Jermy, A. Aitani, J. Čejka, S. Al-Khattaf, Selective synthesis of linear alkylbenzene by alkylation of benzene with 1-dodecene over desilicated zeolites, Catal. Today. 227 (2014) 187-197.

[7] G.C. Laredo, R. Quintana-Solórzano, J.J. Castillo, H. Armendáriz-Herrera, J.L. Garcia-Gutierrez, Benzene reduction in gasoline by alkylation with propylene over MCM-22 zeolite with a different Brönsted/Lewis acidity ratios, Appl. Cat. A: Gen. 454 (2013) 37-45.

[8] T. Odedairo, S. Al-Khattaf, Comparative study of zeolite catalyzed alkylation of benzene with alcohols of different chain length: H-ZSM-5 versus mordenite, Catal. Today. 204 (2013) 73-84.

[9] I. Craciun, M. Reyniers, G.B. Marin, Liquid-phase alkylation of benzene with octenes over Y zeolites: Kinetic modeling including acidity descriptors, J. Catal. 294 (2012) 136-150.

[10] Z. Zhao, W. Wang, W. Qiao, G. Wang, Z. Li, L. Cheng, HY zeolite catalyst for alkylation of α-methylnaphthalene with long-chain alkenes, Microporous Mesoporous Mater. 93 (2006) 164-170.

[11] P. Hudec, A. Nociar, A. Smiešková, T. Jakubík, Liquid-phase alkylation of benzene by long-chain linear α-olefins over Y and mordenite type zeolite catalysts. Influence of Si/Al ratio, Stud. Surf. Sci. Catal. 158, Part B (2005) 1795-1802.

[12] R. Anand, S.S. Khaire, R. Maheswari, K.U. Gore, V.R. Chumbhale, N-Alkylation of aniline with ethanol over HY and dealuminated HY zeolites, Appl. Catal A: Gen. 242 (2003) 171-177

[13] R. Anand, R. Maheswari, K.U. Gore, V.R. Chumbhale, Selective alkylation of catechol with t-butyl alcohol over HY and modified HY zeolites, Catal. Commun. 3 (2002) 321-326.

[14] D. Venu Gopal, B. Srinivas, V. Durgakumari, M. Subrahmanyam, Vapor-phase alkylation of indole with methanol over zeolites, Appl. Cat. Gen. 224 (2002) 121-128.

[15] K. Zhang, H. Zhang, G. Xu, S. Xiang, D. Xu, S. Liu, H. Li, Alkylation of phenol with tert-butyl alcohol catalyzed by large pore zeolites, Appl. Cat. Gen. 207 (2001) 183-190.

[16] Z. Da, P. Magnoux, M. Guisnet, Liquid phase alkylation of toluene with 1-heptene over a HFAU zeolite: evidence for transalkylation between toluene and non-desorbed products, Appl. Cat. Gen. 182 (1999) 407-411.

[17] J. Aguilar, F.V. Melo, E. Sastre, Alkylation of biphenyl with methanol over Y zeolites, Appl. Catal. Gen. 175 (1998) 181-189.

[18] N. Viswanadham, G. Muralidhar, T.S.R.P. Rao, Cracking and aromatization properties of some metal modified ZSM-5 catalysts for light alkane conversions, J. Mol. Catal. Chem. 223 (2004) 269-274.

[19] L.A. Pine, P.J. Maher, W.A. Wachter, Prediction of cracking catalyst behavior by a zeolite unit cell size model , J. Catal. 85 (1984) 466.

[20] F.A. Khowatimy, Y. Priastomo, E. Febriyanti, H. Riyantoko, W. Trisunaryanti, Study of Waste Lubricant Hydrocracking into Fuel Fraction over the Combination of Y-Zeolite and ZnO Catalyst, Pro. Environ. Sci. 20 (2014) 225-234.

[21] A. Jentys, G. Warecka, J.A. Lercher, Surface chemistry of HZSM-5 studied by time-resolved IR spectroscopy, J. Mol. Catal. 51 (1989) 309-327.

[22] D. Tzoulaki, A. Jentys, J. Pérez-Ramírez, K. Egeblad, J.A. Lercher, On the location, strength and accessibility of Brønsted acid sites in hierarchical ZSM-5 particles, Catal. Today. 198 (2012) 3-11.

[23] J.A. van Bokhoven, Chapter 24 - Strong Brønsted Acidity in Alumina-Silicates: Influence of Pore Dimension, Steaming and Acid Site Density on Cracking of Alkanes, in: V. Valtchev, S. Mintova, M. Tsapatsis (Eds.), Ordered Porous Solids, Elsevier. 1 (2009) 651-668.

[24] A.G. Pelmenschikov, R.A. van Santen, J.H.M.C. van Wolput, J. Jänchen, The IR transmission windows of hydrogen bonded complexes in zeolites: a new

interpretation of IR data of acetonitrile and water adsorption on zeolitic Brönsted sites, Stud. Surf. Sci. Catal. 84 (1994) 2179-2186.

[25] C. Pereira, R.J. Gorte, Method for distinguishing Brønsted-acid sites in mixtures of H-ZSM-5, H-Y and silica-alumina, Appl. Catal. Gen. 90 (1992) 145-157.

[26] B. Su, V. Norberg, Characterization of the Brønsted Acid Properties of H(Na)-Beta Zeolite by Infrared Spectroscopy and Thermal Analysis, Zeolites. 19 (1997) 65-74.

[27] H. Fujita, T. Kanougi, T. Atoguchi, Distribution of Brønsted acid sites on beta zeolite H-BEA: A periodic density functional theory calculation, Appl. Catal. Gen. 313 (2006) 160-166.

[28] J. Li, X. Li, G. Zhou, W. Wang, C. Wang, S. Komarneni, Y. Wang, Catalytic fast pyrolysis of biomass with mesoporous ZSM-5 zeolites prepared by desilication with NaOH solutions, Appl. Catal. Gen. 470 (2014) 115-122.

[29] B. Gil, L. Mokrzycki, B. Sulikowski, Z. Olejniczak, S. Walas, Desilication of ZSM-5 and ZSM-12 zeolites: Impact on textural, acidic and catalytic properties, Catal. Today. 152 (2010) 24-32.

[30] K. Sadowska, K. Góra-Marek, J. Datka, Hierarchic zeolites studied by IR spectroscopy: Acid properties of zeolite ZSM-5 desilicated with NaOH and NaOH/tetrabutylamine hydroxide, Vib. Spectrosc 63 (2012) 418-425.

[31] K. Sadowska, A. Wach, Z. Olejniczak, P. Kuśtrowski, J. Datka, Hierarchic zeolites: Zeolite ZSM-5 desilicated with NaOH and NaOH/tetrabutylamine hydroxide, Microporous Mesoporous Mater. 167 (2013) 82-88.

[32] S.J. You, E.D. Park, Effects of dealumination and desilication of H-ZSM-5 on xylose dehydration, Microporous Mesoporous Mater. 186 (2014) 121-129.

[33] M.D. González, Y. Cesteros, P. Salagre, Establishing the role of Brønsted acidity and porosity for the catalytic etherification of glycerol with tert-butanol by modifying zeolites, Appl. Catal. Gen. 450 (2013) 178-188.

[34] K. Sadowska, K. Góra-Marek, M. Drozdek, P. Kuśtrowski, J. Datka, J. Martinez Triguero, F. Rey, Desilication of highly siliceous zeolite ZSM-5 with NaOH and NaOH/tetrabutylamine hydroxide, Microporous Mesoporous Mater. 168 (2013) 195-205.

[35] H. Mochizuki, T. Yokoi, H. Imai, S. Namba, J.N. Kondo, T. Tatsumi, Effect of desilication of H-ZSM-5 by alkali treatment on catalytic performance in hexane cracking, Appl. Catal. Gen. 449 (2012) 188-197.

[36] V.M. Benítez, C.R. Vera, C.L. Pieck, F.G. Lacamoire, J.C. Yori, J.M. Grau, J.M. Parera, Silica supported superacid isomerization catalysts, Catal. Today. 107–108 (2005) 651-656.

[37] J.R. Sohn, D.H. Seo, Preparation of new solid superacid catalyst, zirconium sulfate supported on γ-alumina and activity for acid catalysis, Catal. Today. 87 (2003) 219-226.

[38] K. Arata, H. Matsuhashi, M. Hino, H. Nakamura, Synthesis of solid superacids and their activities for reactions of alkanes, Catal. Today. 81 (2003) 17-30.

[39] A. Corma, V. Fornés, M.I. Juan-Rajadell, J.M.L. Nieto, Influence of preparation conditions on the structure and catalytic properties of SO42−/ZrO2 superacid catalysts, Appl. Cat. Gen. 116 (1994) 151-163.

[40] I. Mejri, M. Younes, A. Ghorbel, P. Eloy, E.M. Gaigneaux, Characterization and reactivity of aerogel sulfated zirconia-ceria catalyst for n-hexane isomerization, J. Porous Mater. 17 (2010) 545-551.

[41] B.M. Reddy, P.M. Sreekanth, V.R. Reddy, Modified zirconia solid acid catalysts for organic synthesis and transformations, J. Mol. Catal. Chem. 225 (2005) 71-78.

[42] O. N. Masatomi, H. T. Kinoshita, T. M. Tokushima, J. Naruto, Manufacture of Levulinic acid, Patent U.S 3,752,849, (1971).

[43] International Zeolite Association (IZA).(2014). http://www.iza-online.org/

[44] R. Karimi, B. Bayati, N. Charchi Aghdam, M. Ejtemaee, A.A. Babaluo, Studies of the effect of synthesis parameters on ZSM-5 nanocrystalline material during template-hydrothermal synthesis in the presence of chelating agent, Powder Technol. 229 (2012) 229-236.

[45] J.W. Jun, I. Ahmed, C. Kim, K. Jeong, S. Jeong, S.H. Jhung, Synthesis of ZSM-5 zeolites using hexamethylene imine as a template: Effect of microwave aging, Catal. Today. 232 (2014) 108-113.

[46] B. Beagley, J. Dwyer, F.R. Fitch, R. Mann, J. Walters, Aluminum distribution and properties of faujasites. Basis of models and zeolite acidity, J. Phys. Chem. 88 (9) (1984) 1744-1751.

[47] R.L. Wadlinger, G.T. Kerr, E.J. Rosinski, Catalytic composition of a crystalline zeolite, US Patent No. 3,308,069 , Mobil Oil Corporation, (1967).

[48] A. Corma, A. Martínez, Zeolites in refining and petrochemistry, Stud. Surf. Sci. Catal. 157 (2005) 337-366.

[49] G. Luo, L. Kang, M. Zhu, B. Dai, Highly active phosphotungstic acid immobilized on amino functionalized MCM-41 for the oxidesulfurization of dibenzothiophene, Fuel. Process. Technol. 118 (2014) 20-27.

[50] K.U. Nandhini, B. Arabindoo, M. Palanichamy, V. Murugesan, Al-MCM-41 supported phosphotungstic acid: Application to symmetrical and unsymmetrical ring opening of succinic anhydride, J. Mol. Cat. Chem. 243 (2006) 183-193.

[51] Y. Izumi, K. Urabe, M. Onaka (Eds.), Zeolites, Clay and Heteropoly Acids in Organic Reactions, 99 ed., Kodansha/VCH, Tokyo, (1992).

[52] K. Wilson, J.H. Clark, Solid acids and their use as environmentally friendly catalysts in organic synthesis, Pure Appl. Chem. 72 (7) (2000) 1313-1319.

[53] P.Trens, J.W. Peckett, V.N. Stathopoulos, M.J. Hudson, P.J. Pomonis, Phosphotungstate anions supported on spherical beads of carbon as highly efficient catalysts for the dehydration of propan-2-ol to propene, Appl. Catal. Gen. 241 (2003) 217-226.

[54] E. Escalona Platero, M. Peñarroya Mentruit, C. Otero Areán, A. Zecchina, FTIR Studies on the Acidity of Sulfated Zirconia Prepared by Thermolysis of Zirconium Sulfate, J. Catal. 162 (1996) 268-276.

[55] G.D. Yadav, J.J. Nair, Sulfated zirconia and its modified versions as promising catalysts for industrial processes, Microporous Mesoporous Mater. 33 (1999) 1-48

[56] T. Kim, R.S. Assary, H. Kim, C.L. Marshall, D.J. Gosztola, L.A. Curtiss, P.C. Stair, Effects of solvent on the furfuryl alcohol polymerization reaction: UV Raman spectroscopy study, Catal. Today. 205 (2013) 60-66.

[57] B.Saha, M.Mahdi A.Omar, Advances in 5-hydroxymethylfurfural production from biomass in biphasic solvents, Green Chem. (2014) 16-24.

[58] M.Mellmer, C.Sener, J.Marcel, R. Gallo, J. Luterbacher, D.M.Alonso, J.Dumesic, Solvent Effects in Acid-Catalyzed Biomass Conversion Reactions, Angewandte Chemie International Edition, 53 (2014) 11872-11877

[59] N.P. Vasilakos, D.M. Austgen, Hydrogen-Donor Solvents in Biomass Liquefaction, ind. Eng. Chem. Process Des.Dev, 24 (1985) 304-311

[60] R.A. van Santen, Theory of Brønsted Acidity in Zeolites, Stud. Surf. Sci. Cat. 85 (1994) 273-294.

[61] K. Sadowska, K. Góra-Marek, M. Drozdek, P. Kuśtrowski, J. Datka, J. Martinez Triguero, F. Rey, Desilication of highly siliceous zeolite ZSM-5 with NaOH and NaOH/tetrabutylamine hydroxide, Microporous Mesoporous Mater. 168 (2013) 195-205.

[62] F. Lónyi, J. Valyon, on the interpretation of the NH_3-TPD patterns of H-ZSM-5 and H-mordenite, Microporous Mesoporous Mat. 47 (2001) 293-301.

[63] L. Rodríguez-González, F. Hermes, M. Bertmer, E. Rodríguez-Castellón, A. Jiménez-López, U. Simon, The acid properties of H-ZSM-5 as studied by NH3-TPD and 27Al-MAS-NMR spectroscopy, Appl. Catal. Gen. 328 (2007) 174-182.

[64] N. Topsøe, K. Pedersen, E.G. Derouane, Infrared and temperature-programmed desorption study of the acidic properties of ZSM-5-type zeolites, J. Cat. 70 (1981) 41-52.

[65] N.R. Meshram, S.G. Hegde, S.B. Kulkarni, Active sites on ZSM—5 zeolites for toluene disproportionation, Zeolites. 6 (1986) 434-438.

[66] M.I. Zaki, M.A Hasan, F.A Al-Sagheer, L. Pasupulety, In situ FTIR spectra of pyridine adsorbed on SiO_2 –Al_2O_3,TiO_2, ZrO_2 and CeO_2: general considerations for the identification of acid sites on surfaces of finely divided metal oxides, Colloids and Surfaces A: Phys. Eng. Asp. 190 (2001) 261–274

[67] Rohm and Haas website, 2005, www.amberlyst.com.

[68] D.R. Brown, P.F. Siril, H.E. Cross, New polystyrene sulfonic acid resin catalysts with enhanced acidic and catalytic properties, J. Mol. Cat. A: Chemical 279 (2008) 63-68

Chapter 6. Study of “superacid” catalysts sulfated lanthanum-zirconium oxide in the synthesis of levulinic acid from furfuryl alcohol.

Table of contents

6.1. Summary 157

6.2. Introduction 158

6.3. Experimental 159

6.3.1. Preparation of catalysts 159

6.3.2. Techniques of characterization 160

6.3.3 Activity tests 160

6.4 Results and discussion 161

6.4.1 Results of characterization 161

6.4.2 Catalytic activity measurements 164

6.5. Conclusions 167

6.6 References 168

6.1. Summary

In this chapter the activity of “superacid” catalysts type La_xZrO_2/SO_4^{2-} in the hydration reaction of furfuryl alcohol (FA) to levulinic acid (LA) is studied. Superacid catalysts are materials referenced in literature as catalysts with high values of acidity. For this study, the catalysts were prepared by co-precipitation method, using ultrasound at low temperature and then calcined at 923 K, resulting an oxide mixture of both metals. The characterization of catalysts included the energy dispersion X-ray analysis (EDX), X-ray photoelectron spectroscopy (XPS) and ammonia temperature-programmed desorption (NH_3-TPD).

The results of activity showed high reactivity of FA, but a low selectivity to LA. Such as obtained in previous chapter 4, the formation of furan resins and other byproducts caused the decrease in yield to LA. Although a slight increase in yield to LA was observed using La_xZrO_2/SO_4^{2-} respect to monometallic ZrO_2/SO_4^{2-}, the yield to LA only reached a 10 %. The results of characterization by EDX and XPS analysis revealed a low presence of lanthanum in the catalysts with higher nominal La/Zr ratio, probably caused by leaching in some step of the preparation procedure. The activity tests also indicated that major product obtained after 3 hours of reaction was 2(3)-furanone-5-methyl, which was formed from FA.

6.2. Introduction

The superacid solid catalysts were named in chapter 1, section 1.3.1.4 where the strong acidity of zirconium oxide sulfate and its ability to catalyze many reactions as alkylation, isomerization and esterification were emphasized [1-6]. In order to determine how the sulfate species enhances the surface acidity of zirconia, different authors have studied the surface using mainly X-ray photoelectron spectroscopy (XPS) [7, 8]. Hino et al.(2006) and Jin et al.(1986) [8,9] proposed the surface structure to be SO_4^{2-} combined with Zr elements in bridging bidentate state as shown in Scheme 6.1. In Scheme 6.1, the S=O double bond in sulfate complex is much stronger than simple metal sulfate, therefore, Lewis acid strength of Zr^{4+} is greater by the inductive effect of S=O in the complex. In presence of water, the Lewis acid sites are converted to Bronsted acid sites via proton transfer.

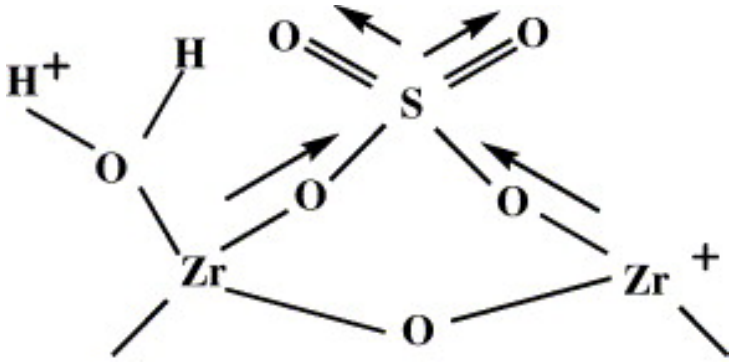

Scheme 6.1 Surface structure proposed for sulfated zirconia [8].

Xiang Feng et al. (2009) [10] and Matsuhashi et al. (1999) [4] reported that the ZrO_2/SO_4^{2-} super acid material has excellent acid properties, but its structural stability should be further improved. Therefore, it becomes necessary the incorporation of an element which increase the stability of catalyst such as lanthanum. The incorporation of lanthanum not only increases the stability of catalyst, also increases the acidity by the increase in formation of hydroxyl groups, which are fixed to links of sulfated zirconia

and lanthanum oxides. In recent studies, Xiang Feng et al. (2009) [10] developed the synthesis and characterization of solid acid sulfated zirconia-lantanum (La_xZrO_2/SO_4^{2-}) as superacid catalyst to apply to multiple reactions. They found that content of lanthanum in solid acid had influence on the acidity of catalyst. These results were taken into consideration for this study, including the preparation method used.

6.3. Experimental

6.3.1. Preparation of catalysts

As described above the catalysts were prepared according to results obtained by Xiang Feng et al. (2009) [10], they reported increasing in acidity when 0.6 mol% La/Zr ratio was used. According to these results 0.00, 0.53 % and 1.06 % (expressed as La/Zr mol%) were used for the preparation. The named catalysts were prepared by multistage precipitation. Firstly, aqueous ammonium solution (28 mol% NH_3) was added into a solution of $ZrN_2O_7*xH_2O$ (6 g) and $La(NO_3)_3$ (0.06 g) under ultrasonic stirring until pH=9.0. The precipitate which is a mixture of zirconia and lanthanum hydroxide was aged for 4 h at 255 K.

Secondly, the precipitate was filtered, and washed many times until all nitrates present were eliminated. The precipitate was dried at 383 K for 6 h and then the dry solid was immersed in a solution of 0.5 mol/L H_2SO_4 for 12 h and filtered again. Finally, the precipitate was dried at 383 K and calcined at 923 K at 5 K/min for 4 h. The above procedure was repeated using 0.12 g of $La(NO_3)_3$. The catalysts synthesized were named as ZrO_2/SO_4^{2-}, $La_{0.53}ZrO_2/SO_4^{2-}$ and $La_{1.06}ZrO_2/SO_4^{2-}$; being the 0.53 and 1.06, the lanthanum-zirconia ratio expressed in mol%.

6.3.2. Techniques of characterization

The elemental composition of solids was determined by Energy Dispersion X-ray analysis (EDX) using a scanning electron microscope (Hitachi S3600N SEM) equipped with an EDX detector (Thermo Ultra Dry) at an acceleration voltage of 15 kV. Before analysis, the samples were dried and powdered for more homogeneity.

Measurements of X-ray Photoelectron Spectroscopy (XPS) were performed in a system *SPECS* (Berlin, Germany) equipped with analyzer Phoibos 150 1D-DLD and monochromatic radiation Al Kα (1486.6 eV). An initial analysis of elements present was carried out (wide scan: step energy 1 eV, dwell time 0.1 s, pass energy 80 eV), and detailed analysis of the elements present were performed (detail scan: step energy 0.1 eV, dwell time 0.1 s, pass energy 30 eV), with an electron exit angle of 90°. The spectra were fitted using the software *CasaXPS 2.3.16.*

Ammonia Temperature Programmed Desorption (NH_3-TPD) was used in order to measure the amount and strength of acid sites of the catalysts. The TPD profiles were monitored by a thermal conductivity detector and recorded from 373 to 823 K at heating rate of 10 K/min. 15 mg of catalyst was pretreated in a He flow (30 mL/min) at 773 K for 1h to remove the physisorbed water and the crystal water. The sample was cooled to 373 K and then, NH_3 was absorbed using pulsed injections at 373 K until saturation, then TCD signal was recorder.

6.3.3 Activity tests

Test of activity were developed in the micro reactors described in chapter 3, section 3.6.1. Due to the low yields to LA obtained without solvents (as evidenced in the chapter 4, Table 4.3), in addition to positive results showed in chapter 5 (Figure 5.2), in which the solvents with ketone group exerts as inhibitor of resin formation, acetone was selected as solvent for the catalytic activity. Acetone was valued in previous chapters with positive results due to its capacity to avoid formation of furan resins in this reaction, in addition to the complete solubility of all reagents which allows a single phase in the reaction system (excluding the catalyst).

In a standard procedure, the catalyst (100 mg) was loaded to the reactor, followed by the addition of FA (0.2 mL), deionized water (2 mL) and acetone (7.8 mL). Air was previously removed from the reactor by purging with a N_2 flow during 1 min. Then, the glass-pressure reactor was located in an oil bath, heated by a hot-plate magnetic-stirrer device. The reactant mixture was stirred at 800 rpm to start the catalytic reaction. Different glass-pressure reactors were used for each experiment. The reaction in all of them started at the same time. After different reaction time (1 and 3 hours), each reactor was taken out the oil bath and the reaction was stopped immediately immersing the reactor in cold water (277 K). The reaction mixture was quantitatively transferred and subsequently filtered with a millipore filter of 0.22 μm for their immediate analysis by GC, and MS-GC as described in chapter 3, section 3.4.1.

6.4 Results and discussion

6.4.1 Results of characterization

The metallic content of zirconium and lanthanum in the catalysts was analyzed by EDX technique. The signal of the scanning electron microscope is shown in Figure 6.1. Five points focused at 250 μm were selected to determine the elemental composition of the materials corresponding to its average. The lanthanum shows low peak intensity in both catalysts, this indicates that lanthanum possibly was removed by leaching during some stage of preparation. The results obtained by EDX and XPS analysis (Table 6.1) show that lanthanum content was not increased as the expected nominal values. The XPS analysis also shows that sulfate ion is present on the surface of catalyst as shown in Figures 6.2a and 6.2b (Binding energy: 169 eV). The results reported in Table 6.1 show an increase in sulfur content associated with the incorporation of lanthanum on the catalyst. As the sulfating process was equivalent for all catalysts, it is deduced that interactions between bimetallic lanthanum and zirconium oxides with sulfate ion were greater than interactions with monometallic zirconium oxide.

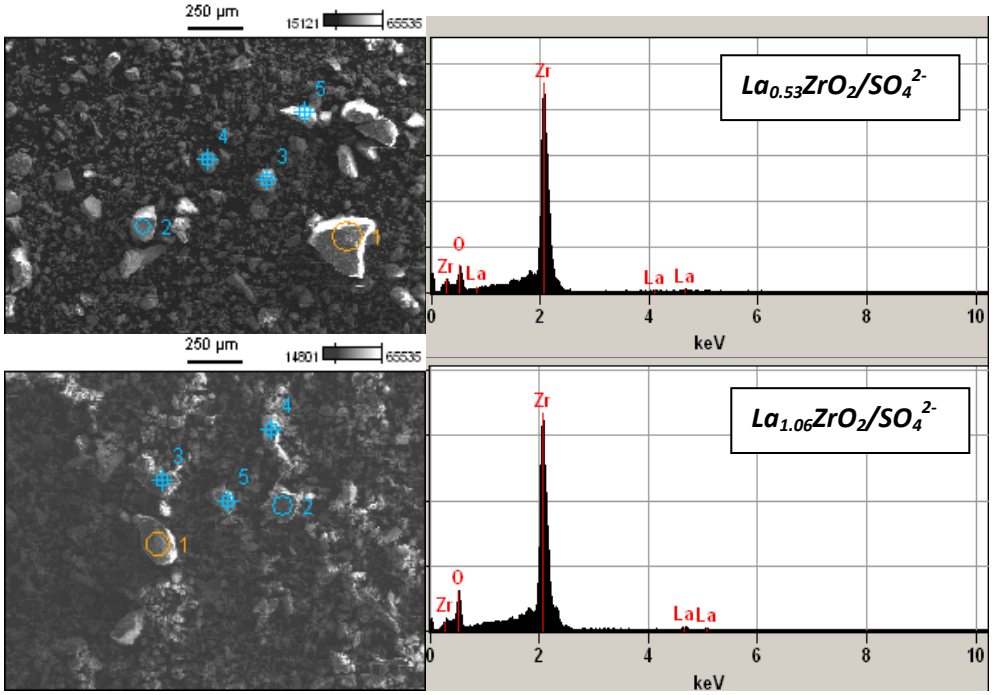

Figure 6.1 Signal of energy dispersion X-ray analysis for $La_{0.53}ZrO_2/SO_4^{2-}$ and $La_{1.06}ZrO_2/SO_4^{2-}$.

Table 6.1. Elemental quantification of catalysts by EDX and XPS analysis

Catalyst	Elemental composition by EDX analysis (atom %)		Surface elemental composition By XPS analysis (atom %)			
	Zr	La	Zr	La	S	O
ZrO_2/SO_4^{2-}	28.19	-	29.7	-	3.9	66.4
$La_{0.53}\,ZrO_2/SO_4^{2-}$	27.55	0.76	26.4	0.2*	6.6	66.8
$La_{1.06}\,ZrO_2/SO_4^{2-}$	28.72	0.74	27.6	0.2*	7.1	65.1

La: 0.53 and 1.06 are the nominal ratios La/Zr (mol%) used for the synthesis. *detection limit: 0.2.

Table 6.2, reports the results of acidity obtained by TPD-NH_3 method for the catalysts studied. All samples showed a combined weak and strong acid strength. However, a decrease of weak acid strength as opposed to increase of strong acid strength was observed by the incorporation of lanthanum. The above named interactions between zirconium oxides with ion sulfate in addition to lanthanum interactions resulted in high values of total acidity.

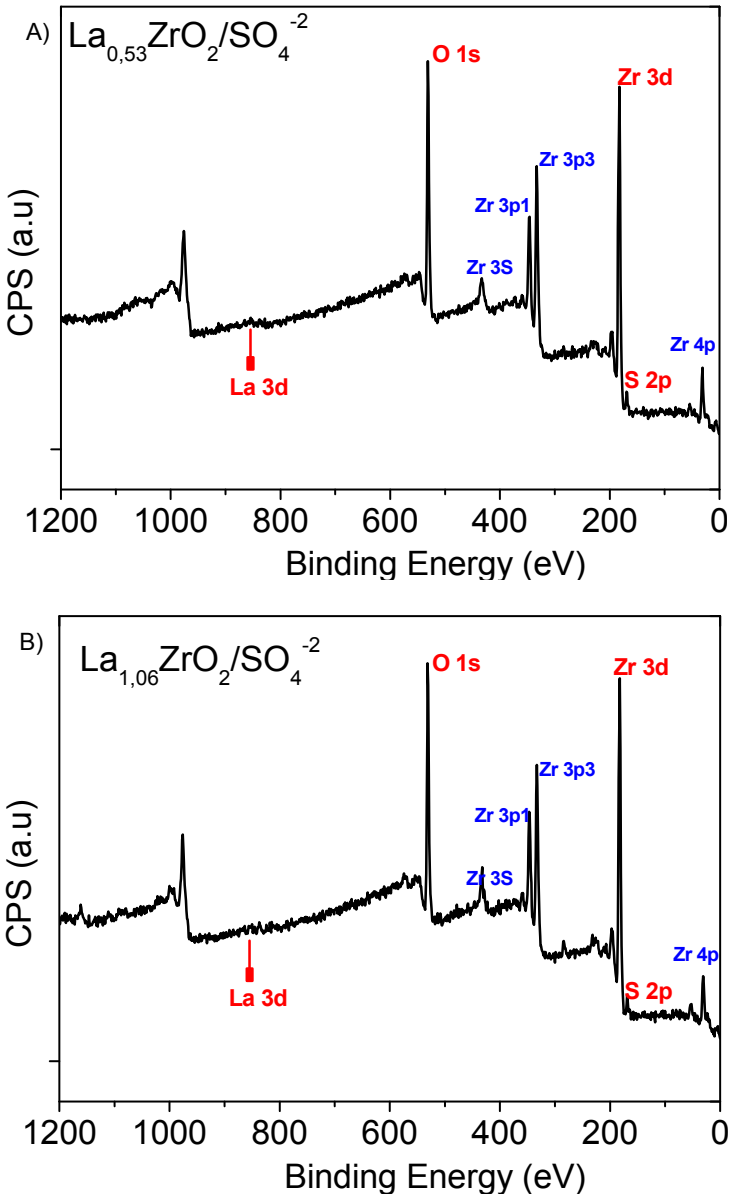

Figure 6.2 XPS data analysis for A) $La_{0.53}ZrO_2/SO_4^{2-}$, B) $La_{1.06}ZrO_2/SO_4^{2-}$.

Table 6.2. Total acidity determined by TPD-NH_3

Catalyst	*Acid strength *(mmol NH_3/g)*		Total acidity *(mmol NH_3/g)*
	Weak	Strong	
ZrO_2/SO_4^{2-}	0.166	0.175	0.341
$La_{0.53}ZrO_2/SO_4^{2-}$	0.125	0.226	0.351
$La_{1.06}ZrO_2/SO_4^{2-}$	0.088	0.425	0.513

*Average acid strenght (weak): 450 K; **Average acid strenght (strong): 850 K.

6.4.2 Catalytic activity measurements

The catalysts have been evaluated in the hydration reaction of furfuryl alcohol to levulinic acid. As shown in Figure 6.3, all catalysts were active for this reaction, reaching complete conversion after 3 hours of reaction. However, as in previous chapter 4, the yield to LA was low due to formation of byproducts, mainly furan resins. The differences in conversion between ZrO_2/SO_4^{2-} and La_xZrO_2/SO_4^{2-} reached up to 40 points (%) at 1h, indicating that lanthanum increased the activity of catalysts in the reaction described. Although the quantification of lanthanum on surface of catalysts by XPS analysis was below to the detection limit (Table 6.1), a slight increase in the sulfur content of $La_{1.06}ZrO_2/SO_4^{2-}$ generated a higher acidity (Table 6.2), which caused the higher conversion than other.

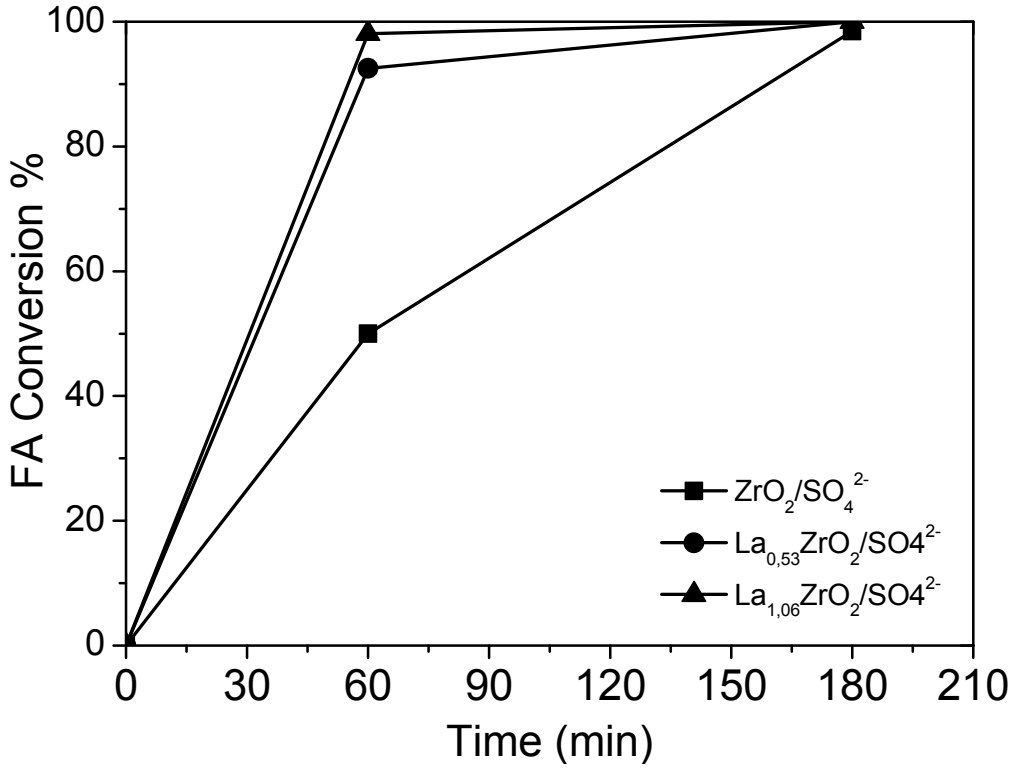

Figure 6.3. Evolution of furfuryl alcohol conversion with reaction time for La_xZrO_2/SO^{2-}, operation conditions: 413K, autogen pressure, purge with nitrogen gas, 100 mg of catalyst, 0.2 mL of FA, 2 mL of H_2O, 7.8 mL of acetone as solvent.

The results summarized in Table 6.3 also show that activity of catalysts in the formation of levulinic acid increased with the incorporation of lanthanum. However, the maximum yield to LA obtained only reached a 10 % over a period of 3 hours reaction. The content in the reactor after the end of reaction evidences the presence of furan resins (unquantified) and others compounds which are represented in Scheme 6.2. Some authors proposes that ring opening of 2(3H)-furanone,5-methyl can form LA in a mechanism of reversible reaction [11], therefore, it can be considered as an intermediate product. According to the studied in chapter 4, the 4-HCP is not precursor of LA, this is considered as a byproduct of reaction from FA, which is precursor of cyclopentanone. While other compound as 1,3 cyclopentanedione has not been reported as precursor of LA.

Table 6.3 Summary of FA conversions and yields to LA on reaction time

Catalyst	Yield to LA		Conversion of FA	
	Time		Time	
	1h	3 h	1h	3 h
ZrO_2/SO_4^{2-}	0	1.4	50.0	98.5
$La_{0.53}ZrO_2/SO_4^{2-}$	0	4.5	92.5	100.0
$La_{1.06}ZrO_2/SO_4^{2-}$	0	10.0	98.1	100.0

Operation conditions: 413K, autogenous pressure, purge with nitrogen gas, 100 mg of catalyst, 0.2 mL of FA, 2 mL of H_2O, 7.8 mL of acetone as solvent.

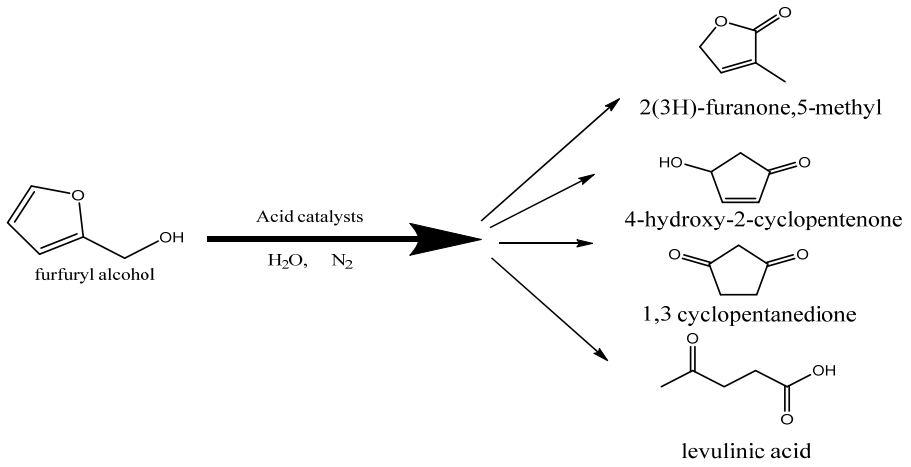

Scheme 6.2. Main products obtained from FA, with ZrO_2/SO_4^{2-} and La_xZrO_2/SO_4^{2-} catalysts.

The distribution of products identified by GC-MS (Figure 6.4), shows that 2(3)-furanone-5-methyl, 4-HCP and LA, were the main products obtained after 3 hours of reaction for all catalysts tested. The higher signal obtained in all cases correspond to 2(3)-furanone-5-methyl, which is formed mainly in the first minutes of reaction, this product was identified in the MS-GC with a probability of 78 %. Such as above described, undesired furan resins were obtained, thus decreasing yield to LA; this was noticeable by its adhesion to the walls of the reactor.

Figure 6.4 also shows that peak area of levulinic acid (LA) increased considerably when catalysts with lanthanum were used. The increase of peak area intensity is proportional to the increases of total acidity for LA and inversely proportional for 2-(3H)-furanone, 5-methyl.

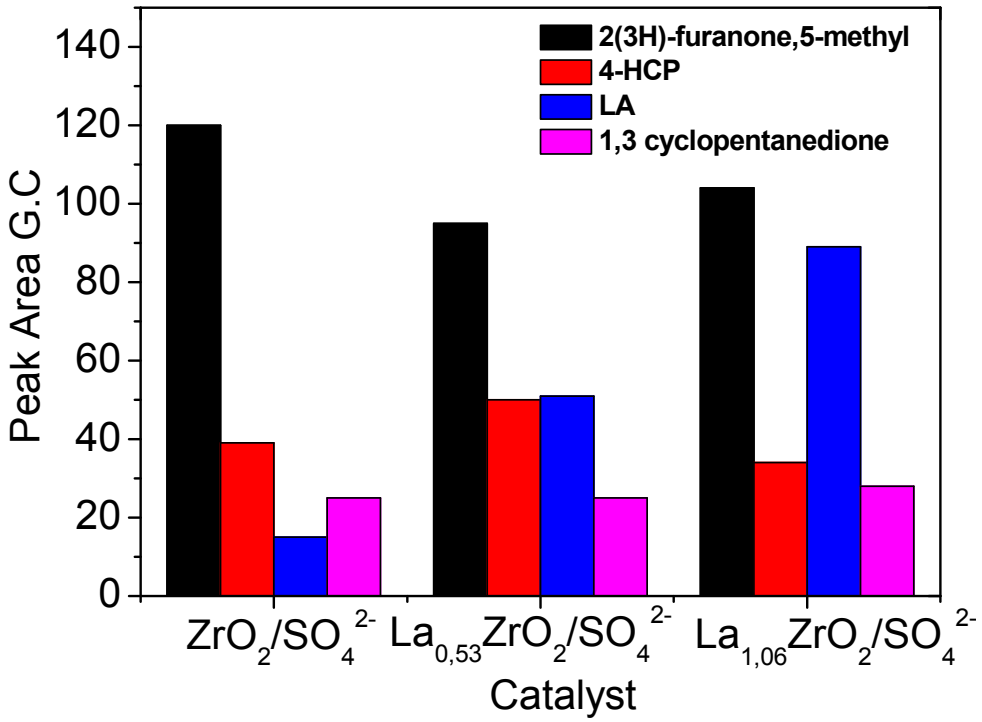

Figure 6.4 Distribution of by-products obtained with La_xZrO_2/SO_4^{2-}catalysts. Operation conditions: 413K, autogen pressure, purge with nitrogen gas, 100 mg of catalyst, 0.2 mL of FA, 2 mL of H_2O, 7.8 mL of acetone as solvent, 3 hours of reaction.

6.5. Conclusions

The set prepared of superacid catalysts, containing sulfated lanthanum and zirconium oxides, showed a high activity in the reaction of FA in aqueous media reaching conversions up to 100 %. However, the distribution of products obtained, indicates a low selectivity to levulinic acid. The lanthanum present in the catalyst generated a slightly increase in yield to LA.

The lanthanum oxide analyzed was lower than expected, implying a loss in some stage of synthesis; this fact was verified by EDX and XPS analysis. Furan resins were observed in the reactor after the reaction; other compounds were also identified by MS-GC, these included the 2(3)-furanone-5-methyl and 4-HCP as the main byproducts obtained.

The method of preparation used was effective for the obtaining of sulfated zirconium oxide, but the results were not as expected in the lanthanum oxide incorporation. So, it is proposed for future tests the election of other methods of preparation including higher ratios of lanthanum respect to zirconium. The selection of the method of preparation was made based on the positive results obtained by others author [10].

The activity tests were developed selecting acetone as an acceptable solvent of FA, to increase the yield to LA, it is considered necessary the optimization of main variables as quantity of catalyst and the use of other metal ratios in the bimetallic catalysts La_xZrO_2/SO_4^{2-}.

Although the incorporation of lanthanum was not as expected, an increase up to 10 percentage points of LA yield was obtained with $La_{1.06}ZrO_2/SO_4^{2-}$ compared to ZrO_2/SO_4^{2-}, because of the increase in the strong acid strength.

6.6 References

[1] B.M. Reddy, P.M. Sreekanth, V.R. Reddy, Modified zirconia solid acid catalysts for organic synthesis and transformations, J. Mol. Catal. Chem. 225 (2005) 71-78.

[2] K. Arata, H. Matsuhashi, M. Hino, H. Nakamura, Synthesis of solid superacids and their activities for reactions of alkanes, Catal. Today. 81 (2003) 17-30.

[3] J.R. Sohn, D.H. Seo, Preparation of new solid superacid catalyst, zirconium sulfate supported on γ-alumina and activity for acid catalysis, Catal. Today. 87 (2003) 219-226.

[4] H. Matsuhashi, H. Shibata, H. Nakamura, K. Arata, Skeletal isomerization mechanism of alkanes over solid superacid of sulfated zirconia, Appl. Cat. Gen. 187 (1999) 99-106.

[5] G.D. Yadav, J.J. Nair, Sulfated zirconia and its modified versions as promising catalysts for industrial processes, Microporous Mesoporous Mater. 33 (1999) 1-48.

[6] K. Arata, Solid Superacids, Adv. Cat. 37 (1990) 165-211.

[7] M. - Hino, K. - Arata, - Synthesis of solid superacid catalyst with acid strength of H0[less-than-or-eq]-16.04, - J. Chem. Soc, Chem. Commun. - 851.

[8] M. Hino, M. Kurashige, H. Matsuhashi, K. Arata, The surface structure of sulfated zirconia: Studies of XPS and thermal analysis, Thermochimica Acta. 441 (2006) 35-41.

[9] T. Jin, T. Yamaguchi, K. Tanabe, Mechanism of acidity generation on sulfur-promoted metal oxides, J. Phys. Chem. 90 (1986) 4794-4796.

[10] C. Xiang feng, C. Tong Yun, H. Ke liang, Superacid Catalyst $SO_4^{2-/}ZrO_2$-La_2O_3 Prepared by Ultrasonic Co-precipitation and Low Temperature Aging, Chin. J. Chem. Phys. 22 (2009) 322-326.

[11] J.A.Dumesic, M.W.Ryan, Production of methyl-vinyl ketone from levulinic acid, Patent: WO2011087962 (2011).

Chapter 7. Valorization of furfuryl alcohol as an alternative to produce 4-hydroxy-2-cyclopentenone and cyclopentanone.

Table of contents

7.1. Summary 170

7.2. Introduction 171

7.3. Experimental 173

7.3.1. Activity tests 173

7.3.1.1. Activity tests for obtaining 4-hydroxy-2-cyclopentenone (4-HCP) from furfuryl alcohol (FA), using Nb_xUSY catalysts (first stage) 173

7.3.1.2. Activity test for obtaining cyclopentanone (CPN) from 4-hydroxy-2-cyclopentenone (4-HCP), using $Pt*WO_x/Al_2O_3$ catalysts (second stage) 174

7.3.1.3. Activity test for the direct production of cyclopentanone from furfuryl alcohol, using $Pt*WO_x/Al_2O_3$ catalysts. 174

7.4. Results and discussion 174

7.4.1. Results of characterization of Nb_xTiO_2 and Nb_xUSY catalysts 174

7.4.2. Results of characterization of Pt/Al_2O_3, WO_x/Al_2O_3 and $Pt*WO_x/Al_2O_3$ 185

7.4.3. Catalytic activity 189

7.4.3.1. Obtaining of 4-hydroxy-2-cyclopentenone (4-HCP) 189

7.4.3.2. Obtaining of cyclopentanone (CPN) from 4-hydroxy-2-cyclopentenone (4-HCP) 190

7.4.3.3. Study of obtaining cyclopentanone (CPN) from furfuryl alcohol (FA) in one stage, using Pt/Al_2O_3, WO_x/Al_2O_3 and $Pt*WO_x/Al_2O_3$ catalysts 192

7.5. Conclusions 200

7.6. References 201

7.1. Summary

In this chapter a series of catalysts based on acid metal oxides were studied in the aqueous reaction of furfuryl alcohol (FA). The catalysts evaluated were niobium oxides supported on ultra stable Y zeolite (Nb_xUSY) and titanium dioxide (Nb_xTiO_2). Initially, niobium catalysts were synthesized by precipitation and wet impregnation methods using different weight percentage (x) respect to support, mainly to obtain levulinic acid. However, the activity to levulinic acid was low and the catalysts were active to form principally a product identified as 4-hydroxy-2-cyclopentenone (4-HCP).

The 4-HCP is a precursor of cyclopentanone (CPN) and cyclopentanol (CPOL) which are highly commercial chemicals. Therefore, a further reaction stage was included for obtaining CPN from 4-HCP using heterogeneous catalysis. In the second stage platinum and wolframium supported on aluminum oxide (γ-Al_2O_3) were used as catalysts.

In the first stage, the best results to 4-HCP were achieved using Nb_xUSY catalysts prepared by precipitation method. The incorporation of niobium in the support generated a significant change in the original structure of zeolite. The global yield to cyclopentanone was 45 mol%.

The catalytic activity in a direct stage from FA to CPN was also studied in this chapter using the bimetallic platinum-wolframium catalyst supported on alumina ($Pt*WO_x/Al_2O_3$) and its monometallic counterparts (Pt/Al_2O_3 and WO_x/Al_2O_3). The catalytic activity was tested after a previous optimization of main variables as temperature, pressure, and concentration of reagents. The results of activity were similar to the ones obtained in two stages, in this case the maximum selectivity to CPN reached a 42 mol%.

7.2. Introduction

The results obtained in previous chapters in the reaction of furfuryl alcohol (FA) in aqueous media using heterogeneous catalysis, showed that levulinic acid (LA), 4-hydroxy-2-cyclopentenone (4-HCP) and furan resins were the main products obtained. In chapters 4 and 5, it has been demonstrated that catalysts with high acidity and mesoporosity were selective to levulinic acid. However, some catalysts containing metal oxides have sizeable mesoporosity but low acidity, which gives rise to other derivative compounds different to LA, as the 4-HCP.

In recent years, the 4-HCP has been used as precursor of antibiotics and antimicrobial products [1, 2], but its direct application is still to be defined. The use of 4-HCP as reagent precursor of CPN is an alternative to provide an added value.

Cyclopentanone is a cyclic ketone, colorless liquid, with a peppermint-like odor used mainly in synthesis of pharmaceuticals and perfumery products; also is used as solvent for electronic applications [3]. CPN is mostly obtained by chemical synthesis from adipic acid at high temperatures in multistep processes using a closed vessel reactor [3]. Some authors have included studies about their obtention from furfural. Yanliang et al. (2013) showed a 65 % yield to CPN from furfural and 36 % from FA, using a bimetallic Ni-Cu/SBA15 catalyst (40 bar, H_2) [4]. Hronec et al. (2012) included a new route from furfural and furfuryl alcohol in aqueous medium with palladium and platinum catalysts under hydrogen pressure (80 bar), obtaining 76 % yield to CPN from furfural and 61 % from furfuryl alcohol [5, 6]. Minghao et al. (2014) presented a 70 % yield to CPN from furfural using Ni/CNTs catalyst (50 bar) [7]. And recently, Hongyan et al. (2014) published 95.8 % yield to CPN from furfural using a Cu-Ni-Al/ hydrotalcite catalyst (40 bar) [8].

In this chapter, the study to obtain 4-HCP and cyclopentanone (CPN) as alternative products derived from FA via heterogeneously catalyst has been analyzed. Initially, the study was performed in two stages (see Scheme 7.1).

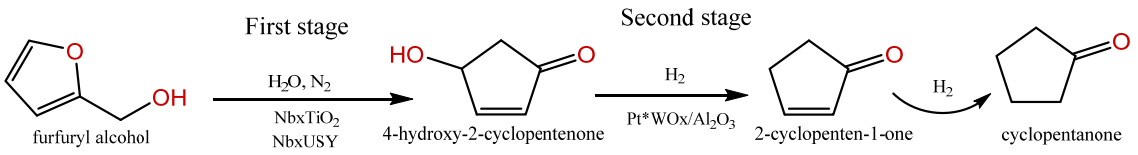

Scheme 7.1. Mechanism of reaction in two stages for the conversion of furfuryl alcohol to cyclopentanone.

In the first stage, the catalysts prepared were composed of niobium supported on titanium oxide and ultra stable Y zeolite (USY). Niobium oxides are effective catalysts used in various reactions [9-11], its most common oxide forms are Nb^{5+}(Nb_2O_5, total oxidation) and Nb^{4+} (NbO_2, partial oxidation). However, the low surface area of Nb_2O_5 causes a decrease in the activity. Therefore, an alternative is the selection of supports with higher surface area and a moderate acidity.

The supported niobium catalysts have remarkable differences compared to bulk Nb_2O_5*nH_2O. Ultra stable Y zeolite (USY) is a promising support for metals due to its high surface area and combined acidity, Brönsted and Lewis. Titanium oxide is other alternative currently used as a support in various catalytic materials, TiO_2 has low acidity but high surface area, and is most used as support for the incorporation of reducible or oxidizable metals [11].

In the second stage, the reaction of 4-HCP to CPN wascarried out using wolframium (W) and platinum (Pt) supported on alumina oxide (γ-Al_2O_3), the reaction proceeded in hydrogen atmosphere.

The catalysts of platinum supported in γ-Al_2O_3 are materials usually used to catalyze reactions of hydrogenation. However, the high cost of platinum, added to its contribution to undesirable coke formation, creates the need of a decrease in the amount of platinum loaded by the incorporation of other transition metals as wolframium. Bimetallic platinum-wolframium catalyst has been mentioned as an attractive alternative for decreasing the platinum content without affecting its high activity [15]. The platinum catalyst has high activity and selectivity in many reactions such as naphtha reforming and hydrogenolysis of alkanes and cycloalkanes [12-15].

7.3. Experimental

This section describes the procedures used to evaluate the catalytic activity of solid catalysts in the reaction of FA to CPN. Other procedures, as the preparation of catalysts, were described in previous sections 3.3.1, 3.3.2, and 3.3.3 in chapter 3. The description of characterization techniques used were also described in chapter 3, section 3.5. It is noteworthy that metal contents selected for niobium supported on USY zeolite were 1, 4 and 8 wt%, and 1 and 24 wt% of niobium supported on titanium oxide. The catalysts supported on USY zeolite were prepared by wet impregnation method (M1) and precipitation method (M2). In the case of platinum and wolframium catalysts, the values incorporated were fixed as follows: Pt/Al_2O_3 (platinum, 5 wt%,), $Pt*WO_x/Al_2O_3$ (platinum, 5 wt% and wolframium, 5 wt%) and WO_x/Al_2O_3 (wolframium, 5 wt%); these contents were prepared following the procedure published by García et al. (2015) described in chapter 3, section 3.3.3 [15].

7.3.1. Activity tests

7.3.1.1. Activity tests for obtaining 4-hydroxy-2-cyclopentenone (4-HCP) from furfuryl alcohol (FA), using Nb_xUSY catalysts (first stage)

The activity of catalysts was carried out in a series of glass pressure stirred reactors which were described in chapter 3.6.1. The reactors were charged with 50 mg of catalyst and 5 mL of dissolution of FA at 4 vol % in bidestilled water. The air was previously removed from the system by purges with N_2 flow. Then, the temperature in oil bath was fixed at 423 K, and the stirring at 800 rpm to start the reaction. Different glass-pressure reactors were used for each experiment. After the reaction time selected, each reactor was taken out of the oil bath, and the reaction stopped by immersion of reactor in cold water at 277 K.

7.3.1.2. Activity test for obtaining cyclopentanone (CPN) from 4-hydroxy-2-cyclopentenone (4-HCP), using $Pt*WO_x/Al_2O_3$ catalysts (second stage)

The product of reaction obtained in previous section 7.3.1.1 was converted to CPN using the stainless steel reactor described in chapter 3.6.1. The solid catalyst $Pt*WO_x/Al_2O_3$ (75 mg) was loaded to reactor with 20 mL of product obtained in first stage (aqueous mixture of 4-HCP). Previously, the reactor was purged with hydrogen flow to evacuate the air into the reactor. Then, the system was pressurized with hydrogen at 10 bar and the temperature of reaction was set at 423 K. The samples of reaction were taken for its analysis by gas chromatography (described in section 3.4.1).

7.3.1.3. Activity test for the direct production of cyclopentanone from furfuryl alcohol, using $Pt*WO_x/Al_2O_3$ catalysts.

The activity tests for direct production of CPN were carried out in the reactor used in previous section 7.3.1.2. In a typical procedure, 75 mg of catalyst previously reduced on hydrogen media at 723 K was loaded into the reactor. Then, a mixture of FA (4 wt%) and water was added to the reactor. The system was pressurized with hydrogen and the temperature was set at 423 K. The samples of reaction were taken at different times for its analysis and quantification.

7.4. Results and discussion

7.4.1. Results of characterization of Nb_xTiO_2 and Nb_xUSY catalysts

The analysis of temperature programmed oxidation (TPO) showed that at temperatures higher than 573 K, all oxidisable compounds completed the corresponding reactions. The optimal value of calcination temperature for Nb_xTiO_2 catalysts was selected at 573 K. The release of CO and CO_2 was due to the decomposition of the niobium oxalate precursor impregnated on titanium dioxide (Figure 7.1).

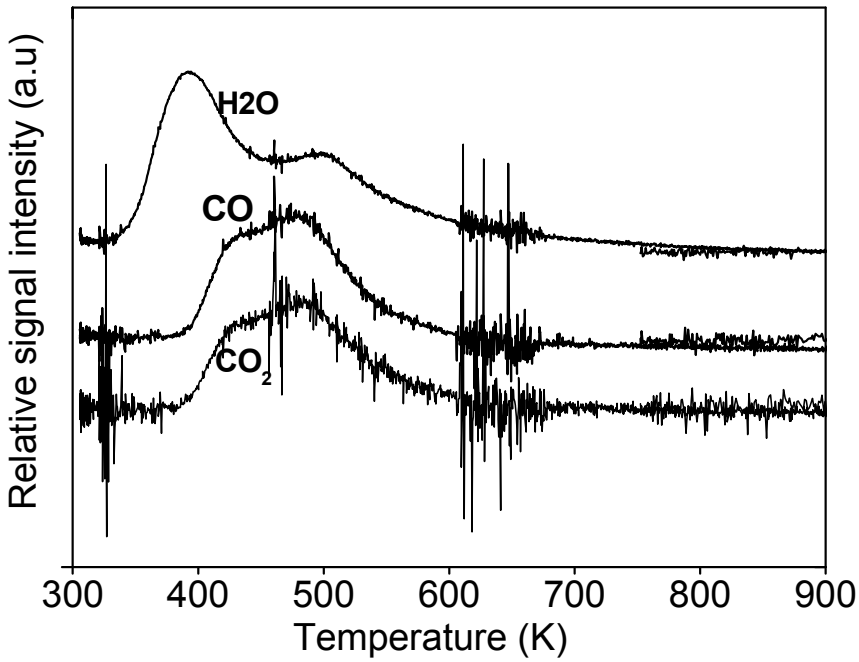

Figure 7.1. Evolution of temperature programmed oxidation (TPO) of Nb_1TiO_2 catalyst. Heating rate at 10 K/min, temperature range of 300 K-900 K.

Thermogravimetric analysis TGA (Figure 7.2) shows that the parent Y zeolite (NH_4-Y zeolite) has a constant weight loss (up to 24.7 %) between 350-750 K, corresponding to elimination of ammonia and intracrystalline water. In the case of Nb_xUSY, two slight peaks can be seen by oxidation of niobium species with maximum peaks at 450 K and 650 K. Consequently, the temperature of calcination was set at 773 K for all Nb_xUSY catalysts.

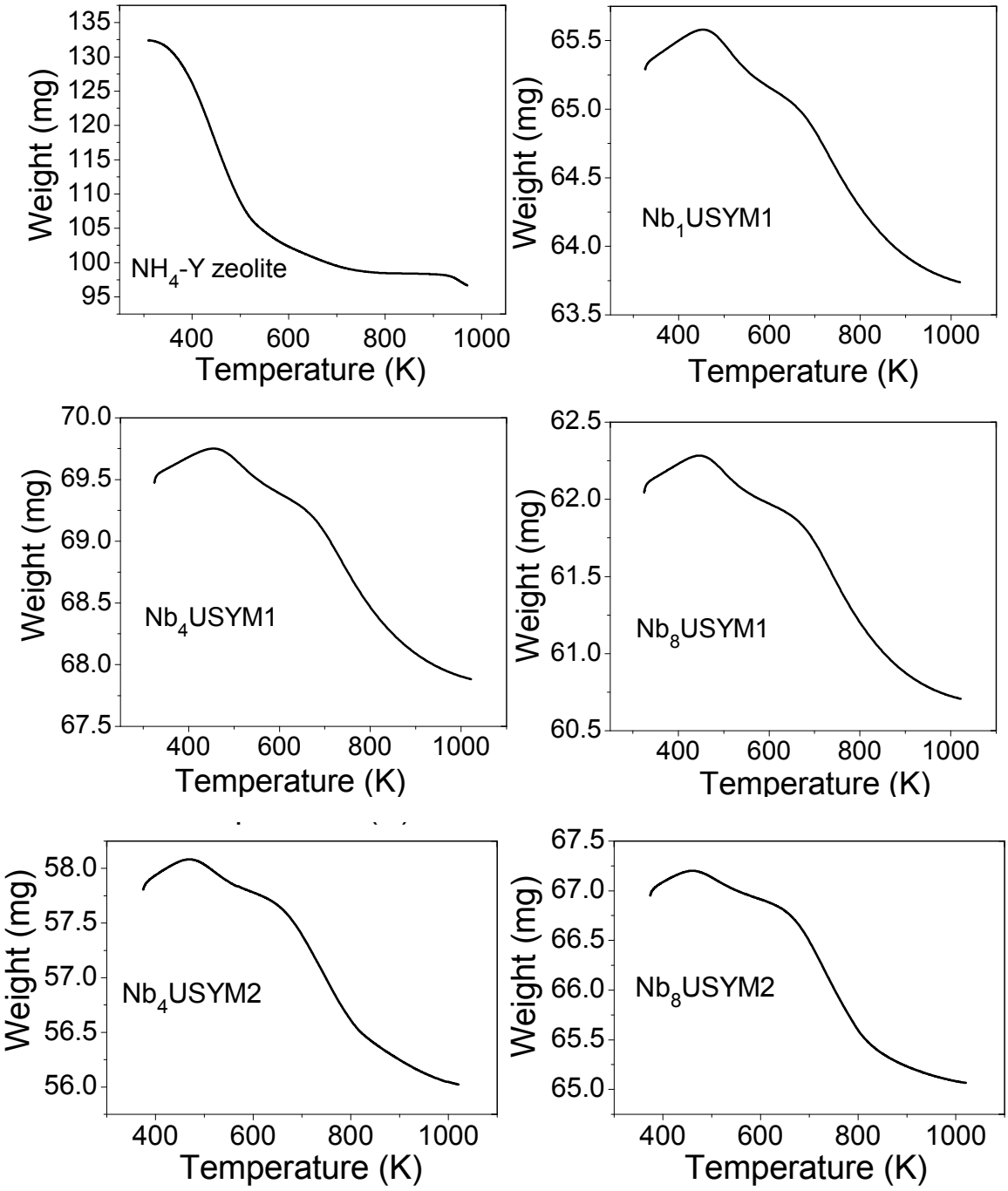

Figure 7.2. Thermogravimetric analysis (TGA) of H-USY and Nb_xUSY catalysts. Analysis by two thermal cycles, first cycle with N_2: (323 K-723 K), second cycle with O_2: (323 K-1023 K). M1: preparation by wet impregnation method, M2: preparation by precipitation method.

Textural properties of catalysts are presented in Table 7.1. The results show a substantial reduction in surface area when niobium oxide was incorporated to zeolite. In the case of materials prepared by wet impregnation method (M1), the surface area and pore volume decreases considerably due to pore plugging. In the case of catalysts prepared by precipitation method (M2), the surface area and pore volume loss were less evident, except for the catalyst with higher niobium content; so that in M2 method, the distribution of particles of niobium in surface was more homogeneous than M1. The niobium content is according to desired nominal values incorporated initially to the support.

Table 7.1. Textural properties and chemical composition of Nb_xUSY and Nb_xTiO_2 catalysts

Catalysts	S_{BET} (m^2/g)	D_p (nm)	V_T (cm^3/g)	V_m (cm^3/g)	Nb content (wt %)	Nb/Ti surface atom ratio
H-USY	361	3.4	0.331	0.203	-	-
Nb_1USYM1	28	2.1	0.124	0.017	0.67	-
Nb_4USYM1	26	1.9	0.115	0.016	4.36	-
Nb_8USYM1	34	2.2	0.118	0.021	6.53	-
Nb_1USYM2	165	1.5	0.246	0.092	0.73	-
Nb_4USYM2	54	1.7	0.132	0.031	3.99	-
Nb_8USYM2	10	1.4	0.352	0.006	8.62	-
TiO_2	77	3.7	0.173	-	-	
Nb_1TiO_2	59	2.6	0.159	-	-	0.034
$Nb_{24}TiO_2$	45	2.3	0.220	-	-	0.056

S: Total surface area; BET: BET method, D_p: Pore diameter, V_T: total pore volume, V_m: micropore volume.

X-ray diffraction analysis (XRD) (Figure 7.3) shows that the crystalline structure of H-USY was modified by the incorporation of niobium oxides. The addition of only 1 wt% of niobium generated a total crystallinity loss for Nb_xUSYM1 catalysts. However, this is less evident for Nb_1USYM2 and Nb_4USYM2, which have a semi-amorphous structure. The XRD differences obtained between M1 and M2 methods indicates a better rearrangement of niobium dispersed in surface for catalysts prepared by M2 method, such as was described in the analysis of surface area and pore diameter.

The XRD analysis for Nb_xTiO_2 (Figure 7.4) showed in all cases characteristic peaks of anatase and rutile phases. In this case, $NbxTiO_2$ did not present alteration of these phases by the incorporation of niobium species.

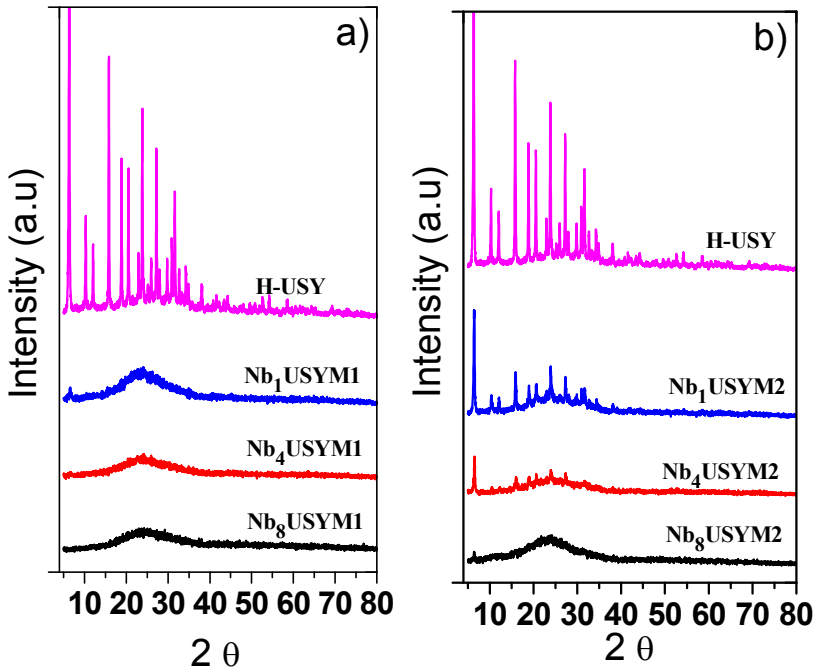

Figure 7.3. X-ray diffraction of zeolite H-USY and Nb_xUSY

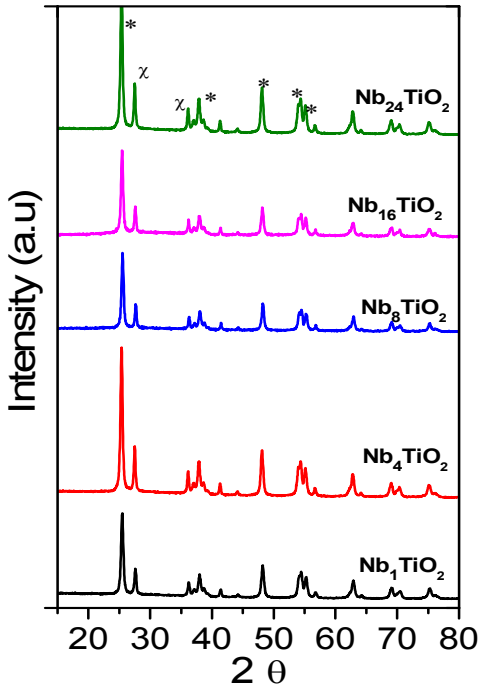

Figure 7.4. X-ray diffraction analysis of Nb_xTiO_2 catalysts. (*) characteristic peak of TiO_2 anatase and (×) characteristic peak of TiO_2 rutile.

The Figure 7.5 shows the XPS analysis for Nb_xTiO_2 catalysts. A high resolution in Nb 3d spectrum is shown, revealing a doublet which is observed approximately in a range of 207- 210 eV, respectively. The above named peaks are attributed to niobium species in oxidation state Nb^{5+}, which is consistent with the results obtained for other authors [10, 11].

The XPS analysis of Nb_xUSYM2 is shown in Figure 7.6, and the results are summarized in Table 7.2. The results show that oxidation of niobium species in Nb_1USYM2 is complete (maximum oxidation state: Nb^{5+}), whereas in the case of Nb_4USYM2 and Nb_8USYM2 are present both oxidation states Nb^{4+} (binding energy: 205) and Nb^{5+} (binding energy: 207).

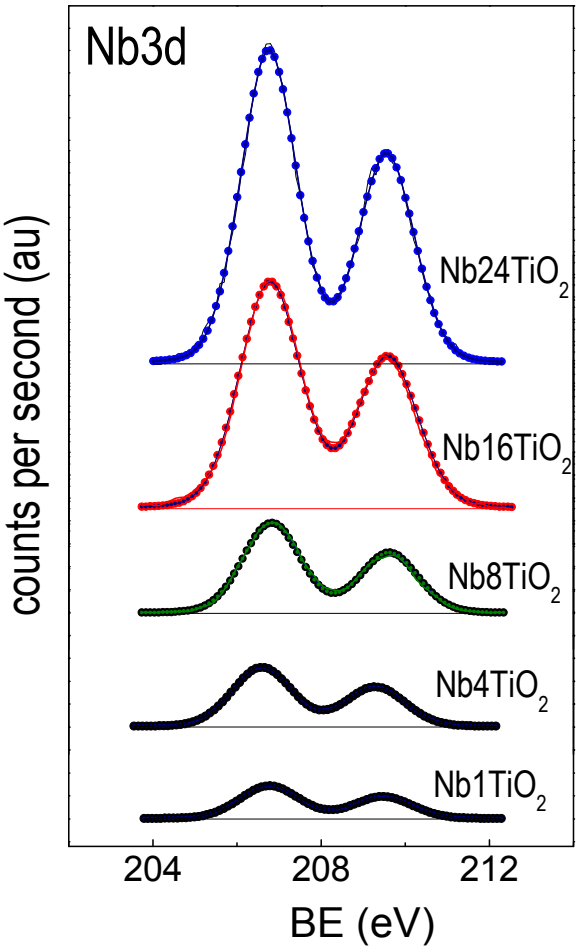

Figure 7.5 XPS analysis of Nb_xTiO_2

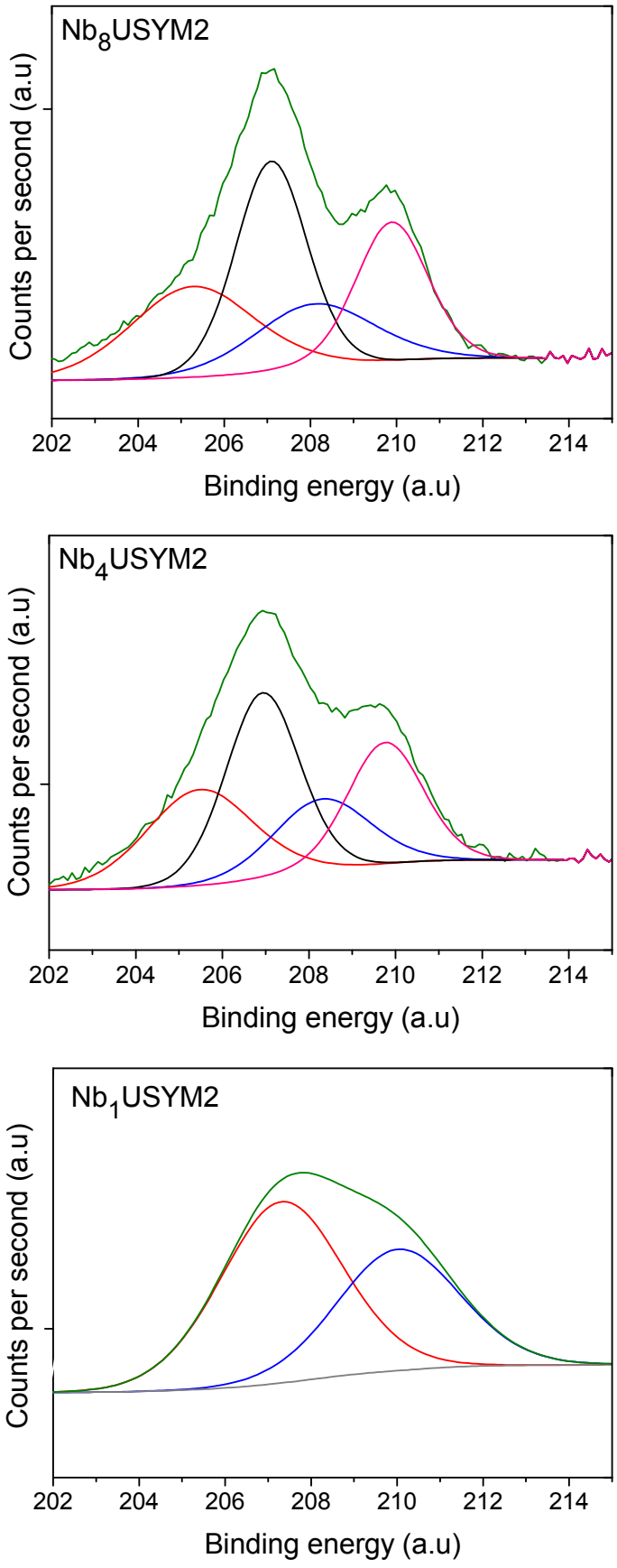

Figure 7.6. XPS analysis of Nb_1USYM2, Nb_4USYM2, Nb_8USYM2.

Table 7.2. Binding energy (eV) and surface content of niobium (Nb) by XPS analysis

Catalyst	Binding energy (eV)	Nb Surface content atomic ratio (%)	Total Nb surface content atomic ratio (%)
Nb_1USYM2	207.31 210.02	0.499 0.335	0.834
Nb_4USYM2	205.47 208.31 206.93 209.76	1.316 0.883 1.776 1.192	5.167
Nb_8USYM2	205.27 208.09 207.09 209.89	2.294 1.539 3.079 2.066	8.978

The Brönsted and Lewis acidity was studied by FTIR-pyridine adsorption method. Infrared spectra of adsorbed pyridine on Nb_xTiO_2 (Figure 7.7) shows predominantly three bands at 1445, 1573 and 1606 cm^{-1}, ascribed to chemisorbed pyridine molecules on Lewis acid sites (PyL) [9, 17, 18]. A slight peak of pyridine adsorbed in Brönsted acid sites (PyB) is observed on TiO_2 at 1546 cm^{-1} (Figure 7.7a), less evident for Nb_8TiO_2 and $Nb_{24}TiO_2$ (Figure 7.7b and 7.7c) respectively; in these cases overlapped peaks were observed. Due to overlapping peaks, the area value was solved integrating the deconvoluted peaks with a Gaussian type fit. The results expressed as Brönsted and Lewis peak area ratios are summarized in Table 7.3. The results show very low values of PyB/PyL ratio indicating high content of Lewis acidity (also observed in Figure 7.7).

On the other hand, Figure 7.8 shows the infrared spectra of pyridine adsorbed on Nb_xUSY catalysts. In contrast to the showed by Nb_xTiO_2, the PyB/PyL ratios are greater than unity (Table 7.3), indicating a higher Brönsted acidity. However, the incorporation of niobium to H-USY, increased the Lewis acid sites (decreased PyB/PyL ratios), indicating that surface niobium oxide is significantly more active when it is coordinated to the Al_2O_3 and SiO_2 surfaces than when it is to TiO_2.

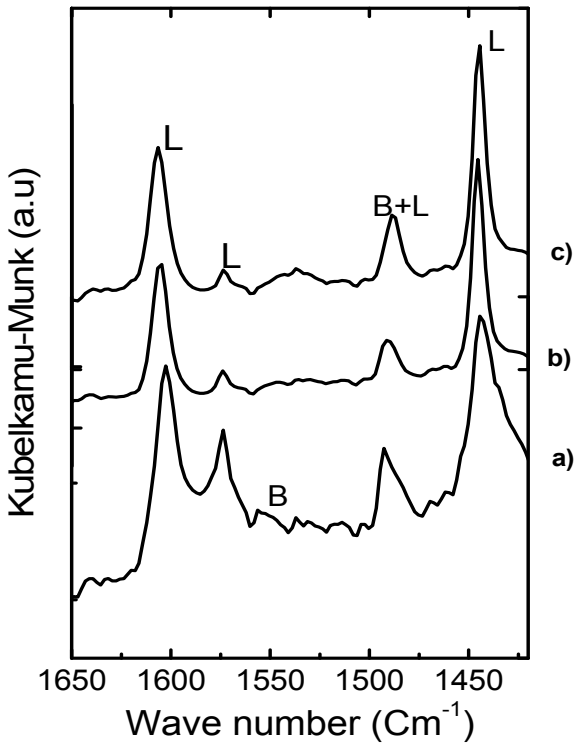

Figure 7.7. Acidity determined by FTIR pyridine adsorption method. 393 K: (a) TiO_2 (b) Nb_8TiO_2 (c) $Nb_{24}TiO_2$.

Table 7.3 Brönsted and Lewis peak areas ratio

Catalyst	*Ratio PyB/PyL
H-USY	5.11
Nb_4USYM1	1.42
Nb_8USYM1	0.30
Nb_4USYM2	5.21
Nb_8USYM2	1.22
TiO_2	0.048
Nb_8TiO_2	0.046
$Nb_{24}TiO_2$	0.051

* determined by peak area deconvolution, PyB: pyridine adsorbed on Brönsted acid site at 1546 cm^{-1}, PyL: pyridine adsorbed on Lewis acid site at 1445 cm^{-1}.

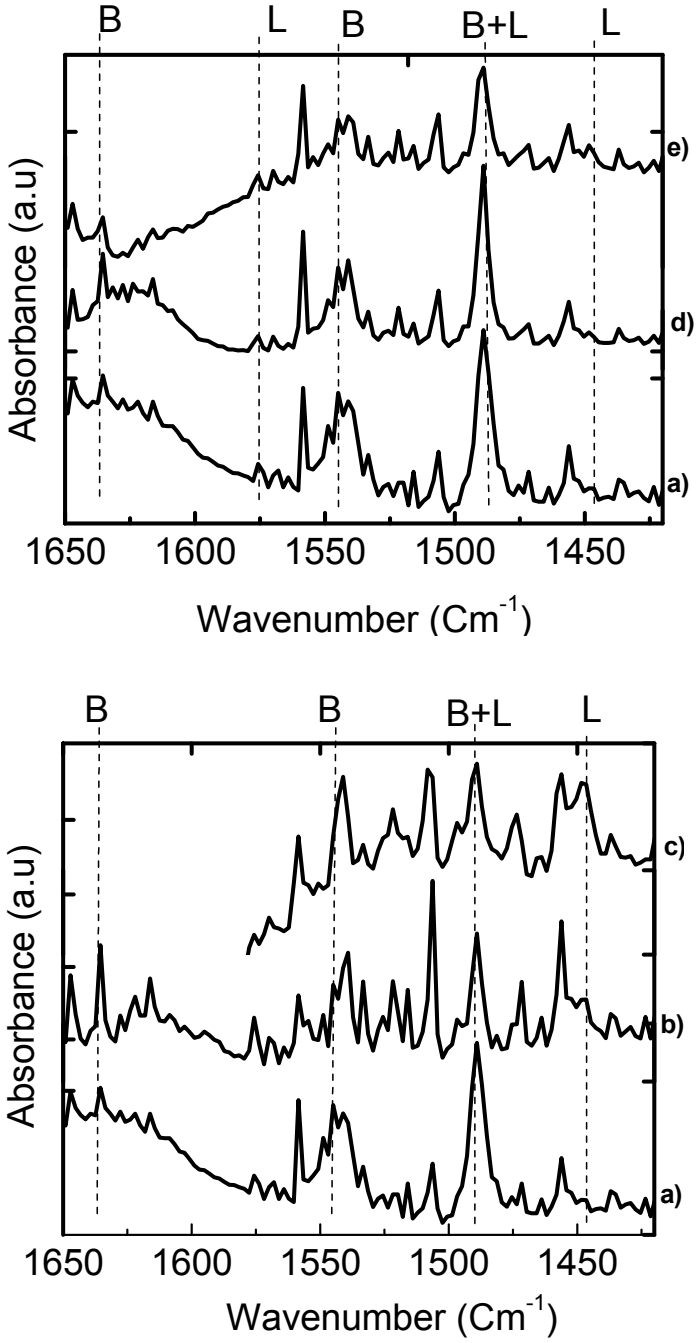

Figure 7.8. Acidity determined by pyridine adsorption FTIR at 473 K: (a) H-USY, (b) Nb_4USYM1, (c) Nb_8USYM1, (d) Nb_4USYM2, (e) Nb_8USYM2.

The total acidity of Nb_xTiO_2 was evaluated by ammonia chemisorption obtained in two successive isothermal cycles represented in Figure 7.9. In the low pressure region, the total amount of ammonia chemisorbed increased quickly, indicating the presence of active acid sites on surface, which give strong acidity interaction with ammonia

molecules. However, at high pressure, the adsorption rate is reduced to linear isotherm. Two straight lines reported in Figure 7.9 are extrapolated to zero pressure and the difference between both intercept points is the maximum irreversible ammonia chemisorbed (Table 7.4).

The results summarized in Table 7.4 shows a slight increase in total acidity by the incorporation of niobium on the support. The total acidity reported for TiO_2 catalyst is 77 μmol NH_3/g, and by the incorporation of niobium oxide, this value increased to 127 μmol NH_3 /g for $Nb_{24}TiO_2$ catalyst. The increase in acidity is due to Lewis acid sites formed by niobium oxides on TiO_2 surface, according to the previously discussed Figure 7.7.

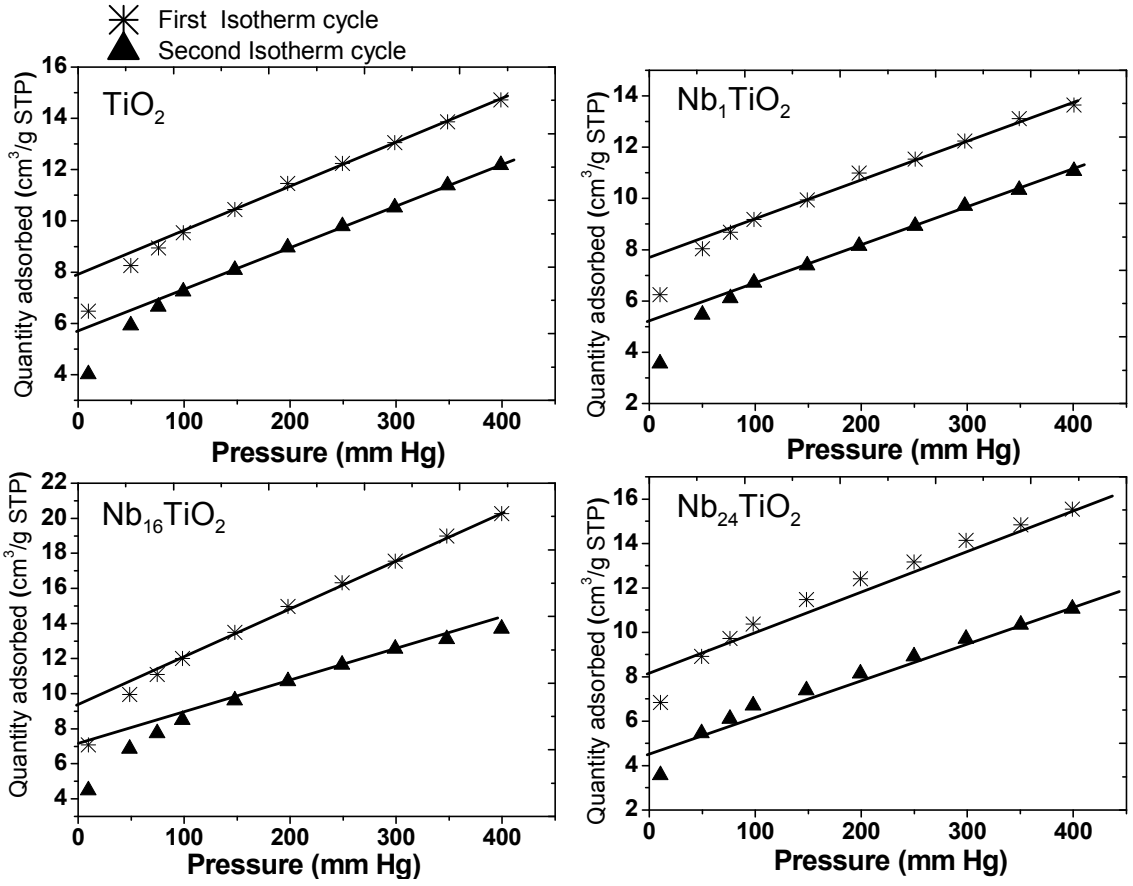

Figure 7.9. Isothermal cycles of ammonia chemisorption for Nb_xTiO_2 at 373 K.

Table 7.4. Total acidity determined by ammonia chemisorption at 373 K

Catalyst	Volume adsorbed of NH_3 (cm^3/g STP)	Total acidity (μmol NH_3/g)
TiO_2	2.392	77
Nb_1TiO_2	2.476	80
$Nb_{16}TiO_2$	3.054	98
$Nb_{24}TiO_2$	3.950	127

7.4.2. Results of characterization of Pt/Al_2O_3, WO_x/Al_2O_3 and $Pt*WO_x/Al_2O_3$

The characterization of Pt/Al_2O_3, WO_x/Al_2O_3 and $Pt*WO_x/Al_2O_3$ catalysts was studied using the following techniques: temperature programmed reduction (TPR), BET surface area analysis, X-Ray diffraction (XRD) and metal content by ICP-OES.

The Figure 7.10 shows a TPR analysis for the catalysts above mentioned. A defined zone of H_2 consumption is observed at 530 K due to reduction of platinum species. And, two less intense peaks are observed at 403 K and 693 K for pt/Al_2O_3 catalyst. The appearance of reduction peak at 723 K for $Pt*WO_x/Al_2O_3$ catalyst is probably due to platinum species interacting with the support γ-Al_2O_3. Therefore, the temperature of reduction was established at 723 K. It is clear that tungsten reduction doesn`t occurs at temperatures lower than 1300 K.

Textural properties are reported in Table 7.5. The impregnation of platinum and wolframium caused very little alteration on surface area compared to original support γ-Al_2O_3, the surface area only decreased a 1 % with wolframium impregnation, a 4 % with platinum and a 9 % when both metals were successively impregnated, while the pore diameter decreased considerably of 7 to 4.7 nm.

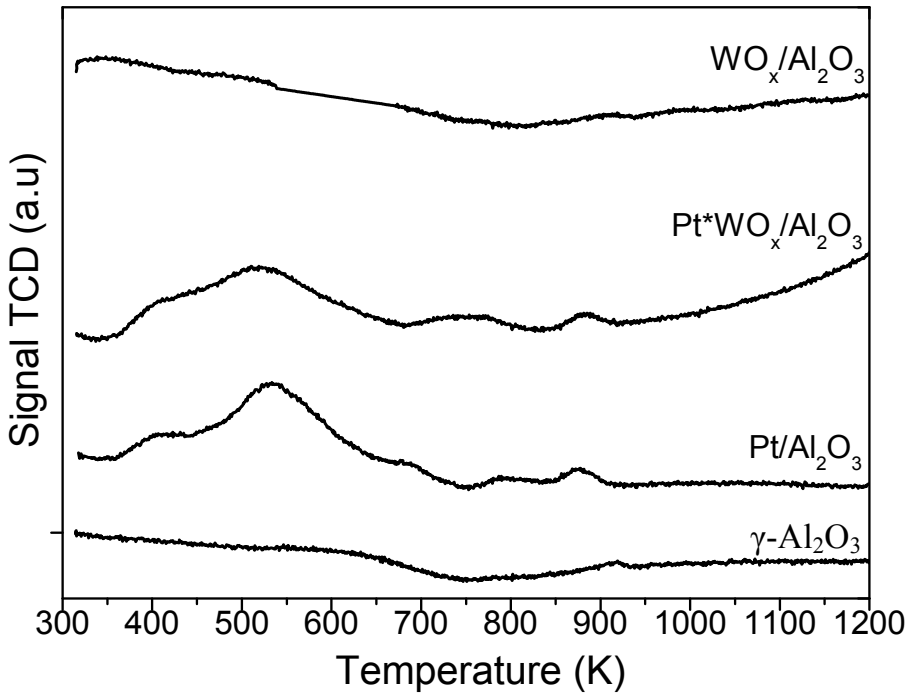

Figure 7.10. Temperature programmed reduction (TPR) of γ-Al_2O_3, WO_x/Al_2O_3, $Pt*WO_x/Al_2O_3$ and $Pt*WO_x/Al_2O_3$ catalysts.

Table 7.5. Textural properties and chemical composition of platinum and wolframium catalysts

Catalysts	S_{BET} (m^2/g)	D_p (nm)	V_T (cm^3/g)	Metal content (wt%)	
				desired	obtained
γ-Al_2O_3	128	7.0	0.221	-	-
Pt/Al_2O_3	123	7.1	0.219	5.0	-
WO_x/Al_2O_3	127	6.8	0.217	5.0	-
$Pt*WO_x/Al_2O_3$	116	4.7	0.203	5.0^{Pt}	3.3^{Pt}
				5.0^{W}	4.0^{W}

S: Total surface area; BET: BET method, V_T: total pore volume; D_p: Pore diameter, Pt: platinum, W: wolframium.

In addition to the above results, the ICP analysis shows that platinum and wolframium contents are slightly lower to desired nominal values incorporated initially to support.

Nitrogen gas adsorption-desorption isotherm for $Pt*WO_x/Al_2O_3$ catalyst (Figure 7.11) correspond to isotherm type IV which is characteristic of mesoporous materials according to IUPAC classification [19]. The adsorption occurs in multilayer, which is reflected into a central region of isotherm ascending as more and more layers of gas are absorbed on the solid surface. Here also the formation of the hysteresis cycle is evident.

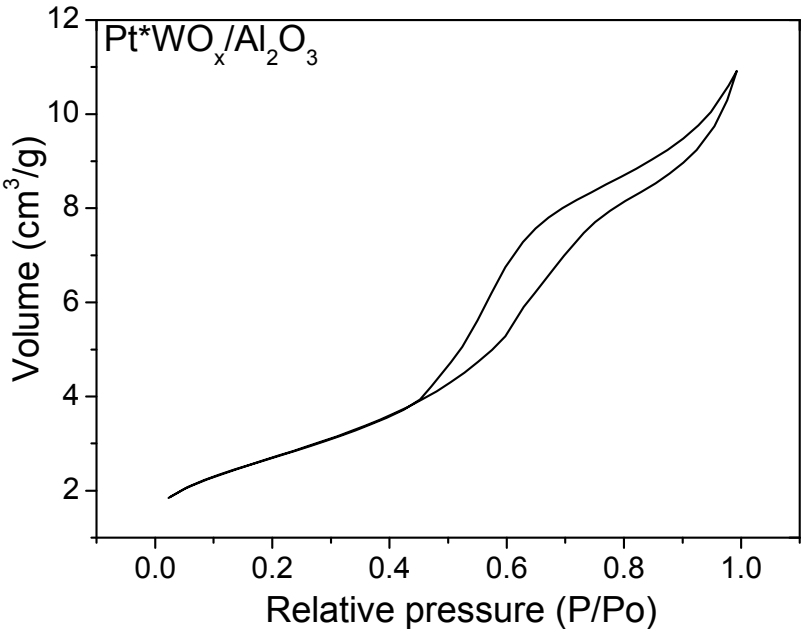

Figure 7.11. Nitrogen adsorption desorption isotherm of $Pt*WO_x/Al_2O_3$ catalyst.

The results of XRD show diffraction peaks of platinum particles appearing at 2 theta: 39°, 46°, and 67°, although the latter value at 67º overlaps with the value of γ-Al_2O_3, such as it can be seen in Figure 7.12. The distribution of wolframium on γ-Al_2O_3 surface presented crystal size values below to 5 nm (Table 7.6), which is indicative of optimal dispersion on surface. Platinum supported over γ-Al_2O_3 showed a semi-crystalline phase which allows differentiation of its peaks. However, when platinum was supported on WO_x/Al_2O_3, the crystallinity decreased considerably.

The results reported in Table 7.6, shows that crystal size of platinum supported on γ-Al_2O_3 and WO_x/Al_2O_3 are relatively high (around 100 nanometers). This suggests that another method of incorporation in surface must be used in futures studies to decrease the crystal size and thereby improve its dispersion.

Table 7.6. Metal particle sizes from XRD measurements

Catalyst	Crystallite size (nm)
Pt/Al_2O_3	~110 [a]
WO_x/Al_2O_3	< 5 [b]
$Pt*WO_x/Al_2O_3$	~100 [a]

a: Platinum, b: Wolframium

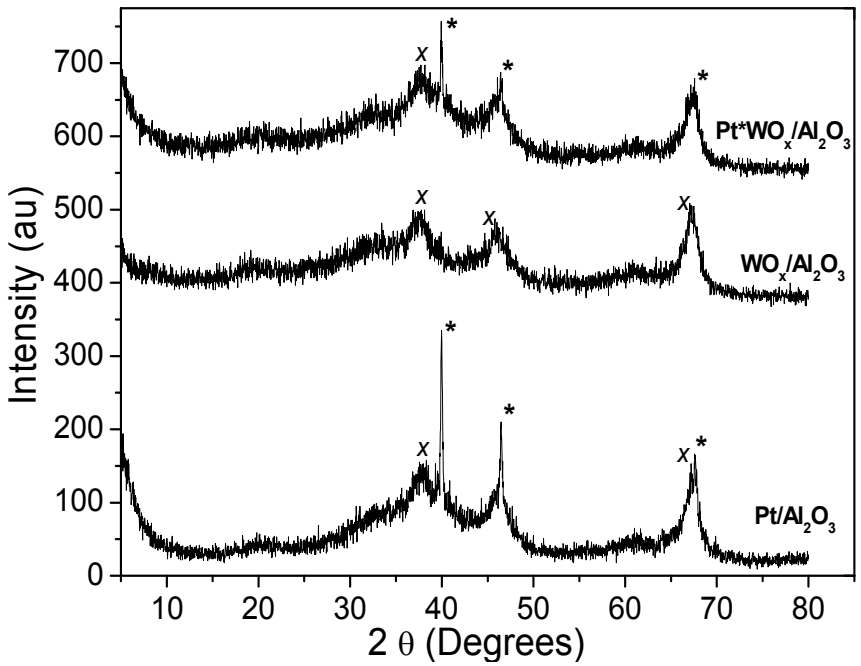

Figure 7.12. X-ray diffraction (XRD) of Pt/Al_2O_3, $Pt*WO_x/Al_2O_3$ and WO_x/Al_2O_3 catalysts. Alumina (*), platinum (x)

7.4.3. Catalytic activity

7.4.3.1. Obtaining of 4-hydroxy-2-cyclopentenone (4-HCP)

Nb_xUSY and Nb_xTiO_2 were used as catalysts for first stage of reaction, which involves the obtaining of 4-HCP from FA in aqueous medium, under conditions specified in section 7.3.1.1. Figure 7.13 shows furfuryl alcohol conversion for Nb_xUSY and Nb_xTiO_2 catalysts. The high reactivity of FA is evidenced: 100% conversion was achieved for all catalysts after 12 hours of reaction. High conversions were obtained in short reaction time for both supports H-USY and TiO_2, in contrast to the obtained for catalysts with niobium incorporated. The above can be related with surface propertie losses caused by the incorporation of niobium (Table 7.1), added to the above mentioned XRD results when crystal structure of H-USY was highly modified by the incorporation of niobium, generating an amorphous structure. This fact can also be confirmed by the activity showed for the catalysts prepared by method M2, where the structural modification of the support was lower, showing higher conversions in short time reaction respect to the obtained with the catalysts prepared by method M1.

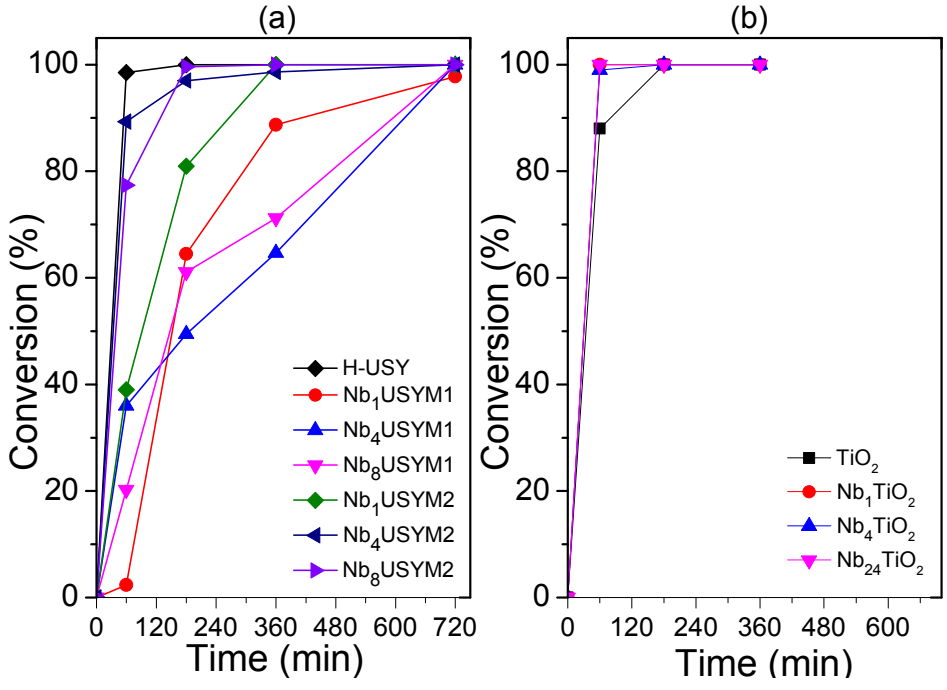

Figure 7.13. Conversion of furfuryl alcohol using a) Nb_xUSY, b) Nb_xTiO_2. Operation conditions: 0.2 ml of FA, 4.8 ml of H_2O, 50 mg of catalyst, 423 K and autogenous pressure

Figure 7.14 shows the relative chromatographic peak areas of 4-HCP obtained using Nb_xUSY and Nb_xTiO_2 catalysts. A high signal intensity of 4-HCP was obtained with Nb_xUSY, respect to Nb_xTiO_2 (showed in Figure 7.14b). This result can be related to Brönsted-Lewis acidity ratio. According to Figure 7.7, the Nb_xTiO_2 has mostly Lewis acid sites, while Nb_xUSY shows combined Brönsted and Lewis acidity (Figure 7.8). Therefore, from the results reported in Table 7.3 and Figure 7.13 is deduced that higher content of Brönsted acid sites increases the FA conversion at higher reaction rate.

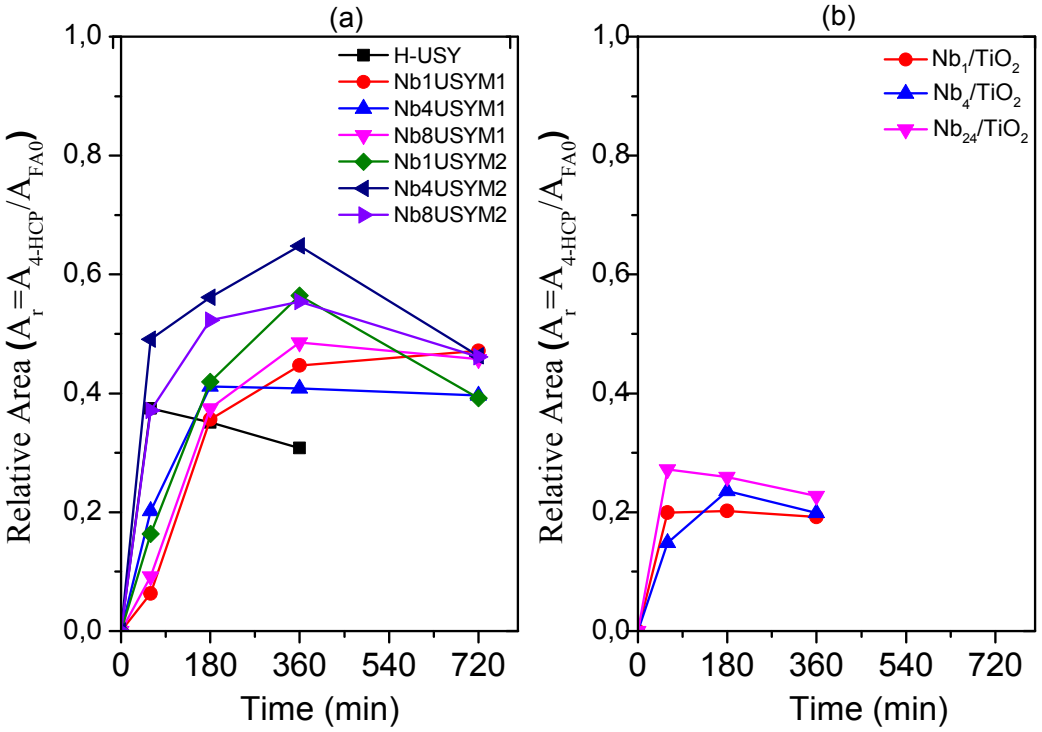

Figure 7.14. Relative peak area of 4-HCP formation for Nb_xUSY and Nb_xTiO_2. Conditions: 0.2 ml of FA, 4.8 ml of H_2O, 50 mg of catalyst, 423 K and autogenous pressure. $A_{4\text{-HCP}}$: 4-HCP chromatogram peak area, A_{FA0}: FA chromatogram peak area in time zero of reaction.

7.4.3.2. Obtaining of cyclopentanone (CPN) from 4-hydroxy-2-cyclopentenone (4-HCP)

Firstly, the 4-HCP necessary for this experimental work was synthesized in our laboratory using the most active catalyst to 4-HCP formation (Nb_4USYM2), according to results obtained in previous section 7.4.3.1. The 4-HCP obtained was used for producing CPN with $Pt*WO_x/Al_2O_3$ catalyst according to description in section 7.3.1.2.

But, under the experimental conditions used, it is also possible to obtain cyclopentanol (CPOL) by hydrogenation of CPN. However, both compounds were not separated by the gas chromatography column employed. Therefore, yield was defined as the moles of CPN plus CPOL obtained respect to FA moles feed in the first stage.

Figure 7.15 shows the CPN + CPOL yield obtained versus reaction time. There it is observed a maximum yield after 2 hours of reaction. This value remains stable for the next hours, thus indicating no formation of other compounds from it. The above is understandable since the signals of both peaks are overlapped, and when CPN is hydrogenated to CPOL, the signal intensity remains almost constant.

The formation of oligomeric resins during the first stage (FA to 4-HCP) can explain the low global yield showed to CPN in second stage. In Figure 7.15 also is shown the 4-HCP behavior. The data represented is the ratio of the peak area of 4-HCP obtained for a sample, respect to the 4-HCP peak area in the feed. The consumption of 4-HCP in reaction is complete after 2 hours, but their consumption at 30 minutes of reaction was very high (about 85 %).

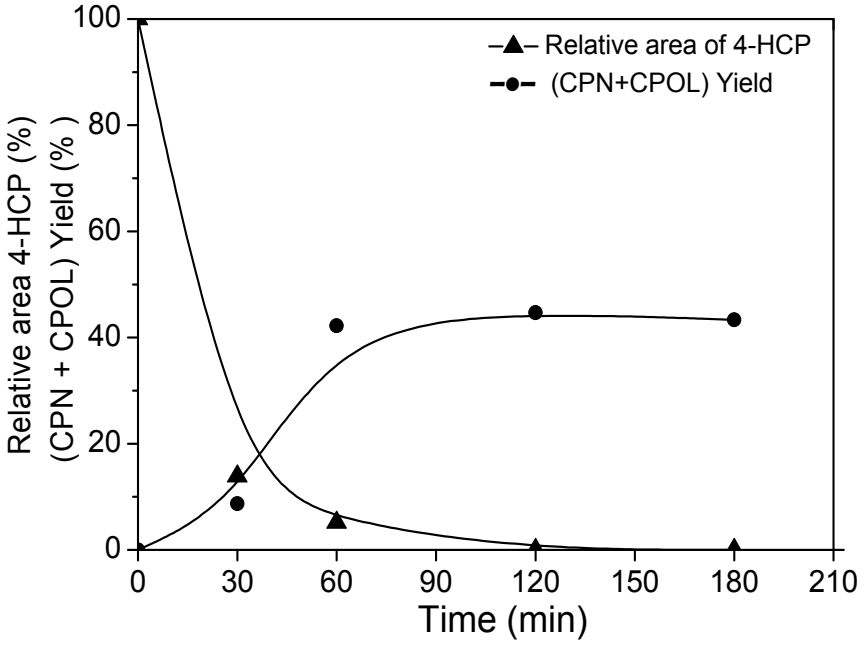

Figure 7.15. Representation of reactants and products in second stage. Yield to (CPN+CPOL) and relative peak area of 4-HCP. Operation conditions: 473 K, 10 bar H_2 pressure, 75 mg of catalyst and 20 mL of product obtained in first stage with Nb_4USYM2 catalyst.

7.4.3.3. Study of obtaining cyclopentanone (CPN) from furfuryl alcohol (FA) in one stage, using Pt /Al_2O_3, WO_x/Al_2O_3 and PtWO_x/Al_2O_3 catalysts*

In last section 7.4.3.2 it was studied the obtaining of CPN from 4-HCP, which previously was obtained from furfuryl alcohol. In this section, the direct obtaining of CPN from FA in aqueous medium by use of Pt/Al_2O_3, WO_x/Al_2O_3 and Pt∗WO_x/Al_2O_3 catalysts was studied.

For a complete study of activity, an optimization of the main variables of operation was included. The process variables studied were: pressure, temperature, concentration of FA feed and reaction time.

The FA conversion for both tested pressures was complete after 1 h of reaction time. Due to the peak superposition signal between CPN and CPOL, which was analyzed in gas chromatograph (G.C), the yields were expressed as the sum of them. The effect of pressure in (CPN+CPOL) yield is represented in Figure 7.16. A substantial difference in yield is observed when the pressure increased from 10 to 20 bar; this increase reached up to 20 % in 180 minutes of reaction. Therefore the increase of hydrogen pressure increases the reaction rate (Figure 7.16), and favors the formation of CPN and CPOL.

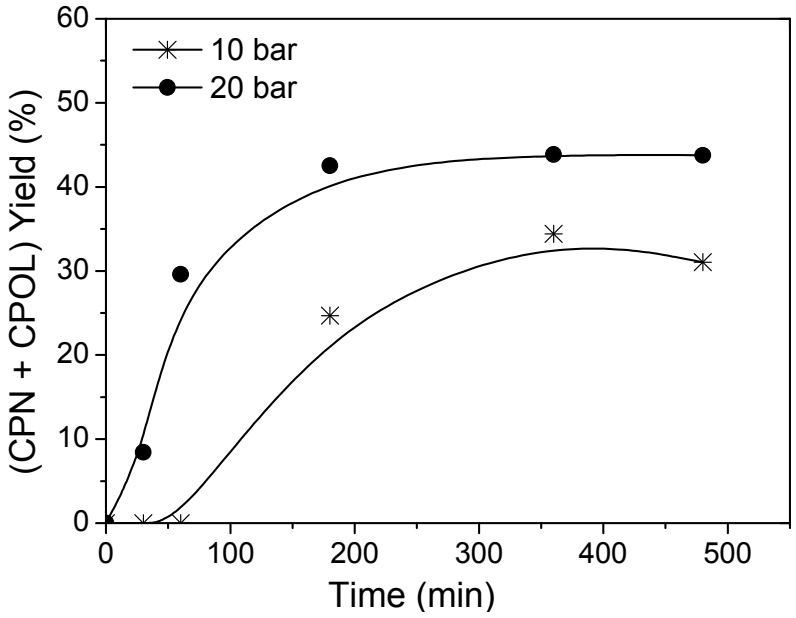

Figure 7.16. Variation of CPN+CPOL yield with the operating pressure. Operation conditions: Temperature (413 K), Catalyst Pt∗WO_x/Al_2O_3 (75 mg), volume of reaction: 20 mL (0.8 ml FA+19.2 ml H_2O), hydrogen gas.

The effect of temperature on yield to reaction products is represented in Figure 7.17. The values selected were 383 K, 413 K and 453 K. In this case, the reaction samples were analyzed by G.C and High-Performance Liquid Chromatography (HPLC), being the main compounds optimally separated and quantified.

Figure 7.17 shows that at the lower temperature tested (383 K), the conversion of FA only reached 45 %, in the same way, low yield to CPN was obtained. When the temperature increased to 413 K, the conversion of FA was complete and the yield to CPN was the highest. At 453 K, a slight decrease of yield to CPN and other compounds was observed, which can be related to the formation of volatile compounds detected in gas phase. Some compounds as 4-HCP and cyclopentenone (CPNE) were not included in Figure 7.17, as it was not possible to quantify, these compounds are precursors of CPN and showed high signal intensity at low temperature. The main compounds obtained to the conditions reported in Figure 7.17 were the following: tetrahydrofurfuryl alcohol (THFA), methyl ethyl ketone (MEK), tetrahydrofuran (THF), CPN and CPOL.

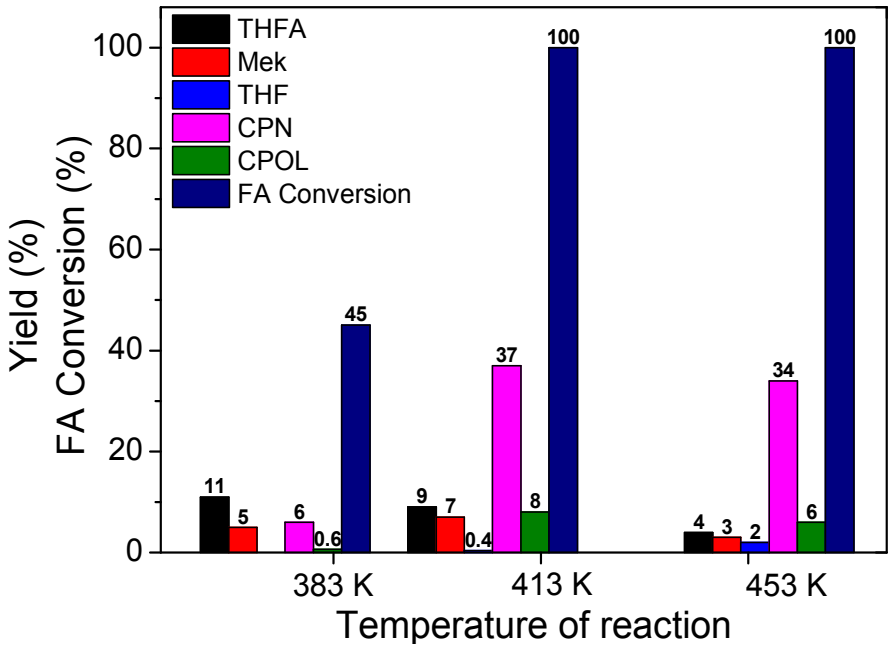

Figure 7.17. Effect of temperature in FA conversion and yields to main products. Operation conditions: 20 bar, gas hydrogen, catalyst of Pt_*WO_x/Al_2O_3 (75 mg), volume of reaction: 20 mL (mixture of 0.8 mL FA and 19.2 mL H_2O).

The quantity of FA fed to the reactor is also an important variable which has influence in the results. In Figure 7.18 is shown the variation of yield to CPN with the mol ratio of FA to catalyst weight (mol FA/g cat). The FA conversion was complete at 1 h of reaction time for all cases. The study of activity in the conditions described in Figure 7.18 showed that yield to CPN increased at low concentration of FA in reaction, reaching differences up to 30 percentage points in CPN yield.

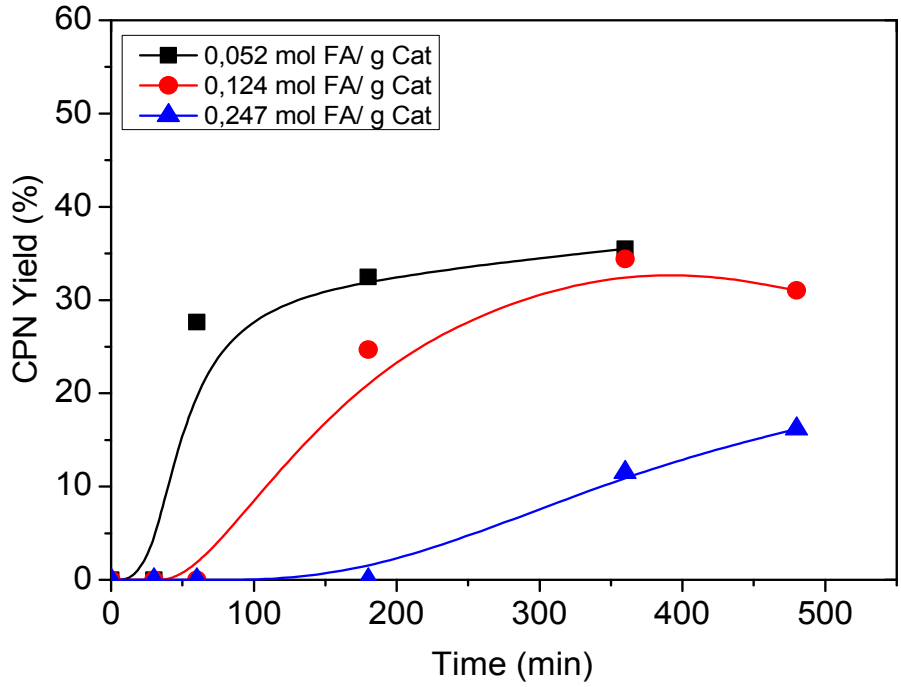

Figure 7.18. Variation of yields to CPN with amount of FA fed (moles FA/ mass of catalyst). Operation conditions: temperature (413 K), pressure (20 bar of hydrogen), catalyst $Pt*WO_x/Al_2O_3$ (75 mg), Total volume of reaction (mixture of FA and H_2O: 20 mL).

Based in the results obtained in the above optimization procedure, the following operation conditions were selected for the activity study of catalyst: 20 bar, 413 K, 75 mg catalayst, 0.8 ml of FA and 19.2 ml H_2O.

At the above mentioned conditions the conversion of FA was studied using Pt/Al_2O_3, WO_x/Al_2O_3 and $Pt*WO_x/Al_2O_3$ catalysts. Figure 7.19 shows that reaction rate is lower for Pt/Al_2O_3 catalyst, respect to other catalysts. The FA conversion with Pt/Al_2O_3 is below 30 percentage points respect to the other catalysts at 1 h of reaction time, although all catalysts showed complete conversion after 3 hours. For explaining this

difference in conversion, Figure 7.20 shows the distribution of the main products obtained for each catalyst, represented as peak area percentage obtained by HPLC analysis. The Figure 7.20a shows that for WO_x/Al_2O_3 catalyst, the high FA conversion obtained in the first hour of reaction, mainly corresponds to the formation of 4-HCP, the reaction mechanism involves the fast reaction of FA to 4-HCP and then the CPN formation from it. However, the catalytic activity of Pt/Al_2O_3 catalyst in reaction (Figure 7.20b) did not include the formation of 4-HCP, in this case, the presence of platinum increased the hydrogenation reactions to form tetrahydrofurfuryl alcohol (THFA), cyclopentanone (CPN), cyclopentanol (CPOL) and an undefined compound (Undefined A). This mechanism is studied in detail later. As the platinum promotes the hydrogenation of CPN to CPOL, a higher formation of CPOL is observed (Figure 720b and 7.20c) than obtained with WO_x/Al_2O_3 (Figure 7.20.a).

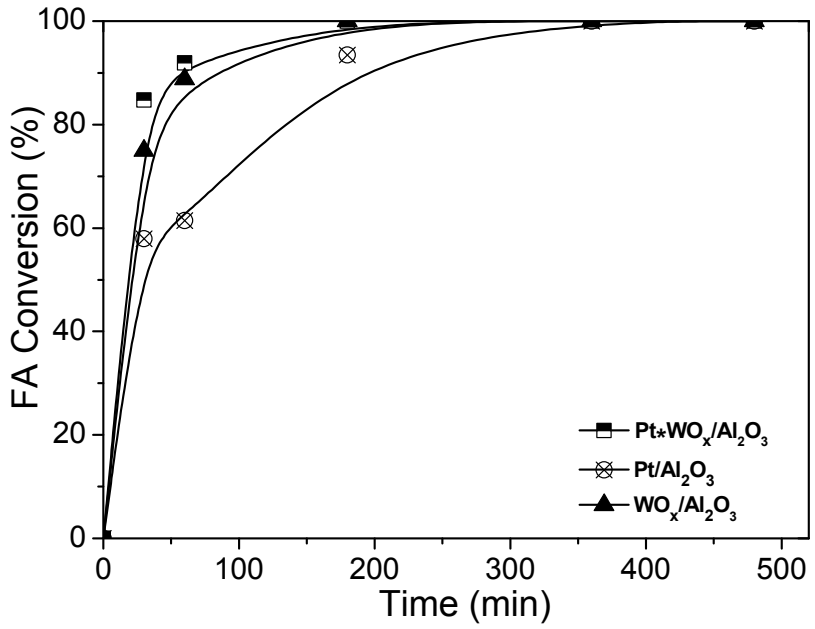

Figure 7.19. Conversion of FA by the use of WO_x/Al_2O_3, Pt/Al_2O_3 and $Pt*WO_x/Al_2O_3$catalysts. Operation conditions: hydrogen pressure: 20 bar, 413 K, 0.8 ml of FA, 19.2 mL H_2O, 75 mg cat.

The activity of $Pt*WO_x/Al_2O_3$ is highly oriented to CPN formation, the main products obtained after 6 h of reaction were: CPN, CPOL, THFA and undefined compound (undefined B). Again, the presence of platinum not has promoted the formation of 4-HCP. The combination of platinum and wolframium oxide on alumina support increased the formation of CPN, such as is shown in Figure 7.20.

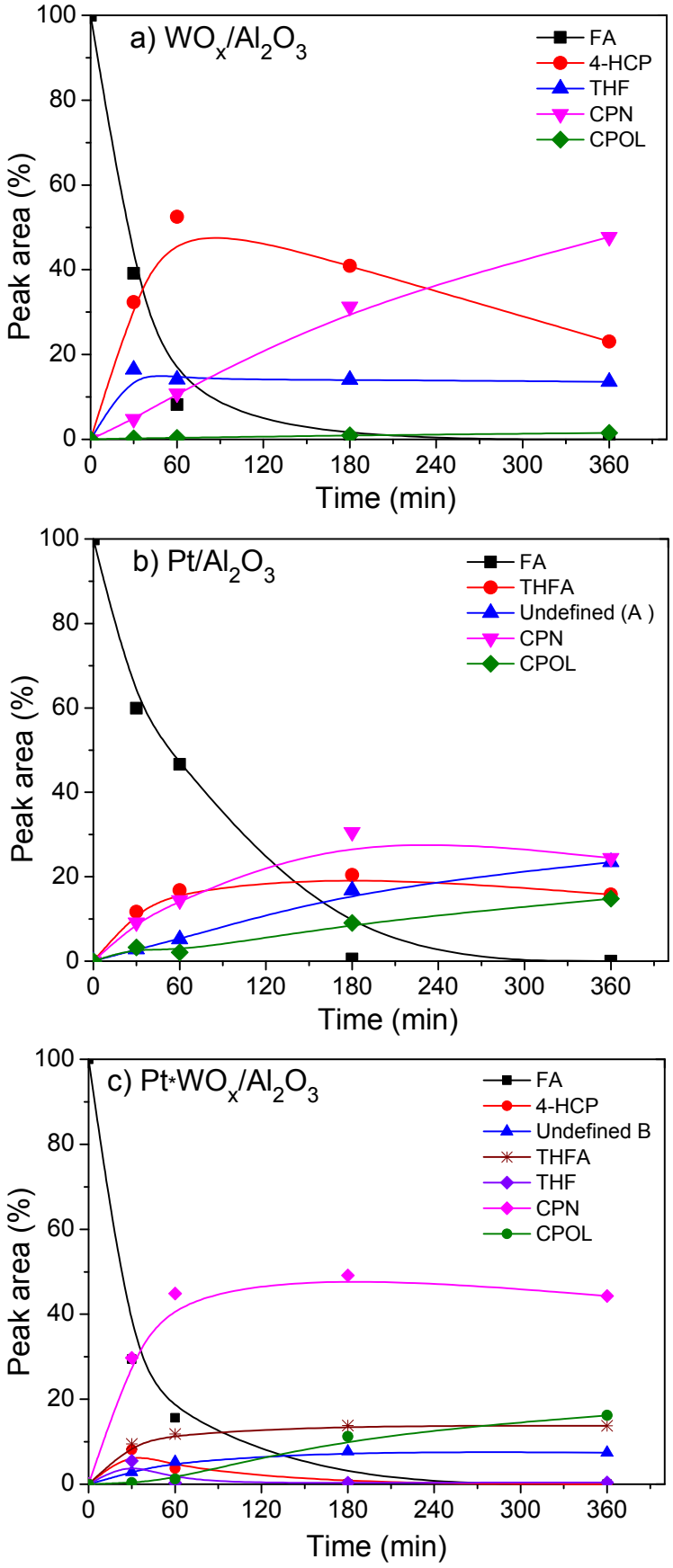

Figure 7.20. Main products obtained by the use of different catalysts. a) WO_x/Al_2O_3, b) Pt/Al_2O_3 and c) $Pt*WO_x/Al_2O_3$. Operation conditions: 413 K, 20 bar H_2, 75 mg of catalyst, volume of reaction: 20 mL (0.8 mL FA+19.2 mL H_2O).

A summary of selectivity to CPN obtained with the catalysts studied is shown in Figure 7.21. The highest selectivity to CPN was obtained using Pt*WO_x/Al_2O_3 catalyst; under optimal conditions, the selectivity to CPN reached up to 42 mol% at low reaction time (1 h). Slightly lower selectivity to CPN was obtained using the WO_x/Al_2O_3 catalyst (39 mol%), although higher reaction time was required (6 hours). The results using Pt/Al_2O_3 showed that selectivity to CPN only reached 30 mol%, while the tests without catalyst presented a CPN selectivity of 20 mol%. The results obtained without catalyst showed that CPN can be obtained without catalyst only by hydrogenation, through the mechanisms that included 4-HCP as main intermediate product.

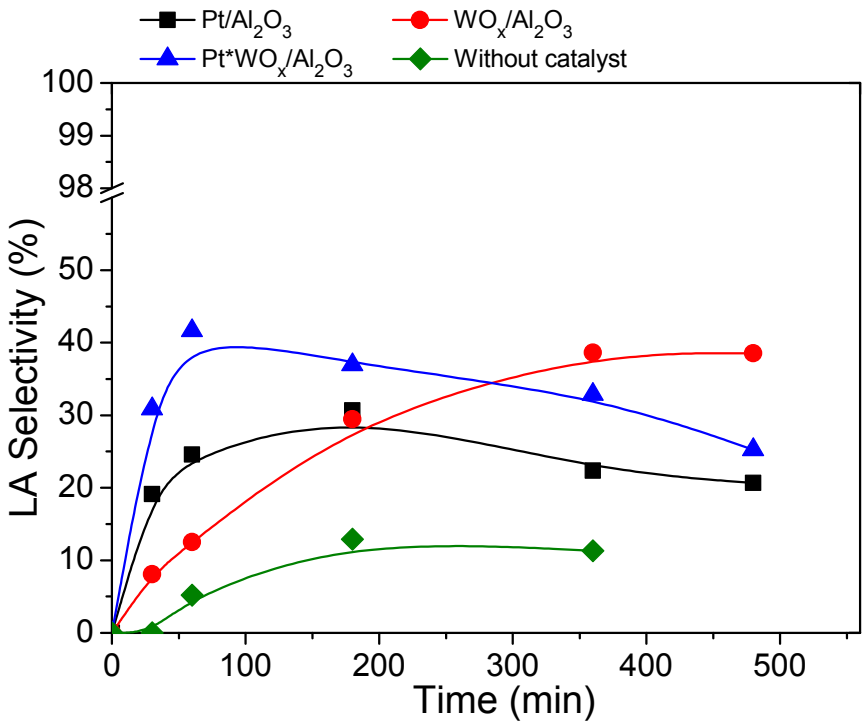

Figure 7.21. Selectivity to CPN using Pt/Al_2O_3, WO_x/Al_2O_3 and Pt*WO_x/Al_2O_3 catalysts. Operation conditions: 413K, 20 bar of H_2, 75 mg catalyst, 0.8 mL of FA, 19.2 mL of H_2O.

The percentage of selectivity to the products obtained for each catalyst is shown in Figure 7.22. The selectivity represented in this figure corresponds to reaction time in which a maximum selectivity to CPN was obtained for each catalyst. The schematized results show that multiple compounds are mostly obtained with Pt/Al_2O_3. In this case, though the selectivity to CPN is low, other products as THFA and CPOL can be obtained as added value; so, the presence of CPOL indicates that it was formed from

hydrogenation of CPN due to the high activity of platinum in the hydrogenation reactions. The formation of THFA only occurs when platinum is present in the catalyst, in this case, the product distribution to form CPN is different. Then the distribution of products proposed is clearly detailed (Scheme 7.2.)

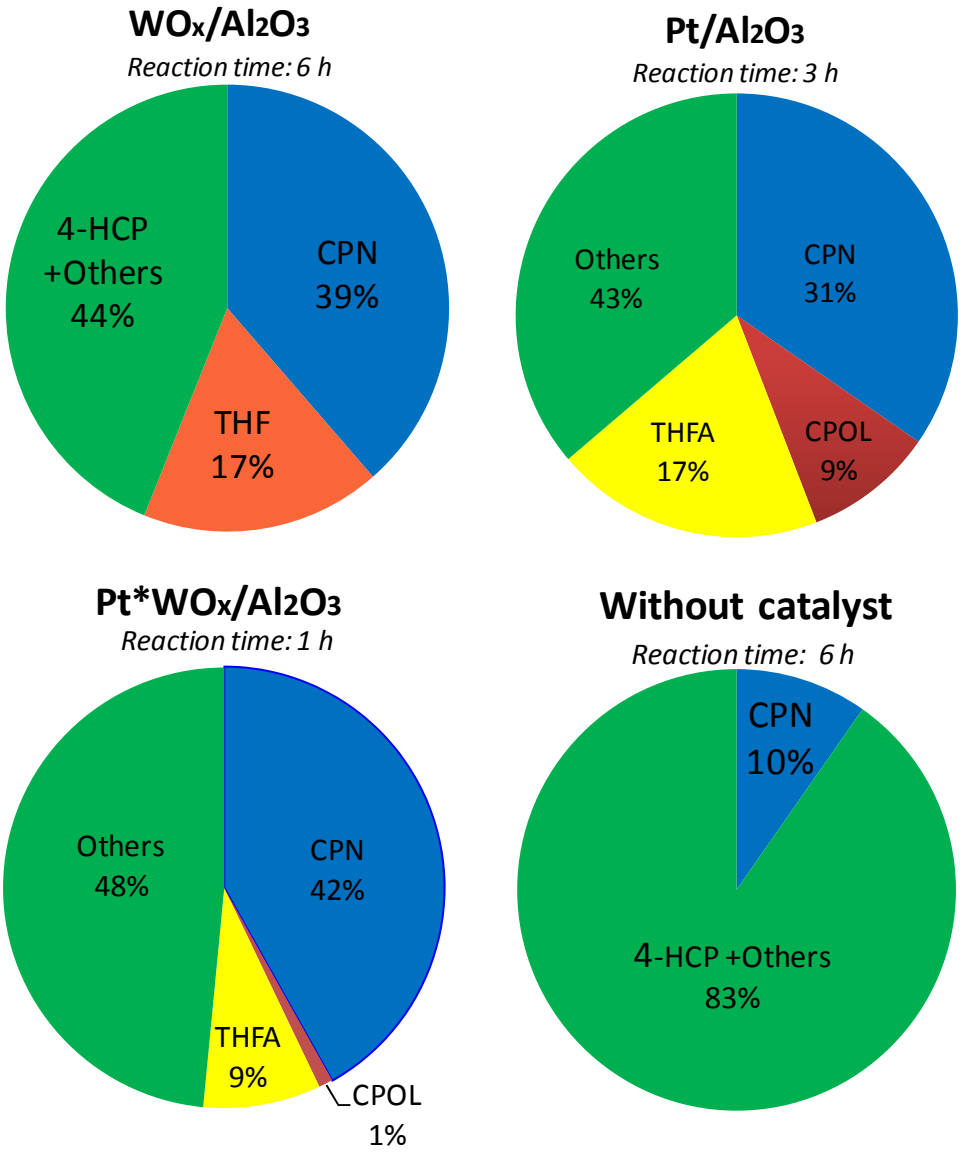

Figure 7.22. Selectivity of products obtained for different catalysts. Optimal conditions: 413 K, 20 bar H_2, 75 mg cat, 0.8 mL FA, 19.2 mL H_2O. Products analyzed by HPLC. Reaction time defined to maximum selectivity obtained for each catalyst. THF: tetrahydrofuran, THFA: tetrahydrofurfuryl alcohol, CPOL: cyclopentanol,CPN: cyclopentanone.

According to the above results showed in Figures 7.20 and 7.22, two different routes of obtaining CPN are possible, depending upon whether the catalyst used contains platinum as active metal in reduced form (Scheme 7.2a). On the other hand, when other active metal (wolframium) in oxide form (calcined) is used as catalyst, the mechanism of obtaining CPN is different (Scheme 7.2b).

According to Scheme 7.2.a, the furfuryl alcohol (FA) is hydrogenated to tetrahydrofurfuryl alcohol (THFA), followed by a dehydration reaction to form cyclopentanone (CPN), which is hydrogenated to cyclopentanol (CPOL). Other products with lower signal intensity are also formed as methyl ethyl ketone (MEK) and 1,4-pentanediol, formed from THFA.

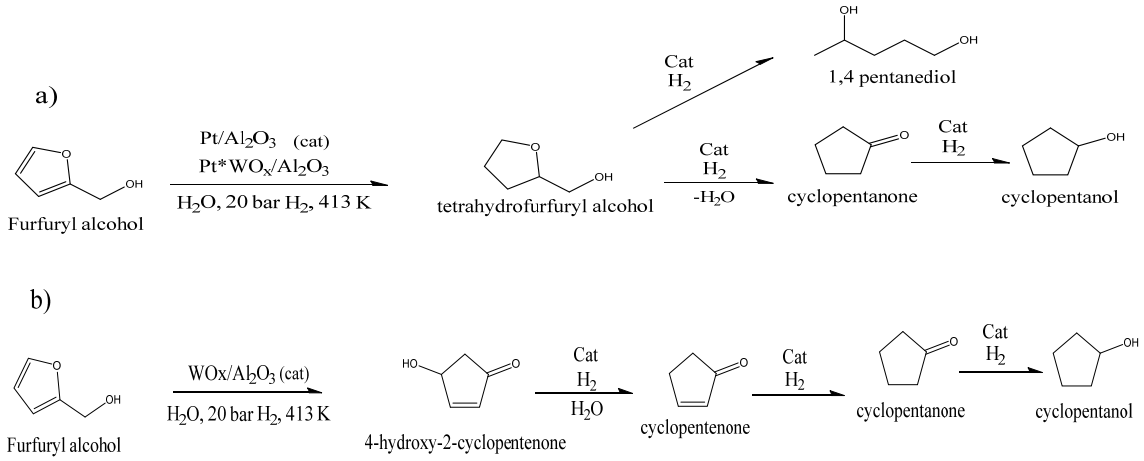

Scheme 7.2. Mechanism of obtaining CPN from furfuryl alcohol. a) reaction mechanism for catalysts with platinum content, b) reaction mechanism for catalysts with metallic oxide content.

The reaction mechanism of obtaining CPN from FA using wolframium oxide catalyst (WO_x/Al_2O_3) proceeds through the obtaining of 4-HCP, which is dehydrated to unstable cyclopentenone (CPNE). Then, this is hydrogenated to CPN, which also is hydrogenated to CPOL.

The yields to CPN in this study were lower than the ones obtained by Hronec et al (61 %) which used a platinum catalyst supported on activated carbon powder [5, 6].

7.5. Conclusions

In this chapter the synthesis of CPN and 4-HCP from furfuryl alcohol was studied. The 4-HCP is a product precursor of various products including CPN. Initially, two stages were proposed for obtaining CPN from FA. In a first stage 4-HCP was obtained using niobium oxide catalysts supported on USY zeolite and TiO_2. In this stage, the niobium supported on TiO_2 showed a lower activity towards 4-HCP than those supported on zeolite USY, which were prepared by wet impregnation and precipitation methods. The catalysts prepared by precipitation method were more active in synthesis of 4-HCP, these showed better dispersion of niobium in surface. The 4-HCP synthesized in first stage (using Nb_4USYM2) was used to produce CPN in a second stage. The study was carried out with the catalyst $Pt*WO_x/Al_2O_3$. The global yield to CPN increased to 45 %. This low yield is attributed to the formation of furan resins in the first stage.

The direct production of CPN form hydrogenation of FA in aqueous media was evaluated by the use of catalysts Pt/Al_2O_3, WO_x/Al_2O_3 and $Pt*WO_x/Al_2O_3$. The reaction proceeded by the formation of 4-HCP as intermediated compound prior to the formation of CPN when WO_x/Al_2O_3 catalyst is used. The incorporation of platinum promotes the hydrogenation reactions in the mechanism, including THFA and THF as intermediate compounds. The desired product CPN also reacts to form CPOL by hydrogenation. To avoid this, the reaction must be stopped at time where maximum yield to CPN is obtained.

The most active catalyst to form CPN was the $Pt*WO_x/Al_2O_3$, which reached a maximum in selectivity up to 42 %. In this case, the low selectivity was attributed to formation of byproducts as tetrahydrofuran (THF), 2-butanone (MEK), 1,4-pentanodiol and other unidentified compound.

7.6. References

[1]. D. Ayhan, S. Ozge, A new and efficient chemoenzymatic access to both enantiomers of 4-hydroxycyclopenten-2-en-1-one, Tetrahedron: Asymmetry 13 (2002) 667-670.

[2]. K. Subhash, N. Nahid, M. Sukumar, Y. Yang, R. Joshua, An efficient synthesis of 4(s)-Hydroxycyclopent-2-enone, J. Org. Chem 60 (1995) 7548-7551.

[3]. C. Wenkang, Method for preparing cyclopentanone from adipic acid Pat: CN103044226A (2013).

[4]. Y. Yanliang, D. Zhongtian, H. Yizheng, L. Fang, W. Feng, G. Jin, X. Jie, Conversion of furfural into cyclopentanone over Ni–Cu bimetallic catalysts, RSC Publishing 15 (2013) 1932-1940.

[5]. M. Hronec, K. Fulajtarová, Selective transformation of furfural to cyclopentanone, Catal. Commun. 24 (2012) 100-104.

[6]. M. Hronec, K. Fulajtarová, T. Liptaj, Effect of catalyst and solvent on the furan ring rearrangement to cyclopentanone, Appl. Catal., A: General 437–438 (2012) 104-111.

[7]. Z. Minghao, Z. Hongyan, N. Lei, X. Guomin, X. Rui, Catalytic Hydroprocessing of Furfural to Cyclopentanol Over Ni/CNTs Catalysts: Model Reaction for Upgrading of Bio-oil, Catal. Lett. 144 (2014) 235-241.

[8]. Z. Hongyan, Z. Minghao, Z. Zuo, X. Guomin, X. Rui, Selective hydrogenation of furfural to cyclopentanone over Cu-Ni-Al hydrotalcite-based catalysts, Korean J. Chem. Eng. 31 (2014) 593-597.

[9]. M.G. Alimukhamedov, F.A. Magrupov, Kinetics of homopolycondensation of furfuryl alcohol., Polym. Sci. Ser B. 49 (2007) 1287-1292.

[10]. T. Kim, R.S. Assary, H. Kim, C.L. Marshall, D.J. Gosztola, L.A. Curtiss, P.C. Stair, Effects of solvent on the furfuryl alcohol polymerization reaction: UV Raman spectroscopy study, Catal. Today 205 (2013) 60-66.

[11] A. Ahmet, M. Holger, H. Dieter, Investigation of acid sites on V_2O_5/TiO_2 catalysts by FTIR with Adsorption of Pyridine, Tr. J. chem. 20 (1996) 38-42.

[12]. M.O. Guerrero-Pérez, M.A. Bañares, Niobium as promoting agent for selective oxidation reactions, Catal. Today 142 (2009) 245-251.

[13]. R. Ladera, E. Finocchio, S. Rojas, J.L.G. Fierro, M. Ojeda, Supported niobium catalysts for MeOH dehydration to dimethyl ether: FTIR studies of acid properties, Catal. Today 192 (2012) 136-143.

[14]. J.C. Rooke, T. Barakat, M.F. Finol, P. Billemont, G. De Weireld, Y. Li, R. Cousin, J. Giraudon, S. Siffert, J. Lamonier, B.L. Su, Influence of hierarchically porous niobium doped TiO_2 supports in the total catalytic oxidation of model VOCs over noble metal nanoparticles, Appl. Catal., B: Environmental 142–143 (2013) 149-160.

[15] S. García-Fernández, I. Gandarias, J. Requies, M.B. Güemez, S. Bennici, A. Auroux, P.L. Arias, New approaches to the Pt/WOx/Al2O3 catalytic system behavior for the selective glycerol hydrogenolysis to 1,3-propanediol, J. Catal. 323 (2015) 65-75.

[16]. Z. Sarbak, Characterization and infrared study of the effect of Cr, Mo and W on carbon deposition on platinum/alumina, Appl. Catal,. A: General. 177 (1999) 85-97.

[17] B. Chakraborty, B. Viswanathan, Surface acidity of MCM-41 by in situ IR studies of pyridine adsorption, Catal. Today 49 (1999) 253-260.

[18] A. Ramanathan, R. Maheswari, D.H. Barich, B. Subramaniam, Microporous Mesoporous Mater. 190 (2014) 240-247.

[19] International Union of Pure and Applied Chemistry (IUPAC), IUPAC Manual os Symbols and Terminology, Pure Appl. Chem. 31 (1972) 578.

Chapter 8. Conclusions and proposals for future research on this topic.

8.1. Conclusions

The production of levulinic acid (LA) from furfuryl alcohol (FA) by heterogeneously catalized reactions has been studied in the present work. This reaction is included in the so called biorefinery processes, which are been widely studied in recent years by the broad variety of chemical that can be obtained from biomass. In each chapter, the main conclusions about catalysts and process conditions have been explained according to the results obtained. Consequently, a summary of the main conclusions about the work described in this manuscript is presented below.

1- The initial screening of acid catalysts indicated that catalysts with organic structure, Amberlyst, attained a high yield to levulinic acid. By the use of these catalysts, the yield reached up to 63 % in continuous flow and 44 % in batch system, in both cases with total conversion of furfuryl alcohol. The mesoporosity and Brönsted acidity were the main characteristics of these materials influencing the results obtained. The high mesoporosity provided easy access of reactants to acid sites on the organic structure.

2- The formation of undesired furan resins was among the high causes in the decrease of yield to LA. This side reaction is associated with concentration of FA in the reaction medium, where the furan resins formation increased considerably. An additional drawback of this resin formation is the active sites blockage due to its deposition onto the catalyst surface. Therefore, a low concentration of FA should be used. At first, it seems that dilution of FA adding more water is a simple and low cost solution for this issue. But high water concentration increased the selectivity to the formation of 4-hydroxy-2-cyclopentenone (4-HCP) as main product. The alterative found in the present work consisted in the addition of cyclopenthyl methyl ether (CPME) as co-solvent, insoluble in water. Then the FA was “stored” in organic phase, crossing the interphase as it was consumed in the reaction, thus maintaining a low FA concentration in the aqueous phase.

3- Although the results obtained with the Amberlyst were positives, it should be noted that its organic structure presented thermal-mechanical limitations being unviable its reuse. As the optimal temperature of reaction was set to values very close to the maximum specified for these catalysts, the structure of the catalysts was thermally affected. In addition to the above, high losses of sulfonic groups were reported, attributed to leaching in aqueous media, these losses amounted up to 65 % (reported as sulfur loss).

4- Given the thermo-mechanical instability of the Amberlyst catalysts, a series of catalysts with inorganic structure was evaluated. The H-ZSM5 zeolite showed higher yields to LA compared to other catalysts as H-β zeolite, heteropolyacids (PTA) and super acids (ZrO_2/SO_4^{2-}). The combined Brönsted and Lewis acidity of H-ZSM5, added to the structure of ZSM-5, showing well defined pores and channels (mostly mesoporosity), allowed to obtain a yield to LA up to 58 mol%, in a semi continuous system. The yield to LA increased by the incorporation of methyl ethyl ketone (MEK) as solvent of FA in the feed, minimizing the formation of undesired furan resins. After optimization of main operation conditions in a semicontinuous system the yield to LA increased to 77 mol%.

5- The modification of SiO_2:Al_2O_3 ratio in the H-ZSM5 zeolites was also investigated respect to its change in porosity and exchange capacity. The desilicated H-ZSM5 with a lower Si/Al ratio (H-ZD(23)) showed the best yield to LA (81 mol%), which represents 11 percentage points higher than the parent H-Z(23). In the case of H-Z(23), the desilication was effective due to the mesoporosity, keeping its acid properties. The desilication process of H-Z(50) was also effective respect to the increase of mesoporosity and pore diameter. However, the yield to LA decreased considerably due to acidity loss; as the number of strong acid sites dropped.

6- The catalysts type La_xZrO_2/SO_4^{2-} known as “superacid catalyst”, showed high activity in the aqueous reaction of FA. A conversion of 100 % was reached at 3 hour of reaction; nevertheless, the selectivity to LA was low. Although lanthanum

oxide was not completely incorporated according to the nominal value set in the preparation (verified by EDX and XPS analysis), this catalysts showed selectivity to LA, as opposed to the results obtained with ZrO_2/SO_4^{2-}, in which the yield to LA was close to zero. By the use of La_xZrO_2/SO_4^{2-}, the yield to LA increased 9 percentage points attributed to the increase of strong acidity.

7- The study over the activity of niobium (Nb) catalysts supported on titanium oxide (TiO_2) and ultra stable Y zeolite (USY) in the aqueous reaction of FA was evaluated initially with the purpose of obtaining levulinic acid (LA). However, these catalysts showed very low selectivity to LA, in contrast to the high formation of 4-hydroxy-2-cyclopentenone (4-HCP). As 4-HCP is not yet highly commercialized a further reaction stage was included for obtaining cyclopentanone (CPN) using platinum and wolframium catalysts supported on alumina ($Pt*WO_x/Al_2O_3$). The global yield to CPN (including two stages) was 45 mol%. In first stage, the niobium supported on USY and prepared by precipitation method (Nb_xUSYM2) was more active to 4-HCP, showing an better dispersion of niobium in the surface. In this stage, the low yields were attributed to the formation of furan resins, as other compounds were not detected. The study about the obtaining of CPN in one-stage from FA in aqueous media was also evaluated by the use of monometallic supported Pt/Al_2O_3, WO_x/Al_2O_3 and bimetallic $Pt*WO_x/Al_2O_3$ catalysts. The maximum selectivity to CPN amounted to 43 mol% by the use of bimetallic $Pt*WO_x/Al_2O_3$. In this case, furan resins were not obtained, accordingly, the distribution of products included the 4-HCP, tetrahydrofurfuryl alcohol (THFA), cyclopentenone (CPNE), tetrahydrofuran (THF) and cyclopentanol (CPOL). These results showed that one-stage production of CPN from FA is an effective reaction process, because furan resins were not obtained, and the by-products obtained can be given an added value, doing the overall process economically feasible.

8.2. Proposals for future research on this topic

In addition to the above conclusions, a series of proposals outlined from the main results obtained are described below. These proposals are mainly aimed to the contribution of improvements in this topic, given the experience acquired over this research.

As was mentioned above, in the obtaining of levulinic acid from furfuryl alcohol in aqueous media, the best result were obtained using the commercial zeolite H-ZSM5 with the lowest Si/Al ratio and after being subjected to a desilication process. The desilication process was positive due to the increase of mesoporosity, which clearly favors the yield to LA. The reusability of catalysts was possible by activation at 823 K in air, keeping its activity. Based on this background, it is proposed an activity study in a packed bed reactor, such as was done in chapter 4, in which the Amberlyst was used as catalyst. In principle the reaction in packed bed reactor is economically more feasible than semicontinuous processes, being easier the "in situ" activation of catalysts (by calcination) and higher operation time. For this process is proposed the use of co-solvent to be soluble in water and furfuryl alcohol, to maintain low concentrations avoiding the furan resins formation and 4-hydroxy-2-cyclopentenone (4-HCP) which are favored at high water concentration. Added to this, the pressurization of the reactor with hydrogen can be included. According to results obtained in the semicontinuous reactor, the inhibition effect in the formation of furan resins of hydrogen was higher than when nitrogen was used.

On the other hand, given that La_xZrO_2/SO_4^{2-} showed a promising selectivity to LA respect to the parent ZrO_2/SO_4^{2-}, new studies are suggest respect to other synthesis methods, in order to increase the percentage of lanthanum added to the catalyst.

Participation in conferences

- 7th International Conference on Green and Sustainable Chemistry (GSC-7)

Tokyo, Japan; July 2015

http://www.jaci4gsc7.org/

Title: "Solid acid catalysts in the synthesis of levulinic acid from furfuryl alcohol".

- Oral presentation

- International conference on catalysis ICC 2014

Beijing,China; June 2014

http://www.engii.org/workshop/ICC2014June/

Title: "Niobium and Platinum-Wolframium catalysts in the conversion of furfuryl alcohol to cyclopentanone. Reaction in two stages".

- Oral presentation

- 7th International Conference on Environmental Catalysis ICEC-2012

Lyon, France; September 2012

http://www.icec2012.fr/en/home.html

Title: "Levulinic acid from Furfuryl alcohol, Catalyzed by Amberlyst resins. Batch and continuous process".

- Poster presentation

- International Symposium on Catalysis for Clean Energy and Sustainable Chemistry

Alcobendas Madrid, Spain; June 2012

http://www.energy.imdea.org/events/2012/international-symposium-catalysis-clean-energy-sustainable-chemistry-ccesc2012

Title: "Synthesis of levulinic acid from furfuryl alcohol catalyzed by Amberlyst ion–exchange resin.

- Poster presentation